UNIVERSITY OF SZEGED
DOCTORAL SCHOOL OF GEOSCIENCES

APPLYING CORRELATIVE BIOME MODELS TO ADDRESS CERTAIN PHYTOGEOGRAPHICAL ISSUES OVER DIFFERENT SPACE AND TIME WINDOWS

KORRELATÍV BIOM MODELLEK ALKALMAZÁSA BIZONYOS NÖVÉNYFÖLDRAJZI KÉRDÉSEK ÉRTÉKELÉSE CÉLJÁBÓL KÜLÖNBÖZŐ TÉR- ÉS IDŐABLAKOK MELLETT

PhD dissertation

ZOLTÁN SZELEPCSÉNYI

Supervisor:
PROF. PÁL SÜMEGI DSC
full professor
Department of Geology and Palaeontology
University of Szeged

Co-Supervisor:
NÁNDOR FODOR PHD
senior research fellow
Agricultural Institute
Eötvös Loránd Research Network

External Consultant:
HAJNALKA BREUER PHD
assistant professor
Department of Meteorology
Eötvös Loránd University

UNIVERSITY OF SZEGED
FACULTY OF SCIENCE AND INFORMATICS
DEPARTMENT OF GEOLOGY AND PALAEONTOLOGY

SZEGED
2022

‘I could calculate your chance of survival, but you won’t like it.’
The Hitchhiker’s Guide to the Galaxy, *Douglas Adams, 1979*

Table of contents

1 Introduction

Bioclimatic classification methods (BCMs) are tools used to transform a set of climate and soil variables into an index-class that can be directly related to biome-level vegetation units (Tapiador et al. 2019). Although the BCMs have been developed for discovering regional differences in climate and potential vegetation (Mucina 2019), the access to projections of future climate change led necessarily to investigations using these tools for assessing the potential effects of climate change on vegetation. In the mid-1980s, Emanuel et al. (1985) were the first to apply one of the simplest BCMs, called Holdridge life zone (HLZ) system (Holdridge 1947, 1967), to the simulated temperature alterations under unchanged precipitation patterns, demonstrating that climate change can induce large shifts in vegetation distribution at high latitudes. A decade later, the hypothesis of warming-driven range shift of woody plants was already supported by long-term observations from both mountain (e.g., Grabherr et al. 1994; Kullman 2001) and lowland regions (e.g., Lescop-Sinclair and Payette 1995; Sturm et al. 2001).

By the early 2000s, a large body of evidence had accumulated that climate change is forcing the flora to react, at levels from individuals (e.g., shifts in phenological phases) to communities (e.g., changes in species composition) (see e.g., Walther et al. 2002). This decade has seen a surge in studies linking species distribution data to contemporary climate data in order to extrapolate this link to future climates (Araújo et al. 2019). In this algorithm, called species distribution modelling (see Elith and Leathwick 2009), besides topographic and soil variables, various bioclimatic variables derived from monthly climatologies (multi-year averages) for temperature and precipitation are usually used as environmental predictors. In the 2000s, this approach began to be used in large numbers in conservation biology for both teaching and practical purposes (Pearson 2007). This can be explained by the fact that it has become easier to access datasets related to species occurrence (e.g., Global Biodiversity Information Facility, GBIF: Yesson et al. 2007) and climatic conditions (e.g., WorldClim: Hijmans et al. 2005).

In the second half of the 2000s, a number of coordinated research projects (e.g., PRUDENCE: Christensen et al. 2007a; ENSEMBLES: van der Linden and Mitchell 2009) have undertaken to provide fine-scale climate data for impact studies, by means of dynamical downscaling of climate fields derived from global climate models (GCMs) (Giorgi 2019). Access to outputs of regional climate model (RCM) and GCM simulations derived from, among others, these projects laid the groundwork for those distribution modelling studies whose main goal was to assess possible responses of main forest-forming tree species to estimated climate change, in Hungary (e.g., Czúcz et al. 2011; Rasztovits et al. 2012; Móricz et al. 2013) and Serbia (e.g., Stojanović et al. 2013, 2014; Miletić et al. 2021). Regional studies of beech in Hungary (Czúcz et al. 2011; Móricz et al. 2013) and Serbia (Stojanović et al. 2013, 2014) using various species distribution models (SDMs) have reached similar conclusions: towards the end of the twenty-first century, a significant proportion of beech stands might be outside of the climatically suitable habitat for this species. Recently, Miletić et al. (2021) predicted a strong habitat loss of five tree species (beech, silver fir, Norway spruce, black pine, and Scots pine) for the far future, in Serbia. As a climatic predictor, the vast majority of these studies used also the Forestry Aridity Index (*FAI*, unitless: Führer et al. 2011), which has been basically developed to delineate different climate categories applied in forestry practice. The classification system in question, however, included the community type "forest-steppe" without a lower xeric limit, which was eventually introduced by Mátyás et al. (2018) in the context of assessing the effects of future climate change. This simple modification

fixed a major shortcoming of the classification system, considering that the transitional zone between forests and grasslands must also be taken into account when mapping the vegetation of Hungary (see Varga et al. 2000).

Given that most BCMs optimized at a global scale (e.g., Köppen climate classification scheme: Köppen 1936) are not able to capture the spatial variability of climate within a relatively small domain (Szelepcsényi et al. 2009), there are relatively few studies that have evaluated the projected changes in spatial patterns of bioclimatic classes, at a regional or national level in the Carpathian Region. The few examples found show, however, that by applying these classification methods to sufficiently high-resolution climate data, the marginal biome types of the region, such as the tundra both in the Tatra Mountains of the Carpathians (Skalák et al. 2018) and in the Prokletije Mountains of the Dinaric Alps (Mihailović et al. 2015), can also be identified. In addition to an assessment of recent conditions in Serbia, Mihailović et al. (2015) have applied one of the best-known BCM, the Köppen scheme, to bias-corrected climate outputs of RCM simulations forced by two different emission scenarios. It has been found that in the future, the coverage of climate categories reflecting warmer and drier conditions could significantly increase, while the type "tundra" may totally disappear from the country, regardless of the emission scenario used. To evaluate future changes in spatial distribution of Köppen climate classification zones within Central Europe, Skalák et al. (2018) have used bias-adjusted climate simulations generated using two different RCMs under one emission scenario. It has been concluded that although the type Cfb (temperate climate with no dry season and warm summer) will remain the dominant type in the region, it will shift toward higher altitudes and replace types reflecting cooler conditions, which will practically vanish by the end of the century. The results from the above-mentioned two studies therefore show that the temperature signal simulated by the RCMs is large enough to cause transitions between classes within the region in question, so there is no need to rule out the use of BCMs in this study configuration.

In addition, the Köppen scheme is still being used to this day in so-called paleo data–model comparisons (see Harrison 2013), in order to convert outputs from paleoclimate simulations into the distribution patterns of vegetation (e.g., Oh and Shin 2016; Wu et al. 2021). Comparative studies of this kind use (raw) climate simulation data and proxy archives, such as fossil pollen records (Brewer et al. 2013), in a common framework. The first global data–model comparisons, also carried out as part of a coordinated research project, the Cooperative Holocene Mapping Project (COHMAP: COHMAP Members 1988), were primarily aimed at evaluating the capabilities of climate models, and providing feedback on areas needing improvement (see e.g., Prentice et al. 1998; Webb et al. 1998). A data–model comparison using pollen data can be made basically in two ways, either by collating pollen-inferred climate with that simulated by climate models (e.g., Webb et al. 1998; Mauri et al. 2014), or by comparing biome distribution estimated using paleoclimate model outputs with plant communities reconstructed from pollen assemblages (e.g., Prentice et al. 1998; Tian et al. 2018). The key step in these comparisons is thus to make the climate model outputs and paleo data directly comparable to each other by some transformation procedures.

To translate climate model outputs into biome distribution patterns, comparisons focusing on the Late Quaternary climates carried out within the COHMAP (e.g., Prentice et al. 1998; Williams et al. 1998) have used the BIOME model (Prentice et al. 1992) which has been developed as a diagnostic tool for mapping the potential natural vegetation (PNV) and land cover features, basically in the context of the future climate change. In terms of the implementation logic, the BIOME model shows a similarity with the model developed by Box (1981a) for predictive

vegetation modelling, which builds on two important ecological insights: (i) vegetation responds to changes in climatic conditions at the species level rather than at the biome level, and (ii) species can be grouped based on their physiognomic characteristics. These findings are already important because they have provided the theoretical basis for defining the so-called plant functional type (PFT), i.e., the basic unit of calculation used in most global vegetation models. (According to Prentice and Cowling (2013), the PFT is a "group of plants assumed to have similar properties and responses to environmental changes".)

However, despite the structural similarity, there are two major differences between the two above-mentioned predictive vegetation models:

- In the Box model, each plant type is characterized by lower and upper limits of each of the selected bioclimatic indices, based on the "current" observed correlations between vegetation and climate. In contrast, when developing the BIOME model, threshold values were assigned to each PFT only in cases where a known or hypothesized physiological response had been identified.
- In the Box model, to describe moisture conditions, the ratio of the annual precipitation to the annual potential evapotranspiration, i.e., the moisture index (*MI*, dimensionless) is used. However, the value of *MI* does not directly reflect the drought stress inhibiting plant growth, thus to account for the plant-available moisture, the BIOME model uses the Priestley–Taylor coefficient (Priestley and Taylor 1972), which is computed as the ratio of actual to equilibrium evapotranspiration at an annual time scale. These water balance components are estimated using a process-based simulation model (for details, see Cramer and Prentice 1988; Prentice et al. 1993). For this reason, the use of the BIOME model, in contrast to the Box model and the BCMs, besides temperature and precipitation data, requires also a meteorological variable directly related to radiation, and optionally soil parameters. The initial version of the model uses monthly mean daily values of the relative sunshine duration for estimating the components of the net radiation.

Thus, the BIOME model represents an important step in the development from totally statistical models to more physiologically grounded models, the so-called dynamic global vegetation models (DGVMs). However, this topic is beyond the scope of the present dissertation. For an overview of this modelling approach, see Prentice and Cowling (2013).

To transform fossil pollen assemblages into biome types, comparisons focusing on the Late Quaternary climates carried out within the COHMAP (e.g., Prentice et al. 1998; Williams et al. 1998) have used a vegetation reconstruction approach developed by Prentice et al. (1996), the so-called biomization scheme. This reconstruction method, given that it was specifically developed to create a common language for data–model comparisons, builds on the PFT concept used in the BIOME model. The essence of the approach in question is to assign pollen types (taxa) to one or more PFTs (considering the climatic tolerances and requirements of taxa), and then describe a set of biomes based on their PFT compositions. In practice, each taxon in the pollen sample is taken into account based on its relative abundance value (i.e., the percentage of individuals for the given species within the community) in the calculation of biome scores, and the procedure ends with the selection of the biome type with the highest score. In terms of technical implementation, several attempts have been made over the last 25 years to improve the initial version of the method (e.g., introduction of intermediate PFT scores: Peyron et al. 1998; modification of the taxa/PFT composition of each biome type: Williams et al. 1998; use of arboreal taxa as climate indicators in the differentiation of non-arboreal biome types: Tarasov et al. 1998; inclusion of transitional vegetation types in the set of biomes: Sun et al. 2020). The biomization approach was inherently designed to reconstruct the PNV using pollen data (see Prentice et al. 1996), but over time on the

basis of this classification technique, an additional algorithm has also been developed to reconstruct anthropogenic land use changes (see pseudo-biomization: Woodbridge et al. 2014).

In consideration of the literature discussed above, this dissertation investigates the following research questions:

1. Can the impacts of recent climate change in the Carpathian Region be properly assessed using the HLZ system or not? How did the spatial and altitudinal distribution patterns of HLZ types alter in the Carpathian Region in the last century? (These questions are discussed in Chapter 2.)
2. Does a modified version of the HLZ system, which is based on theoretical considerations, have the ability to identify the potential distribution of forest-steppe ecotone (i.e., a boundary zone between closed forests and treeless steppes) in the Carpathian region or not? What is the degree of agreement between climate-derived vegetation maps generated by different versions of the HLZ system and an expert-based PNV map? (These questions are discussed in Chapter 2.)
3. What changes are expected in the distribution of HLZ types in the Carpathian Region in the future? Is there a significant trend in the projected shifts in the mean centres of HLZ types or not? How are altitudinal ranges of HLZ types likely to change in the future? What conclusions can we draw if the HLZ system is combined with an ensemble of bias-corrected regional climate model outputs? What is the uncertainty of the predicted changes considering the inter-model variability? (Chapter 3 is dedicated to answering these questions.)
4. Is the spatial distribution of biomes able to be properly simulated using only monthly climatologies of temperature and precipitation, and location data? Can monthly mean daily values of the relative sunshine duration required to run more sophisticated biome models be estimated with sufficient accuracy from commonly available meteorological variables or not? How does the quality of estimates change as a result of proposed modifications of the approach which are justified by its applicability in paleoenvironmental studies? (These issues are investigated in Chapter 4.)
5. Is a high-resolution biome map of the Greater Alpine Region (GAR) generated using only monthly temperature and precipitation data (and digital elevation models) consistent with a vegetation map generated by ecological experts using field surveys and other sources, or not? What conclusions can we draw from a comparison of climate- and pollen-inferred biome types of the GAR, in this highly heterogeneous and human-modified landscape? What is the effect of refining the evaluation methodology (e.g., considering near-misses, i.e., assignments to a biome type with similar PFT composition) on the comparison result? (Chapter 5 is devoted to these issues.)

2 Climate of the Carpathian Region in the twentieth century based on various versions of the Holdridge life zone system*

Manuscript published in the *Central European Journal of Geosciences*
Volume 6, Issue 3, 293–307 (2014)
DOI: 10.2478/s13533-012-0189-5

Authors:

Zoltán Szelepcsényi
Department of Geology and Palaeontology
University of Szeged, Hungary

Hajnalka Breuer
Department of Meteorology
Eötvös Loránd University, Hungary

Pál Sümegi
Department of Geology and Palaeontology
University of Szeged, Hungary

Abstract. The Holdridge life zone (HLZ) system has already been applied several times to analyse the effects of climate change on the vegetation. However, a harsh criticism of this model is that it cannot interpret the so-called ecotones (e.g., forest-steppe). Thus, in this study, both the core and transitional HLZ types are also separately determined within the model. Then, both a simplified version of the HLZ system and one of the variants of this widely used version are applied to the monthly climatological fields from the well-known CRU TS 1.2 climate database. HLZ maps are created for the Carpathian Region (43.5° N to 50.5° N, 15.5° E to 28° E), for five 20-year time periods in the twentieth century. The accuracy of the result maps is estimated by comparison to an expert-based vegetation map, by means of Cohen's Kappa statistic. Finally, temporal changes in the spatial and altitudinal distribution patterns of each HLZ type are investigated. The coverage of the boreal region was decreased by 59.5% during the last century, and in parallel, the warm temperate zone became two and a half times larger than it used to be. The mean centres of those HLZ types which were not related to mountains shifted northward during the investigated time period. In the case of the most abundant HLZ types, the mean distributional altitude increased. By modifying of the simplified model, the potential distribution of the forest-steppe ecotone can also be identified.

Keywords: Holdridge life zone system; transitional zone; forest-steppe; mean centre shift; Kappa statistic

* This chapter is the updated version of the final manuscript of the paper "The climate of Carpathian Region in the 20th century based on the original and modified Holdridge life zone system", accepted in 2014.

2.1 Introduction

Alexander von Humboldt (von Humboldt 1806; von Humboldt and Bonpland 1807) has recognized that widely separated regions have structurally and functionally similar vegetation if their climates are similar. Thus, the major vegetation groups and vegetation boundaries can be appropriately used to classify various climates. Those approaches which are based on the relationship between vegetation and climate can be referred to as bioclimatic classification methods. One of the best-known of these methods is the so-called Holdridge life zone (HLZ) system (Holdridge 1947, 1967).

In the course of developing his model, Holdridge (1947, 1967) supposed that structural and functional characteristics of the vegetation are basically determined by qualitative and quantitative features of its ecophysiological processes. Furthermore, he found that these characteristics can properly be separated from each other at the biome level, and because of this, the so-called life zone was chosen as the basic unit of his classification. Both the terms "life zone" and "biome" have very similar content. According to the definition described by Holdridge (1967), however, a Holdridge life zone (HLZ) type is only determined by the climatic conditions. By synthesizing his field experiences, Holdridge (1947, 1967) developed a very simple geometric model to formalize the relationship between his classification units (HLZ types) and the three most important bioclimatic indices (see below).

Holdridge (1947, 1967) attempted to develop a simple model that takes into account effects of both cold and heat stress on the vegetative growth and, furthermore, some basic laws of plant physiology, e.g., the law of the minimum (Liebig 1840) and the law of diminishing returns (Mitscherlich 1909). However, numerous ecological and climatological aspects are not considered by the HLZ system; for this reason, the model has been criticized several times (e.g., Lugo et al. 1999; Kappelle et al. 2003). The four most important criticisms are as follows: (a) the seasonal variations of the meteorological variables are not taken into account, (b) the transitional HLZ types which are substantively very similar to the so-called ecotones (i.e., the transitional areas between two biomes) are not determined, (c) the issue of succession (i.e., temporal changes in the species composition) is not included and (d) the effects of soil physical properties, soil salinity and the limiting factors of nutrient uptake on ecophysiological processes are ignored.

Although Holdridge (1967) also knew that the validity of the results provided by his model was weakened by its inability to identify the transitional zones (e.g., forest-steppe), he made no recommendations to solve this issue. Holdridge (1947, 1967) developed his model to map the vegetation distribution at the global scale; and as the use of transitional HLZ types would have greatly complicated the interpretation of the results, eventually he dispensed with their use. In our previous work (Szelepcsényi et al. 2009), however, it was concluded that in a regional analysis, it is advisable to use the transitional HLZ types. The exact definitions of these transitional HLZ types can be found in Fan et al. (2013). Here, however, two critical remarks about this work are added: (a) the consistency of the new vegetation classes identified by the model with the actual vegetation types had not been investigated and (b) their designations are too complicated. In this study, we attempt to address also these issues.

The HLZ system has been basically developed to identify spatial differences in climate (see Holdridge 1967). By recognizing the climate change, however, the application area of this model has been significantly altered. The so-called HLZ maps were first used by Emanuel et al. (1985) to assess the effects of possible climate change on vegetation. Even though the alteration in

precipitation was not considered, this study showed for the first time that climate change can induce drastic shifts in vegetation distribution at high latitudes.

Since then, the HLZ system has been applied several times to map the ecological impacts of the recent climate change at a regional scale, for example, in various regions of China (Yue et al. 2001, 2005a; Zheng et al. 2006; Zhang et al. 2011; Fan et al. 2012). In these studies, the spatial and altitudinal distribution and the mean centre of each HLZ type and their temporal changes have been primarily assessed, along with the alterations in the diversity and the patch connectivity of HLZ types. For example, Yue et al. (2001) have detected a decreasing trend in the diversity of HLZ types in China over the past decades which may be associated with the observed alteration of the environmental stability. In the Loess Plateau of China, Fan et al. (2012) found that the coverage of humid and perhumid HLZ types showed a significant decrease during the second half of the twentieth century, and in parallel, the extent of the HLZ types warm temperate desert scrub and warm temperate thorn steppe showed a considerable increase. In the Inner Mongolia of China, Zhang et al. (2011) observed that the mean centres of HLZ types shifted northeastward over the last half century, resulting a decrease (increase) in the coverage of grassland and forest (desert).

In spite of the criticisms summarized above, it seems to us that the HLZ system can be applied within certain limits to estimate the effects of climate change on vegetation. For this reason, the aim of this study is twofold: (a) to identify the potential distribution of forest-steppe ecotone, through the use of transitional HLZ types and (b) to map the impacts of climate change in the Carpathian Region for the last century, by using the two selected variants of the HLZ system. The distribution patterns of HLZ types are characterized by the relative coverage, the mean centre and the mean distributional altitude. In this study, temporal changes in these features are analysed in the context of climate change. Because the HLZ system has been developed for the tropical region (see Holdridge 1967), it is necessary to evaluate the accuracy of HLZ maps for the mid-latitudes. For this reason, HLZ maps created here are compared to an expert-based vegetation map. During this validation procedure, the degree of agreement between the maps is measured by using the Kappa statistic developed by Cohen (1960).

2.2 Data

2.2.1 Climatic data

The HLZ system requires daily or monthly time series of temperature and precipitation. In this study, the monthly climatological fields are derived from the well-known CRU TS 1.2 climate database (Mitchell et al. 2004) provided by the Climate Research Unit (CRU) of the University of East Anglia. This dataset covers all Europe (34° N to 72° N, 11° W to 32° E) for the period 1901–2000. The dataset was constructed by using an “anomaly” approach (New et al. 1999, 2000). In this procedure, the so-called station anomalies were interpolated to a predefined grid, considering the basic geographical variables (latitude, longitude and altitude) as parameters; and then these grids were combined with gridded reference climatologies to obtain the final dataset. The density of the climate station network was extremely low in certain periods of the last century; furthermore, many of stations have only recently been added to the network. Consequently, some biases and errors in the gridded data are possibly generated by the interpolation procedure, especially in areas with complex topography and low station density. However, one of the advantages of this interpolation method is that long and uninterrupted time series of the climate variables are available for all Europe. The gridded data were created with a spatial resolution of

10 arc-min (~20 km in mid-latitudes). The dataset also includes a digital elevation model, which is used to calculate the mean distributional altitude of each HLZ type.

In this study, the target area is the Carpathian Region (43.5° N to 50.5° N, 15.5° E to 28° E). The average values of monthly mean temperature and monthly total precipitation are computed for five 20-year time periods in the twentieth century (P1: 1901–1920, P2: 1921–1940, P3: 1941–1960, P4: 1961–1980, P5: 1981–2000). The two selected versions of the HLZ system are applied to these mean fields.

2.2.2 An expert-based vegetation map

In some ways, the HLZ system is a very simple model of the potential vegetation distribution (see Yates et al. 2000). Thus, the accuracy of a HLZ map can be estimated by comparison to another vegetation map, in the framework of a validation procedure. During the selection of the vegetation map used as a reference, we have to consider over what space and time windows the model is applied. Indeed, these parameters indirectly describe the degree of the anthropogenic pressure, on the basis of which, in turn, the three basic types of the vegetation state can be distinguished in accordance with the classification determined by Bartha (2005) (Fig. 2.1): actual vegetation (AV), reconstructed natural vegetation (RNV) and potential natural vegetation (PNV).

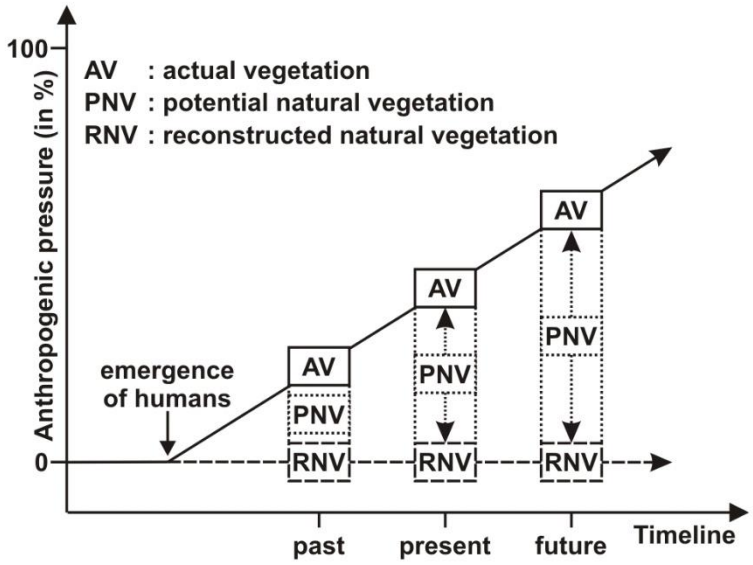

Fig. 2.1 Vegetation states as a function of the anthropogenic pressure (by assuming a linear degradation in time). Adapted from Bartha (2005)

According to the commonly used definition described by Tüxen (1956), the term "PNV" expresses a hypothetical natural state of vegetation that shows the biotic potential of nature under the given climatic conditions, in the absence of human influence and disturbance. It is easy to see that when the model described by Holdridge (1967) is applied to an observational climate database, a vegetation state which is similar to the PNV can be diagnosed. This is also supported by the fact that an interpretation of the succession is completely absent from the HLZ system, similarly to the term "PNV" (see Bartha 2005). Therefore, by applying the HLZ system to such climate databases, only the climatic component of the site potential can be determined.

Considering all of these, in the validation procedure, an expert-based PNV map constructed by Bohn et al. (2003) is used as a reference map. This map displays the potential distribution of the dominant natural plant communities consistent with the current climatic and edaphic conditions (Bohn et al. 2003). In this case, the attribute "current" does not express a given 30-year long

reference period, but a much longer but undetermined period of time, as the recent climatic change was not taken into account during the creation of the map (see Bohn et al. 2003). The most important sources for the national contribution of Hungary to this PNV map were the natural vegetation maps created by Zólyomi (1967, 1981). These maps show a reconstructed vegetation state which could have existed prior to the age of deforestation, agricultural mechanization, large river regulation and drainage. Therefore, considering the content of the reference map and the features of the applied climate database, the HLZ maps for the period 1901–1920 (the maps P1) are selected for the validation procedure.

The validation procedure requires that the maps that are compared have the same spatial resolution and distinguish the same classes. For this reason, the preselected expert-based PNV map stored in a geospatial vector data format is converted into raster format. As a first step, the data are projected to the commonly used WGS-84 geodetic coordinate system, and then the individual polygons are reclassified according to the predefined reclassification rules for the formations (see Section 2.4.1), by using the ESRI ArcGIS 9.3.1 software. In the next step, by means of the GDAL software (Mitchell and GDAL Developers 2014), the European map is constricted to the above-mentioned target domain. Finally, this vector map is converted into the grid of the applied climate database, by using the function "rasterize" in the R package "raster" (Hijmans and van Etten 2014). In this conversion procedure, the function "modal" is applied.

In the target area, a total of nine zonal and five azonal formation classes can be identified according to the expert-based vegetation map (see Table 2.1). Depending on the reclassification rules applied, azonal vegetation types that are determined by non-macroclimatic conditions cover 15.0–15.3% of the target domain. For this reason, these areas are eliminated from the validation procedure along with additional seven grid cells that are labelled as "other".

Table 2.1 Formation classes observed in the target area according to the expert-based vegetation map of Bohn et al. (2003) (B–N: zonal vegetation (mainly determined by macroclimatic conditions); P–U: azonal vegetation (mainly determined by edaphic conditions))

Type	Code	Formation class
Zonal	B	Arctic tundras and alpine vegetation
	C	Subarctic, boreal and nemoral-montane open forests, as well as subalpine and oro-Mediterranean vegetation
	D	Mesophytic and hygromesophytic coniferous and mixed broadleaved-coniferous forests
	F	Mesophytic deciduous broadleaved and mixed coniferous-broadleaved forests
	G	Thermophilous mixed deciduous broadleaved forests
	J	Mediterranean sclerophyllous forests and scrub
	K	Xerophytic coniferous forests and scrub
	L	Forest-steppe (meadow steppes or dry grasslands alternating with deciduous broadleaved forests or xerophytic scrub)
	M	Steppes
	N	Oroxerophytic vegetation (thorn cushion communities, tommilares, mountain steppes, partly scrub)
Azonal	P	Coastal dune and (inland) halophytic vegetation
	R	Tall reed and tall sedge swamps, aquatic vegetation
	S	Mires
	T	Fen and swamp forests
	U	Vegetation of floodplains, estuaries and freshwater polders

2.3 Methods

2.3.1 The simplified version of the Holdridge life zone (HLZ) system

Holdridge (1967) has classified the various climates according to the types of potential vegetation. Namely, in order to determine requirements for the adequate functioning of ecophysiological processes of each plant type, Holdridge (1947, 1967) has developed three bioclimatic indices for his classification system: mean annual biotemperature (*ABT*, in °C), total annual precipitation (*APP*, in mm), and potential evapotranspiration ratio (*PER*, unitless).

Holdridge (1967) perceived that the vegetative growth and thus the net primary productivity are possible only in a certain temperature range. This remark was used in the definition of the mean annual biotemperature (*ABT*). Initially, negative effects related only to the frost damage were recognized by Holdridge (1947); and because of this, values below 0 °C had to be substituted with 0 °C in the calculation of the *ABT*. Later, he discovered that the heat stress inhibits the growth of plants similarly to the cold stress. For this reason, it was proposed by Holdridge (1967) to apply the above-mentioned substitution rule also for the values above 30 °C. Holdridge (1947) firstly suggested using values of the monthly mean temperature to compute the value of *ABT*; but later, it was already preferred to use daily temperature data (see Holdridge 1967). In this study, by using monthly data, the value of *ABT* is calculated as follows:

$$ABT = \frac{1}{12}\sum_{i=1}^{12} T_{bio,i} \ , \tag{2.1}$$

where $T_{bio,i}$ is the monthly mean biotemperature for the *i*-th month (in °C), which can be determined by the following formula:

$$T_{bio,i} = \begin{cases} 0, & \text{if } T_i < 0 \\ T_i, & \text{if } 0 \le T_i \le 30 \\ 0, & \text{if } T_i > 30 \end{cases}, \tag{2.2}$$

where T_i is the monthly mean temperature for the *i*-th month (in °C).

The potential evapotranspiration ratio (*PER*) expresses at an annual timescale what is the ratio of the maximum amount of water that could be evaporated and transpired by sufficiently wet soil and plant surfaces under given atmospheric conditions to the quantity of precipitation (i.e., the amount of water made available for potential use in evaporation and transpiration) (see Holdridge 1967). Accordingly, the value of *PER* is computed as the ratio of the annual potential evapotranspiration (*APE*, in mm) to the annual precipitation (*APP*, in mm). Although there are several estimation techniques for potential evapotranspiration (see Xu and Singh 2002), in this study, in accordance with the relevant literature (e.g., Yue et al. 2001; Zhang et al. 2011), the value of *APE* is calculated by using the following simple formula (Holdridge 1959):

$$APE = 58.93 \cdot ABT, \tag{2.3}$$

where *ABT* is the mean annual biotemperature (in °C).

The HLZ system is one of the best methods which uses only monthly temperature and precipitation data to describe terrestrial ecosystems. Each HLZ type has an exact definition for each above-mentioned bioclimatic index. Holdridge (1947, 1967) developed a very simple geometric model to formalize relationships between HLZ types and bioclimatic indices. This model, which is commonly labelled as the Holdridge life zone (HLZ) chart, is a triangular coordinate system (Fig. 2.2) in which the bioclimatic indices are depicted on logarithmic axes in accordance with the law of diminishing returns (Mitscherlich 1909). The threshold of ~17 °C ($2^{(\log_2 12+0.5)}$ °C ≈ 16.97 °C) for the *ABT* is determined as a frost or critical temperature line which represents the dividing line between the warm temperate and subtropical regions within this system (Holdridge 1967). On the warmer side of this line, the plants are commonly sensitive to the lower temperatures (see Holdridge 1967).

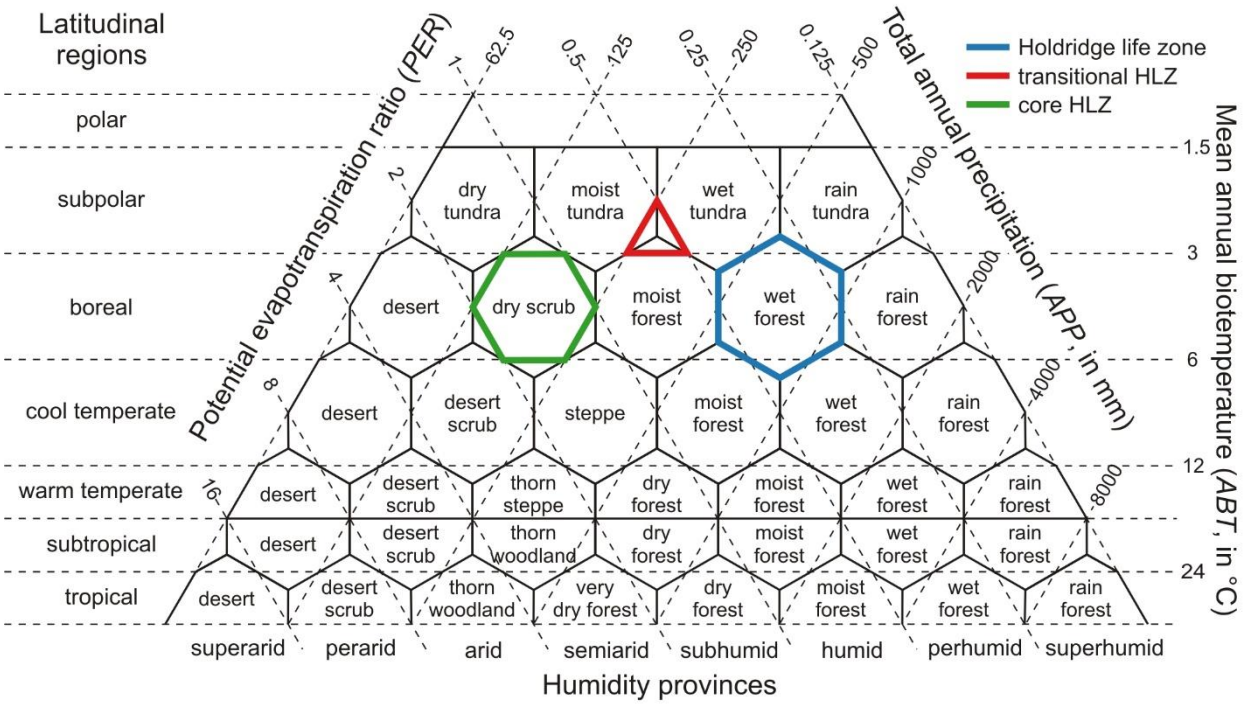

Fig. 2.2 A simplified version of the Holdridge life zone (HLZ) chart developed by Holdridge (1967). Consult text for further explanation

The plotting of thresholds of the above-mentioned bioclimatic indices in the HLZ chart leads to emerge a set of hexagons and triangles. In Fig. 2.2, these hexagons denoted by dashed lines indicate the so-called core HLZ types, while the so-called transitional HLZ types are circumscribed by equilateral triangles marked by dashed lines in the HLZ chart. Although Holdridge (1967) has outlined the theoretical background of transitional HLZ types, considering the difficulties related to the interpreting of the results obtained by his model, he eventually dispensed with their use. For this reason, each equilateral triangle was divided into three equal parts which were formed by connecting the three vertices of the triangle to the centroid; in the next step, these smaller triangles were attached to the adjacent hexagons declaring the core HLZ types. As a result, in the HLZ chart, larger hexagons are obtained, which are denoted by solid lines in Fig. 2.2. Hereinafter, these larger hexagons are considered to be the basic units of the HLZ system. In this system, a location with a value of *ABT* below 1.5 °C but with sufficient moisture and rainfall is defined as a separate class named “polar desert”.

The HLZ system has been developed for the tropical region (see Holdridge 1967). In the model, besides the latitudinal regions, altitudinal belts have also been assigned on the basis of the values of *ABT*. The reason for this is that Holdridge (1967) found it necessary to determine which is the most important limiting factor of the *ABT* (and thus the vegetative growth): the distance from the Equator or the elevation. The model, which uses also the altitudinal belts, is not appropriate to classify vegetation at the global scale, due to the high number of classes used. For this reason, most impact studies (e.g., Yue et al. 2001, 2005a; Zheng et al. 2006; Zhang et al. 2011; Fan et al. 2012), which apply the HLZ system to map the potential vegetation, ignore the altitudinal belts. This simplified version of the HLZ system distinguishes 38 vegetation classes, which are listed in Table 2.2. For simplicity, this model is hereinafter referred to as the “original” model.

Table 2.2 Vegetation classes distinguished by the simplified version of the Holdridge life zone (HLZ) system, used in this study, and their abbreviations

Code	Name
PD	Polar desert
SpDt	Subpolar dry tundra
SpMt	Subpolar moist tundra
SpWt	Subpolar wet tundra
SpRt	Subpolar rain tundra
BD	Boreal desert
BDs	Boreal dry scrub
BMf	Boreal moist forest
BWf	Boreal wet forest
BRf	Boreal rain forest
CtD	Cool temperate desert
CtDs	Cool temperate desert scrub
CtS	Cool temperate steppe
CtMf	Cool temperate moist forest
CtWf	Cool temperate wet forest
CtRf	Cool temperate rain forest
WtD	Warm temperate desert
WtDs	Warm temperate desert scrub
WtTs	Warm temperate thorn steppe

Code	Name
WtDf	Warm temperate dry forest
WtMf	Warm temperate moist forest
WtWf	Warm temperate wet forest
WtRf	Warm temperate rain forest
StD	Subtropical desert
StDs	Subtropical desert scrub
StTw	Subtropical thorn woodland
StDf	Subtropical dry forest
StMf	Subtropical moist forest
StWf	Subtropical wet forest
StRf	Subtropical rain forest
TD	Tropical desert
TDs	Tropical desert scrub
TTw	Tropical thorn woodland
TVdf	Tropical very dry forest
TDf	Tropical dry forest
TMf	Tropical moist forest
TWf	Tropical wet forest
TRf	Tropical rain forest

2.3.2 One of the modified variants of the simplified HLZ system

One of the most serious criticisms of the HLZ system is that the vegetation type identified by the model does not always coincide with the vegetation type observed in actual landscapes (e.g., sampling points from grasslands are often incorrectly assigned by the model to a closed vegetation type). One of the reasons for this is probably that transitional HLZ types have not been determined as separate vegetation units within the model. The HLZ system has been optimized at the global scale. If the core and transitional HLZ types had also been introduced into the model, the HLZ system would have been able to distinguish 89 vegetation classes (38 core HLZ types and 51 transitional HLZ types). However, the plotting of this large number of classes would have made it impossible to visualize the relevant vegetation types.

In this study, a regional analysis is performed, so it is considered appropriate to use core and transitional HLZ types (see Szelepcsényi et al. 2009). These new vegetation classes are determined by taking into account thresholds for the latitudinal regions (Table 2.3) and for the humidity provinces (Table 2.4).

Table 2.3 Latitudinal regions according to Holdridge (1967) (*ABT*: mean annual biotemperature)

Latitudinal regions	*ABT* (in °C)
polar	0–1.5
subpolar	1.5–3
boreal	3–6
cool temperate	6–12
warm temperate	12–17
subtropical	17–24
tropical	24–30

Table 2.4 Humidity provinces according to Holdridge (1967) (*PER*: potential evapotranspiration ratio)

Humidity provinces	*PER* (unitless)
superhumid	0.125–0.25
perhumid	0.25–0.5
humid	0.5–1
subhumid	1–2
semiarid	2–4
arid	4–8
perarid	8–16
superarid	16–32

In contrast to the original model, here, a given transitional HLZ type is not apportioned among the adjacent core HLZ types, but is defined as a separate unit. Each of these new vegetation units is labelled as follows: (i) to form the first section of the label, both the latitudinal belt and the humidity range are assigned, and then (ii) to obtain the final label, these terms are added to a combination of the two adjacent core HLZ types derived from the same latitudinal region. The list of these new vegetation classes is shown in the legend of Fig. 2.3. Those transitional HLZ types which are contiguous with only one core HLZ type are not defined in the system, therefore, only 43 transitional HLZ types are determined. Each transitional HLZ type which is simultaneously adjacent to open and closed vegetation types is labelled as forest-steppe. The forest-steppe ecotone is a transitional vegetation belt between closed forests and treeless steppes, where closed forest patches alternate with dry grasslands, forming a mosaic-like vegetation pattern (Varga et al. 2000). Actually, the main reason for defining the transitional HLZ types is to identify the position of this ecotone and to assess temporal changes in its spatial characteristics.

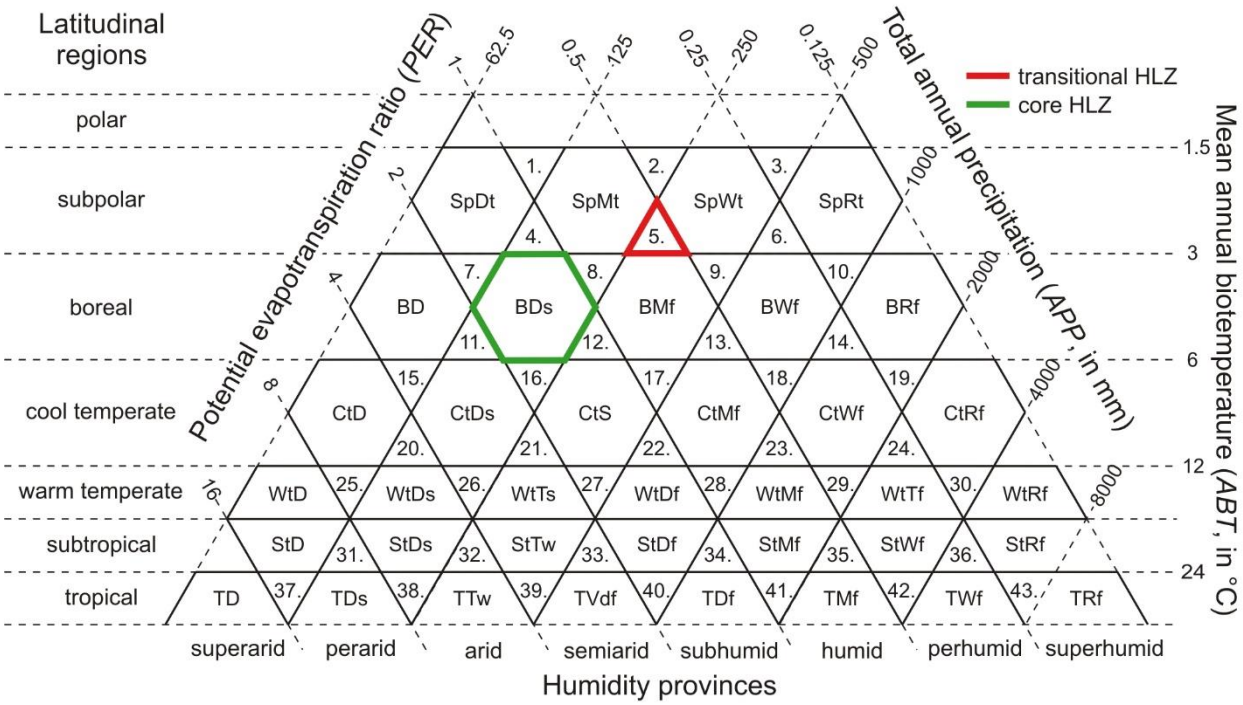

1. subpolar humid dry-moist tundra
2. subpolar perhumid moist-wet tundra
3. subpolar perhumid wet-rain tundra
4. subpolar subhumid dry-moist tundra
5. subpolar humid moist-wet tundra
6. subpolar perhumid wet-rain tundra
7. boreal subhumid desert – dry scrub
8. boreal humid dry scrub – moist forest
9. boreal perhumid moist-wet forest
10. boreal superhumid wet-rain forest
11. boreal semiarid desert – dry scrub
12. boreal subhumid forest-steppe
13. boreal humid moist-wet forest
14. boreal perhumid wet-rain forest
15. cool temperate semiarid desert – desert scrub
16. cool temperate subhumid desert scrub – steppe
17. cool temperate humid forest-steppe
18. cool temperate perhumid moist-wet forest
19. cool temperate superhumid wet-rain forest
20. cool temperate arid desert – desert scrub
21. cool temperate semiarid desert scrub – steppe
22. cool temperate subhumid forest-steppe
23. cool temeprate humid moist-wet forest
24. cool temperate perhumid wet-rain forest
25. warm temperate arid desert – desert scrub
26. warm temperate semiarid desert scrub – thorn steppe
27. warm temperate subhumid forest-steppe
28. warm temperate humid dry-moist forest
29. warm temperate perhumid moist-wet forest
30. warm temperate superhumid wet-rain forest
31. subtropical perarid desert – desert scrub
32. subtropical arid desert scrub – thorn woodland
33. subtropical semiarid thorn woodland – dry forest
34. subtropical subhumid dry-moist forest
35. subtropical humid moist-wet forest
36. subtropical perhumid wet-rain forest
37. tropical perarid desert – desert scrub
38. tropical arid desert scrub – thorn woodland
39. tropical semiarid thorn woodland – very dry forest
40. tropical subhumid very dry – dry forest
41. tropical humid dry-moist forest
42. tropical perhumid moist-wet forest
43. tropical superhumid wet-rain forest

Fig. 2.3 The modified HLZ chart, namely a nomogram for a variant of the simplified HLZ system which is suitable for identifying the so-called core and transitional HLZ types. Core (transitional) HLZ types are marked by *combinations of uppercase and lowercase letters* (*Arabic numerals*). Notations for core HLZ types that match class labels used in the simplified HLZ system, referred to as the original model within the text, are listed in Table 2.2

Bioclimatic constraints for core and transitional HLZ types which are newly introduced into the simplified version of the HLZ system are explained in Fig. 2.3. For example, limits for the core HLZ type "boreal dry scrub" are as follows: (a) 3 °C < *ABT* < 6 °C, (b) 125 mm < *APP* < 250 mm, and (c) 1 < *PER* < 2. Furthermore, as indicated by Fig. 2.3, the type of potential vegetation is identified as the transitional HLZ type "subpolar subhumid moist-wet tundra" if the following three conditions are fulfilled at the same time: *ABT* ≤ 3 °C, (b) *APP* ≥ 250 mm, and (c) *PER* ≥ 0.5. For simplicity, the classification model built by these rules is hereinafter referred to as the "modified" model. In the following sections, except in the case of Section 2.4.1, for vegetation

classes related to the modified model, abbreviations are not used, and in every case it is indicated whether the given class represents a core or a transitional HLZ type.

2.3.3 Kappa statistic

During our investigations, in the first step, the validation of the different classification methods is performed for the Carpathian Region. For this purpose, our result maps are compared to an expert-based vegetation map, through the use of the Kappa statistic developed by Cohen (1960).

The Kappa statistic (κ) is calculated according to the following formula:

$$\kappa = \frac{p_o - p_e}{1 - p_e}, \tag{2.4}$$

where p_o is the proportion of agreement and p_e is the overall proportion of chance-expected agreement. In order to determine variables of the formula, it is necessary to define a so-called contingency table. In cell (x, y) of this table, it has to be displayed what is the probability that the category x on map A agrees with the category y on map B. A value in the main diagonal shows the probability that a given point on map A, which is classified into the respective category, falls into the same category on map B. The value of p_o is obtained by adding the individual values in the main diagonal. By summing the values of row x (column y), the probability that category x (category y) can be found on map A (map B) can be determined. The value of p_e is computed by summing the products of row and column sums of the same category.

The value of κ can vary between 0 and 1, with 0 representing totally different patterns and 1 indicating complete agreement. Threshold values used here for separating the different degrees of agreement for the Kappa statistic follow those determined by Monserud and Leemans (1992) (Table 2.5). We provide only a short overview of the Kappa statistic because Monserud and Leemans (1992) have already described the mathematical background of the model in detail.

Table 2.5 The relationship between the Kappa statistic (κ) and the degree of agreement according to Monserud and Leemans (1992)

Degree of agreement	Kappa statistic (κ)
no	0.00–0.05
very poor	0.05–0.20
poor	0.20–0.40
fair	0.40–0.55
good	0.55–0.70
very good	0.70–0.85
excellent	0.85–0.99
perfect	0.99–1.00

2.3.4 Spatial characteristics of HLZ types

During our investigations, the distribution patterns of HLZ types are characterized by the relative extent, the mean centre and the mean distributional altitude. As Yue et al. (2006) and Zhang et al. (2011) have shown, the so-called mean centre is suitable for diagnosing changes in the spatial distribution of HLZ types. The calculation of the mean centre of each HLZ type is based on a simple arithmetic mean of longitude and latitude of grid cells classified in the respective HLZ type. To calculate the mean distributional altitude (MDA), the same methodology is applied, but here to the values of altitude.

One of the objectives of this study is to compute the distance and direction of shift of the mean centre from P1 to P5 for each HLZ type. The distance of this shift is calculated as a great circle distance following Fenna (2007), while its direction is computed according to Yue et al. (2006).

2.4 Results

2.4.1 Validation of classification methods

According to Berényi (1943), the performance of a given bioclimatic classification method is determined by its ability to reflect the correlations between vegetation and climate. Thus, as a first step, the validation of the two above-presented models is performed for the Carpathian Region. The maps P1 are compared to an expert-based vegetation map, by using the Kappa statistic introduced by Cohen (1960).

As indicated above (see Section 2.2.2), the validation procedure requires that the compared maps distinguish the same classes. For this reason, the various maps have to be translated into the same vegetation classes, by means of a set of rules (see Table 2.6). In the validation experiment for the original model, we distinguish two classes: forest and steppe, while in the case of the modified model, the vegetation type "forest-steppe" can be determined as a separate class because of the use of the transitional HLZ types. In the case of the original model, the formation "forest-steppe" is firstly assigned to the class "forest" (α.), while in the second case to the class "steppe" (β.). Further assignments of both formations and HLZ types to the main vegetation types clearly depend on their openness (see Table 2.6).

Table 2.6 Reclassification rules for both formation classes and Holdridge life zone (HLZ) types observed in the target area (*uppercase letter* (formation): notations can be found in Table 2.1; *combination of uppercase and lowercase letters* (α. and β. HLZ type in the original model, γ. core HLZ type in the modified model): notations can be found in Table 2.2; *Arabic numeral* (transitional HLZ type in the modified model): notations can be found in Fig. 2.3)

Class	**Formations**			**HLZ types (original model) (α., β.)**	**HLZ types (modified model) (γ.)**
Forest	C, D, F, G, J, K			BRf, BWf, CtWf, CtMf, WtMf, WtDf	BRf, BWf, CtWf, CtMf, WtMf, WtDf
	α. L	β. –	γ. –		10., 14., 18., 23., 28.
Steppe	M, N			CtS	CtS
	α. –	β. L	γ. –		
Forest-steppe	α. –	β. –	γ. L	–	17., 22.

Our results are compared with findings of other similar investigations (Lugo et al. 1999; Zheng et al. 2006). The most important features of the validation experiments that were performed by Lugo et al. (1999) and Zheng et al. (2006) are summarized in Table 2.7, complemented by our own results.

Table 2.7 Main features of the various validation experiments for the Holdridge life zone (HLZ) system

	Lugo et al. (1999)		**Zheng et al. (2006)**	**This study**		
				original		**modified**
				α.	**β.**	**γ.**
Kappa statistic (κ)	0.39	0.43	0.43	0.28	0.46	0.39
Degree of agreement	poor	fair	fair	poor	fair	poor
Location	conterminous United States of America		Xinjiang Uygur Autonomous Region	Carpathian Region		
Area	8 080 464 km^2		1 660 001 km^2	716 390 km^2		
Spatial resolution	2.5 arc-min		0.5 arc-min	10 arc-min		
Time window	1961–1990		1971–1980	1901–1920		
Reference map	Bailey (1976)	Küchler (1964)	Hou et al. (1982)	Bohn et al. (2003)		
Vegetation definition	potential natural	potential natural	actual	(potential/reconstructed) natural		
Number of classes used	4		12	2		3

In the Xinjiang Uygur Autonomous Region, Zheng et al. (2006) validated the HLZ system for the period 1971–1981, by using the actual vegetation (AV) map of the People's Republic of China (Hou et al. 1982) as a reference map (see Table 2.7). For the validation procedure, the AV map was reclassified; each AV type was assigned to one of the HLZ types observed in the target domain, and so 12 classes were used. This was a very strict condition for the validations, but this effect was offset by a high spatial resolution used (0.5 arc-min). Yue et al. (2005b) found that both the spatial extent and the spatial resolution of the applied database have an important role in the various vegetation studies (e.g., ecological diversity, vegetation dynamics). This effect is also clearly outlined in Table 2.7. Eventually, Zheng et al. (2006) found "fair" (κ = 0.43) agreement between their maps.

In the conterminous USA, Lugo et al. (1999) performed the validation of the HLZ system for the period 1961–1990 at a spatial resolution of 2.5 arc-min (see Table 2.7). Vegetation maps of Bailey (1976) and Küchler (1964) were used for the validation procedure. Four classes were used for the reclassification of their maps: forest, grassland, scrubland and non-vegetated. In spite of the relatively high spatial resolution and the small number of classes used, their comparisons indicated only "poor" and "fair" agreements between their maps.

In this study, the various maps are prepared with a spatial resolution of 10 arc-min, which is relatively poor considering the above-mentioned studies, so it is justifiable to use only a few classes for the reclassification of our maps. Another problem is that the majority of the azonal vegetation types can be observed in the central part of the Carpathian Region in which the majority of the transitional HLZ types is also found. As it is totally unambiguous that the HLZ system is more sensitive to the transitional HLZ types, this effect also greatly hampers the model validation.

For the original model, we can register "poor" (α. κ = 0.28) and "fair" (β. κ = 0.46) agreement between our maps (Table 2.7). In the case of the modified model, even by introducing a further class, the degree of agreement is still only "poor" (γ. κ = 0.39). Because of the more strict conditions, the fact that the value of the Kappa statistic for the modified model is more than the mean of the two former values can be understood as an advancement. Considering all this, the findings of the reference studies (Lugo et al. 1999; Zheng et al. 2006) and our results are very similar. Thus, the selected models can be correctly applied also in the Carpathian Region.

2.4.2 Spatial distribution pattern of HLZ types

2.4.2.1 The original version of the HLZ system

The recent climate change can be appropriately detected also by assessing the temporal changes in the spatial distribution pattern of HLZ types. For example, Table 2.8 lists those HLZ types which can be registered in the Carpathian Region during the last century, along with their relative coverage values for the previously defined 20-year time periods. In addition, the horizontal distribution pattern of HLZ types for the periods 1901–1920 (P1) and 1981–2000 (P5) is shown in Fig. 2.4.

Table 2.8 Relative coverage (in percentages) of each Holdridge life zone (HLZ) type in the target area for the periods 1901–1920 (P1), 1921–1940 (P2), 1941–1960 (P3), 1961–1980 (P4) and 1980–2000 (P5)

HLZ type	P1	P2	P3	P4	P5
Boreal wet forest (BWf)	5.07	3.32	3.10	3.44	2.64
Boreal rain forest (BRf)	0.43	0.18	0.06	0.18	0.09
Cool temperate steppe (CtS)	9.58	8.44	10.96	5.83	13.02
Cool temperate moist forest (CtMf)	69.91	70.00	67.49	70.86	61.56
Cool temperate wet forest (CtWf)	8.01	8.17	5.34	8.93	5.86
Warm temperate dry forest (WtDf)	6.23	9.00	12.34	9.98	15.60
Warm temperate moist forest (WtMf)	0.77	0.89	0.71	0.77	1.23

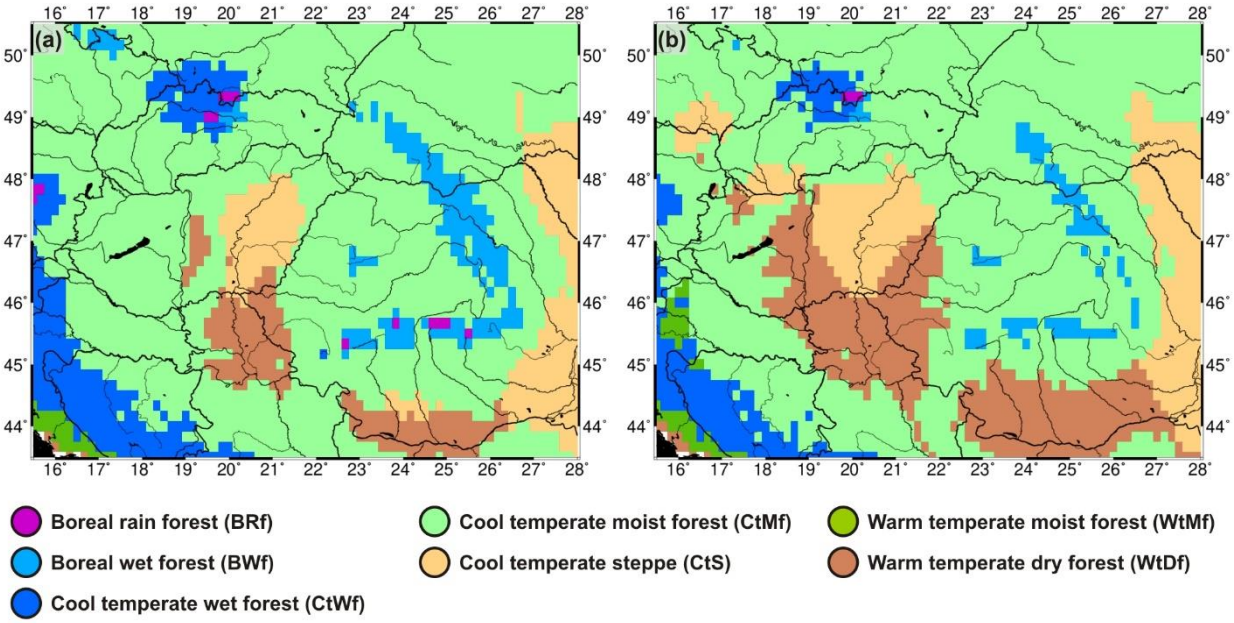

Fig. 2.4 Spatial distribution of Holdridge life zone (HLZ) types in the Carpathian Region for the periods (**a**) 1901–1920 and (**b**) 1981–2000. The maps are created by applying the original version of the HLZ system driven by climate data provided by the CRU TS 1.2 database

In P1, the dominant HLZ type was the cool temperate moist forest (CtMf) in the Carpathian Region, covering about 70% of the total area (Table 2.8). At the beginning of the century, the second most abundant HLZ type was the cool temperate steppe (CtS), with an areal proportion of 9.6%. About one third of this vegetation class covered the centre of the Carpathian Basin (Fig. 2.4) where the annual precipitation sum was the lowest, considering the whole region. The rest of this vegetation class in P1 can be found to the east and south of the Carpathians. The third in the

coverage ranking was the cool temperate wet forest (CtWf), covering approximately 8% of the target area. This class can be found at higher altitudes at the beginning of the last century. In P1, the dominant HLZ type of the Wallachia, and of the north of Serbia was the warm temperate dry forest (WtDf). The relative extent of this HLZ type was little more than 6%. In the Eastern and Southern Carpathians, the climatic conditions in P1 were suitable for the boreal wet forest (BWf), by causing a coverage of about 5% for this class. At the same time, the boreal rain forest (BRf) covered the highest peaks of the Carpathians, which were the coldest and rainiest areas of the whole region.

Comparing the maps P1 and P5, it can be clearly seen that by the end of the century, climatic conditions in the Carpathian Region have changed substantially: the spatial distribution pattern of HLZ types was remarkably altered. However, it is also important to investigate what kinds of changes have taken place from P1 to P5. However, in the case of the original model, the changes in heat and moisture properties cannot be properly addressed because each HLZ type covers partly or fully three ranges, for both types of properties.

However, we feel it is also necessary to investigate what kinds of HLZ transformations have taken place from P1 to P5. For this reason, we define a so-called transformation matrix (not shown) in which the proportions of areas affected by HLZ transformations are indicated. HLZ transformation can be observed over approximately one fifth of the target domain, taking into account the last century. The two greatest changes were attributed to the transformations from CtMf to WtDf and from CtMf to CtS, which affected 8.2 and 4.5% of the total area, respectively (see Fig. 2.4).

2.4.2.2 The modified version of the HLZ system

By modifying the HLZ system, it is possible to circumscribe the position of the forest-steppe, which is one of the most important ecotones in the Carpathian Region. Through the use of transitional HLZ types, we can typify the climate of the target domain in more detail. For the periods 1901–1920 (P1) and 1980–2000 (P5), the spatial distribution pattern of the vegetation classes newly introduced into the HLZ system is presented by Fig. 2.5, while for the five preselected 20-year time periods, values of the relative coverage of each class are shown in Table 2.9. During the last century, seven core and seven transitional HLZ types can be identified in the target area. The results show that by the end of the century, one core and two transitional HLZ types totally disappeared from the Carpathian Region (see Table 2.9).

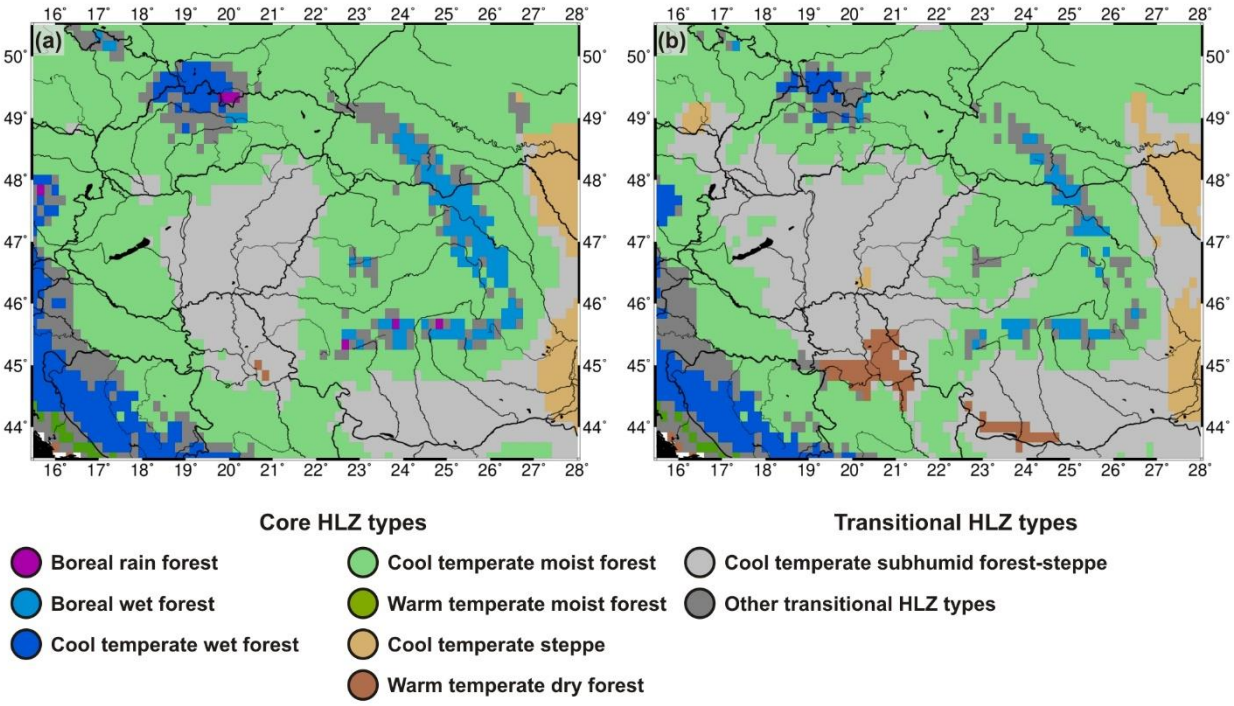

Fig. 2.5 Spatial distribution of core and transitional Holdridge life zone (HLZ) types in the Carpathian Region for the periods (**a**) 1901–1920 and (**b**) 1981–2000. The maps are created by applying the modified version of the HLZ system driven by climate data provided by the CRU TS 1.2 database. With the exception of the type "cool temperate subhumid forest-steppe", transitional HLZ types are plotted by an aggregated class

Table 2.9 Relative coverage (in percentages) of each core/transitional Holdridge life zone (HLZ) type in the target area for the periods 1901–1920 (P1), 1921–1940 (P2), 1941–1960 (P3), 1961–1980 (P4) and 1980–2000 (P5). The *symbol* – refers to those cases where the given class in the given time period cannot be observed in the target domain

	HLZ type	**P1**	**P2**	**P3**	**P4**	**P5**
Core	Boreal wet forest	3.25	1.90	1.57	1.60	1.47
	Boreal rain forest	0.21	0.09	–	0.15	–
	Cool temperate steppe	3.87	5.83	6.85	0.89	4.33
	Cool temperate moist forest	58.80	58.83	56.13	58.27	50.63
	Cool temperate wet forest	5.53	5.56	3.53	6.54	4.02
	Warm temperate dry forest	0.12	0.40	2.00	0.18	1.97
	Warm temperate moist forest	0.40	0.46	0.12	0.46	0.31
Transitional	Boreal superhumid wet-rain forest	0.09	0.03	–	–	–
	Boreal perhumid wet-rain forest	0.52	0.46	0.34	0.71	0.18
	Cool temperate humid forest-steppe	0.21	–	0.18	–	–
	Cool temperate perhumid moist-wet forest	4.39	4.18	4.30	4.67	3.44
	Cool temperate subhumid forest-steppe	19.90	19.40	21.98	24.26	30.27
	Cool temperate humid moist-wet forest	2.43	2.61	2.43	2.06	2.79
	Warm temperate humid dry-moist forest	0.28	0.25	0.58	0.21	0.58

Due to the introduction of transitional HLZ types, the most extensive vegetation class in P1 was the core HLZ type "cool temperate moist forest", covering 58.8% of the target domain (Table 2.9). According to the modified model, the second in the coverage ranking was the transitional HLZ type "cool temperate subhumid forest-steppe", covering approximately one fifth of the target area.

In P1, this type covered the Great Hungarian Plain, the Wallachian Plain and a small patch along the Hungarian upper section of the Danube (Fig. 2.5a). The third most abundant vegetation class was the core HLZ type “cool temperate wet forest” with an areal proportion of 5.5%. This type can be observed in the high altitudes of the Dinaric Alps, Alps and Northwestern Carpathians, at the beginning of the century. In contrast, the highest peaks of the Eastern and Southern Carpathians can be separated by the core HLZ type “boreal wet forest” (Fig. 2.5a), covering 3.3% of the target domain. In P1, the second most extensive transitional vegetation class was the transitional HLZ type “cool temperate perhumid moist-wet forest” with an areal proportion of 4.4%, covering the other mountainous areas. At the beginning of the century, considering only the core HLZ types, the relative coverage exceeded 3% just for the core HLZ type “cool temperate steppe”, except in the case of the above-mentioned vegetation classes (Table 2.9). In P1, however, this vegetation type can only be observed to the east of the Carpathians. In P1, the rest of the core/transitional HLZ types covered about 4.3% of the target area, mainly outside the Carpathian Basin.

Assessing temporal changes in the relative coverage of each core/transitional HLZ type (see Table 2.9) provides a good opportunity to map the dynamics of climatic ranges. For example, during the whole study period, more than half of the target domain was covered by the core HLZ type “cool temperate moist forest”. Furthermore, it can clearly be seen from Table 2.9 that the relative extent of the HLZ type “cool temperate subhumid forest-steppe” never fell below 19%, in the last century. The introduction of transitional HLZ types into the model allows an accurate assessment of climate change in terms of the heat and moisture properties. In the entire study period, the relative coverage of the cool temperate zone exceeded 95%. From P1 to P3, the extent of the superhumid, perhumid and humid provinces permanently decreased, while in the case of the subhumid range, the same value was increased. As we have seen before, climatic conditions in P4 were more humid than in the previous ones. In P4, the relative coverage of the subhumid province was 25.3%, which was the second smallest, considering the five investigated time periods. Taking into account the respective coverage rankings, in P5, the relative extent of the humid, perhumid and superhumid ranges was the smallest: 54.3, 9.1 and 0%, respectively. While at the same time, the coverage of the subhumid province reached its maximum value of 36.6%. From P1 to P5, the extent of the boreal region decreased by 59.5%, and in parallel, the warm temperate zone became two and a half times larger than it used to be. At the end of the century, the subhumid province was one and a half times as large as in P1, while from P1 to P5, the coverage of the humid and perhumid provinces decreased by 12.6 and 33.5%, respectively (Table 2.9).

The transformations between the HLZ types can be assessed by using a transformation matrix (not shown). From P1 to P5, the proportion of the area affected by these HLZ transformations was 24.4%. During the last century, four dominant HLZ transformations can be observed. By the end of the century, the core HLZ type “cool temperate moist forest” was replaced by the transitional HLZ type “cool temperate subhumid forest-steppe” over about 12% of the target domain. Considering the total area, the second greatest change was the transformation from the transitional HLZ type “cool temperate perhumid moist-wet forest” to the core HLZ type “cool temperate moist forest”, with an areal proportion of 3.3%. For 1.7% of the whole region, the core HLZ type “warm temperate dry forest” was substituted for the transitional HLZ type “cool temperate subhumid forest-steppe”. In case of the transformation to the core HLZ type “boreal wet forest” to the transitional HLZ type “cool temperate perhumid moist-wet forest”, the relative extent of the affected area was 1.5%.

2.4.3 Mean centres of HLZ types

The recent climate change is assessed also in terms of the shift in the mean centre of each HLZ type. Mean centres of the HLZ types defined by the original model are shown in Fig 2.6, for the previously defined 20-year time periods.

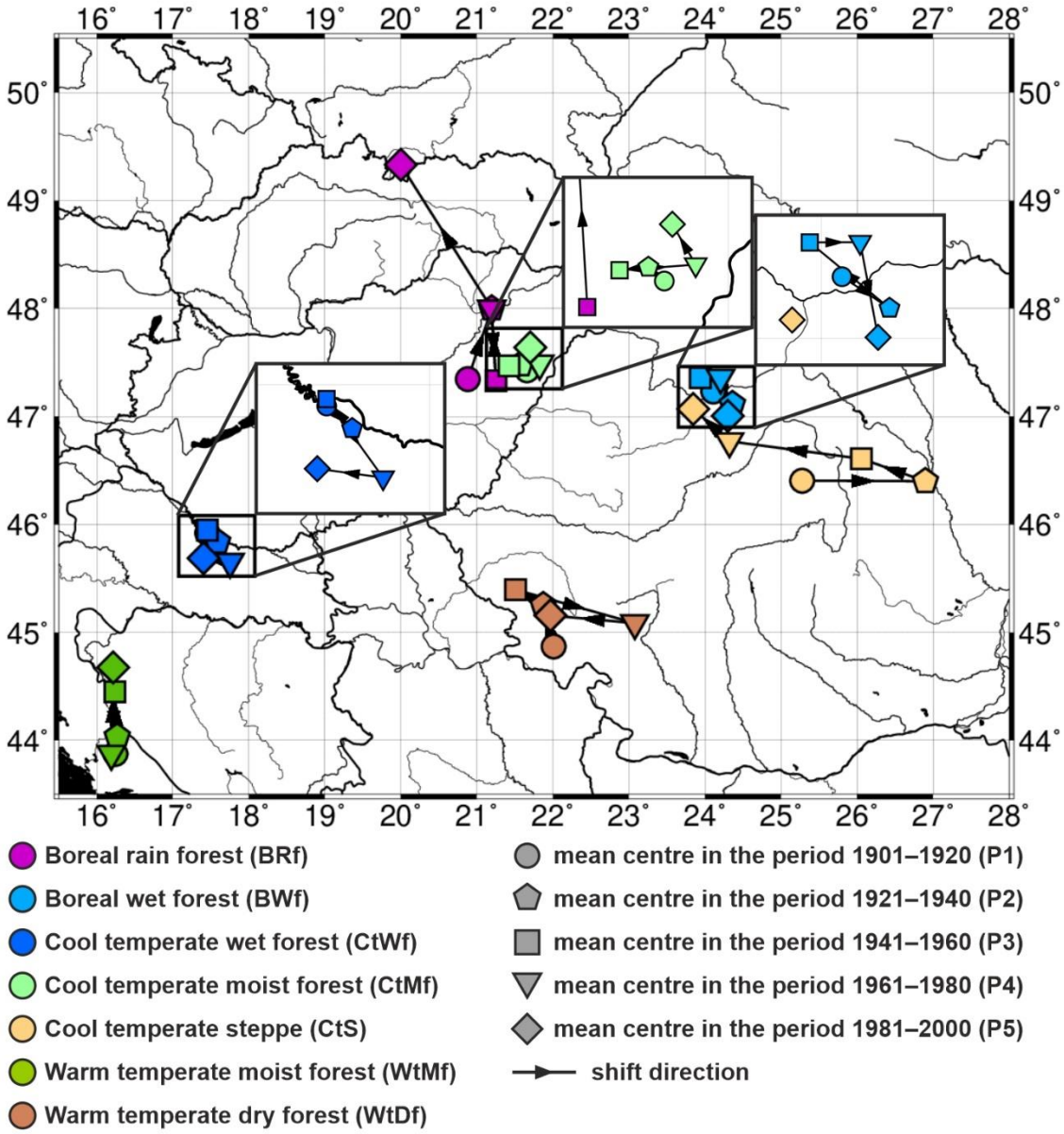

Fig. 2.6 Mean centres of Holdridge life zone (HLZ) types in the Carpathian Region for the periods 1901–1920 (P1), 1921–1940 (P2), 1941–1960 (P3), 1961–1980 (P4) and 1981–2000 (P5)

The exact position of the mean centre is not informative, since the mean centre of a given HLZ type does not necessarily fall into the domain of the respective HLZ type because of its fragmentation. Taking into account all these and the page limitations, here, only the distance and direction of shift of the mean centre from the period 1901–1920 (P1) to the period 1981–2000 (P5) for each HLZ type are evaluated (see Table 2.10 for results obtained by the original model).

Table 2.10 Distance and direction of the shift of the mean centre of each Holdridge life zone (HLZ) type from the period 1901–1920 (P1) to the period 1981–2000 (P5)

HLZ type	From P1 to P5	
	distance (in km)	direction
Boreal wet forest (BWf)	29.35	southeast
Boreal rain forest (BRf)	230.70	northwest
Cool temperate steppe (CtS)	132.68	northwest
Cool temperate moist forest (CtMf)	23.55	north
Cool temperate wet forest (CtWf)	25.77	south
Warm temperate dry forest (WtDf)	32.41	north
Warm temperate moist forest (WtMf)	90.12	north

In terms of the spatial distribution, the examination of shifts in the mean centres is irrelevant for three out of seven HLZ types identified in the Carpathian Region, the boreal HLZ types (BRf, BWf) and the CtWf, since during the last century, these types were directly related to mountains, considering the whole target domain (see Fig. 2.4). From P1 to P5, for three out of the remaining four HLZ types, the mean centre moved northward, while for one HLZ type (CtS), a northeastward shift can be observed (Table 2.10). From P1 to P5, the mean centres of the CtMf, WtDf and WtMf shifted by 23.55, 32.41 and 90.12 km, respectively. In the case of the CtS, a northwestward shift of 132.68 km can be registered during the last century. This high-magnitude shift can be explained by the fact that in P5, this HLZ type appeared also in the northwestern part of the target domain, while in P1, it can be registered only in areas situated to the east of the Danube.

Comparing the results obtained by the original and modified models, it can be found that they are very similar, principally in terms of the direction. So, here, the results for the modified model are not shown in detail. However, it should be emphasized that if the direction of the mean centre shift is taking into account only in relation to the east–west axis, a southward shift of the mean centre can be registered for just three out of eleven HLZ types (not shown): the core HLZ type "boreal wet forest", the core HLZ type "cool temperate wet forest" and the transitional HLZ type "cool temperate perhumid moist-wet forest". Furthermore, it should be noted that compared to the original model, the fragmentation of vegetation types was much higher in the case of the modified model, due to the high number of classes used and the "coarse" resolution of the applied climate database. For this reason, for most vegetation classes used in the modified model, the mean centre shows a shift of even higher magnitude between the various time periods than in the case of the original model.

2.4.4 Altitudinal distribution pattern of HLZ types

2.4.4.1 The original version of the HLZ system

Besides the horizontal distribution of the HLZ types, their vertical distribution is also evaluated. For the original model, features describing the altitudinal distribution pattern of each HLZ type are summarized in Table 2.11: (a) the mean distributional altitude in P1 (MDA_{P1}, in m a.s.l.), (b) the change in the value of MDA for two consecutive time periods t and $t + 1$ ($\Delta MDA_{t/t+1}$, in m), and (c) the change in the value of MDA from P1 to P5 ($\Delta MDA_{P1/P5}$, in m).

Table 2.11 Altitudinal distribution pattern of each Holdridge life zone (HLZ) type: (a) the mean distributional altitude in P1 (MDA_{P1}, in m a.s.l.), (b) the change in the value of MDA for two consecutive time periods t and $t + 1$ ($\Delta MDA_{t/t+1}$, in m), and (c) the change in the value of MDA from P1 to P5 ($\Delta MDA_{P1/P5}$, in m). Negative values of ΔMDA are highlighted in bold

HLZ type	MDA (in m a.s.l.)	ΔMDA (in m)				ΔMDA (in m)
	P1	From P1 to P2	From P2 to P3	From P3 to P4	From P4 to P5	From P1 to P5
Boreal wet forest (BWf)	994.2	+75.9	+32.1	**−45.5**	+83.6	+146.0
Boreal rain forest (BRf)	1304.7	+25.0	+38.3	**−38.3**	**−56.0**	**−31.0**
Cool temperate steppe (CtS)	107.3	+28.6	+2.7	**−30.3**	+25.3	+26.3
Cool temperate moist forest (CtMf)	326.9	+15.8	+29.4	**−36.2**	+56.6	+65.5
Cool temperate wet forest (CtWf)	716.3	+17.0	+76.3	**−72.4**	+64.6	+85.5
Warm temperate dry forest (WtDf)	91.4	+2.6	+17.4	**−19.5**	+33.9	+34.4
Warm temperate moist forest (WtMf)	416.8	**−28.4**	+9.3	**−11.8**	**−43.5**	**−74.5**

Table 2.11 confirms our earlier statement that in the last century, the boreal HLZ types and the CtWf were related to mountains. For the CtWf, BWf and BRf, the value of MDA_{P1} is 716.3, 994.2 and 1304.7 m a.s.l., respectively. For most HLZ types, the value of MDA increased between any two consecutive time periods, with the exception of the shifts from P3 to P4. Based on changes in the value of MDA, apart from two exceptions, HLZ types show an upward shift at the end of the century. From P4 to P5, in the case of the BRf and WtMf, the value of MDA decreased by 56 and 43.5 m, respectively. For the BRf, this decrease can be explained by the fact that by the end of the last century, this type had totally disappeared from the South Carpathians, and can be observed in P5 only on the northern slopes of the High Tatras (see Fig. 2.4). All in all, for the five dominant vegetation classes, the value of MDA increased from P1 to P5, namely, during the last century, the HLZ types moved toward higher elevations (Table 2.11).

2.4.4.2 The modified version of the HLZ system

Temporal changes in the values of MDA are evaluated also for core and transitional HLZ types identified in the Carpathian Region (Table 2.12). In the target domain, seven core and seven transitional HLZ types can be registered in P1, however, not all types can be observed in the next four time periods, and so the shift in the value of MDA cannot be calculated in all cases.

Table 2.12 Altitudinal distribution pattern of each core/transitional Holdridge life zone (HLZ) type: (a) the mean distributional altitude in P1 (MDA_{P1}, in m a.s.l.), (b) the change in the value of MDA for two consecutive time periods t and $t + 1$ ($\Delta MDA_{t/t+1}$, in m), and (c) the change in the value of MDA from P1 to P5 ($\Delta MDA_{P1/P5}$, in m). Negative values of ΔMDA are highlighted in bold. The *symbol* – refers to those cases where the value of ΔMDA cannot be computed

	HLZ type	MDA (in m a.s.l.)	ΔMDA (in m)				ΔMDA (in m)
		P1	From P1 to P2	From P2 to P3	From P3 to P4	From P4 to P5	From P1 to P5
Core	Boreal wet forest	1059.6	+54.9	+50.5	**−46.3**	+65.3	+124.4
	Boreal rain forest	1363.9	**−90.2**	–	–	–	–
	Cool temperate steppe	115.0	+16.0	+14.3	**−37.0**	+14.7	+8.1
	Cool temperate moist forest	339.8	+16.0	+27.6	**−35.1**	+60.8	+69.3
	Cool temperate wet forest	765.7	+32.9	+43.1	**−53.8**	+80.9	+103.1
	Warm temperate dry forest	102.8	**−3.7**	**−2.4**	**−36.6**	+28.1	**−14.5**
	Warm temperate moist forest	487.7	**−41.4**	+167.2	**−190.0**	+100.9	+36.7
Transitional	Boreal superhumid wet-rain forest	1467.3	+179.7	–	–	–	–
	Boreal perhumid wet-rain forest	1032.3	+102.3	+55.8	**−81.4**	+140.2	+216.9
	Cool temperate humid forest steppe	295.1	–	–	–	–	–
	Cool temperate perhumid moist-wet forest	785.6	+57.9	+46.7	**−43.1**	+51.5	+113.1
	Cool temperate subhumid forest steppe	114.4	+8.4	+13.1	**−16.3**	+37.5	+42.7
	Cool temperate humid moist-wet forest	406.0	**−38.2**	+78.8	**−119.1**	+64.1	**−14.3**
	Warm temperate humid dry-moist forest	206.3	+12.9	+80.8	**−94.5**	**−9.0**	**−9.8**

Considering the shifts from P1 to P2 (see Table 2.12), the largest decrease in the value of MDA can be found in the case of the core HLZ type "boreal rain forest", with a value of 90.2 m. Taking into account the same shifts, the second largest increase in the value of MDA can be registered for the transitional HLZ type "boreal perhumid wet-rain forest", with a value of 102.3 m. This can be explained by the fact that in the Southern Carpathians, the former type was replaced by the latter type, from P1 to P2 (not shown). The former vegetation class falls into the superhumid province, whereas the latter class is assigned to the perhumid range. According to this, the aridity process is well illustrated also by shifts in the values of MDA. From P2 to P3, apart from one exception, all calculable changes in the value of MDA refer to an upward shift of the vegetation. In accordance with the above-presented results, from P3 to P4, the value of MDA decreased for all vegetation classes. With the exception of the transitional HLZ type "warm temperate humid dry-moist forest", the values of MDA increased form P4 to P5. To conclude, from P1 to P5, the value of MDA increased for most HLZ types (Table 2.12), which suggests that during the last century, HLZ types shifted to higher altitudes.

2.5 Summary

Holdridge (1967) had developed the Holdridge life zone (HLZ) system to identify spatial differences in climate at a global scale. In some ways, however, the HLZ system is a very simple model of the potential vegetation distribution (see Yates et al. 2000). In the course of developing the model, some aspects had been forced to ignore. For example, the so-called transitional HLZ

types were not determined as separate vegetation units within the model because, as a result, the model would have distinguished too many classes, and the plotting of this large number of classes would have made it impossible to visualize the relevant vegetation types. In our previous work (Szelepcsényi et al. 2009), however, it was found that in a regional analysis, it is advisable to use the transitional HLZ types. In this study, the widely used version of the HLZ system is modified, namely both the core and transitional HLZ types are determined as separate classes.

As the HLZ system has been developed for the tropical region (see Holdridge 1967), it is necessary to evaluate the accuracy of HLZ maps for the mid-latitudes. For this reason, HLZ maps prepared here are compared to an expert-based map of the potential natural vegetation (PNV), created by Bohn et al. (2003). The degree of agreement between the maps is estimated by using the Kappa statistic developed by Cohen (1960). These comparisons indicate "poor" and "fair" agreements between the maps that are consistent with the findings by other studies in extratropical regions (e.g., Lugo et al. 1999; Zheng et al. 2006).

Furthermore, here, the original and modified versions of the HLZ system are applied also to an observational climate database, in order to map the impacts of the recent climate change in the Carpathian Region for the last century. During our investigations, temporal changes in the relative coverage, the mean centre and the mean distributional altitude (MDA) are evaluated for each HLZ type.

In the target area, seven HLZ types can be observed by using the original model. The results show that the dominant HLZ type of the Carpathian Region was the cool temperate moist forest (CtMf) during the whole study period. This type covered more than 60% of the total area in each of the five preselected 20-year time periods. At the beginning of the century, seven core and seven transitional HLZ types can be registered by using the modified variant of the HLZ system. Due to the introduction of transitional HLZ types, the spatial pattern of vegetation classes is significantly rearranged: (a) the first in the coverage ranking is the core HLZ type "cool temperate moist forest", with an areal proportion of 50–60% (depending on the study period), whereas (b) the second most abundant vegetation class is the transitional HLZ type "cool temperate subhumid forest-steppe", covering a significant part of the lowland areas. In the period 1901–1920 (P1), the latter type covered about one fifth of the target domain, whereas at the end of the century, the relative coverage of this vegetation class became one and a half times larger than in P1. Comparing the distribution pattern of this transitional HLZ type in the period 1981–2000 (P5) and the potential areas of the forest-steppe ecotone (see Varga et al. 2000), a big overlap can be found between them.

One of the objectives of this study is to assess temporal shifts in various measures of the central tendency for HLZ types. Similar trends can be found for both models, so here, findings only for the original model are summarized. From P1 to P5, the mean centres of those HLZ types which were not related to mountains shifted northward. Furthermore, the results show that from P1 to the period 1941–1960 (P3), the value of MDA increased for all HLZ types, apart from one exception, whereas from P3 to the period 1961–1980 (P4), a decrease in this parameter can be registered for all HLZ types. The reason for this is the fact that the climate in P4 was slightly rainier and cooler than in P3. All in all, for the five most abundant HLZ types, the value of MDA increased during the last century. The registered changes in the spatial distribution pattern of HLZ types refer to northward and/or upward shifts of the vegetation, which are consistent with the recently observed shifts of the natural ecosystems (e.g., Walther et al. 2002, 2005; Kharuk et al. 2007).

In summary, the effect of recent climate change on the potential vegetation in the Carpathian Region could be well presented by applying the selected versions of the HLZ system. Through the

use of the modified model, the climate of this region could be typified in much more detail. By introducing the transitional HLZ types, it is possible to circumscribe the position of the forest-steppe, which is one of the most important ecotones in the study region. We think that the HLZ system, this relatively simple bioclimatic classification method, is suited to use as an effective visualization tool for disseminating current and future climate change information. For this reason, our further purpose is to evaluate the ecological impacts of also the projected climate change for the Carpathian Region, by using these models, following the example of other similar studies (e.g., Chen et al. 2003; Yue et al. 2006).

Acknowledgments. This research was supported by the European Union and the State of Hungary, co-financed by the European Social Fund in the framework of TÁMOP 4.2.4. A/2-11-1-2012-0001 'National Excellence Program'. The authors gratefully acknowledge the Climatic Research Unit of the University of East Anglia, UK, for providing the monthly high-resolution dataset CRU TS 1.2. The authors are also grateful to the developers of the R package "raster" (https://github.com/rspatial/raster) for making their source code available to everyone. We would like to thank Ágnes Havasi (Eötvös Loránd University, Hungary) for language polishing of the updated version of our manuscript.

3 Assessment of projected climate change in the Carpathian Region using the Holdridge life zone system

Manuscript published in the *Theoretical and Applied Climatology*
Volume 131, Issue 1–2, 593–610 (2018)
DOI: 10.1007/s00704-016-1987-3

Authors:

Zoltán Szelepcsényi
Department of Geology and Palaeontology
University of Szeged, Hungary

Hajnalka Breuer
Department of Meteorology
Eötvös Loránd University, Hungary

Anna Kis
Department of Meteorology
Eötvös Loránd University, Hungary

Rita Pongrácz
Department of Meteorology
Eötvös Loránd University, Hungary

Pál Sümegi
Department of Geology and Palaeontology
University of Szeged, Hungary

Abstract. In this paper, expected changes in the spatial and altitudinal distribution patterns of Holdridge life zone (HLZ) types are analysed to assess the possible ecological impacts of future climate change for the Carpathian Region, by using 11 bias-corrected regional climate model simulations of temperature and precipitation. The distribution patterns of HLZ types are characterized by the relative extent, the mean centre and the altitudinal range. According to the applied projections, the following conclusions can be drawn: (a) the altitudinal ranges are likely to expand in the future, (b) the lower and upper altitudinal limits as well as the altitudinal midpoints may move to higher altitudes, (c) a northward shift is expected for most HLZ types and (d) the magnitudes of these shifts can even be multiples of those observed in the last century. Related to the northward shifts, the HLZ types warm temperate thorn steppe and subtropical dry forest can also appear in the southern segment of the target area. However, a large uncertainty in the estimated changes of precipitation patterns was indicated by the following: (a) the expected change in the coverage of the HLZ type cool temperate steppe is extremely uncertain because there is no consensus among the projections even in terms of the sign of the change (high inter-model variability) and (b) a significant trend in the westward/eastward shift is simulated just for some HLZ types (high temporal variability). Finally, it is important to emphasize that the uncertainty of our results is further enhanced by the fact that some important aspects (e.g., seasonality of climate variables, direct CO_2 effect, etc.) cannot be considered in the estimating process.

3.1 Introduction

Nowadays, several methods are available to analyse the potential effects of climate change on vegetation distribution (see Prentice et al. 2007; Elith and Leathwick 2009; McMahon et al. 2011). Considering the applied approaches, models of plant distribution can be divided into two major groups: correlative and mechanistic models. Correlative models determine a statistical relationship between vegetation distribution and environmental variables (e.g., climate, soil, etc.); then this link is applied to predict the potential distribution of vegetation under the altered environmental conditions (Yates et al. 2000; Elith and Leathwick 2009). Mechanistic models simulate the growth and main physiological processes (e.g., photosynthesis, respiration, etc.) of some idealized plant types considering changes in the environmental conditions (Cramer 2002; Prentice et al. 2007). Nowadays, the distribution of vegetation is most commonly modelled at the following two levels of organisation: species and biome.

Considering the object of prediction and the modelling approach, four basic techniques of modelling of plant distribution can be assigned: (a) correlative biome models (e.g., Holdridge 1947, 1967; Box 1981b), (b) correlative species distribution models (see Elith and Leathwick 2009), (c) dynamic global vegetation models (DVGMs) (e.g., Lund–Potsdam–Jena DVGM, LPJ-DVGM: Sitch et al. 2003) and (d) mechanistic species distribution models (e.g., PHENOFIT: Chuine and Beaubien 2001). Transitions between the basic techniques are continuous; several hybrid models have been developed in the past (see Cramer 2002; Dormann et al. 2012).

Both modelling approaches have several disadvantages; therefore, it can only be conceptually claimed that process-based models are better than statistical approaches. Mechanistic models have large data requirement, and in order to successfully apply these models, several ecological processes have to be known in more detail (Chen et al. 2003). In turn, one of the largest disadvantages of correlative models is that they are based on the current distribution patterns, namely, equilibrium between vegetation and environmental factors is assumed.

Mechanistic models are more applicable for global/continental assessments because of those modelling approaches. At regional/local scale, correlative models are more widespread. In the recent past, for example, Falk and Mellert (2011), Rasztovits et al. (2012) and Zimmermann et al. (2013) used correlative models to predict the potential distribution of main forest-forming species in Europe. Modelling the distribution of biomes using correlative techniques is not typical on our continent. A simple climate–vegetation scheme, the so-called Köppen climate classification system (Köppen 1936) or one of its modified versions, is commonly applied to assess the sensitivity of European natural ecosystems to projected climate change (e.g., de Castro et al. 2007; Fábián and Matyasovszky 2010; Feng et al. 2012).

Considering the terminology, the Holdridge life zone (HLZ) system (Holdridge 1947, 1967) can be regarded as the first correlative biome model (Cramer 2002). The model takes into account some basic laws of plant physiology; however, several important factors are not considered (e.g., seasonality of climate variables, physical properties of soil, etc.). Yates et al. (2000) compared Holdridge's model to three process-based biogeography models for the conterminous USA under current and altered climate. They found that the reproduction ability of the HLZ system is almost as good as more complex biogeography models', so this simple model is applicable with certain restrictions to assess potential impacts of climate change on natural ecosystems. In this case, however, we cannot afford to ignore the following conclusions of de Castro et al. (2007): (a) the future climate simulations show large uncertainties, (b) the relationship between vegetation and

climate in the future will not necessarily be the same as the current one and (c) the climate–vegetation schemes consider only a limited number of clusters.

The so-called HLZ maps were first used by Emanuel et al. (1985) to assess the effects of climate change on vegetation. Even though the alteration of precipitation was not considered, this investigation showed for the first time that climate change can induce drastic changes in vegetation distribution at high latitudes. Since then, this model has been applied several times to analyse the possible ecological impacts of the estimated climate change at a regional scale, for example, in China (Chen et al. 2003; Yue et al. 2006; Li et al. 2015) and India (Chakraborty et al. 2013). The above-mentioned investigations differ substantially from each other considering the input data. For the estimation of changes in Holdridge's bioclimatic indices, Yue et al. (2006) and Li et al. (2015) used global climate model (GCM) outputs, which they downscaled using different statistical techniques. In the case of investigations of Yue et al. (2006), the GCMs were forced by the early IS92a emission scenario (Leggett et al. 1992), while the GCMs used by Li et al. (2015) already applied the so-called Representative Concentration Pathways (RCP) scenarios (Moss et al. 2008) to simulate the response of the global climate system. Chakraborty et al. (2013) applied the HLZ system for a gridded observational database and three alternative scenarios. To our knowledge, outputs from a regional climate model (RCM) simulation were first used by Chen et al. (2003) to create HLZ maps. Climate change was defined by a doubling of the atmospheric CO_2 concentration; the simulation was prepared by using the RegCM2 regional climate model (Giorgi et al. 1993) coupled with the CSIRO global climate model (Watterson et al. 1995).

To our knowledge, assessment of the projected changes in the distribution of HLZ types was carried out using RCM outputs neither for the Carpathian Region, nor for Europe. One possible reason for this is that in the framework of the PRUDENCE project (Christensen et al. 2007a), the first harmonized set of RCM experiments in Europe, the possible effects of climate change on terrestrial ecosystems were assessed by Morales et al. (2007) using the LPJ-GUESS process-based vegetation model (Smith et al. 2001) on the one hand, and by de Castro et al. (2007) using the Köppen–Trewartha climate classification method (Trewartha and Horn 1980) on the other hand; and in further investigations (e.g., Wolf et al. 2008; Hickler et al. 2012; Gallardo et al. 2013), these ecosystem models were favoured, too.

For the last century, shifts in the horizontal and vertical distribution pattern of each HLZ type in the Carpathian Region have been analysed by Szelepcsényi et al. (2014a, b). The results showed that the mean centres of those HLZ types which were not related to mountains shifted northward during the twentieth century. In addition, it has also been found that the altitudinal midpoint of the dominant HLZ types moved to higher elevations in the selected time period. Nevertheless, Breuer et al. (2017) have recently analysed the climate change for the twentieth century in Hungary, by using another climate classification method, the revised Thornthwaite method (Feddema 2005). Unfortunately, they have not applied the thresholds associated with vegetation boundaries for both thermal and moisture indices (e.g., Mather and Yoshioka 1968); therefore, their investigation does not directly pertain to the potential vegetation.

In this paper, expected shifts in the spatial and altitudinal distributions and the mean centres of the HLZ types are investigated for the Carpathian Region, in accordance with the above-mentioned studies (Szelepcsényi et al. 2014a, b). In order to construct HLZ maps, bias-corrected temperature and precipitation fields of 11 RCM simulations from the ENSEMBLES project (van der Linden and Mitchell 2009) are used. Analyses are performed not only for each RCM simulation but also for their so-called ensemble mean. Expected changes of the distribution pattern of HLZ types, of the relative extent, of the mean centre and certain altitudinal points of each HLZ type are

investigated. Results of the ensemble mean and those simulations which provide the minimal and maximal changes in the distribution pattern of HLZ types are presented in detail. In addition, the direction, the magnitude and the uncertainty of changes are analysed for each HLZ type. Moreover, projected trends in the coordinates of mean centre and the positions of the selected altitudinal points are detected for each HLZ type in the case of all projections. So it is investigated whether each HLZ type will shift along one of the spatial axes in the Carpathian Region, according to the selected projections.

3.2 Data and methods

3.2.1 Climatic data and study area

The HLZ system requires daily or monthly time series of temperature and precipitation. The necessary data for this study are derived from 11 RCM experiments of the ENSEMBLES project (van der Linden and Mitchell 2009). Table 3.1 lists the 11 selected projections, along with their acronyms, responsible institutes and main references. The following statements apply to each single selected simulation: (a) all of them cover all Europe for the period 1951–2099, (b) all of them were prepared with a horizontal resolution of 15 arc-min (~25 km in mid-latitudes) and (c) all of them apply the SRES A1B emission scenario (Nakicenovic and Swart 2000) after the year 2000 (van der Linden and Mitchell 2009). The necessary initial and boundary conditions are provided by three different GCMs: HadCM (Gordon et al. 2000) developed at the Met Office Hadley Centre, ECHAM5 (Roeckner et al. 2003) developed at the Max Planck Institute, and ARPEGE (Déqué et al. 1998) developed at Météo-France.

Table 3.1 List of the selected regional climate model (RCM) experiments, the corresponding acronyms, driving global climates models (GCMs), responsible institutes and main references

Acronym	Driving GCM	RCM	Institute	Reference
EH	HadCM3Q0	CLM2.4.6	ETHZ (Eidgenössische Technische Hochschule Zürich, SUI)	Böhm et al. (2006)
HH	HadCM3Q0	HadRM3Q0	HC (Hadley Centre for Climate Prediction and Research, GBR)	Jones et al. (2004)
CH	HadCM3Q16	RCA3.0	C4I (Community Climate Change Consortium for Ireland, IRL)	Samuelsson et al. (2011)
SH	HadCM3Q3	RCA3.0	SMHI (Sveriges Meteorologiska och Hydrologiska Institut, SWE)	Samuelsson et al. (2011)
SE	ECHAM5-r3	RCA3.0	SMHI (Sveriges Meteorologiska och Hydrologiska Institut, SWE)	Samuelsson et al. (2011)
IE	ECHAM5-r3	RegCM3	ICTP (International Centre for Theoretical Physics, ITA)	Pal et al. (2007)
KE	ECHAM5-r3	RACMO2.1	KNMI (Koninklijk Nederlands Meteorologisch Instituut, NED)	van Meijgaard et al. (2008)
ME	ECHAM5-r3	REMO5.7	MPI (Max-Planck-Institut für Meteorologie, GER)	Jacob and Podzun (1997)
DE	ECHAM5-r3	HIRHAM5	DMI (Danmarks Meteorologiske Institut, DEN)	Christensen et al. (2007b)
DA	ARPEGE	HIRHAM5	DMI (Danmarks Meteorologiske Institut, DEN)	Christensen et al. (2007b)
CA	ARPEGE	RM5.1	CNRM (Centre National de Recherches Météorologiques, FRA)	Radu et al. (2008)

Comparing RCM simulations to observations, Dobor et al. (2015) have shown that the selected RCM simulations contain biases and errors in the target area. In Hungary, these RCM simulations are able to represent monthly average temperature values properly, aside from a slight overestimation (which does not exceed 1 °C). In the case of precipitation, an overall overestimation can be detected, except in summer, when mostly underestimation occurs (Pongrácz et al. 2011). For this reason, first of all, a bias correction method is applied to the raw data, and then the corrected data are used for the further analyses.

Several bias correction methods exist, and all of them have their advantages and disadvantages (Teutschbein and Seibert 2012), so it may be questionable whether to apply a bias correction or not. Nevertheless, in some cases, it is necessary to eliminate the systematic errors of simulations, hence bias correction is inevitable, but we always have to be aware of its limitations. Firstly, we have to mention that the main assumption of the method is stationarity, which is not probable in climate change conditions. Secondly, relations between different variables, spatiotemporal field consistency and conservation principles can be violated. Furthermore, the choice of the correction method is an additional factor of uncertainty (Ehret et al. 2012; Teutschbein and Seibert 2013). For the main goals of this paper, bias correction is absolutely necessary because for the present analysis absolute values of variables are needed.

In this study, a percentile-based bias correction is applied, which is based on the assumption that two data sets are statistically identical if their cumulative density functions (CDFs) are the same. So the key of the applied method is that the empirical CDF of the simulated data set is fitted to the empirical CDF of the observed data set (Déqué 2007; Wang et al. 2016). Therefore, correction factors should be defined using the inverses of the CDFs for a calibration period. Then, it is possible to correct all simulated data assuming that the bias statistics are constant in time. Additive correction factors should be applied for temperature data, while multiplicative correction

method should be chosen in the case of precipitation. The factors should be defined using daily data for each month, for each grid cell. In this paper, the observed daily data are derived from the E-OBS gridded dataset (version 3.0) (Haylock et al. 2008), for the period 1951–2000. The values of daily mean temperature are corrected in this study, while the corrected values of daily precipitation sum are calculated by Pongrácz et al. (2014). A detailed description of the method used in this study is available in Wang et al. (2016), where it is labelled as quantile mapping method.

In this paper, the target area is the Carpathian Region (Fig. 3.1), so the correction technique is applied only for the following region: 43.625°–50.625° N, 13.875°–26.375° E. In the next step, the values of monthly mean temperature and monthly total precipitation are calculated for each RCM simulation, and then the ensemble means are computed for both climate variables, for each month. The ensemble mean (EM) is defined as the average of the 11 RCM simulations. For the analyses, three 30-year long time periods (T1: 1961–1990, T2: 2021–2050, T3: 2061–2090) and 28 decades (D1: 1951–1960, D2: 1956–1965, D3: 1961–1970, etc.) are selected. In the case of all simulations and the EM, the average values of monthly mean temperature and monthly total precipitation are computed for each chosen time period, for each grid cell. The HLZ system is applied for these mean fields, since Claussen (1996) has suggested that applying 10- and 30-year averages helps eliminate the large year-to-year fluctuation in climate variables, and so in this way, biome distribution could be estimated appropriately.

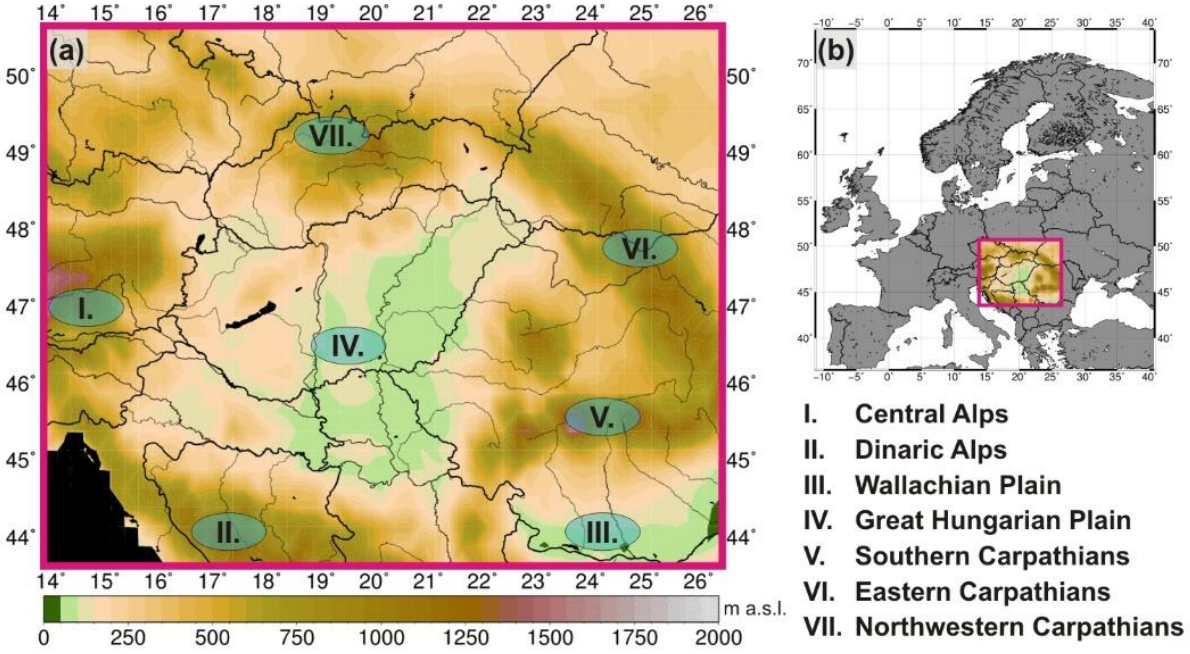

Fig. 3.1 The Carpathian Region. The target area's (**a**) topography and (**b**) location in Europe, indicating the major geographical regions, which are mentioned in the text

The E-OBS gridded observational dataset (Haylock et al. 2008) includes a digital elevation model, which is used to localize altitudinal ranges of the HLZ types. Due to the applied horizontal resolution and spatial averaging, this elevation model cannot represent appropriately the real terrain at some points of the target area. In order to manage the effects of this problem, our assessment focuses on shifts in altitudinal midpoints rather than lower and upper altitudinal limits; furthermore, we assess the directions and tendencies of vertical shifts in more detail, instead of their magnitudes.

3.2.2 Holdridge life zone system

Holdridge (1947, 1967) developed a geometric model which is able to determine the potential vegetation type under the given climatic conditions. The model uses three bioclimatic indices: mean annual biotemperature (*ABT*), total annual precipitation (*APP*), potential evapotranspiration ratio (*PER*). It is important to know that the indices are depicted on logarithmic axes in the so-called life zone chart. A widely used, simplified version of this geometric model (life zone chart) is shown in Fig. 2.2 in Chapter 2.

Holdridge (1967) has recognized that the vegetative growth and thus the net primary productivity are possible only in a certain temperature range. This remark was used in the definition of the *ABT*. In accordance with the above, in this study, as in many others (e.g., Chen et al. 2003; Li et al. 2015), the *ABT* is determined as the sum of monthly mean temperatures divided by 12, with the provision that values above 30 °C or below 0 °C are substituted with 0 °C.

The *PER* is defined as the ratio of the annual potential evapotranspiration (*APE*, in mm) to the annual precipitation (*APP*, in mm). The *APE* can be simply estimated according to the following formula (Holdridge 1959):

$$APE = 58.93 \cdot ABT\ , \tag{3.1}$$

where *ABT* is the mean annual biotemperature (in °C).

Considering the definition, the required data and the performance, the method of Thornthwaite (1948) could be an appropriate choice among the most widely known temperature-based models for potential evapotranspiration (e.g., Thornthwaite 1948; Blaney and Criddle 1950; Hargreaves and Samani 1985). However, in accordance with the relevant literature (e.g., Chen et al. 2003; Li et al. 2015), in the present study, the value of *APE* is calculated using Eq. 3.1. Nevertheless, it is important to note that according to former comparisons (Tuhkanen 1980), in high latitudes, the values of *APE* calculated by Holdridge's formula are lower compared to those estimated by Thornthwaite's method; while in tropical and subtropical regions, the opposite is true. This statement can be underpinned by those thermal thresholds which are applied in the related climate–vegetation schemes (Thornthwaite 1948; Holdridge 1967).

The HLZ system has been developed for the tropical region (Holdridge 1967). In the model, besides the latitudinal regions, altitudinal belts have also been assigned based on the values of *ABT*. The reason for this is that Holdridge (1967) found it necessary to determine which is the most important limiting factor of the *ABT* (and thus the vegetative growth): the distance from the Equator or the elevation. However, the most climate change assessments using HLZ maps (e.g., Velarde et al. 2005; Yue et al. 2006) omit the altitudinal belts, so they use a simplified version of the HLZ system. This kind of simplification of the model described by Holdridge (1967) is justified by the following: (a) the model includes many classes which are difficult to assign to the widely accepted vegetation classes (Yates et al. 2000) and (b) due to the large number of classes, it is relatively complicated to implement this scheme and to evaluate the results. Some variations of the HLZ system (e.g., Henderson-Sellers 1994; Yates et al. 2000) are known, but most of them cannot eliminate the three most important limitations: (a) the lack of different soil–vegetation–atmosphere interactions, (b) limited representation of the seasonality of climate variables and (c) the omission of direct CO_2 effect. In spite of these well-known limitations, nowadays, this model is commonly used to map the possible ecological effects of climate change (e.g., Li et al. 2015; Khalyani et al. 2016), due to its simplicity and general accuracy.

As we could see, there are many opportunities to modify the model (e.g., parameterization of the *APE*, vegetation classification, daily vs. monthly temperature data, etc.). One of the simplified

versions of the HLZ system ("version with no altitudinal belts"), which is used in the present study, is described by Szelepcsényi et al. (2014a). In addition, we should also mention that Szelepcsényi et al. (2014a) presented a variant of this simplified HLZ system, which allowed them to localize one of the most important ecotones of the Carpathian Region, the forest-steppe zone.

3.2.3 Mean centre calculation

There are several methods to determine central tendency (see Burt et al. 2009), one of these methods is the so-called mean centre. As Yue et al. (2006) and Li et al. (2015) have shown that this measure is suitable for analysing the spatial distribution of HLZ types, thus this method is used in the present investigation. The calculation of the mean centre of each HLZ type is based on a simple arithmetic mean of longitude and latitude of grid cells classified in the respective HLZ type. It is evident, as we will see later, that the area, covered by the respective HLZ type, not always includes the mean centre.

One of the objectives of this study is to compute the distance and direction of shift of the mean centre from T1 to T3 for each HLZ type in the case of all projections. The distance of this shift is calculated as a great circle distance following Fenna (2007), while its direction is computed according to Yue et al. (2006).

3.2.4 Mann-Kendall test for trend

The Mann-Kendall test (Mann 1945; Kendall 1975) is a very popular tool for detecting the presence or absence of an increasing or decreasing trend within a time series. This is a rank-based test, which is robust to missing values. Comparing to the parametric trend tests, a benefit of this test is that the data need not conform to any particular distribution. There is only one key requirement to apply this test: data should be serially independent, because the presence of a positive or negative serial correlation affects to correctly identify the significance of trend (Hamed and Rao 1998; Yue and Wang 2004). Recently, several approaches have been developed in order to solve this problem (see Khaliq et al. 2009). Among these efforts, the most widely accepted and applied approaches are pre-whitening (PW), trend-free pre-whitening (TFPW), block bootstrap (BBS) and variance correction (VC).

In this study, the VC method is applied as proposed by Hamed and Rao (1998). The VC method is based on the assumption that serial correlation alters only the variance of the test statistic. The test used in this study differs from the one described by Hamed and Rao (1998) basically in one aspect: missing values in the time series are not replaced, thus serial correlation coefficients are calculated according to Limonard (1978).

The test is applied to assess trends in the coordinates of the mean centre and the positions of the lower and upper altitudinal limits, as well as the altitudinal midpoint for each HLZ type. The above parameters are calculated for each decade from 1951 to 2090 with a lag of 5 years. So ideally, the sample size is 28 for each HLZ type. However, as we will see later, not all HLZ types can be detected in every time period. Therefore, we should mention that significance of the test is determined only when the length of the equidistance time series (the sample size including the missing values) is greater than or equal to 8.

3.2.5 Kappa statistic

During our investigation, we define those simulations which predict the minimal and maximal distributional changes. For this purpose, the HLZ map for the period 1961–1990 (the map T1)

should be compared to the map T3 using Kappa statistic (Cohen 1960), for each projection. That RCM simulation is declared to provide the minimal (maximal) distributional change, for which the degree of agreement between maps T1 and T3 is maximal (minimal) based on the value of Kappa statistic, considering all projections.

The Kappa statistic (κ) is determined according to the following formula:

$$\kappa = \frac{p_o - p_e}{1 - p_e}, \tag{3.2}$$

where p_o is the proportion of agreement and p_e is the overall proportion of chance-expected agreement. In order to determine variables of the formula, it is necessary to define a so-called contingency table. In cell (x, y) of this table, it has to be displayed what is the probability that the category x on map A agrees with the category y on map B. A value in the main diagonal shows the probability that a given point on map A, which is classified into the respective category, falls into the same category on map B. The value of p_o is obtained by adding the individual values in the main diagonal. By summing the values of row x (column y), the probability that category x (category y) can be found on map A (map B) can be determined. The value of p_e is computed by summing the products of row and column sums of the same category.

The value of κ can vary between 0 and 1, with 0 representing totally different patterns and 1 indicating complete agreement. We provide only a short overview of the Kappa statistic because Monserud and Leemans (1992) have already described the mathematical background of the model in detail.

3.3 Results

3.3.1 Spatial distribution pattern of HLZ types

First of all, the spatial distribution pattern of HLZ types is presented according to the EM and those RCM simulations which provide (based on the values of the Kappa statistic) the minimal (DE: HIRHAM5/ECHAM5-r3) and maximal (CH: RCA3.0/HadCM3Q16) distributional changes (Fig. 3.2). In T1, the dominant HLZ type is the cool temperate moist forest (CtMf) in the target domain, which coincides with the results of Szelepcsényi et al. (2014a). In the centre of the Carpathian Region and also in some parts of Wallachian Plain, the cool temperate steppe (CtS) can be observed. The Central Alps, the Dinaric Alps and some parts of the Carpathians can be separated by the cool temperate wet forest (CtWf), the boreal wet forest (BWf) and the boreal rain forest (BRf). (In these mountainous areas, the alpine tundra should also occur sporadically (see Bohn et al. 2003); however, this biome type cannot be found on the above HLZ maps, due to the "coarse" horizontal resolution of the applied RCM simulations.) In T3, the dominant HLZ type is projected to be the warm temperate dry forest (WtDf) and simultaneously, the coverage of the CtMf can be reduced. In T3, a new HLZ type, the warm temperate thorn steppe (WtTs) is likely to appear in the southern part of the Great Hungarian Plain and in the Wallachian Plain, too. In T3, some grid cells in the southwestern segment of the target area can fall into the category of subtropical dry forest (SDf). According to the simulation of CH, which provides the maximal distributional change, the CtS can disappear in the western parts of the domain. In the Central Alps and in the Dinaric Alps, the warm temperate moist forest (WtMf) is estimated to occur in T3. The agreement between maps T1 and T3 is poor/very-poor according to all projections (see the top right corner of maps T3 in Fig. 3.2); so the distributional change of HLZ types is probably remarkable in the Carpathian Region.

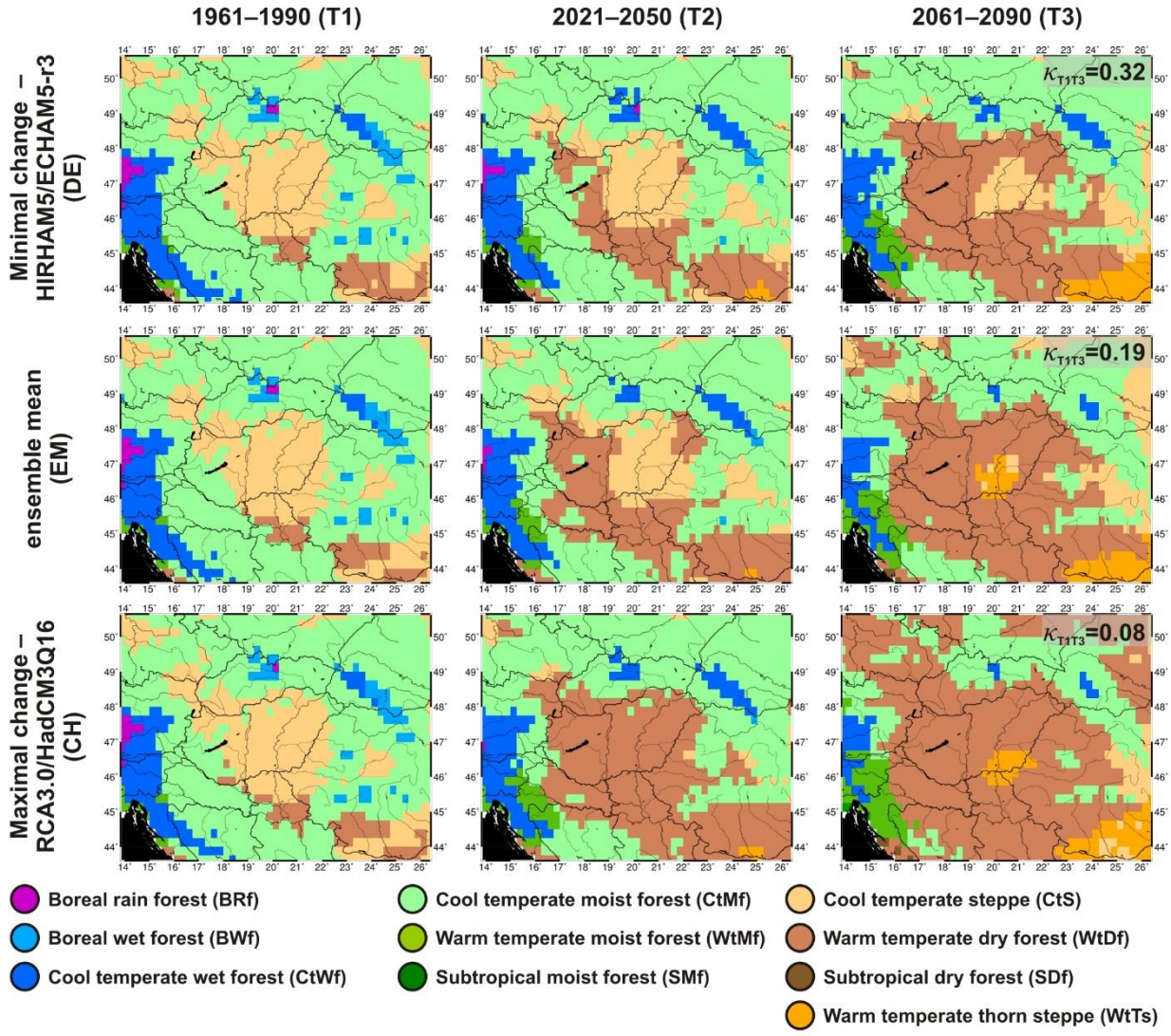

Fig. 3.2 Spatial distribution of Holdridge life zone (HLZ) types in the Carpathian Region for the periods 1961–1990 (T1), 2021–2050 (T2) and 2061–2090 (T3) according to the ensemble mean (EM) of the selected RCM simulations and those RCM simulations which provide the minimal and maximal changes in the distribution pattern of HLZ types. In the top right corner of maps T3, the Kappa statistic is shown, which indicates the degree of agreement between maps T1 and T3 for each projection

In Fig. 3.3, the inter-model difference in the relative coverage of each HLZ type is presented by the so-called skeletal box plots, just like in the case of the following analysed parameters. The reference periods for the bias correction (1951–2000) and for the assessment (1961–1990) are not identical. Therefore, considering individual RCM simulations, calculated values referring to T1 are not necessarily the same as we will see in the following assessments.

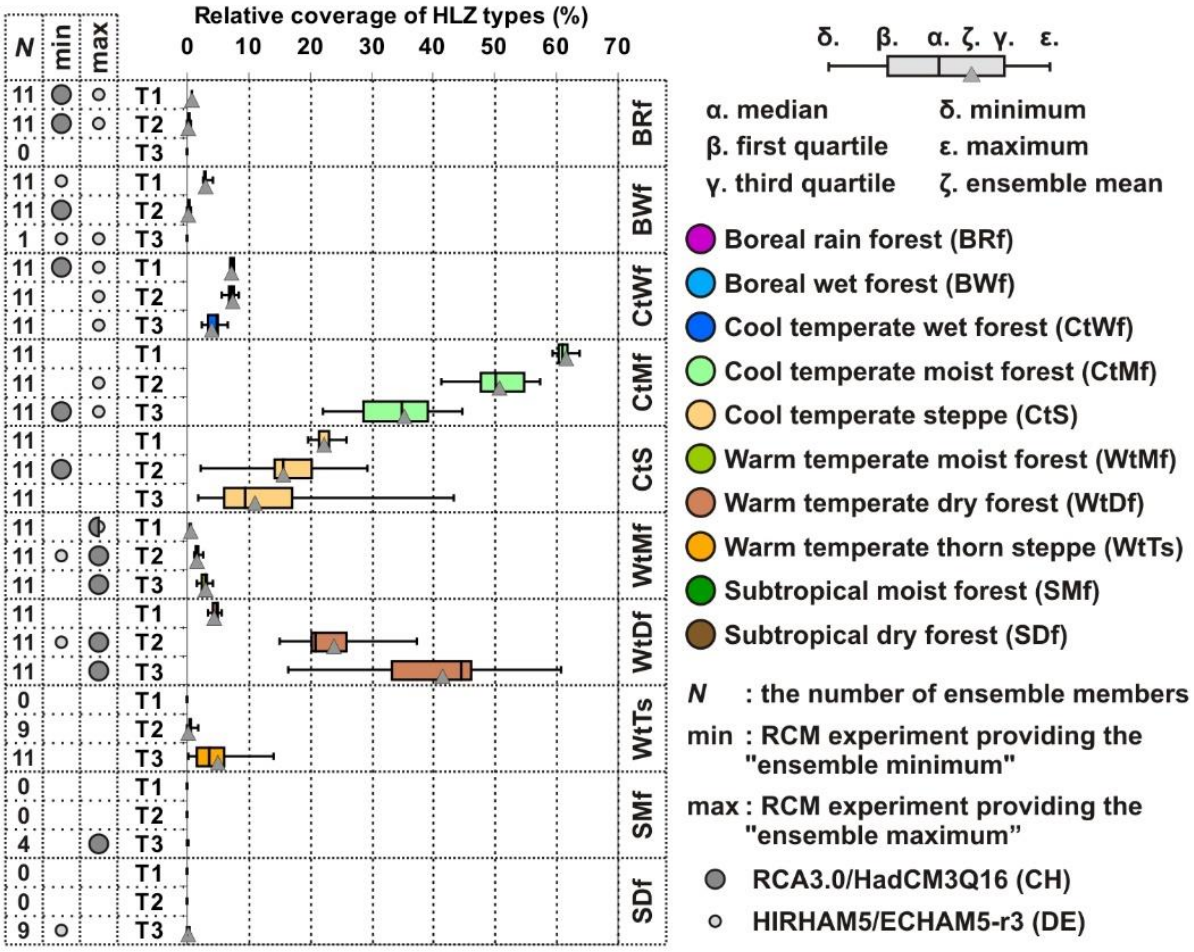

Fig. 3.3 Inter-model difference in the relative coverage of each Holdridge life zone (HLZ) type in the target area for the periods 1961–1990 (T1), 2021–2050 (T2) and 2061–2090 (T3) is shown by box plots. The *triangle* refers to the ensemble mean (EM). In the first column, the number of those ensemble members which indicate the respective HLZ type in the actual time period is shown. In the second (third) column, it is shown whether the minimum (maximum) of coverage values for the respective HLZ type in the actual time period is provided by RCA3.0/HadCM3Q16 (CH; *large circle*) or HIRHAM5/ECHAM5-r3 (DE; *small circle*)

In T1, the relative extent of the BWf can be 2.6–4.2% depending on the RCM simulation (Fig. 3.3); while in T3, this HLZ type appears only by one RCM simulation (CH). Taking into account all ensemble members, the uncertainty is very high in the case of the CtS, because the areal proportion of this HLZ type may change from 19.6–25.8% (T1) to 1.9–43.2% (T3), considering its minimal and maximal values. Hence, taking into account the whole spectrum, even the sign of the change cannot be determined for this HLZ type. However, most of the RCM simulations (8 out of 11) project a smaller relative extent for the CtS than 13.5%, which is substantially less (by about 6%) than its minimal value in T1, considering all RCM simulations. According to the EM, the coverage of the CtS will be halved from T1 to T3 (namely, from 22.3 to 11.1%). Nevertheless, expansion of this HLZ type for the far future is estimated by only two RCM simulations, both of which were driven by ARPEGE. According to the simulation of DA (HIRHAM5/ARPEGE), the extent of the CtS is projected to be twofold by T3 (compared to T1).

In T1, the WtDf can cover 3.3–5.6% of the target area depending on the RCM simulation (Fig. 3.3). The sign of the change is clear for this HLZ type; in T3, the WtDf may become a dominant biome type in the target area. However, in this case, the magnitude of changes is uncertain: 6 out

of 11 RCM simulations project that this HLZ type will cover 43–47.5% of the selected domain in the far future, while three RCM simulations estimate that its value will be 31–34% in T3. According to the EM, the extent of the WtDf can be fourfold in T2 compared to T1 (from 4.4 to 23.9%), while in T3 even 41.6% of the target domain may be covered by this HLZ type.

Appearance of two subtropical HLZ types, the SDf and SMf (subtropical moist forest), is estimated by nine and four RCM simulations, respectively, but their relative coverage will not exceed 0.5% together according to all projections (Fig. 3.3). Furthermore, all RCM simulations estimate that the BRf will disappear from the Carpathian Region by T3.

In T2, the relative extent of the CtMf is projected to be slightly less compared to T1 (this value for the EM is 61.6% in T1 and 50.7% in T2); the largest decrease (from 61.1 to 41.8%) is estimated by the simulation of EH (CLM2.4.6/HadCM3Q0), and the smallest (from 59.9 to 57.3%) by the simulation of DE. For T3, a further decrease is projected for this HLZ type: 6 out of 11 RCM simulations estimate that less than 35% of the target area will be covered by the CtMf. The minimal value (22.1%) of relative coverage for the CtMf is projected by the simulation of CH (maximal distributional change), while its maximal value (44.7%) is estimated by the simulation of DE (minimal distributional change) (Fig. 3.3).

Most of the RCM simulations (9 out of 11) project that the WtTs will appear in the Carpathian Region in T2 (Fig. 3.3); however, the spatial extent is less than 1% according to all projections, except the simulation of EH (1.8%). In T3, appearance of the WtTs is quite certain according to the projections. Its relative coverage is larger than in T2, it can exceed 10% according to the simulation of EH and HH (HadRM3Q0/HadCM3Q0), however this value for the EM is only 4.9%.

In Fig. 3.4, a transformation matrix from T1 to T3 is presented. Letters in the matrix above the main diagonal indicate shifts in climate from “wet” to “dry” and/or from “cold” to “warm” conditions. It is important to emphasize that 17 out of the 20 projected transformation types are above the main diagonal, hence drier and/or warmer climatic conditions are likely to occur in T3, generally. Four dominant HLZ transformations are expected. The proportion of area affected by the transformation g (from CtMf to CtS) is projected to be 7.1% according to the EM; while considering individual RCM simulations, this value is 0.8% minimally and 23.1% maximally. In the case of the transformation i (from CtMf to WtDf), the relative extent of the affected area can vary between 12.4 and 39.3%; however, according to 7 out of 11 RCM simulations, it can be reduced to the 21.5–26% interval. Considering the transformation m (from CtS to WtDf), the uncertainty is relatively high, as 4 out of 11 RCM simulations estimate that the relative coverage of the affected area is less than 10%, while 6 projections estimate that it is more than 15% (this value for the EM is 14.5%). Finally, the transformation n (from CtS to WtTs) is projected to be remarkable. According to the EM, the proportion of the affected area is 3.9%. Considering five RCM simulations, this value can vary between 0.6 and 1.7%, while taking into account all selected RCM simulations, it can be 0.6–12.3%. The CtS occurs in three cases out of these four emphasized transformations. The relative extent of the area affected by these transformations can vary widely. This underpins our former conclusion related to Fig. 3.3, namely the expected tendency in the coverage of the CtS is uncertain. The rest of the HLZ transformations affect less than 5% of the total area, individually.

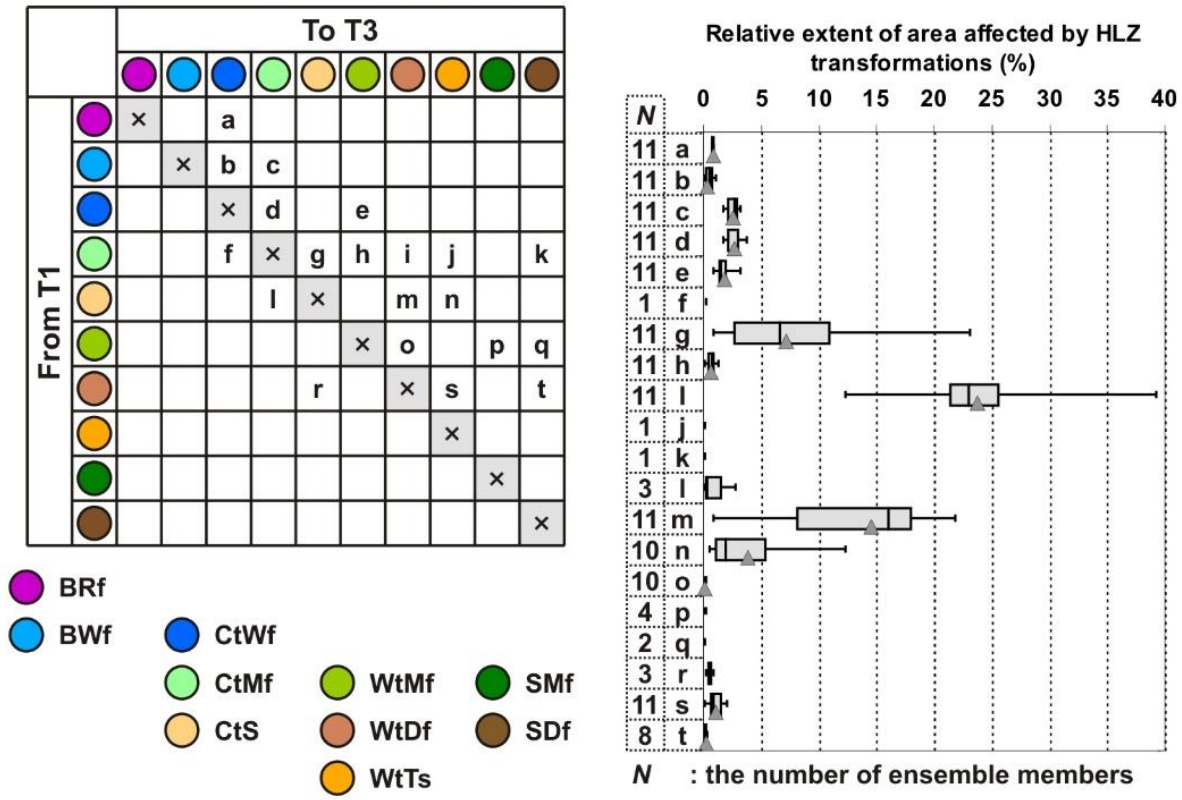

Fig. 3.4 Holdridge life zone (HLZ) transformations in the Carpathian Region from the period 1961–1990 (T1) to the period 2061–2090 (T3) considering all projections. On the left panel, the *letters* (a–t) in the matrix refer to those HLZ transformations which are indicated by at least one of the RCM simulations in the target area. On the right panel, the inter-model scatter in the relative extent of the area affected by these HLZ transformations is shown by box plots. The *triangle* refers to the ensemble mean (EM). The number of ensemble members is also indicated for each HLZ transformation. The abbreviations of HLZ types can be found in Fig. 3.3. At the bottom of the left panel, we can see that a certain HLZ type indicates a "warmer"/"colder" and/or "wetter"/"drier" climatic condition compared to other HLZ types. In this legend, humidity (thermal) characteristic is changing vertically (horizontally). The HLZ types in the uppermost (lowermost) row refer to the wettest (driest) climatic conditions on an annual basis, while in the first (last) column those HLZ types can be observed which indicate the coldest (warmest) conditions

3.3.2 Mean centres of HLZ types

The shift in the mean centre of each HLZ type is also analysed. Because of page limitations, only the shifts from T1 to T3 are assessed, basically. Taking into account that the mean centre of a given HLZ type does not necessarily fall into the domain of the respective HLZ type because of its fragmentation, therefore related maps are presented only in Appendix A.1. However, Fig. 3.5 shows the inter-model spread in the magnitude and direction of the shift only for those five HLZ types which can be observed in both T1 and T3. In order to plot directional data, the so-called circular box plots (Abuzaid et al. 2012) are used. From T1 to T3, the mean centres of the CtS and WtDf are likely to shift by 255.2 ± 92.5 and 278.5 ± 34.3 km, respectively (average ± standard deviation of the 11 RCM simulations). The magnitude of the shift can be remarkable for these HLZ types; however, the range of the projections is wide: the projected minimum–maximum change is 102–414 km in the case of the CtS and 214–333 km in the case of the WtDf. Here, it is also important to mention that the average distance between the easternmost and westernmost

points of the target area is 946 km. In the case of the CtWf, CtMf and WtMf, the expected magnitude of the shift is smaller than in the above-mentioned cases; they are 105.6 ± 19.3, 73.6 ± 20.2 and 57.3 ± 11.3 km, respectively. In the case of the WtMf and WtDf, the uncertainty of the shift direction can be small. From T1 to T3, the mean centre of the WtMf is likely to move to northeast, while for the WtDf, a northwestward shift is expected at the same time. The mean centres of the CtMf and CtS are projected to move to north and northeast, respectively, by 7 out of the 11 selected projections. Southward shift from east–west axis is shown by only two RCM simulation/HLZ type pairs.

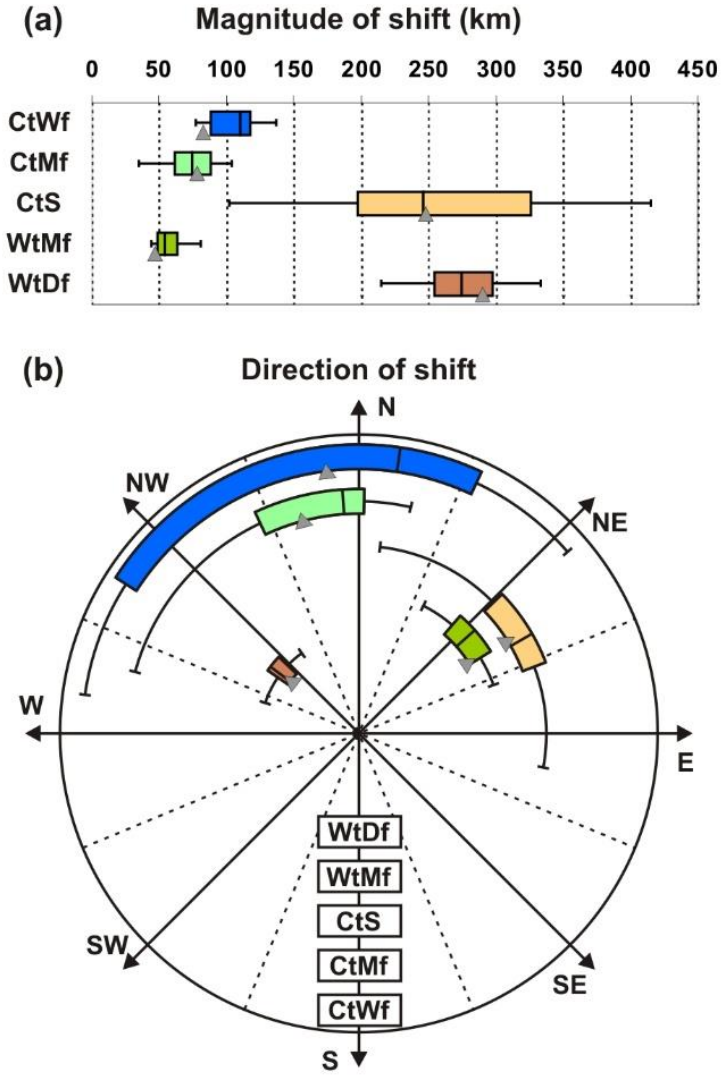

Fig. 3.5 Inter-model spread in the (**a**) magnitude and (**b**) direction of the shift of the mean centre of each Holdridge life zone (HLZ) type from the period 1961–1990 (T1) to the period 2061–2090 (T3) is shown by box plots. Shifts are presented only for those HLZ types which can be indicated by all RCM simulations in the target area in both time periods. Linear (circular) box plots are used for magnitude (directional) data. The *triangle* refers to the ensemble mean (EM). The abbreviations of HLZ types can be found in Fig. 3.3

Shift of the mean centre from T1 to T3 can be assessed only for the five above-mentioned HLZ types. In order to detect the expected tendencies of mean centre shifts for all HLZ types, trends in longitude and latitude coordinates of those mean centres which are calculated for each decade from 1951 to 2090 with a lag of 5 years are estimated (Fig. 3.6). A change in the latitude (longitude)

coordinate refers to a northward/southward (westward/eastward) shift. In the case of the CtWf, CtMf, CtS, WtMf and WtDf, the mean centre is estimated to shift northward according to most of the projections (9 out of 11 RCM simulations project a significant trend at least at a confidence level of 90%), which confirms our former results (Fig. 3.5). In the case of the WtDf, all RCM simulations estimate that the northward shift is significant at a confidence level of 95%. Almost all RCM simulations project a significant southward shift in the case of the BRf and BWf (the trend is significant according to nine RCM simulations at least at a confidence level of 90 and 80%, respectively). The mean centre of the WtTs is likely to move northward according to three RCM simulations at least at a confidence level of 90%. For the WtDf, a westward shift is estimated by all projections, which is significant at a confidence level of 95% according to nine RCM simulations. A westward (eastward) shift is expected also in the case of the BRf (BWf): nine RCM simulations project a significant increasing (decreasing) trend in the longitude coordinate at least at a confidence level of 90% (95%). In the case of the CtS and WtMf, an eastward shift is shown at least at a confidence level of 90%, by seven RCM simulations.

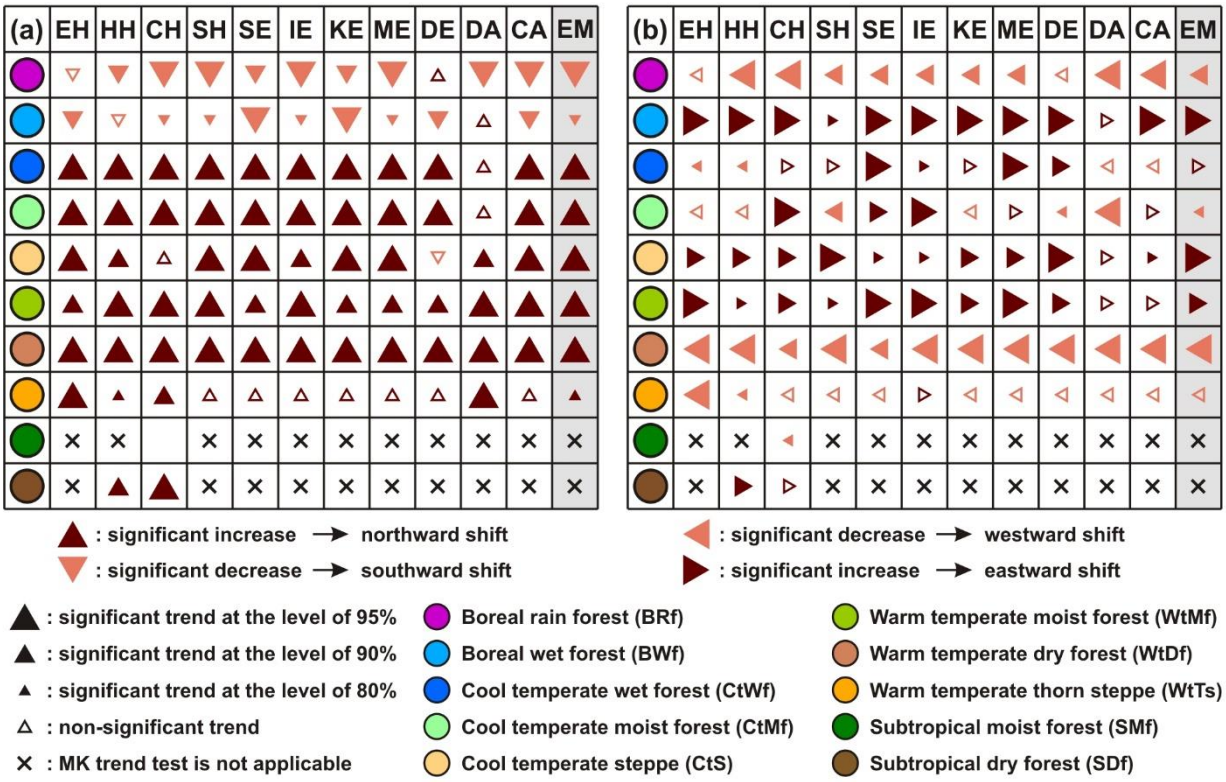

Fig. 3.6 Trends in the (**a**) latitude and (**b**) longitude coordinates of the mean centre of each Holdridge life zone (HLZ) type according to the selected RCM simulations (whose acronyms are listed in Table 3.1) and their ensemble mean (EM). On the left (right) panel, the uncertainty of northward/southward (westward/eastward) shifts is presented. A *larger filled triangle* means that the trend is significant at a higher confidence level. The *empty triangle* indicates a non-significant trend. In the case of *blank rubric* no trend could be detected. The *symbol* × refers to those cases where the Mann-Kendall (MK) trend test is not applicable

3.3.3 Altitudinal distribution pattern of HLZ types

In this subsection, the altitudinal distribution pattern of HLZ types is assessed. Figure 3.7 shows the altitudinal ranges of the HLZ types for T1, T2 and T3 according to the EM and the previously selected RCM simulations (DE, CH), which are identified using Kappa statistic (see Section 3.3.1).

Figure 3.7 confirms our former statement that the two boreal HLZ types (BRf, BWf) directly relate to mountainous areas in the study area. Based on the results of the highlighted projections, in the target area the BRf (BWf) cannot be detected in T1 below 1171 m a.s.l. (728 m a.s.l.). (These relatively low values are explained by the horizontal resolution and spatial averaging related to the applied digital elevation model, as we have indicated earlier.) In T1, the altitudinal range width (i.e., the difference between the maximum and minimum elevations) of the BRf (BWf) is 450.2 m (833 m) according to the EM; while in T2, this value is expected to be 154.9 m (390.6 m). So the results suggest that the altitudinal range width for the boreal HLZ types will probably be reduced; moreover, these HLZ types may even disappear in the far future, and they will be replaced by cool temperate forests (CtMf, CtWf) (Fig. 3.4). This kind of vegetation transformation is consistent with recently observed altitudinal vegetation shifts in undisturbed forests (e.g., Beckage et al. 2008). In parallel, the altitudinal range width is likely to increase in the case of the CtS, WtMf and WtDf. Namely, from T1 to T3, this value for the CtS, WtMf and WtDf is estimated to change from 447.1 to 807.4 m, from 204.8 to 699.7 m and from 365 to 819.8 m, respectively, based on the results of the EM (Fig. 3.7). In those cases, where shifts in the altitudinal midpoints can be detected from T1 to T2 or from T2 to T3, an upward shift can be observed as well, considering the three preselected projections. The lower altitudinal limit is expected to shift toward higher altitudes for all HLZ types, with the exception of the CH/CtS RCM simulation/HLZ type pair from T2 to T3. So the selected projections mostly agree on the direction of changes; however, there are substantial differences considering the details. Take for example the so-called altitudinal core ranges, which are identified by the 25th and 75th percentiles of elevations. In T3, for some HLZ types, the upper margins of the altitudinal core ranges highly vary depending on RCM simulation (DE, EM and CH, respectively): (a) 672.7 m, 797.7 m and 856.5 m a.s.l. for CtMf; (b) 464.4 m, 407.4 m and 819.4 m a.s.l. for CtS; and (c) 789.6 m, 789.6 m and 1001 m a.s.l. for WtMf.

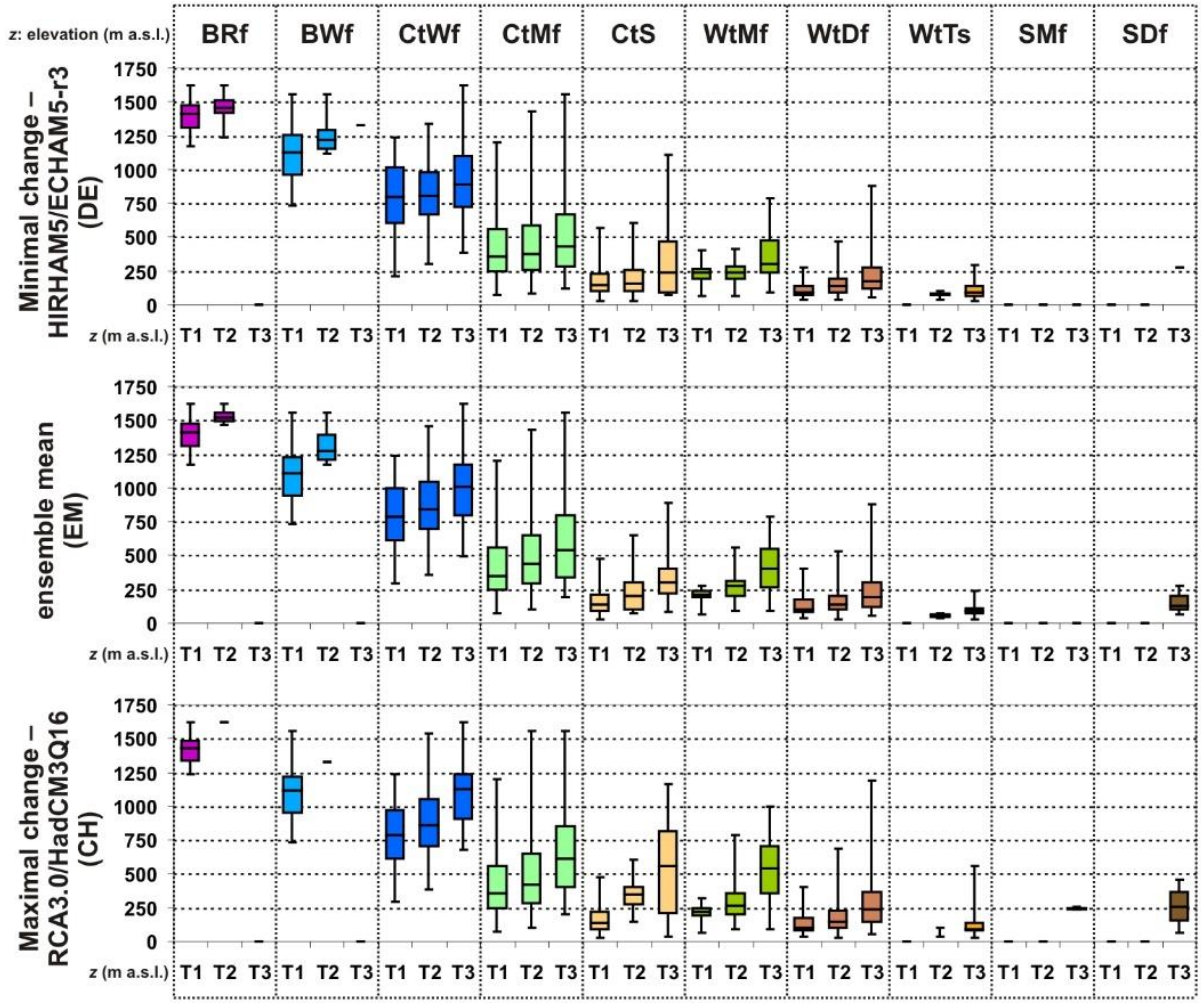

Fig. 3.7 Altitudinal distribution of Holdridge life zone (HLZ) types in the Carpathian Region for the periods 1961–1990 (T1), 2021–2050 (T2) and 2061–2090 (T3) according to the ensemble mean (EM) of the selected RCM simulations and those RCM simulations which provide the minimal (DE) and maximal (CH) distributional changes. The *box* indicates the so-called altitudinal core range (which is identified by the 25th and 75th percentiles of elevations), while the altitudinal midpoint (which is identified by the median) is shown as a *horizontal line in the box*. The *ends of the whiskers* indicate the lower and upper altitudinal limits (which are identified by the minimum and maximum of elevations). The abbreviations of HLZ types can be found in Fig. 3.6

As indicated by Fig. 3.7, the magnitude of shift in each altitudinal range is uncertain. So in the following, the ensemble range of the projected changes in three selected altitudinal points, namely the altitudinal midpoint, the lower and upper altitudinal limits, is examined, again for the five dominant HLZ types (Fig. 3.8). From T1 to T3, the altitudinal midpoints of the CtWf, CtMf, CtS, WtMf and WtDf are likely to move to higher altitudes by 180.1 ± 82.8, 212.1 ± 78.1, 167.7 ± 89.6, 160.4 ± 81.4 and 96.5 ± 24.7 m, respectively. The same values for the upper altitudinal limit are as follows: 387.7 ± 0, 360.9 ± 6.3, 420 ± 173.3, 524.5 ± 127.4 and 501.3 ± 153 m, respectively. So generally, increases for the upper altitudinal limit are expected to be greater than for the altitudinal midpoint. However, the range of the projections is very wide for some HLZ types, similar to the above analysed spatial parameters. For example, the projected minimum–maximum values of shift in the upper altitudinal limit for the CtS, WtMf and WtDf are 182.1–719.9 m, 290.9–683.2 m and 289.2–787.1 m, respectively. Furthermore, the lower altitudinal limits are likely to

shift toward higher elevations, but these shifts cannot be greater than 200 m, except in the case of the CtWf. From T1 to T3, the lower altitudinal limit for this HLZ type will be shift upward by 263.4 ± 68.6 m. Moreover, the upper altitudinal limit of the WtDf can either move to lower altitudes according to one projection (IE: RegCM3/ECHAM5-r3).

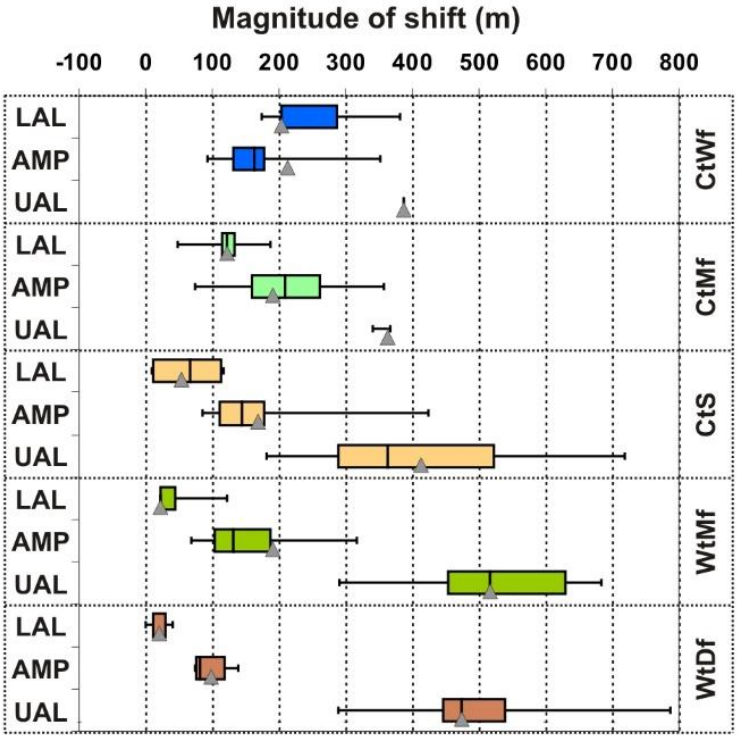

Fig. 3.8 Inter-model spread in the shift of the selected altitudinal points (LAL: lower altitudinal limit, AMP: altitudinal midpoint, UAL: upper altitudinal limit) of each Holdridge life zone (HLZ) type from the period 1961–1990 (T1) to the period 2061–2090 (T3) is shown by box plots. The value of the ensemble mean (EM) is denoted by a *triangle*. Changes are presented only for those HLZ types which can be indicated by all RCM simulations in the target area in both time periods. The abbreviations of HLZ types can be found in Fig. 3.6

3.4 Discussion

Shifts in spatial and altitudinal distribution of HLZ types are determined by the spatial and temporal changes in bioclimatic indices (*ABT*, *APP*, *PER*) of the HLZ system. It is important to note that the applied version of the HLZ system cannot identify the so-called ecotones (transitional zones); hence, main biome types (e.g., forest and steppe) are separated by sharp boundaries which are assigned not empirical limits of climatic variables. Contrary to most biome models, the HLZ system does not focus on thresholds describing boundaries among biome types, hence it classifies based on the distance from the ideal (theoretical) point in the 3-dimensional space of bioclimatic indices (see Yue et al. 2001). Therefore, the model may react extremely sensitively to relative slight changes of the indices inside of the so-called transitional zones. We would like to emphasize that in accordance with the recently observed changes (Szelepcsényi et al. 2014a), the coverage of transitional zones can increase in the target domain (from T1 to T3, from 28.7 ± 0.9 to 38.1 ± 4.4%), which can adversely affect the robustness of modelling results. Furthermore, it is

important to note that the validity of our results is limited because the HLZ system omits seasonal changes in the climatic variables.

3.4.1 Latitudinal and longitudinal range shifts of HLZ types

The results of Pongrácz et al. (2011) indicate that the mean annual temperature is likely to increase by 2–5 ºC for the end of the twenty-first century in the target area. In accordance with this, in the whole Carpathian Region, a significant increasing trend of the *ABT* can be detected in the future (not shown), which implies that the climate will be warmer on an annual basis. This significant temperature rise, in accordance with former simulation results (e.g., Sykes and Prentice 1996; Hickler et al. 2012), may induce a northward shift of climatically determined ecosystem types (Fig. 3.6a).

Pongrácz et al. (2011) have also shown, considering spatial averages, that the precipitation sum will decrease in summer and increase in winter in the Carpathian Region according to the projections; however, considering the value of *APP*, the simulated changes are uncertain and non-significant. In the case of the *APP* and *PER*, which indicate humidity conditions, the uncertainty is quite high, considering both temporal variability and inter-model scatter. Signs of the changes in *APP* are estimated to be different basically in the southern and northern segments of the target domain; in the southern (northern) regions 2–3 (2–4) RCM simulations project a significant decreasing (increasing) trend of the *APP* (not shown). Uncertainty in the projected humidity conditions combined with the modelling approach used in the HLZ system and the complex topography of the study region induce jointly that depending on the RCM simulation, (mostly non-significant) trends are estimated with opposite signs in the case of the westward/eastward shift of the CtWf, CtMf and WtTs (Fig. 3.6b).

Those HLZ types which are adapted to cooler and wetter conditions (e.g., the BRf and BWf) probably occur in patches (mostly in the mountains), due to the topography of the selected domain. While the projected warming and drying affect the mountains in the Carpathian Region with dissimilar intensity according to the applied RCM simulations (see Pongrácz et al. 2011), patches of these HLZ types may shrink by different magnitudes; furthermore, these patches can disappear at different times (e.g., Fig. 3.2). So, for example, a significant eastward shift of the BWf (Fig. 3.6b) can be explained by that its areal extension may shrink faster in the Northwestern Carpathians than in the Eastern and Southern Carpathians; moreover, the applied RCM simulations project its disappearance earlier from the Northwestern Carpathians than from the Eastern and Southern Carpathians.

Westward/eastward shifts of those HLZ types which are not related to mountains are clearly associated with the projected expansion of the WtDf. The estimated spread of the WtDf can be explained by that the value of *ABT* may increase substantially in the plain areas located along a northwest–southeast transect, forming appropriate conditions for that HLZ type which favours drier and warmer conditions. Parallel with the expansion of the WtDf, the CtWf and CtS may shift from the centre of plain areas to the edge of the selected domain (e.g., Fig. 3.2). By the end of the twenty-first century, the CtS may totally disappear from the western regions of the target area (lowland regions between the Central Alps and the Northwestern Carpathians and the Great Hungarian Plain), which explains its significant eastward shift (Fig. 3.6b). In the case of the CtWf, mostly another type of adaptation strategies, the vertical (upward) migration is estimated by the applied RCM simulations (Fig. A.2).

3.4.2 Altitudinal range shifts of HLZ types

According to the EM and the preselected RCM simulations (DE, CH), the altitudinal range width of HLZ types will probably increase, except in the case of boreal HLZ types (BRf, BWf) (Fig. 3.7). The results suggest that the lower and upper altitudinal limits as well as the altitudinal midpoints are likely to move to higher elevations for most HLZ types (Fig. 3.8 and Fig. A.2). The upward shift of woody plants is usually linked to the temperature increase (e.g., Kullman 2001; Peñuelas and Boada 2003). This statement is confirmed by the fact that the upper forest limit is determined by temperature basically; hence, here, the warming usually creates more favourable abiotic conditions for trees and improves the succession processes (Körner 2012).

In the target domain, a similar reaction of vegetation has already been observed under recent climate change: Martazinova et al. (2011) in the Ukrainian Carpathians and Treml and Chuman (2015) in the Sudetes have detected that the treeline advanced upward at a rate of 0.5 and 0.3–0.43 m year^{-1}, respectively, during the last century. They found these altitudinal shifts are associated with observed temperature changes. Nevertheless, it is important to emphasize the main conclusions of Harsch et al. (2009): (a) the air temperature is not the only factor which determines the position of treeline (and so woody plant), as the direct effects of temperature can be hidden by interactions with other factors (e.g., precipitation, disturbance, plant–plant interactions); (b) but it is possible that vegetation response lags behind, or it appears only if warming exceeds a certain threshold. Considering these aspects, our results can be accepted only as a first guess.

Furthermore, we would like to highlight once again that the horizontal resolution of the applied database is relative "coarse" for the mountainous areas, so this can have a certain degree of distortive effect on our results, especially those relating to the upper altitudinal limit. Hence, in our opinion, it is advisable to compare our results to such outcomes, which have similar spatial resolution (~25 km).

3.4.3 Harmful effects of climate change on boreal forests

Our results, which are in accordance with other simulation results (e.g., Sykes et al. 1996; Hickler et al. 2012), indicate that projected changes may have remarkable effects on boreal HLZ types. The relative coverage of these ecosystem types can be substantially reduced; moreover, they can even disappear from the target area (Fig. 3.3). Since the estimated temperature is too high for these HLZ types both in the northernmost and highest points of the target domain, these vegetation types neither with a northward shift (Fig. 3.6a), nor with an upward shift (Fig. 3.7) can response to the possible temperature increase. Furthermore, their adaptation is more difficult, because they already cover only a small area fragmentally (Fig. 3.2).

However, we could not take into consideration in our investigation, but our results are modulated by the fact that the longer growing period and decreasing frequency and severity of frost events are favourable for broad-leaved species (temperate forest), thus giving them a competitive advantage over coniferous species (boreal/alpine forest) (Woodward 1987). Nevertheless, because a correlative model is used in this study, we could not take into consideration that the decreased resistance to insects and the recurrent wildfires may further worsen living conditions of boreal tree species at the lower/southern boundaries of their distribution (Fischlin et al. 2009).

3.4.4 Magnitudes of projected range shifts of HLZ types

Effects of projected alterations can be assessed by comparing them to historical changes. Hence, in the followings magnitude of changes in coverage and shifts in central tendencies (mean centre and altitudinal midpoint) are compared to the results of Szelepcsényi et al. (2014a, b) referring to the twentieth century (however, the current and former investigations' target domains are not identical). So in order to compare the results of these studies, the velocity of changes (changes in extension, shifts in mean centre and altitudinal midpoints) is determined.

Assuming linear shifts (see Treml and Chuman 2015), the velocities are calculated by a two-step procedure for each study: (i) a shift in the given spatial parameter is determined as the difference between the first and last periods and then (ii) this value is divided by the difference between those numbers which label the given time periods. The number, which labels the selected time period, is calculated by the median of the years of the time period; if the number of years is even, we round it down to the nearest integer. In the investigations of Szelepcsényi et al. (2014a, b), the first (last) period is the period 1901–1920 (1980–2000); while in this study, velocities are calculated as differences between T1 and T3.

Comparison can be done only for cool (CtWf, CtMf, CtS) and warm (WtMf, WtDf) temperate HLZ types. Results based on the observational database are basically compared to the EM; however, in the case of the mean centre and the altitudinal midpoint (in the following paragraphs), the minimum and maximum of the projected changes, considering all RCM simulations, are also shown in brackets.

In the last century, extensions of the WtMf and WtDf increased at a rate of 44 and 894 $km^2\ year^{-1}$; while in the future, these rates can be 179 and 2815 $km^2\ year^{-1}$ according to the EM (Fig. 3.2). So the expansion of these HLZ types can be 3–4 times as fast as in the past. Areas of the CtWf and CtMf declined at a rate of 205 and 797 $km^2\ year^{-1}$ over the twentieth century. According to the applied RCM simulations, these downward trends probably will not be reversed. In the future, according to 8 out of the 11 selected RCM simulations, the velocity of area loss of the CtMf can exceed twice the value observed in the past (1594 $km^2\ year^{-1}$). In addition, based on the results of six RCM simulations, the coverage of the CtWf can reduce in the future at least at a rate which is observed over the last century (Fig. 3.3). The extension of the CtS decreased at a rate of 328 $km^2\ year^{-1}$ in the last century; it can reduce at a rate of 852 $km^2\ year^{-1}$ according to the EM (Fig. 3.2). However, the uncertainty of the simulations is quite high (Fig. 3.3): the area of this HLZ type is estimated to increase at a rate of ~1600 $km^2\ year^{-1}$ (DA), while a reducing trend by a similar magnitude can also occur (SE: RCA3.0/ECHAM5-r3).

The mean centres of the CtWf, CtMf, CtS and WtDf are shifted at a rate of 0.32, 0.29, 1.66 and 0.41 km $year^{-1}$, respectively, in the Carpathian Region during the twentieth century. In the future, these values are projected to be 0.83 km $year^{-1}$ (0.77–1.37 km $year^{-1}$), 0.78 km $year^{-1}$ (0.35–1.04 km $year^{-1}$), 2.48 km $year^{-1}$ (1.02–4.15 km $year^{-1}$) and 2.9 km $year^{-1}$ (2.14–3.33 km $year^{-1}$), respectively (Fig. 3.5). Thus, for most HLZ types, the velocities of the future mean centre shifts are estimated to be 1.5–2.5 times as large as in the past, according to the EM. In the case of the WtDf, a drastic velocity increase is expected: according to 10 out of the 11 selected RCM simulations, its mean centre probably shifts at a rate six times larger than the historical value for this HLZ type. A decrease in the magnitude of the mean centre shift can occur only in the case of the WtMf; its rate, which was 1.13 km $year^{-1}$ in the past century, can be declined in the future (0.44–0.81 km $year^{-1}$) (Fig. 3.5).

During the twentieth century, the altitudinal midpoints of the CtMf, CtS and WtDf shifted to higher elevations at a rate of 0.51, 0.46 and 0.24 m year^{-1}, respectively. According to the selected projections, the rates of this vertical (upward) shift are projected to be 1.9 m year^{-1} (0.75–3.57 m year^{-1}), 1.68 m year^{-1} (0.85–4.25 m year^{-1}) and 0.98 m year^{-1} (0.75–1.39 m year^{-1}), respectively (Fig. 3.8). Besides the clear (increasing) trend, it can be seen that the uncertainty in the magnitude of these changes is quite high. This uncertainty is confirmed by inter-model differences (the difference between the minimum and maximum rates), which are usually larger than the absolute values of the rate for EM, except in the case of the WtDf. However, it is important to note that according to the EM, projected future changes can be 3.5–4 times as fast as in the last century, in the case of the three preselected HLZ types. Over the last century, decreasing tendency for the altitudinal midpoint can be recognized only in the case of the WtMf; it can be reversed in the future, this HLZ type can move toward higher elevations at a rate of 1.9 m year^{-1} (0.69–3.17 m year^{-1}) (Fig. 3.8).

3.5 Conclusions

In this paper, Holdridge life zone (HLZ) types of the Carpathian Region were analysed by using 11 bias-corrected RCM simulations of temperature and precipitation from the ENSEMBLES project. Our investigations focused on the spatial and altitudinal distribution patterns of HLZ types. Parameters describing distribution patterns of HLZ types were determined for three 30-year long time periods (T1: 1961–1990; T2: 2021–2050; T3: 2061–2090) and also for 28 decades. Simulations, which provide the maximal and minimal distributional changes, were selected by using Kappa statistics. The sign and the uncertainty of the projected changes are analysed by using the modified Mann-Kendall test for the parameters of spatial and altitudinal distribution referring to decades.

The results show that the dominant HLZ type is the CtMf in the Carpathian Region in T1. The applied RCM simulations project that this dominancy for T3 can be reduced; furthermore, spatial distribution patterns of HLZ types can be modified substantially. The boreal HLZ types (BRf, BWf) are estimated to disappear from the region, whereas the WtTs and SDf can appear, which can be found nowadays, for example, in Spain and Turkey (Leemans 1990; Tatli and Dalfes 2016). The relative extent of humid (CtMf, WtMf, SMf) and perhumid (BWf, CtWf) HLZ types is projected to decrease by 41 ± 12 and 58 ± 13% from T1 to T3, respectively. The relative coverage of warm temperate HLZ types (WtMf, WtDf, WtTs) in T3 can be estimated to be 10 times as much as in T1, while in the case of cool temperate HLZ types (CtWf, CtMf, CtS), the same value can be reduced by one or two thirds from T1 to T3. The recently detected increasing temperature trend is likely to continue in the future in the target area (see Pongrácz et al. 2011), for which as a response, northward and/or upward shifts of biome types are estimated. So according to the applied RCM simulations, the lower and upper altitudinal limits and also the altitudinal midpoints of HLZ types are likely to move to higher altitudes; furthermore, most of the HLZ types are estimated to shift northward in the Carpathian Region. Considering the magnitude of the projected changes, the uncertainty is quite high. However, comparing the recently observed changes of parameters describing spatial and altitudinal distribution patterns, future shifts are likely to be remarkable. It is also important to note that the projected migration rate of HLZ types is larger than the currently estimated migration ability of trees (e.g., see Huntley and Birks 1983; Treml and Chuman 2015). The east–west-oriented mountain chains in Europe (e.g., the Alps, the Carpathians) represent

barriers for north/south migration of species and biomes, so for this reason and because of anthropogenic disturbances, this kind of adaptation strategy of vegetation can hardly be observed in nature (Jump et al. 2009). Eventually, worsening local climatic conditions induce mainly an increase of mortality and/or the alteration of species composition in particular ecosystems (e.g., see Fischlin et al. 2009; Allen et al. 2010b).

To conclude, the effect of possible climate change on potential vegetation in the Carpathian Region could be well presented by using the HLZ system. However, it is important to remark that besides the mentioned cautions of de Castro et al. (2007), our investigation could take into account neither direct effects of CO_2 on growth and water use efficiency of plants (van de Geijn and Goudriaan 1996), nor effects of expected seasonal changes in heat and water fluxes. Nevertheless, we think that our assessment can be an appropriate base for the following impact studies: (a) assessing expected changes in climatic suitability for agricultural production (see Ewel 1999), (b) estimating economic costs of climate change impacts on protected areas (e.g., Velarde et al. 2005) and (c) other investigations applying landscape metrics (e.g., Yue et al. 2001, 2006). In addition, hopefully in the near future, there will be an opportunity to prepare a strategy for sustainable forest management in our region, which takes into account possible responses of not only different forestry climate categories and main forest-forming species (e.g., Führer et al. 2011; Rasztovits et al. 2012), but also of various biome/HLZ types to projected climate change, in order to resolve some scale-dependent problems.

Acknowledgments. This research was supported by the European Union and the State of Hungary, co-financed by the European Social Fund in the framework of TÁMOP 4.2.4. A/2-11-1-2012-0001 'National Excellence Program'. The ENSEMBLES dataset used in this work was funded by the EU FP6 Integrated Project ENSEMBLES (Contract number 505539), whose support is gratefully acknowledged. We acknowledge the E-OBS dataset from the EU FP6 project ENSEMBLES (http://ensembles-eu.metoffice.com) and the data providers in the ECA&D project (http://www.ecad.eu). We are really grateful for János Geiger (University of Szeged, Hungary) for his valuable advices in the trend analysis. We would like to thank Ágnes Havasi (Eötvös Loránd University, Hungary) for careful proof reading of the manuscript. Finally, we gratefully thank the anonymous reviewers for their valuable suggestions and constructive comments that helped us to improve the quality of the manuscript.

4 Estimating relative sunshine duration from commonly available meteorological variables for simulating biome distribution in the Carpathian Region

Manuscript published in the *Hungarian Geographical Bulletin*
Volume 71, Issue 1, 3–19 (2022)
DOI: 10.15201/hungeobull.71.1.1

Authors:

Zoltán Szelepcsényi
Institute of Archaeology
Research Centre for the Humanities
Eötvös Loránd Research Network, Hungary

Hajnalka Breuer
Department of Meteorology
Eötvös Loránd University, Hungary

Nándor Fodor
Agricultural Institute
Centre for Agricultural Research
Eötvös Loránd Research Network, Hungary

Abstract. Bright sunshine duration (BSD) data are required for simulating biomes using process-based vegetation models. However, monthly global paleoclimate datasets that can be used in paleo data–model comparisons do not necessarily contain BSD or radiation data. Considering the theoretical and practical aspects, the scheme of Yin (Theor. Appl. Climatol. 64(1–2):61–68, 1999) is here recommended to estimate monthly time series of relative BSD using only monthly climate and location data. As a case study for the Carpathian Region, the efficiency of both the original and a variant of that scheme is analysed in this paper. The alternative scheme has high applicability in paleoenvironmental studies. Comparison of the estimated and observed BSD data shows that from May to August, the value of relative root mean squared error in more than 90% of the study area does not exceed the threshold of 20%, indicating an excellent performance of the original estimation scheme. It is also found that though the magnitude of overestimation for the alternative algorithm is significant in the winter period, the proposed method performs similarly well in the growing season as the original. Furthermore, concerning modelling the distribution of biomes, simulation experiments are performed to assess the effects of modifying some configuration settings: (a) the generation of relative BSD data, and (b) the algorithm used to create quasi-daily weather data from the monthly values. Under both the recent humidity conditions of the study region and the spatial resolution of the climate dataset used, the results can be considered sufficiently robust, regardless of the configuration settings tested. Thus, using monthly temperature and precipitation climatologies, the spatial distribution of biomes can be properly simulated with the configuration settings proposed here.

Keywords: sunshine duration, water balance, biome, plant functional types, data–model comparisons, CarpatClim

4.1 Introduction

Today there are a number of tools available to translate climate model outputs into vegetation distribution patterns (see e.g., bioclimatic classification methods: Prentice 1990; correlative vs. mechanistic biome models: Yates et al. 2000; species distribution models: Elith and Leathwick 2009). Bioclimatic classification methods (BCMs) are tools used to transform a set of climate and soil variables into an index-class that can be directly related to biome-level vegetation units (Tapiador et al. 2019). Correlative models determine a statistical relationship between vegetation distribution and environmental variables (e.g., climate, soil, etc.); then this link is applied to simulate the potential distribution of vegetation under the altered conditions (Yates et al. 2000; Elith and Leathwick 2009). From this point of view therefore, BCMs (e.g., Köppen 1936) can be considered the simplest correlative biome models. Mechanistic biome models, in contrast, focus on mechanisms determining survival and performance of plants by simulating processes in soil–vegetation–atmosphere systems, such as water, carbon and nutrient cycles (Prentice et al. 2007).

Paleoclimatological and paleoenvironmental studies often use both outputs from climate model simulations and proxy archives, such as fossil pollen records, in a common framework. These studies represent a special area of called paleo data–model comparisons (Harrison 2013) that have essentially two distinct purposes: (a) to understand the mechanisms of past climate and environmental shifts (e.g., Miller et al. 2008; Mauri et al. 2014), and (b) to provide feedback on the performance of climate/environmental reconstruction approaches (e.g., Prentice et al. 1998; Webb et al. 1998). These comparisons can be made in two ways, either by collating pollen-inferred climate with that simulated by climate models (e.g., Webb et al. 1998; Mauri et al. 2014), or by comparing biome/species distribution estimated using paleoclimate model outputs with vegetation reconstructed from pollen assemblages (e.g., Prentice et al. 1998; Miller et al. 2008).

Currently, more and more global datasets are made publicly available that provide bias-corrected monthly climatologies (multi-year averages) from paleoclimate simulations, in order to support distribution modelling experiments in various research areas (e.g., paleobiogeography, archaeology). However, these datasets differ significantly in terms of spatial resolution, temporal coverage and time step, and in terms of which climate variables they contain information on. Beyer et al. (2020), for example, published a monthly global dataset (hereinafter HadCM3-120k), with a horizontal resolution of 0.5°, for temperature, precipitation, cloud cover, relative humidity, and wind speed, and additional parameters related to bioclimatic and biogeochemical conditions, covering the last 120,000 years at a temporal resolution of 1,000–2,000 years. For this, medium-resolution simulations generated by the HadCM3 general circulation model (GCM) for the last 120,000 years were combined with high-resolution simulations prepared by the HadAM3H GCM for the last 21,000 years, and a recent observational dataset. (For details of the above-mentioned GCMs, see Valdes et al. 2017.) Then, Krapp et al. (2021) extended access to the climate variables in question for the last 800,000 years by performing a statistical-based reconstruction using the above-mentioned simulations. And recently, Karger et al. (in review) shared with the scientific community their dataset, called CHELSA-TraCE21k v1.0, that includes monthly climatologies for both temperature and precipitation, and other bioclimatic variables, with a spatial resolution of 30 arc-sec at a 100-year time step for the last 21,000 years. For this, a transient simulation generated by the CCSM3 GCM (He 2011) was downscaled considering the temporal change of orography.

The HadCM3-120k was specifically generated to feed mechanistic biome models, while the CHELSA-TraCE21k v1.0 was clearly developed to support paleoecological studies using

correlative species distribution models (SDMs). In SDMs (e.g., MaxEnt: Phillips et al. 2006), bioclimatic variables, i.e., annual and seasonal measures derived from monthly values of temperature and precipitation, are generally used as environmental predictors, besides topographic variables. In contrast, due to the simulation of energy and water fluxes, for applying mechanistic biome models, a meteorological variable directly related to radiation (e.g., cloud cover, sunshine duration) is also required, besides temperature and precipitation data. Beyer et al. (2020) and Krapp et al. (2021), relying on their own datasets, also estimated the evolution of the global biome distribution using one of the best-known mechanistic biome models, called BIOME4 (Kaplan 2001). The BIOME*n* models (e.g., BIOME: Prentice et al. 1992; BIOME4) estimate the net radiation as a function of latitude, temperature, and bright sunshine duration (BSD). Thus, to apply the above-mentioned vegetation model to their own datasets, the authors used different empirical linear relationships (Doorenbos and Pruitt 1977; Hoyt 1977) to convert cloud cover data to the percentage of possible sunshine hours. Unfortunately, the CHELSA-TraCE21k v1.0 does not contain cloudiness or BSD data, so it is not directly suitable for feeding the above-mentioned BIOME*n* models. However, estimating BSD data from commonly available meteorological variables may be a solution to overcome the lack of data.

Although there are several estimation methods for calculating monthly values of BSD (see Kandirmaz et al. 2014), in this study, the use of a method developed by Yin (1999) is recommended. Yin (1999) used monthly data of 729 worldwide stations for finding a generic algorithm that captures global variability of BSD data in relation to temperature, precipitation, and geographic location. Regression models for estimating monthly mean daily values of BSD are usually set only for smaller regions due to limited access to reliable station data (e.g., Italy: Stanghellini 1981), and/or use parameters that are not readily available from global gridded climate datasets (e.g., the number of wet days per month: Castellvi 2001). Thus, what makes the method proposed by Yin (1999) special is that it is globally parameterized and uses only monthly climate and location data that are widely available.

To our knowledge, by means of gridded climate datasets, the performance of the estimation scheme proposed by Yin (1999) has not yet been evaluated. Our current level of knowledge would indicate that there is currently no global gridded observational dataset to which the following three statements are true without exception: (i) it contains monthly values for BSD, temperature, and precipitation; (ii) it contains monthly meteorological data for a long period without time averaging; and (iii) it was developed based on station observations. Currently, there is only access to global datasets that also use remotely sensed and reanalysis data to produce gridded climate information, and for which values of BSD can only be derived from another meteorological variable (e.g., incoming solar radiation: TerraClimate, Abatzoglou et al. 2018; cloud cover: CRU TS v4, Harris et al. 2020). However, two regional climate databases are known that provide station-based meteorological fields for the above-mentioned three variables, for continuous periods: CarpatClim (Spinoni et al. 2015) and HadUK-Grid (Hollis et al. 2019).

In consideration of the literature discussed above, the first objective of this study is to assess the accuracy of the scheme under discussion using the monthly climate data provided by the CarpatClim dataset. The second goal of this paper is to test how the quality of estimates changes as a result of proposed modifications of the approach, which are justified by its applicability in paleoenvironmental studies. The amount of incoming and outgoing radiation influences the growing conditions of plants, so the error in estimating the relative BSD can cause problems in the modelling of the biome distribution. Therefore, as a case study for the Carpathian Region,

evaluation of the impact of the estimated relative BSD on simulation of energy and water fluxes and biome designation is the third aim of this study.

4.2 Materials and methods

4.2.1 Estimation of monthly mean relative sunshine duration

The monthly mean daily values of relative BSD (*RSD*, dimensionless) for a given month is estimated using the following parametric regression model as recommended by Yin (1999):

$$RSD = e^{\left[-1.65 \cdot p \cdot f_o \cdot \left(1+\sum f_i\right)\right]}, \tag{4.1}$$

with

$$f_o = f\left(R_E\right) \cdot f\left(P\right) \cdot f\left(T, E_p\right) \cdot f\left(\phi\right), \tag{4.2}$$

where

$$f\left(R_E\right) = \left[1 + 0.756 \cdot R_E \cdot \left(3 - R_E\right)\right]^{-1}, \tag{4.3}$$

$$f\left(P\right) = \frac{1 + 0.785 \cdot P}{1 + 0.222 \cdot P}, \tag{4.4}$$

$$f\left(T, E_P\right) = 1 + \frac{\left(7.66 \cdot I_{T<0} - 4.98\right) \cdot T + {E_P}^2}{184}, \tag{4.5}$$

$$f\left(\phi\right) = 1 + 0.512 \cdot \sin\left(\frac{\left(\phi + 15\right) \cdot 2\pi}{77}\right), \tag{4.6}$$

and

$$f_i = \begin{cases} \dfrac{15.6 - T_{am}}{46.3}, & \text{if island or Australia} \\ 0.331 - 0.213 \cdot E_{pam} - \dfrac{\left|T_{am}\right|}{72.5} + \dfrac{\max\left(T_{\min}, 0\right)}{30}, & \text{if North America} \\ 0, & \text{if South America} \\ \dfrac{1}{10.2} + \dfrac{P_7 - P_1}{36.8 \cdot P_{am}} \cdot \left(2.3 - \dfrac{P_7 - P_1}{P_{am}}\right), & \text{if Eurasia} \\ -0.643 + 0.314 R_E + \left(31.8 - T_{am}\right) \cdot \left(\dfrac{T_{am}}{140}\right)^2, & \text{if monsoonal Asia} \\ \dfrac{7.26 - T_{ar}}{32.3}, & \text{if Africa} \end{cases}, \tag{4.7}$$

where p is the station atmospheric pressure in relation to the pressure at sea level, f_o represents global trends, f_i gives regional modifications, $\sum f_i$ is the summation of values of any regional functions that are applicable to a particular location, R_E is the monthly average of hourly solar irradiance for cloudless-sky conditions (in MJ m^{-2} hr^{-1}), P is the monthly mean precipitation intensity (in mm dy^{-1}), T is the monthly mean air temperature (in °C), E_P is the monthly average of daily potential evapotranspiration (in mm dy^{-1}), ϕ is the latitude (in decimal degrees), $I_{T<0}$ is a temperature indicator (1 if $T \leq 0$ °C, and 0 if $T > 0$ °C), T_{am} is the annual mean temperature (in °C), E_{Pam} is the annual average of daily potential evapotranspiration (in mm dy^{-1}), T_{min} is the lowest monthly mean air temperature (in °C), P_7 is the monthly mean precipitation intensity (in mm dy^{-1}) in the warmest month (fixed at July for the Northern Hemisphere, and January for the Southern Hemisphere), P_1 is the monthly mean precipitation intensity (in mm dy^{-1}) in the coldest month (fixed at January for the Northern Hemisphere, and July for the Southern Hemisphere), P_{am} is the

annual mean precipitation intensity (in mm dy^{-1}), T_{ar} is the annual range of monthly mean air temperature (annual diurnal range) (in °C).

The values of R_E are calculated as proposed by Yin (1997a), with a minor modification, using the daytime means of optical air mass and cosine zenith. The former is computed as recommended by Yin (1997a), while the latter is estimated by using Eq. 5 of Yin (1997b). Furthermore, in contrast to the original approach, where the solar constant was fixed at 4.9212 MJ m^{-2} hr^{-1}, its value is corrected, according to Yin (1999), by calendar day for the variable ellipticity of the Earth's orbit using the scheme of Brock (1981). In these calculations, the values of solar declination and daylength are derived by using the approach of Brock (1981). The values of E_P are computed using Eq. A10 of Yin (1998). The value of E_{Pam} is calculated as a weighted mean of the E_P values using the number of days in months as weights.

4.2.2 Simulation of biome distribution

In this study, the BIOME model (Prentice et al. 1992) is applied to simulate the spatial distribution of biome-level vegetation units. First, the presence of each plant functional type (PFT) that is a group of plant types with similar ecophysiological behaviour is estimated under given climatic conditions. To do this, it is necessary to check which of the 14 PFTs defined can occur considering the environmental constraints associated with their climatic tolerances and requirements (Table 4.1). After this, the dominance class value (D) of each PFT is examined and only those in the highest class (with lowest D) present are retained. Finally, to infer the biome type, retained PFTs are combined with each other by taking into account rules formalized in Table 4.2.

Table 4.1 Dominance class (D) and environmental constraints (mean temperature of the coldest month, T_C (in °C), growing degree-days above a 5 °C base, GDD_5 (in °C day), growing degree-days above a 0 °C base, GDD_0 (in °C day), mean temperature of the warmest month, T_W (in °C), and Priestley–Taylor coefficient at an annual time scale, α (dimensionless)) for each plant functional type used in the model

Abbr.	Plant functional type	D	T_C		GDD_0	GDD_5	T_W	α	
			min	max	min	min	min	min	max
tr.e.t	tropical evergreen tree	1	15.5					0.80	
tr.r.t	tropical raingreen tree	1	15.5					0.45	0.95
w-te.e.t	warm temperate evergreen tree	2	5.0					0.65	
te.s.t	temperate summergreen tree	3	−15.0	15.5		1200		0.65	
c-te.c.t	cool temperate conifer tree	3	−19.0	5.0		900		0.65	
bo.e.t	boreal evergreen conifer tree	3	−35.0	−2.0		350		0.75	
bo.s.t	boreal summergreen tree	3		5.0		350		0.65	
sb.suc	sclerophyll/succulent	4	5.0					0.28	
wa.g.s	warm grass/shrub	5					22	0.18	
cl.g.s	cool grass/shrub	6				500		0.33	
cd.g.s	cold grass/shrub	6			100			0.33	
h.d.s	hot desert shrub	7					22		
c.d.s	cold desert shrub	8			100				
p.d	polar desert	9							

Table 4.2 A list of biome types used in the model and their generation rules. Each biome type is arising as a combination of dominant plant functional types

Abbr.	Biome type	Plant functional types
TRRA	Tropical rain forest	tr.e.t
TRSE	Tropical seasonal forest	tr.e.t + tr.r.t
TRDR	Tropical dry forest/savanna	tr.r.t
WAMX	Broad-leaved evergreen/warm mixed forest	w-te.e.t
TEDE	Temperate deciduous forest	te.s.t + c-te.c.t + bo.s.t
COMX	Cool mixed forest	te.s.t + c-te.c.t + bo.e.t + bo.s.t
COCO	Cool conifer forest	c-te.c.t + bo.e.t + bo.s.t
TAIG	Taiga	bo.e.t + bo.s.t
CLMX	Cold mixed forest	c-te.c.t + bo.s.t
CLDE	Cold deciduous forest	bo.s.t
XERO	Xerophytic woods/scrub	sb.suc
WAST	Warm grass/shrub	wa.g.s
COST	Cool grass/shrub	cl.g.s + cd.g.s
TUND	Tundra	cd.g.s
HODE	Hot desert	h.d.s
SEDE	Semi-desert	c.d.s
PODE	Polar desert	p.d

In the BIOME model, the plant-available moisture is characterized by the Priestley–Taylor coefficient (α, dimensionless). Here, the values of α at an annual time scale are computed by using the SPLASH v.1.0 model (Davis et al. 2017), through the simulation of seasonal changes in both surface energy fluxes and climatic water balance. In the BIOME model, in order to quantify heat requirement, the growing degree-days (*GDD*, in °C day) is used, which can be obtained by summing the values of daily temperature above a certain base temperature. To calculate values of *GDD*, the values of daily mean temperature are required; furthermore, besides temperature and precipitation data, the relative BSD must also be used in the SPLASH v.1.0 model, on a daily basis. The methods for generating these daily values are described in more detail below.

4.2.3 Evaluation methodology

Monthly time series of the temperature, precipitation and sunshine duration, along with location data, are required for evaluating the performance of the procedure proposed by Yin (1999). The CarpatClim dataset provide access to the three meteorological variables relevant to the assessment for the time period 1960–2010, with a horizontal resolution of 0.1°, covering nine countries with 5895 grid cells (Fig. 4.1). For this reason, using data derived from this dataset, *RSD* values for each year in the period 1961–2010 are estimated using the scheme developed by Yin (1999), and the estimates are compared to the observed data. Observed values of *RSD* are determined by a two-step procedure, following Spinoni et al. (2015): (i) the monthly amount of BSD to which the CarpatClim dataset provides access is divided by the number of days in a given month to calculate the monthly mean for BSD, and then (ii) this value is divided by the monthly mean for daylength that is calculated using Eq. 8.5.3 of Iqbal (1983). Finally, in each grid cell, values of the root mean square error normalized by the mean value of observed data (*RRMSE*, in percentages) are computed between the observed and estimated 50-year time series of *RSD*, separately for each month.

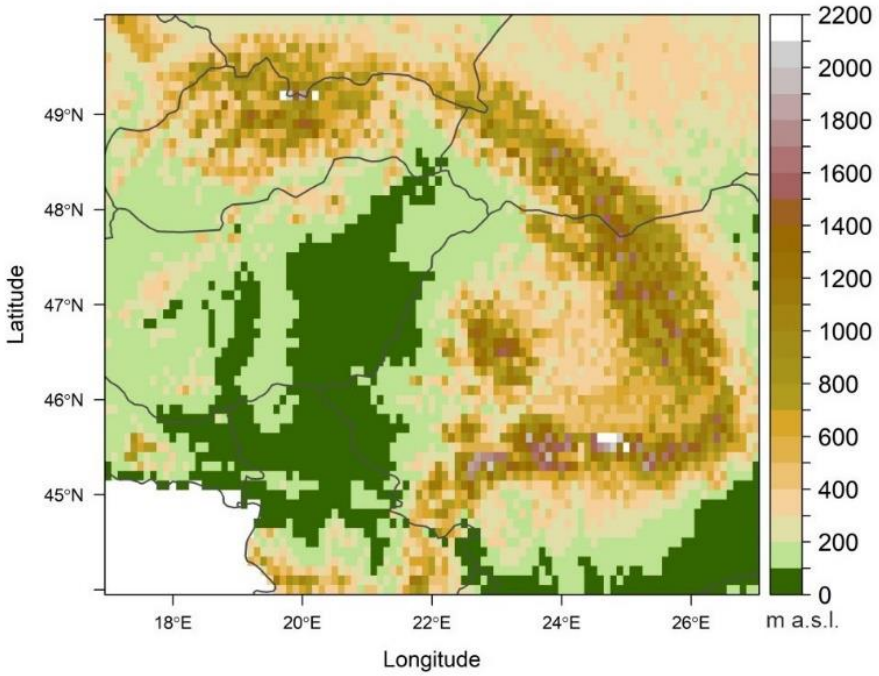

Fig. 4.1 Topography of the Carpathian Region based on the CarpatClim dataset (Spinoni et al. 2015)

To apply the parametric regression model proposed by Yin (1999) to monthly global paleoclimate datasets already described in the introduction, two modifications are needed to use. A feature of such paleoclimate datasets is that they represents climatic conditions averaged over a longer period (typically 30 or 50 years) at each time step. For this reason, it is considered necessary to investigate how the scheme performs when applied to multi-year averages instead of single-year time series. Furthermore, the regression model of Yin (1999) also uses the monthly mean of hourly solar irradiance to estimate the global trend, but uses an algorithm to estimate the value of R_E that cannot be applied without modification in paleoclimatological studies because it does not consider changes in the Earth's orbital parameters. For this reason, here, it is recommended that the value of R_E be calculated using the algorithm used in the SPLASH v.1.0 model, with the addition that orbital parameters are calculated using the method of Berger and Loutre (1991). In this approach, first, the daily solar radiation at the top of the atmosphere is calculated (Eq. 7 in Davis et al. 2017), and then this value is multiplied by the atmospheric transmittivity to obtain the value of daily surface radiation. In this case as well, cloudless conditions are assumed, i.e., the transmission coefficient is taken into account with a universal value of 0.75, however, its value is modified as a function of elevation by using the scheme of Allen (1996). The daylength is calculated via Eq. 1.6.11 in Duffie and Beckman (1991), using the sunset hour angle (Eq. 8 in Davis et al. 2017). Finally, the mean hourly surface radiation is derived as the quotient of the daily surface radiation and the daylength. In this study, using the CarpatClim dataset, values of *RSD* for the period 1981–2010 are computed in two ways: (A) by averaging the time series estimated using the initial scheme for each year, and (B) by applying the scheme to 30-year averages, with the provision that the values of R_E are calculated for year 1995 using the algorithm described above.

When modelling the distribution of biomes, monthly climatologies must be converted to daily values, in order to simulate seasonal changes in both surface energy fluxes and climatic water balance. In the description of the water balance module used in the initial version of the BIOME model, Prentice et al. (1993) have recommended for this that monthly values are interpolated

linearly between mid-month days. However, this approach is unsound because it is not mean-preserving (the monthly means of the interpolated daily values will generally not match the original monthly values). When presenting the SPLASH v.1.0 model, Davis et al. (2017) simply suggested that monthly mean values are assumed constant over each day of the month. This procedure is suitable in terms of the monthly averages, but it generates unrealistic time series. In the 1990s, several mean-preserving methods (see e.g., Epstein 1991; Lüdeke et al. 1994) were developed to address this issue. Here, quasi-daily values are constructed in two ways: (a) monthly averages of temperature and *RSD* are assumed constant, and the monthly precipitation sum is divided equally across each day of the month; and (b) for temperature and *RSD*, the 'harmonic' interpolation technique described by Epstein (1991) is used, with a correction of physically impossible values, and in the case of precipitation, the temporal scaling using an iterative interpolation technique described by Lüdeke et al. (1994) is applied, with a damping variable of 0.7 for each month.

In this study, we assess the effects of the choice of the method used to generate the quasi-daily values and of the source of the BSD data on the results in terms of the spatial distribution of the bioclimatic variables used in the BIOME model. Finally, biome maps simulated under various model configuration settings are compared using the Kappa statistic (Cohen 1960) which value ranges from 0 to 1, with 0 representing totally different patterns and 1 indicating complete agreement.

4.3 Results and discussion

One of the key objectives of this study is to attempt to evaluate the performance of the estimation procedure for *RSD* using data provided by the CarpatClim database. The performance of the scheme proposed by Yin (1999) is assessed based on the root mean square error normalized by the mean value of observed data (*RRMSE*, in percentages) calculated between the observed and estimated values for the period 1961–2010, separately for each month (Fig. 4.2). From May to August, the *RRMSE* value in more than 90% of the study area does not exceed the threshold of 20% below which the model performance can be considered excellent, according to Bellocchi et al. (2002). In the period from April to October, in nearly 99% of the grid cells with elevation smaller than 500 m a.s.l., the value of *RRMSE* is less than 40%, which is the limit of the model performance still considered acceptable based on the work of Bellocchi et al. (2002). In the summer months, the *RRMSE* value in almost 90% of the lower regions (elevation < 500 m a.s.l.) does not even exceed the threshold of 15%. Interestingly, in the winter months, the estimation scheme performs better in the higher than in the lower elevation areas (66 ± 3% and 45 ± 28% of the regions at elevations above and below 500 m a.s.l., respectively, with a threshold of 40%). Although not within the scope of this study, it should be pointed out that the inconsistency between the measured and estimated values found in the Ukrainian section of the Carpathians suggests (Fig. 4.2) that one or even more of the climate fields used in the assessment may contain significant errors in this region. However, an explanation of this requires more detailed analysis.

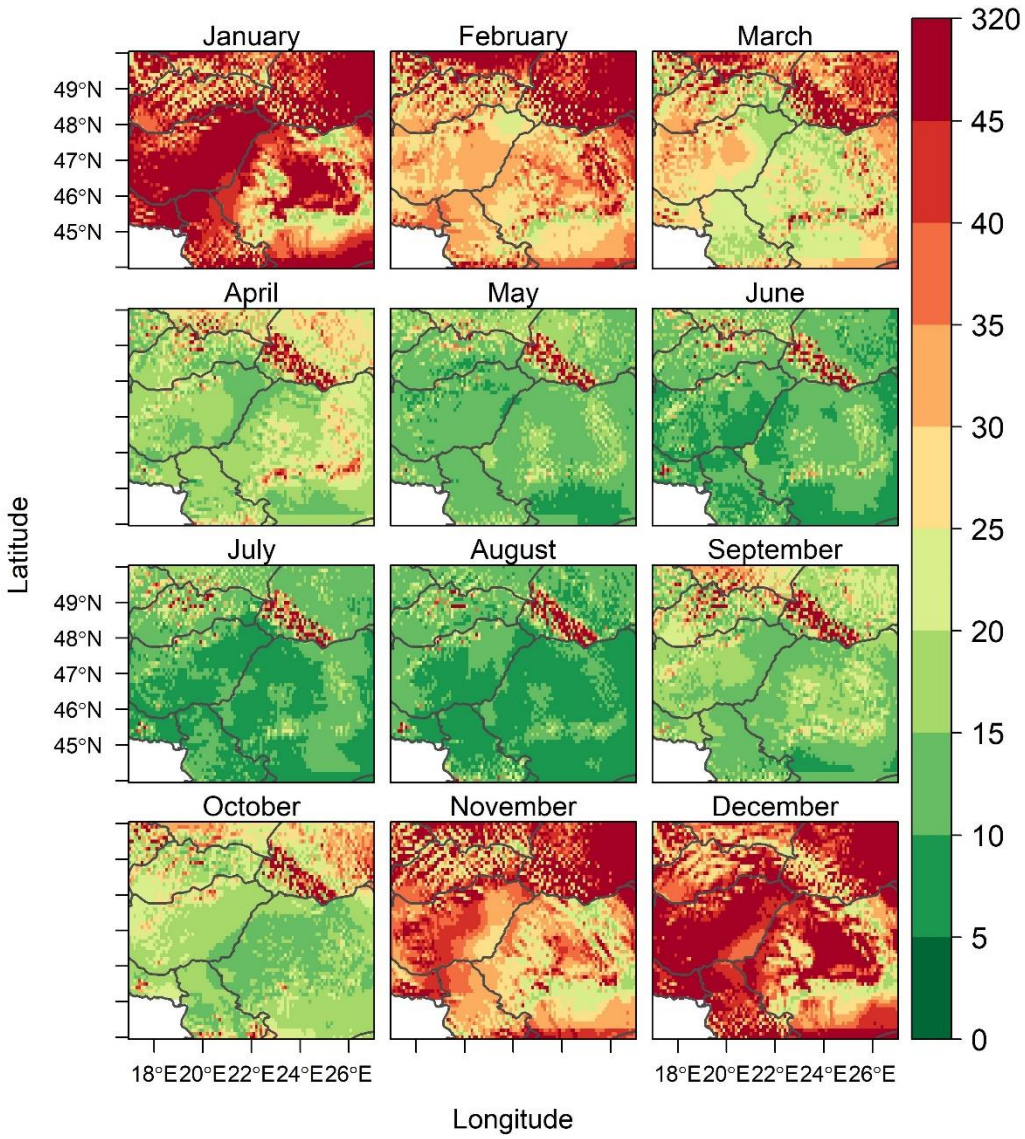

Fig. 4.2 Performance of the regression model developed by Yin (1999) to estimate monthly time series of the relative sunshine duration (*RSD*, dimensionless), based on the root mean square error normalized by the mean value of observed data (*RRMSE*, in percentages). *RRMSE* values are calculated between the observed and estimated values for the period 1961–2010 using the CarpatClim dataset, separately for each month

An important objective of this paper is to assess how the accuracy of the estimates changes when the scheme is adapted for applying to paleoclimate datasets. To study this, values of *RSD* for the period 1981–2010 are calculated in two ways (Fig. 4.3): (A) by averaging the time series estimated using the initial scheme for each year, and (B) by applying the scheme to 30-year averages. The estimated results are compared to the averages of the measured values over the period 1981–2010 (Fig. 4.3b). For the time window used here, we can see that in the period from April to September, the estimation method proposed here performs even better than the initial algorithm. In these months, i.e., in the most important period in terms of the evapotranspiration processes, with one exception, the value of *RRMSE* calculated for the whole study area does not exceed the threshold of 10% (see the second row in Fig. 4.3b), which indicates a very good quality of the estimates. (As previously indicated, the Ukrainian part of the Carpathians is the main contributor to the observed discrepancies.)

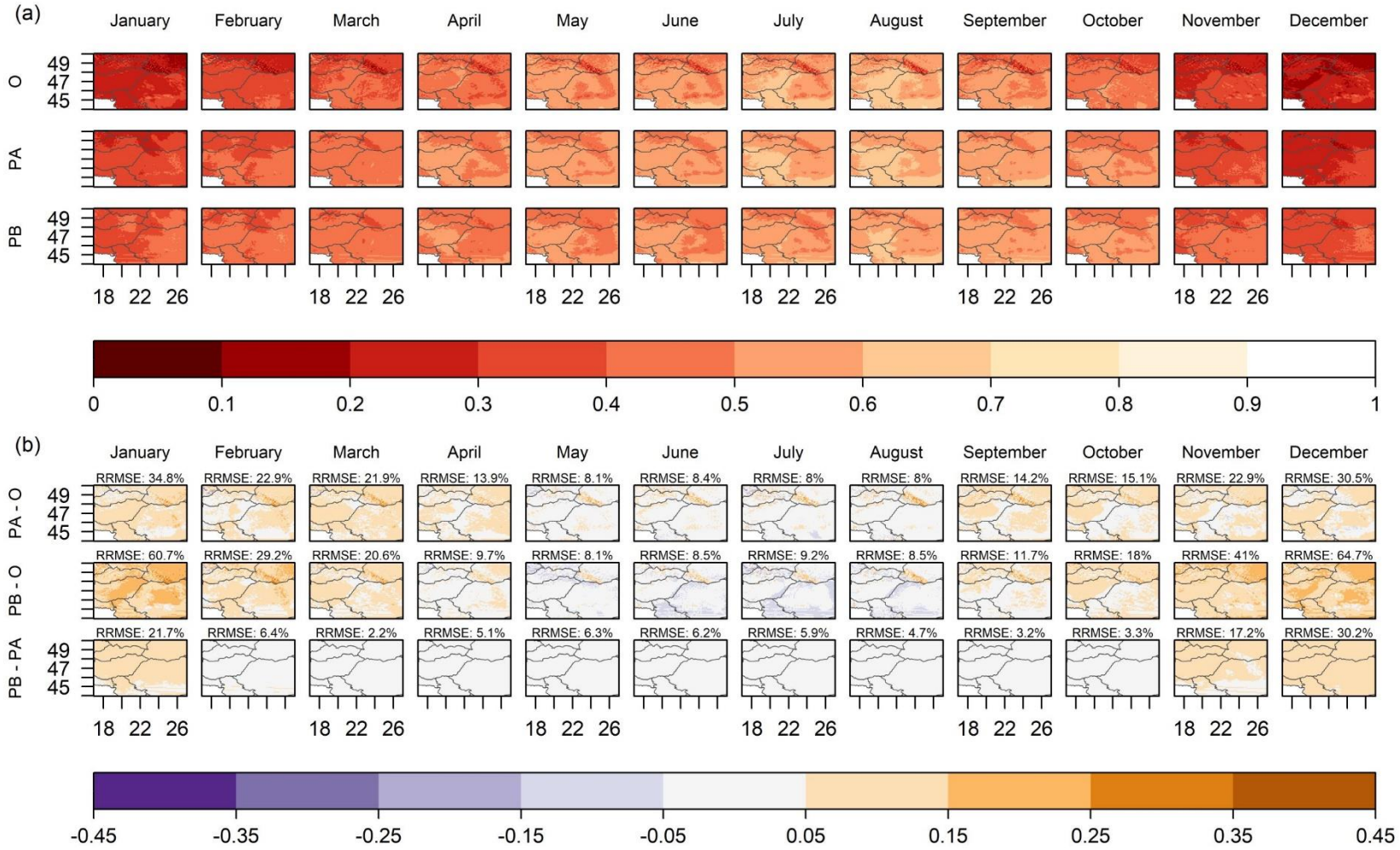

Fig. 4.3 Spatial distribution patterns of monthly mean of relative sunshine duration (*RSD*, dimensionless) in the Carpathian Region for the period 1981–2010: by averaging the observed time series for each year (O); by averaging the time series estimated using the scheme proposed by Yin (1999) for each year (PA); and by applying the scheme to 30-year averages, with the provision that the term related to the solar irradiance in the model (see R_E in Eq. 4.3) is calculated for year 1995 using the algorithm used in the SPLASH v.1.0 model (for details, see Section 4.2.3) (PB). In addition to the values (**a**), the differences from the various sources are also mapped (**b**: PA−O, PB−O, and PB−PA), in the latter case showing the root mean square error normalized by the mean value of reference data (*RRMSE*, in percentages) over the whole target domain

In the context of Fig. 4.3, it is important to underline that when applying the modified estimation scheme to 30-year averages, the overestimation is very high in the winter months (in January, its value exceeds the value of 0.15 over almost half of the region), which, combined with a low (around 0.254 in January) benchmark, results in very high values of *RRMSE*: 60.8% in January and almost 30% in February. For both estimation methods, the difference in winter months, which is also highlighted above in relation to the Fig. 4.2, is probably related to the formation of conditions for cold-air pool (CAP) which is a typical weather situation in the Carpathian Basin (Szabóné André et al. 2021). Namely, the CAP conditions are extremely favourable for the formation of fog which lead to less surface solar radiation. Considering that the model is globally parameterized, it is impractical to expect it to capture such local effects, but fortunately, this model weakness has little relevance in simulating important processes for plants, as it will also be shown later.

The ultimate goal of this study is to examine how sensitive the BIOME model is to change configuration settings. We are interested in how the results change when on the one hand, the measured time series of *RSD* are replaced by estimates produced by different algorithms, and on the other hand, the technique for generating daily weather data is made more sophisticated. For the latter aspect, the simulations are performed in two ways: (a) monthly means are assumed constant over each day of the month, and (b) different mean-preserving interpolation techniques are applied (for details, see Section 4.2.3).

The presence of PFTs is fundamentally dependent on the plant-available moisture, which in the BIOME model is characterized by the α ranging from 0 to 1.26. Its value for the period 1981–2010 is calculated at an annual time scale using the SPLASH v.1.0 model, with a total of six settings (Fig. 4.4). The simulation performed using the measured values of *RSD* and assuming constant monthly means of each meteorological variable over each day of the month is considered as a reference (Fig. 4.4a). Based on this, it can be concluded that there is sufficient moisture in the study area for all woody PFTs related to mid-latitudes (cf. Fig. 4.4a and Table 4.2), with the spatial resolution and time window used here. The change in the methodology for generating daily weather data has little effect on the spatial distributions of this bioclimatic index over the study period: for only 13 out of the 5895 grid cells, the value of α changes by more than 0.005 when the daily data required for the simulation are generated using more sophisticated techniques (see the first row of the second column in Fig. 4.4b). Regardless of the settings, the value of α for the period 1981–2010 does not change over at least one third of the target domain, however, the spatial distribution of these unchanged areas varies depending on the choice of source for the *RSD* data. When using the model driven by sunshine data estimated using multi-year averages, the unchanged areas are limited to the Carpathians that are the wettest regions of the target domain (see the third row in Fig. 4.4b). At this setting, wetter conditions compared to the reference are simulated over more than two thirds of the study area (66.9 and 63.2%, respectively, for constant and interpolated daily data). While simulations using estimated single-year time series of *RSD* show an underestimation in an area of a similar extent (see the second row in Fig. 4.4b). Overall, changing the configuration settings does not have a significant effect on this bioclimatic index, with the *RRMSE* for this index hovering around 1.5%, considering all simulation experiments.

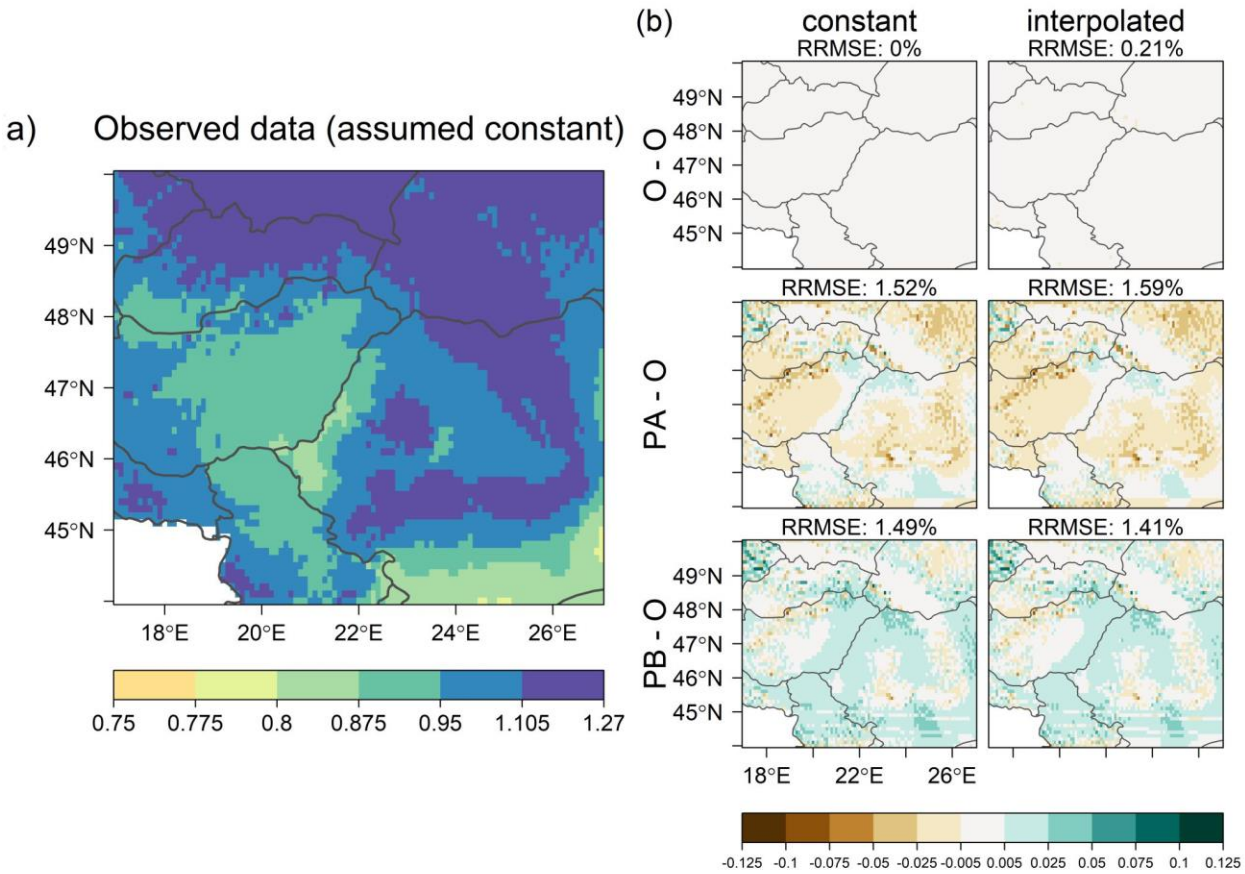

Fig. 4.4 Spatial distributions of the Priestley–Taylor coefficient (α, dimensionless) in the Carpathian Region for the period 1981–2010: (**a**) the values of α are simulated by the SPLASH v.1.0 model using the observed values of monthly means of relative sunshine duration (*RSD*, dimensionless), assuming monthly means for each meteorological variable to be constant over each day of the month; and (**b**) the differences of α values modelled by the initial algorithm and estimated under various model configurations. In each cell of the panel (**b**), the references are derived from the panel (**a**). In each row of the panel (**b**), the estimates are calculated using the *RSD* values derived from various sources: (O) by averaging the single-year time series of the observations; (PA) by averaging the time series estimated using the initial scheme for each year; and (PB) by applying the scheme to 30-year averages. In each column of the panel (**b**), the estimates are calculated using quasi-daily values of each meteorological variable generated by different approaches: (constant) monthly means are assumed constant over each day of the month; and (interpolated) different mean-preserving interpolation techniques are applied (for details, see Section 4.2.3). In the panel (**b**), the root mean square error normalized by the mean value of reference data (*RRMSE*, in percentages) over the whole target domain is shown above each map

Considering all five bioclimatic indices used in the BIOME model, in addition to α, the growing degree-days can also be significantly influenced by the approach used to generate daily temperature values. Thus, a sensitivity analysis is performed also for these two indices. Values of GDD_5 and GDD_0 for the period 1981–2010 are calculated using the two approaches described above, and their spatial distribution (Fig. 4.5) is plotted (mostly) using the thresholds used in the BIOME model (see Table 4.1). Except for the highest peaks of the Carpathians, in the target domain, the value of GDD_5 exceeds the threshold of 1200 °C day, regardless of the settings (Fig. 4.5), and thus, in these regions, the PFT "temperate summergreen tree" (te.s.t) can occur (see Table 4.2), due to the availability of sufficient moisture (Fig. 4.4). Although, in relation to the spatial

distribution of these indices (Fig. 4.5a and 4.5b), a large difference between the two approaches cannot be observed, inter alia due the thresholds used to plotting, but the distribution maps for the differences (Fig. 4.5c and 4.5d) provide additional valuable information. In the case of GDD_5 (GDD_0), the areas with a difference of greater than 30 °C day are mostly located at altitudes lower (higher) than 500 m a.s.l. (cf. Fig. 4.5c/4.5d and Fig. 4.1). For growing degree-days, the difference between the two algorithms is greater in grid cells where the monthly mean temperatures in the first and last months of the growing season are spread around the given base temperature and the annual diurnal range is relatively large. It is easy to understand that under a typical annual temperature course, in cases where the monthly mean temperature is equal to or slightly greater than 5 °C in both April and November, for the GDD_5, a larger amount of heat can be generated from interpolated values than from constant daily data.

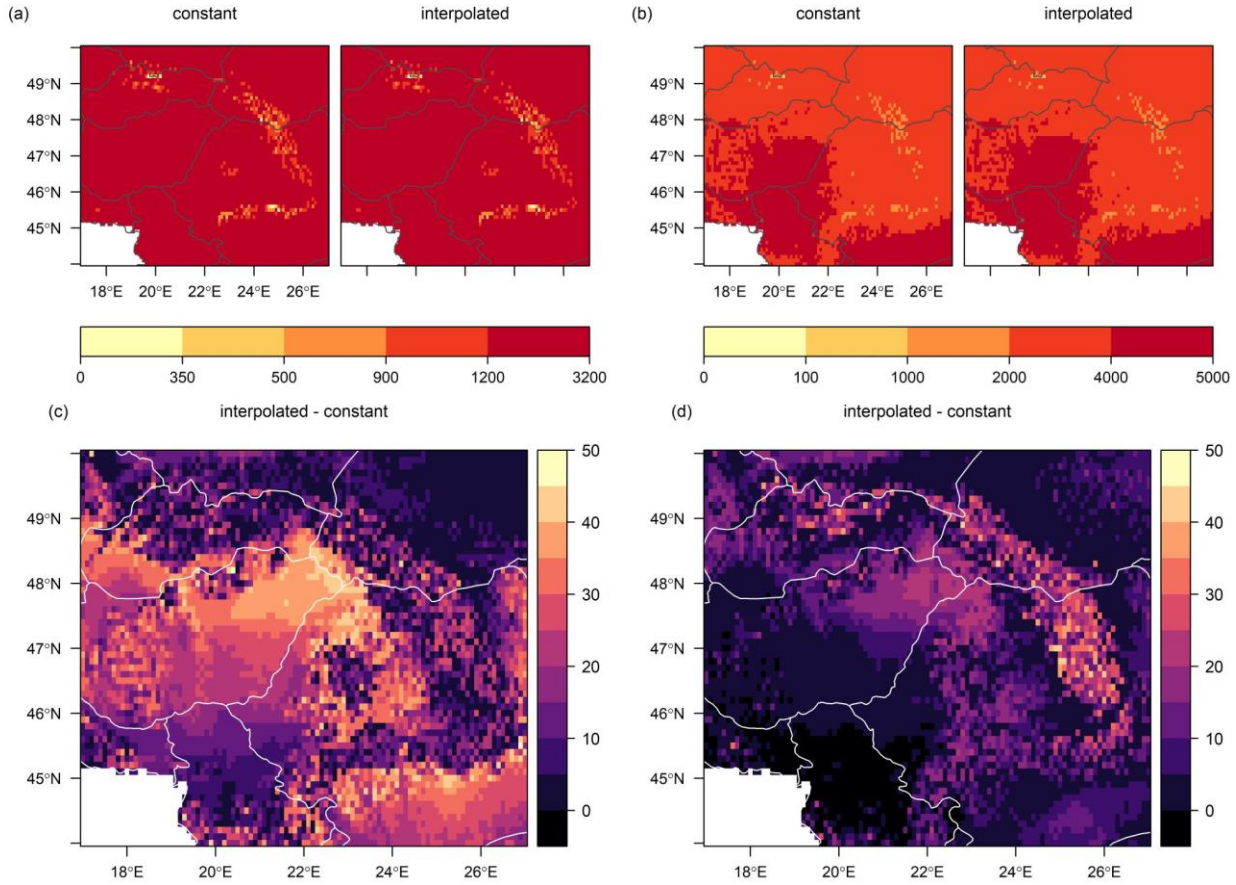

Fig. 4.5 Spatial distributions of growing degree-days above base temperatures of 5 and 0 °C (GDD_5 and GDD_0, °C day) in the Carpathian Region for the period 1981–2010. Panels (**a**) and (**b**) show the spatial distribution of respectively GDD_5 and GDD_0 depending on how the quasi-daily temperature values required to compute these bioclimatic indices are constructed: (constant) monthly means are assumed constant over each day of the month; and (interpolated) the 'harmonic' interpolation technique described by Epstein (1991) is applied. Panels (**c**) and (**d**) show the spatial distributions of the differences between growing degree-days calculated from interpolated and constant daily values, respectively, for GDD_5 and GDD_0

As a final step in this study, it is checked how changing the configuration settings affects the biome designation. Thus, the main results of this study include the distribution maps of biomes under different configuration settings (Fig. 4.6). Here again, the reference simulation is prepared using the measured values of *RSD* and assuming constant monthly means (see the first row of the

first column in Fig. 4.6). For the period 1981–2010, 5 out of the 14 extratropical biome types used by the BIOME model can be observed in the Carpathian Region, at a horizontal resolution of 0.1°. More than half (55%) of the target area is covered by the biome type "temperate deciduous forest" (TEDE), mostly limited to the lowlands (elevation < 250 m a.s.l.). With an areal proportion of 40.7%, the second most dominant biome type in the target domain is the "cool mixed forest" (COMX), covering significant areas in Slovakia, Ukraine and the mountains of Romania. The types "taiga" (TAIG) and "cool conifer forest" (COCO) together cover a total of 4.2% of the study area. As shown in Fig. 4.6, these types appear most markedly in the Eastern Carpathians. The type "tundra" (TUND) covers slightly more than 0.1% of the target area (7 grid cells). Comparing the simulation experiments, it can be found that the choice of source for the time series of *RSD* has no effect on the biome distribution under given space and time conditions: values of the Kappa statistic between the maps derived from the reference simulation and from the remaining two experiments are equal to one, i.e., the spatial distribution patterns of biomes are completely identical (see first column in Fig. 4.6). Biome maps generated using interpolated daily values are consistent with each other (see the second column in Fig. 4.6). Comparing them to the reference map, only a slight mismatch can be found (Kappa statistic = 0.9923). There is a disagreement between biome maps for only 24 of the 5895 grid cells derived using different daily weather data. In all cases, this mismatch is explained by the discrepancy in the spatial distribution of GDD_5 (Fig. 4.5c). The difference is ultimately due to the fact that in some grid cells of the Carpathians, certain heat-demanding woody PFTs (e.g., te.s.t) can occur in the case of the reference simulation, in contrast to the experiments using interpolated daily values. In summary, the BIOME model is insensitive to modify configuration settings considered here.

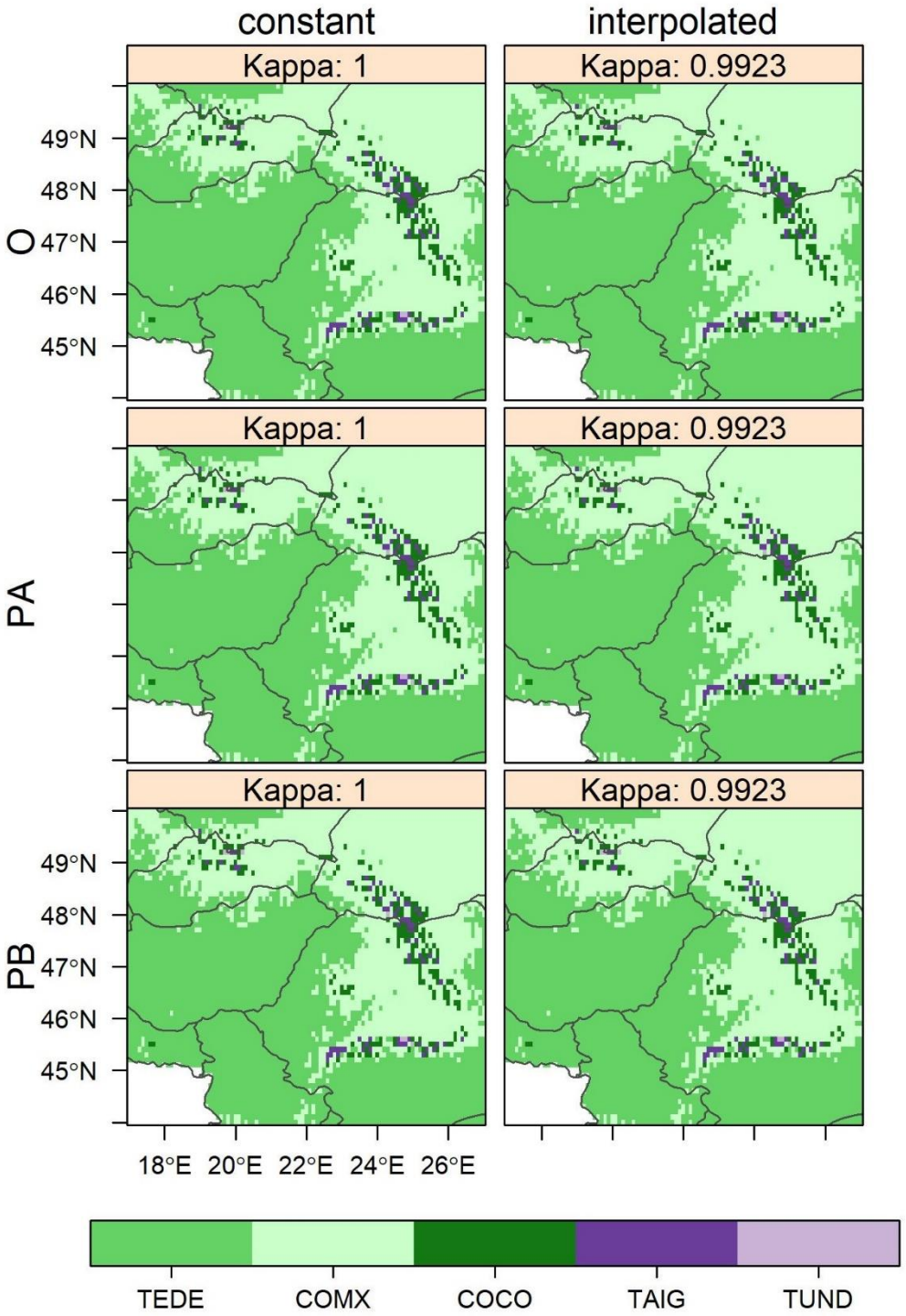

Fig. 4.6 Spatial distribution patterns of biomes simulated by the BIOME model in the Carpathian Region for the period 1981–2010. In each row, the biomes are derived using the sunshine duration data derived from different sources: (O) by averaging the single-year time series of the observations; (PA) by averaging the time series estimated using the initial scheme for each year; and (PB) by applying the scheme to 30-year averages. In each column, the biomes are derived using quasi-daily values of each meteorological variable generated by different approaches: (constant) monthly means are assumed constant over each day of the month; and (interpolated) different mean-preserving interpolation techniques are applied (for details, see Section 4.2.3). Above each maps, the Kappa statistic reflecting the degree of similarity of the distribution patterns is shown, using the map in the first column of the first row as a reference in each case. The abbreviations of biome types can be found in Table 4.2

4.4 Conclusions

In this paper, as a case study for the Carpathian Region, we inspect the efficiency of biome distribution simulation using only monthly temperature and precipitation climatologies. The biome maps were constructed by using a simple process-based vegetation model, the BIOME model, with one minor amendment: the water balance module of the model was replaced by the SPLASH v.1.0 model, thus switching to analytical expressions for calculating daily radiation, evapotranspiration and soil moisture. Monthly temperature and precipitation data, which were required to create the biome maps, were taken from the CarpatClim dataset for the period 1981–2010. The relative BSD data required to run the SPLASH v.1.0 model were taken from the CarpatClim dataset and also estimated by the scheme proposed by Yin (1999) using the above-mentioned temperature and precipitation data. Comparisons between the observed and estimated relative BSD time series for the period 1961–2010 showed that the estimation procedure performed relatively well from late spring to early autumn, i.e., in the most important period in terms of the evapotranspiration processes. It was also examined the effects of two modifications justified by the applicability of the estimation method to paleoclimate datasets: (a) to apply the scheme of Yin (1999) to multi-year averages instead of single-year time series, and (b) to calculate the term related to the solar irradiance in the scheme by applying the algorithm used in the SPLASH v.1.0 model under changing orbital parameters of the Earth. It was found that although the magnitude of overestimation for the modified algorithm is significant in the winter period, the proposed procedure performs similarly well as the initial procedure in the period from March to October. When modelling the distribution of biomes, simulation experiments were performed to assess the effects of modifying some configuration settings of the model: (a) the generation of relative BSD data, and (b) the algorithm used to create quasi-daily weather data from the monthly climatologies. We found that under both the recent humidity conditions of the study region and the spatial resolution of the climate dataset used, the results can be considered sufficiently robust, regardless of the configuration settings tested. The choice of the source of BSD data had no effect on the results, while the choice of the method for temporal downscaling of monthly temperature data had little effect on the distribution patterns of biomes. Thus, the main message of this paper is that using climate data available for Quaternary studies (i.e., monthly temperature and precipitation climatologies), the spatial distribution of biomes can be properly simulated via more sophisticated biome models than BCMs. We believe that by applying the modelling framework outlined here to the data provided by the CHELSA-TraCE21k v1.0, the evolution of biomes over past millennia can be properly mapping.

Acknowledgments. The work of the first author was supported by the European Union and the State of Hungary, co-financed by the European Social Fund in the framework of TÁMOP 4.2.4. A/2-11-1-2012-0001 ‘National Excellence Program’. The work of the second author was partly financed by the János Bolyai Research Scholarship of the Hungarian Academy of Sciences. The authors would like to thank the creators of the CarpatClim dataset (http://www.carpatclim-eu.org/) used in this study for sharing their datasets with the scientific community. The authors are also grateful to the software developers of the SPLASH model (https://bitbucket.org/labprentice/splash) for making available to everyone their source codes.

5 Comparing climate- and pollen-inferred vegetation in the Greater Alpine Region

Manuscript submitted to the *Quaternary Research*

Authors:

Zoltán Szelepcsényi
Institute of Archaeology
Research Centre for the Humanities
Eötvös Loránd Research Network, Hungary

Hajnalka Breuer
Department of Meteorology
Eötvös Loránd University, Hungary

Nándor Fodor
Agricultural Institute
Centre for Agricultural Research
Eötvös Loránd Research Network, Hungary

Pál Sümegi
Department of Geology and Palaeontology
University of Szeged, Hungary

Abstract. In this paper, the biomization is applied to 770 of the most recent fossil pollen assemblages for the Greater Alpine Region (GAR), extracted from the European Pollen Database, providing vegetation reconstructions for 86 pollen sequences. The results are assessed via comparison with a very high-resolution biome map. This map is constructed by using the BIOME model with one amendment, namely that the water balance module is replaced by the SPLASH v.1.0 model. Climate data required for modelling are derived from the HISTALP database, with sunshine duration estimated using temperature and precipitation data. The biomization methodology is not remarkably modified, but the taxon list is expanded. In the comparisons, it is also aimed to consider the effects of uncertainties related to the choice of the spatial scale and the vegetation definitions. It was found that in the case of low altitude pollen sites, even a small expansion of the definition significantly increases the matching percentage. For high altitude sites, the area expansion helps to eliminate the discrepancy. This highlights the fact that classification schemes used here take account of neither ecotones nor anthromes, which significantly impedes comparisons in the GAR where the landscape is topographically complex and significantly modified by humans.

Keywords: phytogeography; biomization; plant functional types; human impact; vegetation transitions

5.1 Introduction

Many tools (e.g., quantitative reconstruction methods: Birks et al. 2010; paleoclimate modelling: Harrison et al. 2016; proxy system models: Evans et al. 2013) are currently available to form an objective picture of the characteristic features of the Quaternary environment and climate as well as their spatial and temporal evolution. By reversing the cause-effect link, past climatic (environmental) conditions can be inferred by transforming proxy data into paleoclimatic (paleoenvironmental) variables using statistical relationships between them (see Juggins and Birks 2012). By using climate models, we can simulate how the climate system has responded to assumed past changes in external forcings (e.g., insolation) and boundary conditions (e.g., vegetation distribution). In another approach, by using so-called forward models (e.g., proxy system models, vegetation distribution models) driven by climate model outputs, the proxy variable (or feature) (e.g., tree ring width, pollen assemblage) that was recorded in proxy archives as a response to environmental forcing can be directly simulated (Evans et al. 2013). Finally, by comparison of the simulated and observed proxy data, it is possible to evaluate the climate model in terms of the simulation of climatic characteristics (e.g., Prentice et al. 1998) or to identify reasonable constraints for the climate model in a paleo data assimilation framework (see Hakim et al. 2016).

Quantitative and qualitative features of past environments and climates are commonly inferred from different biological archives, such as fossil pollen data (e.g., Liu et al. 2019), plant macrofossils (e.g., Orbán et al. 2018), tree ring data (e.g., Alexander et al. 2019), diatoms (e.g., Wang et al. 2018), fossil arthropods (e.g., Tóth et al. 2022), molluscs (e.g., Rousseau 1991; Hertelendi et al. 1992), and vertebrate bones/teeth (Szabó et al. 2021). Taking into account spatial and temporal coverage, however, fossil pollen data are unique compared with other proxy data sources. Pollen grains preserved in sediments provide information about their source region's vegetation and environment, when calculating the ratio of arboreal to non-arboreal pollen taxa or using other more sophisticated vegetation reconstruction approaches.

Over recent decades, among pollen-based vegetation reconstruction approaches, two methods with different theoretical underpinnings have been unsurpassed in terms of the number of applications: the biomization approach (Prentice et al. 1996; Peyron et al. 1998) and the Landscape Reconstruction Algorithm (LRA: Sugita 2007a, b). REVEALS (Regional Estimates of VEgetation Abundance from Large Sites: Sugita 2007a), the LRA model designed for regional-scale reconstruction, simulates processes of pollen dispersal and deposition based on different numerical assumptions (relative pollen productivity, fall speed of pollen, relevant source area of pollen, wind speed and direction, atmospheric conditions), in order to transform pollen data into vegetation cover. The application of this mechanistic model has caveats related to estimates and assumptions (see e.g., Theuerkauf et al. 2016). For this reason, a reconstruction approach based on fuzzy logic, called biomization (Prentice et al. 1996), is widely used to map past vegetation through the determination of dominant biome types (e.g., Cheng et al. 2018; Li et al. 2019; Magyari et al. 2019, 2022).

In addition, a variety of procedures have been developed recently that are suited to construct quantitative land cover reconstructions by using partial results of the biomization algorithm (e.g., Tarasov et al. 2013; Davis et al. 2015; Zanon et al. 2018). Davis et al. (2015) have converted pollen data into plant functional type (PFT) assemblages, and then the data have been interpolated in space and time onto a four-dimensional grid. Finally, forest cover has been estimated as the percentage of arboreal PFTs. Recently, Zanon et al. (2018) created a gridded reconstruction of

European forest cover during the last 12,000 years, which can provide adequate boundary conditions for paleoclimate simulations. Zanon et al. (2018) extended the relationship between pollen and satellite data back in time, by applying the Modern Analog Technique (MAT), based on the conception used by Williams and Jackson (2003) and Tarasov et al. (2007). However, by way of deviation from the original approach, PFT scores (see Peyron et al. 1998), instead of taxon abundances, have been applied in the MAT algorithm in order to avoid non-analogue situations. Tarasov et al. (2013) have proposed an index for the characterization of landscape openness, defined as the difference between the maximum forest biome score and the maximum open biome score. They aimed to correct one of the weaknesses of the biomization scheme, namely that the original method is unable to reconstruct the transitional vegetation types, called ecotones (e.g., forest-steppe), which are indispensable to map the vegetation of Eurasia. Recently, by using this new index, Tian et al. (2018) have presented a series of maps detailing the evolution of East Asian landscape openness during the last 40,000 years.

There are various limitations to reconstruction methods based on the biomization approach depending on both the spatial and temporal frame/resolution of the investigation. Within the original and refined versions of the method, Peng et al. (1995), Prentice et al. (1996), and Tarasov et al. (1998) evaluated the success of the biomization approach for European regions. In connection with the redefinition of PFTs and biomes, as a validation of the method, Bigelow et al. (2003) and Binney et al. (2017) compared the vegetation reconstructed from modern pollen samples with a map of potential natural vegetation (PNV) using a simple error matrix. Recently, Marinova et al. (2018) devoted an entire article to assessing the performance of the biomization scheme and the potential sources of bias, similarly, by using error matrices. In the initial validation experiments (e.g., Tarasov et al. 1998), biome maps that were created by using a simple biogeographical model, called BIOME model (Prentice et al. 1992), were used as references. In contrast, Marinova et al. (2018) used PNV maps that were based on expert assessments for comparisons. These expert-based PNV maps (e.g., Bohn et al. 2003) generally take into account vegetation history, orography, and soils. Thus, if they are applied as a reference in the validation, on the one hand, the effect of anthropogenic disturbance on the reconstruction procedure cannot be directly evaluated, and on the other hand, the use of azonal vegetation types can hinder the comparison in certain cases.

However, it is important to consider the following facts: (a) anthropogenic disturbance of vegetation is a possible source of bias in the biome reconstruction (Peng et al. 1995), and (b) the taxon list of each PFT used in the biomization approach is developed by taking into account the climatic tolerances and requirements of taxa (Prentice et al. 1996). For these reasons, in the benchmarking of the biomization scheme, it is advisable to use biome maps that also reflect climatic conditions (Peng 2000) as a reference. Such maps can easily be generated, for example, by running the above-mentioned BIOME model driven by gridded observational databases of monthly climatic variables, following the conception presented by Prentice et al. (1996).

Over the past 25 years, more and more observational climate databases have become accessible in Europe with improved spatial resolution and temporal coverage, such as the well-known CRU TS 1.2 (Mitchell et al. 2004), the HISTALP (HISTorical instrumental climatological surface time series of the Greater ALPine Region, Auer et al. 2007) and the HadUK-Grid (Hollis et al. 2019). In parallel, a significant improvement has been made in the accessibility of pollen data used in biomization, due to various international collaborative efforts (see European Pollen Database (EPD): Fyfe et al. 2009; Eurasian Modern Pollen Database (EMPD): Davis et al. 2020). Taking this into account, we consider it valuable to carry out the classification accuracy assessment of the biomization scheme again, following the concept proposed by Prentice et al. (1996) and exploit

improvements in climate and pollen data. For example, the above-mentioned HISTALP database contains homogenised monthly temperature and precipitation data covering the period 1801–2014 for the Greater Alpine Region (GAR). At the same time, thanks to the close cooperation between the Alpine Palynological Database and the EPD, the number of freely available fossil pollen samples has significantly increased for the Alpine region. The simultaneous use of these data enables an identification of climate- and pollen-inferred vegetation types for a region with complex topography having diverse flora and climate (Fauquette et al. 2018).

In consideration of the literature discussed above, the aim of this paper is threefold: (i) to construct a very high-resolution distribution map of climate-derived vegetation for the GAR by running the BIOME model driven by HISTALP climate data; (ii) to apply an updated version of the biomization scheme to pollen samples from the EPD; and (iii) to compare climate- and pollen-inferred vegetation by evaluating explicitly the potential sources of bias in the biomization scheme through the use of metadata of the pollen sites and various matching measures.

5.2 Material and methods

5.2.1 Climate-derived biomes

In this study, the well-known biogeographical model developed by Prentice et al. (1992), called the BIOME model, is applied to obtain the distribution of climate-derived vegetation. First, the BIOME model estimates the presence of each PFT (i.e., plant types with similar ecophysiological behaviour) under given climatic conditions. Subsequently, the biome type can be easily inferred if PFTs occurring at the maximal dominance level are combined with each other. Each PFT is described by constraints of bioclimatic indices (BIs) associated with their climatic tolerances and requirements.

In the BIOME model, the plant-available moisture is characterized by the Priestley–Taylor coefficient (α). Here, the values of α at an annual time scale are computed by using the SPLASH v.1.0 model (Davis et al. 2017), through the simulation of seasonal changes in both surface energy fluxes and climatic water balance. In the BIOME model, in order to quantify the heat requirement, the growing degree-days (*GDD*, in °C day) is used, which can be obtained by summing the values of daily temperature above a threshold base temperature.

To calculate values of *GDD*, the values of daily mean temperature are required; furthermore, besides temperature and precipitation data, a meteorological variable directly related to radiation (e.g., cloud cover, sunshine duration) must also be used in the SPLASH v.1.0 model, on a daily basis. In this study, however, data requirements of this model are met by monthly temperature and precipitation fields, taking into account other aspects of the study. To quantify radiation, monthly mean daily values of the relative sunshine duration (*RSD*) are estimated using monthly temperature and precipitation data, as proposed by Yin (1999). Finally, quasi-daily values are constructed using the monthly values of the above-mentioned meteorological variables: (a) for *RSD* and air temperature, the 'harmonic' interpolation technique described by Epstein (1991) is used, with a correction of physically impossible values, and (b) in the case of precipitation, the temporal scaling using an iterative interpolation technique described by Lüdeke et al. (1994) is applied, with a damping variable of 0.7 for each month.

The distribution map of climate-derived biomes is constructed for the GAR, which is defined as being located from 43° to 49° N, and between 4° and 19° E (Fig. 5.1). For this purpose, the selected biogeographical model is applied to the updated monthly temperature and precipitation

fields from the HISTALP database (and to the *RSD* fields derived from the above fields). These data are available on an equidistant grid with a horizontal resolution of 5 arc-min (with a cell size of ~55 km^2 in the middle region). As this degree of detail is not appropriate for biological applications due to its inability to capture the diverse topography of the region along with alpine valleys and mountain peaks, the spatial resolution of meteorological fields is improved by an order of magnitude. For temperature data, the following method is applied: (i) the values of sea level temperature are calculated using the digital elevation model of the HISTALP database and the monthly mean vertical temperature gradients computed by Rubel et al. (2017) from the results of Rolland (2003); (ii) the sea level temperature field is interpolated to a 0.5 arc-min grid of the Global 30 Arc-Second Elevation Dataset (GTOPO30) developed by the U.S. Geological Survey (Gesch et al. 1999); (iii) finally, air temperatures at the elevation of each GTOPO30 grid cell are recalculated using the sea level temperature fields and elevation data (with a cell size of ~0.55 km^2 in the middle of the region). The interpolation procedure is performed using bilinear resampling, via the function "resample" in the R package "terra" (Hijmans 2021). In the case of precipitation, a similar methodology is applied, uniformly computed with a 5% precipitation increase per 100 m altitude increase, following Rubel et al. (2017). This spatial downscaling approach is performed separately for each year, and then the estimation procedure described by Yin (1999) is applied to these downscaled temperature and precipitation fields.

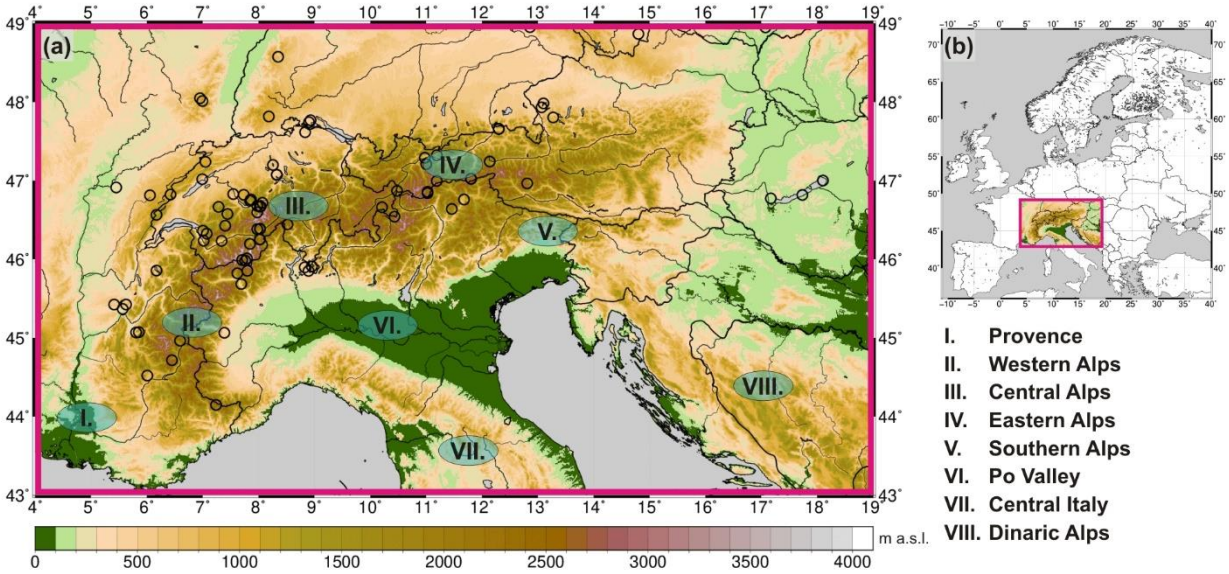

Fig. 5.1 The Greater Alpine Region (GAR). The target area's (**a**) topography and (**b**) location in Europe, indicating the major geographical regions, which are mentioned in the text. The fossil pollen sites, whose data are used in the biomization procedure, are represented by *empty circles*

The updated version of the HISTALP database contains data for the period 1780–2014 in the case of temperature, and for the period 1801–2014 in the case of precipitation. Because of the static view of the applied biogeographical model (see Peng 2000), BIs required to identify biomes are calculated by means of multi-year climatologies. Taking into account the climate regime shift detected globally in the 1980s (Reid et al. 2016), which can be clearly demonstrated in Central Europe by accelerated warming (Philipona and Dürr 2004) and the widespread decline of forests (Kandler and Innes 1995), multi-year climatologies are defined as averages for the years 1801 to 1980. In the calculations, two rules are applied for each grid cell: (i) only those monthly values are considered as part of the time series for which the annual time series are complete in the case of all three variables; (ii) if the number of missing values in the time series exceeds 10% (here, this

threshold is 18 year), the value for the given grid cell has to be interpreted as an error. In the next step, the model described by Prentice et al. (1992) is applied to these mean fields (except for the error grid cells). When running the SPLASH v.1.0 model, only one modification is made: the Earth's orbital parameters are calculated for the year 1890 (i.e., the median of the period 1801–1980) using the method of Berger and Loutre (1991). As the last step, the final product, i.e., the distribution map of climate-derived biomes, is produced using GMT 5.2.1 (Wessel et al. 2013), similarly to the following maps.

5.2.2 Pollen-based biome reconstruction

For transforming pollen data into biome types, Prentice et al. (1996) have proposed a procedure that can also be properly used (with some modifications) to quantitatively reconstruct past climate variables through the use of PFTs, due to the more robust PFT–climate relationship. Over the last 25 years, this universal procedure has been modified several times (e.g., Peyron et al. 1998; Allen et al. 2000; Bigelow et al. 2003). The methodology used here to assign a given pollen assemblage to a biome type follows the one proposed by Peyron et al. (1998) and refined by Tarasov et al. (1998, 1999), with the provision that steps following the designation of the dominant biome type are ignored.

To maximize the utilization of the accessible pollen data, compared to the above-mentioned works, the range of taxa used in this study is expanded, thereby modifying the assignments of pollen taxa to PFTs, and PFTs to biome types. A total of 301 taxa are taken into account in the biomization procedure. The remainders (e.g., *Globularia, Morus,* etc.) are omitted because they occur rarely or with low abundances in pollen spectra, or because they are ambiguous from a taxonomic or ecological point of view. For taxon–PFT and PFT–biome matrices used here, see Tables B.1–3.

One of the most sensitive points in the biomization procedure is the designation of the dominant biome type. By default, the biome type with the highest affinity score is assigned to the pollen spectrum. However, the highest score can belong to several biome types simultaneously. Within the procedure developed by Prentice et al. (1996), this problem was handled by putting the biome types in a particular order. This order was determined by the PFT composition of biome types, considering that the absence of certain PFTs may intuitively assist in decision-making. Bearing this theoretical approach in mind, another algorithm is suggested in this study. Within this procedure (hereinafter referred to as the "smallest hiatus"), for each biome type with the highest score, we calculate the proportion of taxa for which the following criteria are met: (a) all of them are included in the predefined taxon list of the given biome type, but (b) they are not detected in the given pollen spectrum (by using the universal threshold value of 0.5%). Ultimately, the point of the proposed decision-making mechanism is to minimize this ratio.

Fossil pollen data used to reconstruct recent past vegetation are derived from the version of the EPD released on 30 December 2016. The version of the database used here contains 2409 pollen sequences for 1876 sites, though not all possess a reliable chronology (e.g., age–depth models based on calibrated radiocarbon ages). For this reason, following Brewer et al. (2017), the time selection for pollen samples is carried out by using uniformly recalibrated age–depth models prepared by Giesecke et al. (2014). These new chronologies are based on the version of the EPD released on 2 August 2012, nonetheless, quality-controlled age information is provided for just 800 out of the 1204 pollen sites (Brewer et al. 2017). Based on the foregoing, it can be clearly seen that the EPD has broadened significantly between 2012 and 2016, and a large number of samples cannot be taken into account because of the absence of a reliable absolute chronology. For this

reason, following Fyfe et al. (2015), the time selection is extended to all those samples for which a calibrated radiocarbon-based chronology has also been uploaded by the contributing authors.

The biomization procedure is applied to all relevant pollen samples (RPSs). A RPS is defined as that for which: (a) the site is located in the GAR, (b) its calibrated age falls into the time window of 60±90 cal yr BP (1800–1980 CE), and (c) the sum of pollen grains exceeds the threshold of 300 for the taxa involved in this study (Bennett and Willis 2001). Thus, according to the above restrictions, the biomization procedure can be applied to 770 samples of 86 pollen sequences (Fig. 5.1). For metadata describing each sequence used here, see Table B.4. (Given that the pointwise comparison used in this study requires accurate site location information, and as is known, the EPD contains geolocation errors (see Brewer et al. 2017), quality control and correction of spatial data are carried out where the relevant publications are accessed. Table B.4 contains revised spatial data for pollen sequences.)

At the end of the process, the dominant biome type is identified for each pollen sequence. However, the designation becomes problematic if more than one sample belongs to a given sequence. In such a case, it may be possible that more than one biome type can be considered as the dominant type, based on the highest affinity score. To avoid this problem, relative biome scores (RBSs) are defined here, following Allen et al. (2010a). In this study, the RBS is calculated by a two-step procedure: (i) the individual affinity score is divided by the sum of all affinity scores in the given sample, and then (ii) to obtain the final value, these quotients belonging to a given sequence are averaged where it is needed. The final decision is therefore based on these RBSs, with the provision that for identical maximum values, the above-mentioned principle of "smallest hiatus" has to be applied to abundances averaged over the given sequence.

5.2.3 Evaluation of the biomization results

Through the use of a pointwise approach, the vegetation simulated by applying the BIOME model is compared with the vegetation defined based on the RBSs characterizing the pollen sequence, in order to evaluate the performance of the biomization scheme and the potential sources of bias. Besides the visual comparison, we primarily rely on values of the percentage of agreement, but matching measures that more plastically reflect the quality of match are also used for the evaluation.

Based on previous experiences, Marinova et al. (2018) have listed the factors affecting the reliability of the reconstruction as follows: (a) uncertainty in the PFT definitions, i.e., in the assignments of pollen taxa to PFTs, and PFTs to biomes, (b) anomalies in pollen production (i.e., the over-representation of arboreal taxa in the pollen assemblage), (c) variability in the size of the sedimentation basin (i.e., the uncertainty about the choice of the spatial scale of vegetation represented by the pollen), (d) long-distance arboreal pollen transport towards open landscapes (resulting in the poor delineation of biome boundaries), (e) upslope transport of pollen from lowland regions to higher altitudes (resulting in the uncertain delineation of timberline) and (f) anthropogenic disturbance or alteration of the vegetation.

The designation of the dominant biome type leads to a significant loss of information, which can be further exacerbated by determining the quality of the match on a two-class scale. By introducing the concept of near-missing (see Woodbridge et al. 2014), however, the findings can be further nuanced. Here, two possibilities are seen for identifying near-misses (similar cover classes assigned): (a) when accepting the pollen-inferred biome as true, the search window around the location of the pollen site can be broadened for the climate-inferred biome type, and (b) when fixing the climate-inferred biome, the list of those pollen-inferred biome types that are accepted as

matching partners can be expanded further. The former is intended to quantify the impact of the choice of the spatial scale on the quality of reconstruction, while the latter can be suitable for measuring the effects of uncertainties in PFT and biome definitions.

The value of the area expansion required for matching (AEm) shows the side length of the square search window, expressed in grid cell units, to be formed around the grid cell containing the pollen site, in order to find at least one match between the climate- and pollen-inferred biome types. Ideally, the search window does not need to be expanded for matching, so it is most optimal if the value of AEm is zero. If initially there is no match, then, in the next step, the length of the sides of the search window has to be increased by one unit in each direction. If a match is found by this step, then the value of AEm is equal to one.

To determine the value of the definition expansion required for matching (DEm), it must be known first how similar the biome definitions are in terms of taxonomic composition, i.e., for each pollen-inferred biome type, a similarity order must be defined using the Jaccard Similarity Index (JSI: Jaccard 1901). Finally, the value of DEm is obtained by determining the position of the climate-inferred biome type of the grid cell containing the pollen site in the similarity order of the dominant biome type (identified by using pollen data). Ideally, the definition list does not need to be expanded for matching, so it is most optimal if the value of DEm is zero. The JSI values are calculated by using the R package "fossil" (Vavrek 2011). For the similarity orders obtained by applying biome definitions used here and the associated JSI values, see Fig. B.1.

To explicitly evaluate the effects of the above-listed factors on the biomization results, vegetation data for the 86 selected pollen sequences are divided into two groups by means of quantitative characteristics of these factors. Then the above-mentioned matching measures are aggregated separately for these subgroups. To quantify the impact of the degree of landscape openness on the reliability of reconstruction, the values of tree canopy cover (TCC) extracted from the Global Forest Change Dataset (Hansen et al. 2013) for the year 2000 are used. The value of TCC reflects the percentage of the total tree canopy closure in a 1×1 arc-sec grid cell. To account for the human impact on vegetation, we use the map of the human footprint index (HFI) for the year 1993 developed by Venter et al. (2016a). The value of HFI indicates the degree of human pressures on the environment, ranging from 0 (no pressure) to 50 (extremely high pressure), by aggregating multiple indicators, which make aspects such as human population pressure, human land use, and infrastructure measurable. The HFI data are available on an equidistant grid with a horizontal resolution of 30 arc-sec.

To avoid interpretation biases, the TCC and HFI data are first aggregated to the grid of the GTOPO30 using bilinear resampling, via the function "resample" in the R package "raster" (Hijmans 2020). In accordance with Venter et al. (2016b), a given pollen site is considered to be affected by anthropogenic activities when the value of HFI for that 0.5 arc-min grid cell in which the site is located is greater than or equal to 6. Following Hansen et al. (2010), in this study, a grid cell is labelled as forest (i.e., closed vegetation) if the value of TCC is at least 25%.

The TCC and HFI data for the pollen sequences related to RPSs are found in Table B.4, complemented by additional metadata such as the name, geographical location, and elevation of the pollen sites. Altitudinal data are derived also from the GTOPO30. However, pollen sequences where the difference between the grid cell value from the GTOPO30 and the site value from the EPD exceeds 250 m are marked with an asterisk in the "ALT" column of Table B.4. In this context, the terrain ruggedness index (TRI: Wilson et al. 2007) is also calculated from the GTOPO30, using the function "terrain" in the R package "raster". Here, based on the classification by Riley et al. (1999), a terrain of a site is considered to be rugged if the value of TRI is greater than or equal to

240 m. A pollen site is defined as a high-altitude site if the grid cell value of the altitude is not less than 1000 m a.s.l.

A flowchart summarizing procedures for the derivation and comparison of climate- and pollen-based biomes is presented in Fig. 5.2. See above for details.

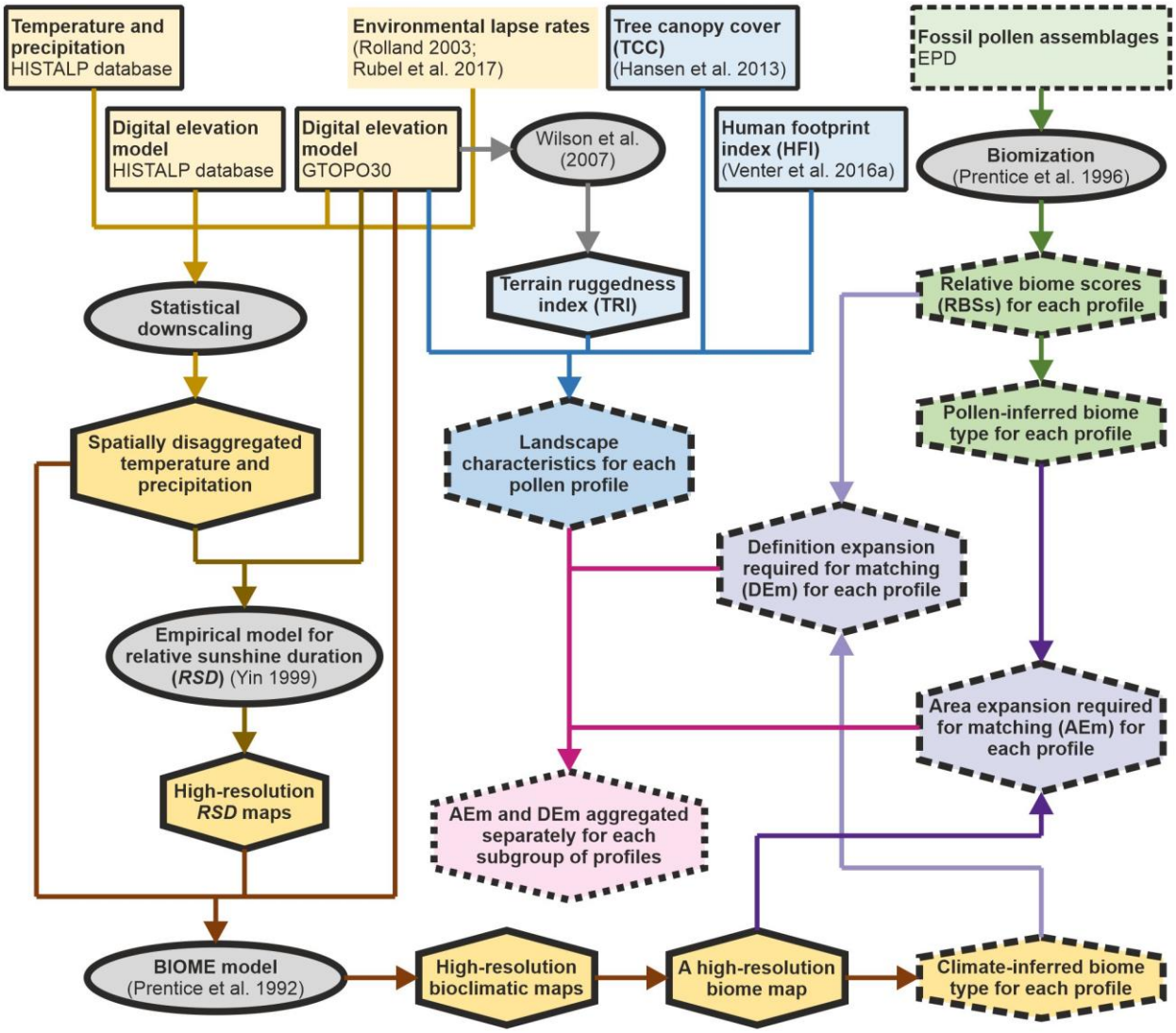

Fig. 5.2 Flowchart showing the steps involved in the used methods to derive and compare climate- and pollen-based biomes. Input data are represented by *rectangles*, procedures by *ellipses* and output data by *hexagons*. An input/output data denoted by *solid lines* is a raster dataset, while a data marked by *dashed lines* contain pollen site information. In the reconstruction of climate-based (pollen-based) biomes, both input and output data are marked with *yellow* (*green*) *polygons*. Supplementary data are distinguished by *blue polygons*, while matching measures obtained in comparisons are denoted by *hexagons with a purple/pink background*. The references in the figure correspond to the citations in the text

5.3 Results

5.3.1 Simulated biome distribution

One of the most important results of this study is the distribution map of climate-based biomes in the GAR for the period 1801–1980 (Fig. 5.3), which is created by means of the BIOME model using climate data provided by the HISTALP database. Due to the lack of climate data, the biome type cannot be identified in the central regions of the Dinaric Alps, but this problem does not inhibit the validation procedure because of the absence of fossil pollen data (see Fig. 5.1).

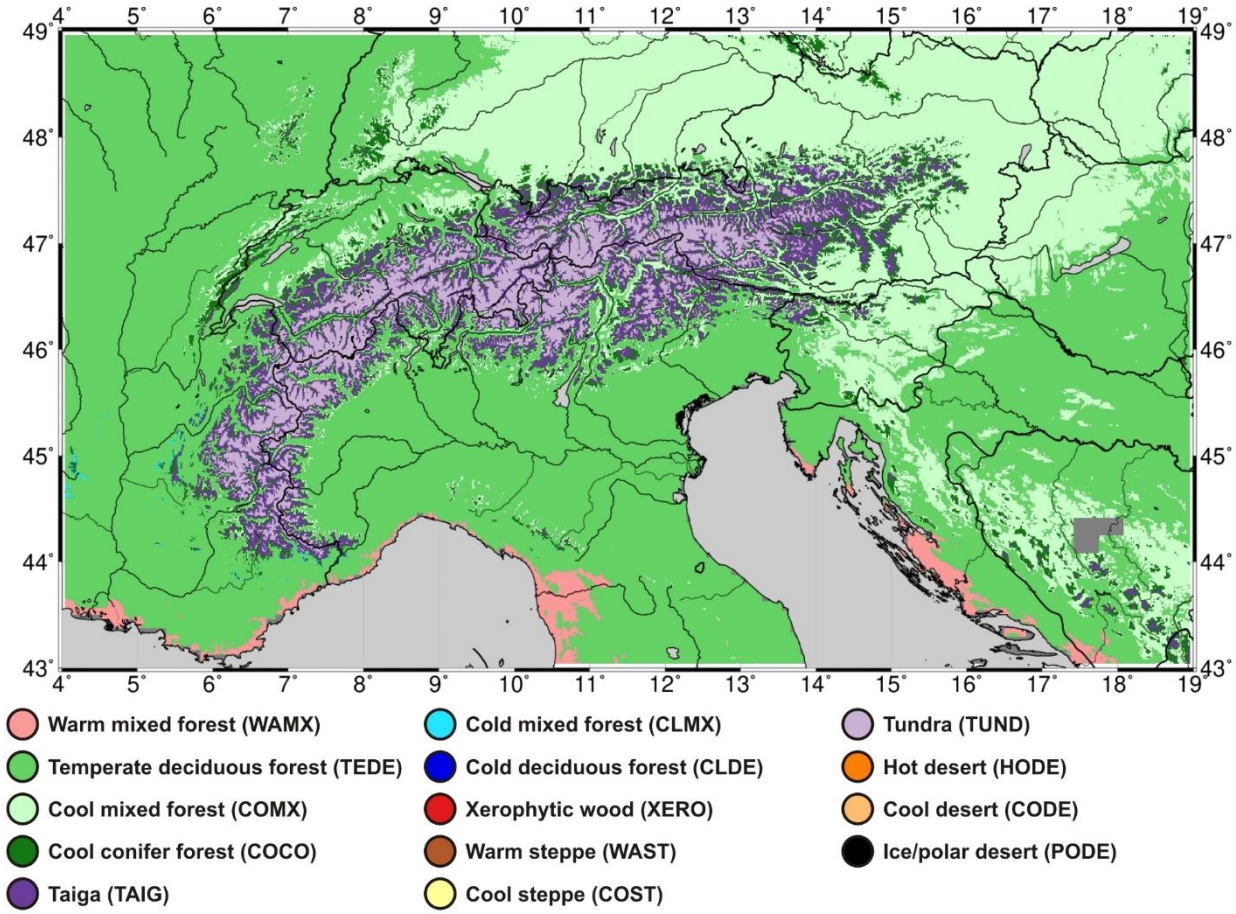

Fig. 5.3 Spatial distribution of the biome types simulated by the BIOME model in the GAR for the period 1801–1980. The observed climate data required for the simulation are derived from the HISTALP database

As shown in Fig. 5.3, under the "current" conditions, 8 out of the 14 extratropical biome types used by the BIOME model can be observed in the GAR, at a horizontal resolution of 0.5 arc-min. Considering the entire target domain, however, the sum of relative coverage of the biome types "cold mixed forest" (CLMX) and "ice/polar desert" (PODE) does not reach 1%. These types can only be sporadically identified in the western segment of the study area.

More than half (54.42%) of the target area is covered by the biome type "temperate deciduous forest" (TEDE). Its distribution is limited to lower regions in the eastern segment of the target domain and in France, as well as to the Po Valley and Central Italy (Fig. 5.3). The biome type "cool mixed forest" (COMX) covers 28.16% of the study area. As shown in Fig. 5.3, the type COMX shows a similar distribution pattern to that of the climate type Dfb (boreal climate with no dry season and warm summer) defined by Köppen (1936) on the map created by Rubel et al. (2017)

for the period 1876–1900. Namely, this biome type can be identified in the areas situated to the north–northeast of the Alps and in the Dinaric Alps. The reason for this is that in the climate classification system of Köppen (1936), the boundary between the warm-temperate and boreal regions is described by the mean temperature of the coldest month (T_C, in °C), while in the BIOME model, the same BI determines what kinds of woody PFTs are present in the GAR, due to the availability of sufficient heat and moisture (Fig. B.3).

A permanent presence of hard winter frosts leads to low (below-freezing) values of T_C, activating the PFT "boreal evergreen conifer" (bec) in the BIOME model. Under the presence of this PFT, the model opts for the type COMX instead of the type TEDE in the designation of biome types (see Table 5 in Prentice et al. 1992). In addition, in the biomization procedure, this PFT is linked to the taxon *Picea* (see Table B.1), the main species of which is the Norway spruce (*Picea abies*). According to Zohner et al. (2016), in the case of *Picea abies*, the predominant climate type refers to the type Dfb, taking into account its native range. Considering these cross-correlations, it can be stated that the definitions of both climate- and pollen-inferred vegetation types used here are sufficiently substantiated.

The biome types "taiga" (TAIG) and "cool conifer forest" (COCO) together cover a total of 11.12% of the target area. As shown in Fig. 5.3, these types appear most markedly on the slopes of the Western and Central Alps, in the Eastern Alps, and sporadically in the Dinaric Alps. The mountain peaks of the Alps, the highest points of the target domain, are mostly dominated by the types TUND and PODE, covering a little less than 5% of the study area. At the same time, in the coastal regions of Croatia, Italy, and France, the dominant climate-inferred vegetation type is the biome type "warm mixed forest" (WAMX) with an areal proportion of only 1.2%, designating the most popular destinations for tourism in this region (see Batista e Silva et al. 2018).

5.3.2 Pollen-inferred biome reconstructions

In the GAR, the biomization is applied to the RPSs derived from the EPD, however, the type of dominant vegetation is ultimately determined for each pollen sequence. A total of 770 samples of 86 sequences meet the strict conditions, and a total of 13 biome types are involved into the biomizaton scheme. Thus, the partial results of the biomizaton procedure, i.e., all RBSs for all pollen sequences can be summarized in a 13 × 86 matrix, but here, these partial results are plotted by a percentage bar chart (Fig. 5.4), in order to facilitate the visual comparison of sequences.

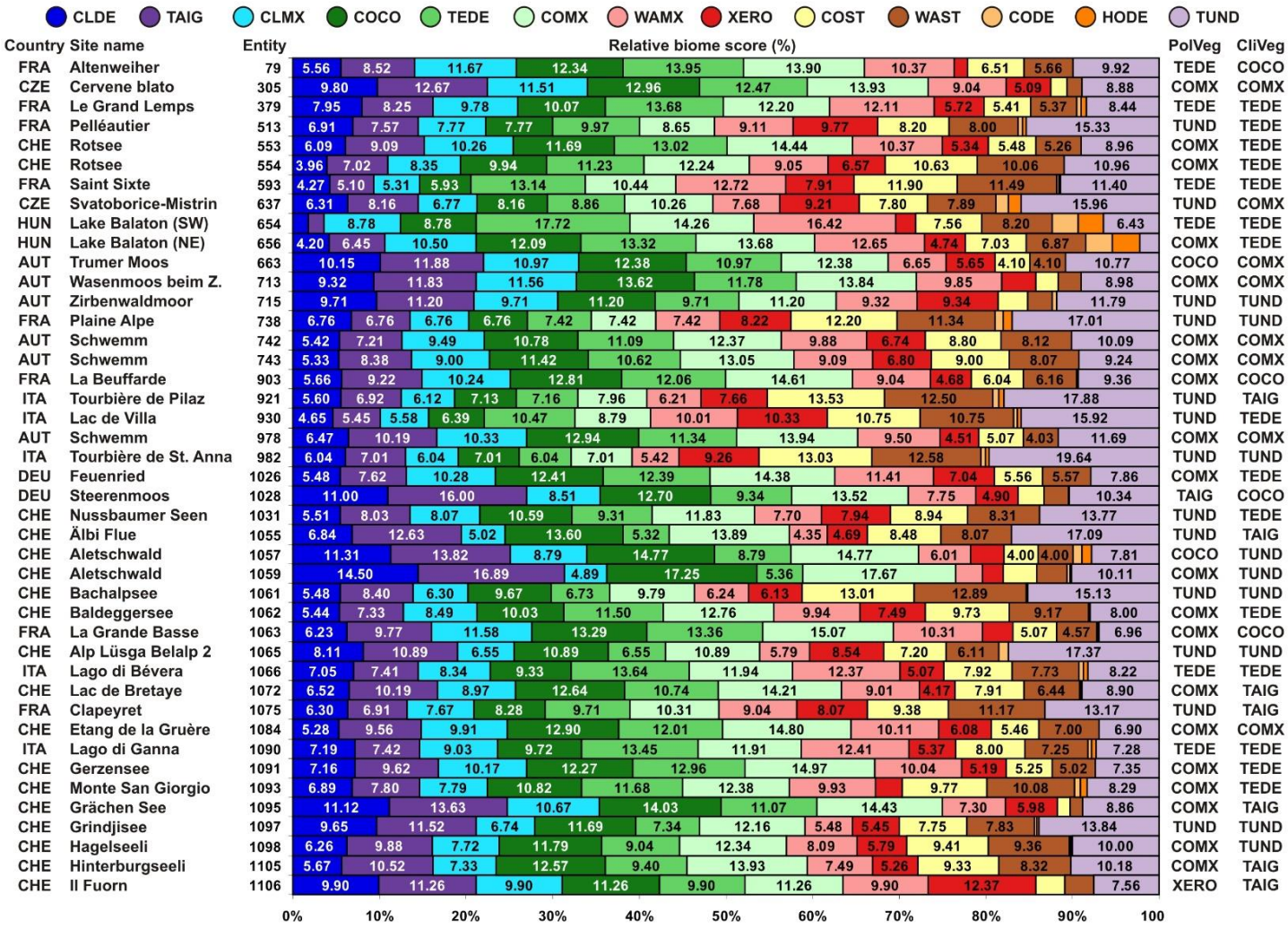

Fig. 5.4 Relative biome scores (RBSs) determined for 86 pollen sequences from the GAR, by using the relevant pollen samples for each pollen sequence; furthermore, the pollen-inferred vegetation (PolVeg) type, which is identified as the dominant type by using these RBSs in the biomization, and the climate-inferred vegetation (CliVeg) type simulated for the period 1801–1980 by the BIOME model (for that 0.5 arc-min grid cell in which the fossil pollen site is located), complemented with metadata (Entity, Site name, Country) for identifying the pollen sequence. RBSs below 4% are not shown in the figure. The abbreviations of biome types can be found in Fig. 5.3

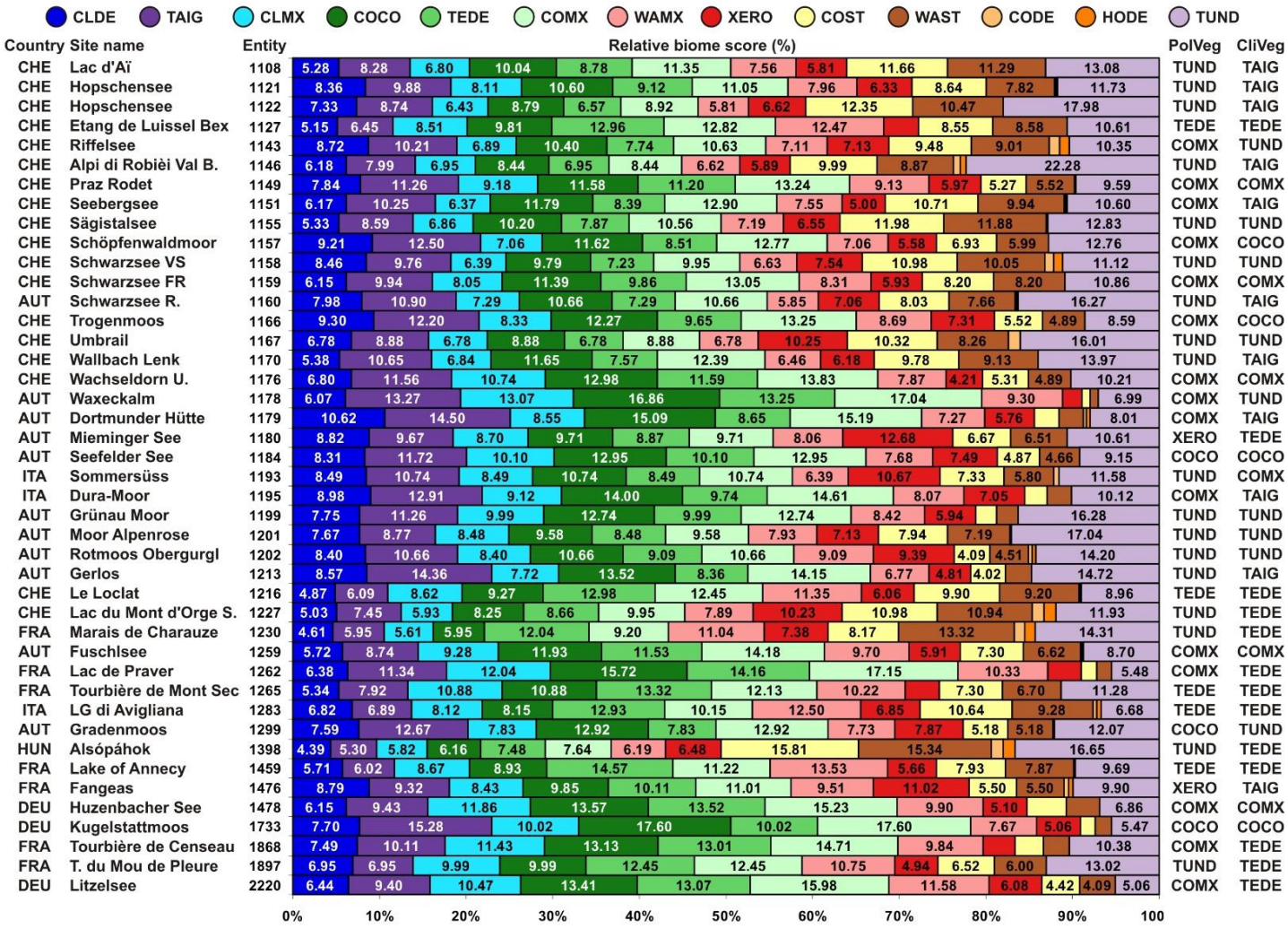

Fig. 5.4 (Continued)

The RPSs are derived from a total of seven countries (Fig. 5.4). Most (36 out of 86) pollen sequences can be found in Switzerland, but Austria and France also contribute substantially to the fossil pollen data, with 17 and 15 pollen sequences, respectively. In addition to a low number of Hungarian and Czech pollen samples, Italy and Germany, despite their large relative spatial coverage, provide only a total of 13 pollen sequences to determine the dominant biome type. Based on the spatial distribution of the pollen profiles involved in this study (Fig. 5.1), it can be found that the higher regions of the Alps and the study area (the eastern segment of the target domain and the lower regions) are over-represented (under-represented), which may distort our validation results.

Based on the RBSs (Fig. 5.4), only 6 of the 13 vegetation types used by the biomization scheme can be identified. For 36% of the pollen sequences, the biomization identifies the dominant vegetation type as the type TUND. For 11 out of 86 sequences of the target area, the pollen-inferred vegetation type is the type TEDE; while a total of 46% of the sequences are assigned to two biome types with very similar PFT compositions: COMX and COCO. Based on the available fossil pollen data, the dominant vegetation type is identified as the type TAIG for one sequence only (Steerenmoos, Germany). The pollen-inferred biome type XERO is assigned to three pollen profiles (one each in Switzerland, Austria, and France).

5.3.3 Comparison of the climate- and pollen-inferred biomes

The superimposing of biomization results on the distribution map of climate-derived vegetation types (Fig. 5.5) provides a good opportunity to evaluate the accuracy of the biomization approach. The biomization scheme estimates the appearance of the biome type TUND along the central chain of the Alps in accordance with climate-based vegetation predictions. Pollen assemblages of sites located in the region covered by the climate-derived vegetation type COMX, which appears sporadically in areas west of 10° E, and in its immediate vicinity, are also often assigned to the same type by the biomization. The biome type COCO, which covers small areas in the GAR in terms of the spatial distribution of climate-derived vegetation and is mostly limited to the Eastern Alps (Fig. 5.3), can be identified for a total of five pollen profiles based on the fossil pollen data. With one exception, the related pollen sites are located either in the Eastern Alps or in areas situated to the north of the Eastern Alps. For this vegetation type, a match between climate- and pollen-inferred biomes can be registered in two cases (Fig. 5.4).

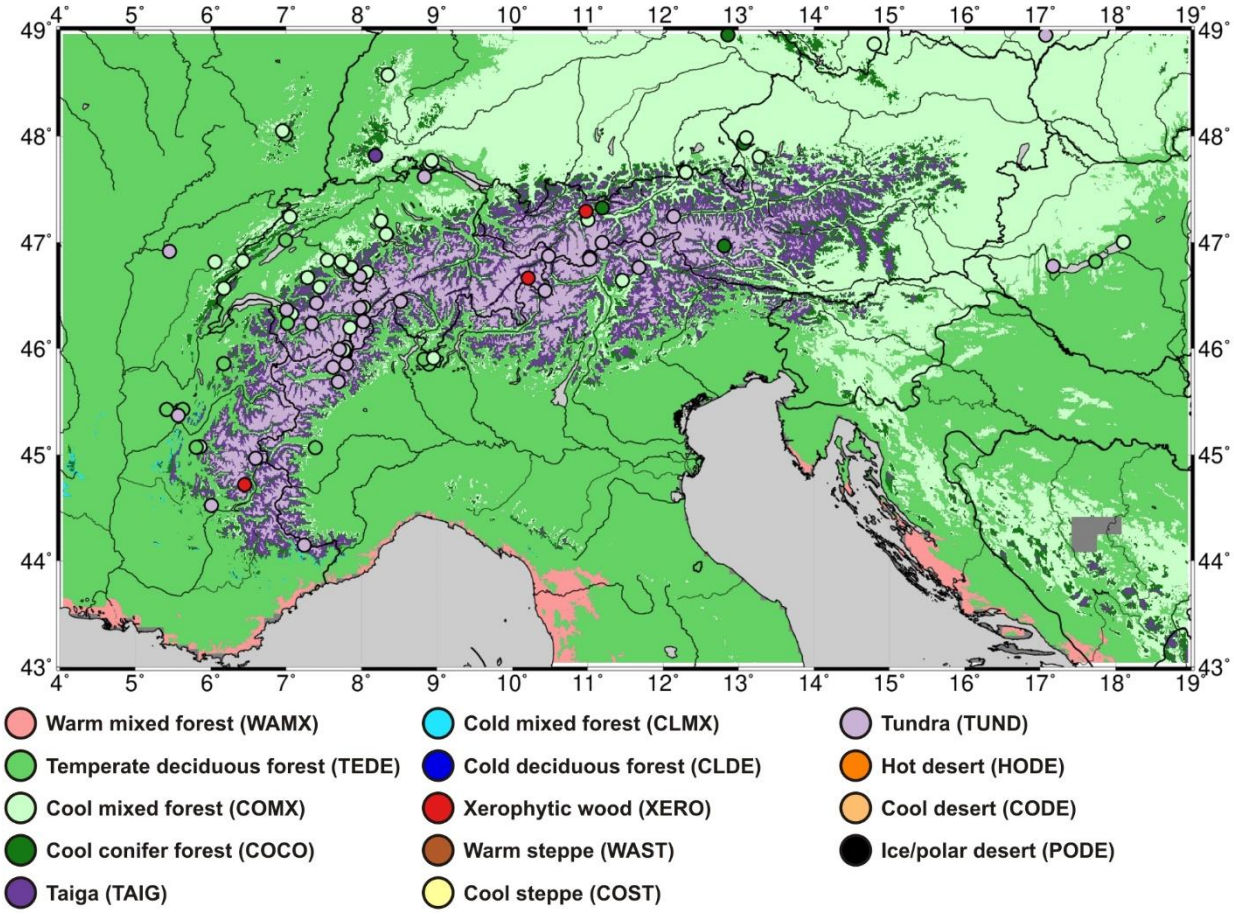

Fig. 5.5 Pollen-inferred biomes superimposed on the distribution map of climate-inferred biome types. The same biome classes are used in both the pollen-based biome reconstruction and the climate-driven BIOME model, with one exception. The type PODE, indicating the lack of vegetation, is not applied in the biomization approach

Along with this, it can be found that the quantitative assessment of the biome reconstructions is less satisfactory. The vegetation type estimated by the biomization scheme is only consistent with the climate-based vegetation type in 35 of the 86 pollen sequences for which the comparison can be carried out (Fig. 5.4), representing a matching rate of only 41%. However, the above proportion may change when subgroups are formed from pollen profile data by using quantitative characteristics which are specialized above, or when near-misses are taken into account.

According to the above classification of pollen sites, we can establish that anthropogenic pressure is likely to negatively affect the accuracy of the reconstruction (Fig. 5.6): only 39% (28 out of 72) of pollen assemblages from sequences strongly affected by human pressure can be biomized in accordance with climate-derived vegetation, while this ratio is 50% (7/14) for the pollen sites weakly affected by anthropogenic pressure. A similar relation is observed when comparing sites with high (HTR: 33%, 3/9) vs. low (LTR: 42%, 32/77) terrain ruggedness. However, it is important to emphasize that due to the relative imbalance of the subgroups formed from the sequences, the effect of these landscape characteristics on the biomization can only be considered in a distorted manner when evaluating.

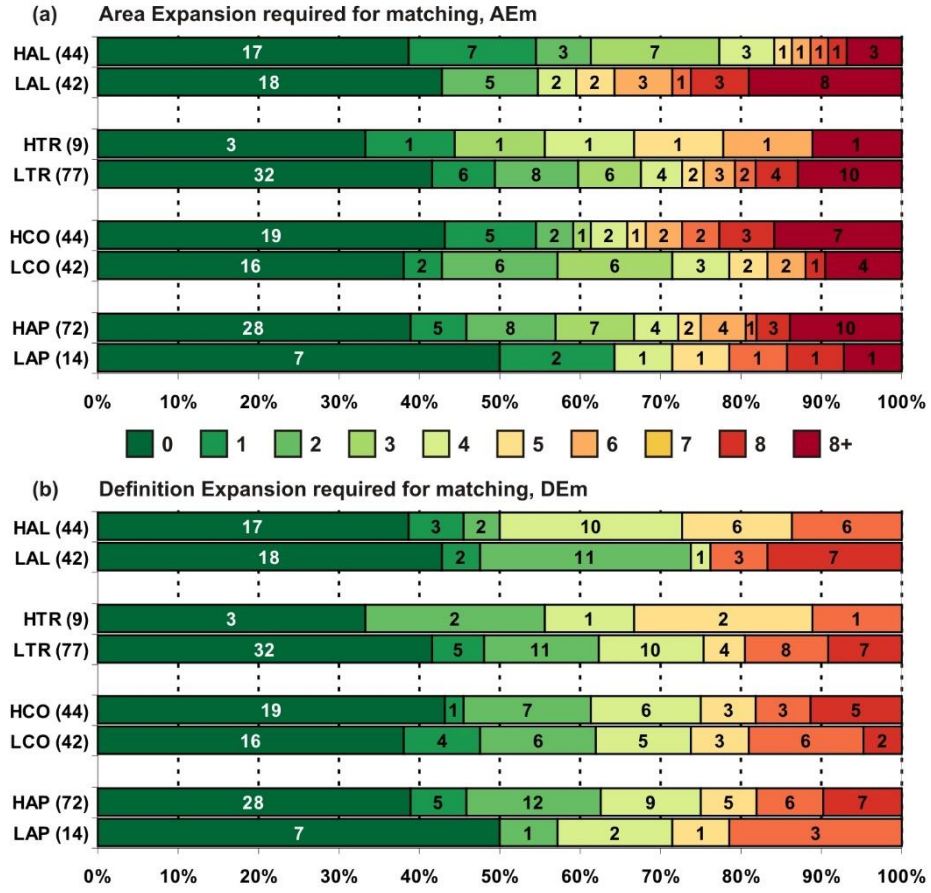

Fig. 5.6 Aggregate values of the matching measures (AEm: area expansion required for matching, DEm: definition expansion required for matching) defined here for subgroups of pollen sequences strongly (HAL, HTR, HCO, HAP) versus weakly (LAL, LTR, LCO, LAP) affected by various impacts (altitude, terrain ruggedness, canopy openness and anthropogenic pressure). The subgroups of strongly affected pollen sites are generated by considering the following landscape characteristics: (a) high altitude (HAL, altitude of >= 1000 m a.s.l.), (b) high terrain ruggedness (HTR, terrain ruggedness index of >= 240 m), (c) high canopy openness (HCO, tree canopy cover of < 25%), and (d) high anthropogenic pressure (HAP, human footprint index of >= 6). For details on generating landscape characteristics, see Section 5.2.3. For the spatial distribution of landscape characteristics and the classification of pollen sites by these characteristics, see Fig. B.2. Site values for the selected landscape characteristics are given in Table B.4

If near-misses are also taken into account, we can make the following statements (see Fig. 5.6): (a) in the case of low altitude sites, even a small expansion of the definition significantly increases the matching rate because if sites with DEm below 4 are identified as a match, this percentage increases from 43 to 74%; (b) for high altitude sites, the area expansion increases the matching ratio because if sites with AEm below 4 are accepted as a match, this percentage increases from 39 to 77%; and (c) for pollen sites under strong anthropogenic pressure, it is common for neither the definition expansion nor area expansion to lead to a match. It should also be noted that in terms of canopy openness, the effect of the definition expansion on consistent matching is similar for the two subgroups, while for sites with low canopy openness, the area expansion better improves the consistency between climate- and pollen-inferred biomes, compared to sites with high canopy openness.

Matching/mismatching patterns between climate- and pollen-inferred biomes (Table 5.1) show (a) the proportion of pollen sites biomized as a given biome type that falls into the same type of climate-derived vegetation zone, and (b) for a given climate-based vegetation class, the proportion of sites where the biomization captures the dominant vegetation type in accordance with the BIOME model. Using this approach, in addition to critical patterns, the possible reasons behind the discrepancies can also be explored. For example, in the case of pollen profiles classified as the climate-inferred biome type TEDE, the designation of the dominant vegetation type based on the fossil pollen data is often inconsistent in terms of the climate-derived vegetation (18 out of 28 sequences) (Table 5.1). However, most of the pollen profiles labelled as the type TEDE based on the fossil pollen data are assigned to the same type according to climatic conditions (10 out of 11 sequences), meaning that the biomization scheme performs well in identifying this biome type. Thus, although the estimation of the type TEDE is reasonable (with a success rate of 91%), 35.7% of the sites located in the region covered by this type of climate-derived vegetation are inconsistently attributed to the type COMX by the biomization procedure. Although it is also important to underline that (a) all 18 sites involved are under high human pressure conditions, and (b) for these pollen samples, even a small expansion of the definition significantly increases the likelihood of a match. The last two statements are also true for the climate-derived vegetation class COCO, for which the discrepancy between pollen- and climate-inferred biomes is always in favour of another forest biome type. See Table 5.1 for more details.

Table 5.1 Matching/mismatching patterns between climate- and pollen-inferred biomes. The column "Reference source: pollen-inferred biome" indicates the percentages of sites assigned by the biomization scheme to a given biome type that fall into the same type of climate-derived vegetation region. The column "Reference source: climate-inferred biome" shows the proportions of pollen sites within a given climate-derived vegetation region that are biomized as the same type. The main features underlying the observed discrepancies are given, and remarks on near-misses are also summarized. The abbreviations of biome types can be found in Fig. 5.3

Biome	Reference source: pollen-inferred biome	Reference source: climate-inferred biome
TAIG	0.0% (0/1); for the only site assigned to this pollen-inferred biome type, the climate-derived vegetation class is the type COCO.	0.0% (0/18); for pollen sites classified as this climate-derived vegetation type, pollen data are biomized as TUND (10), COMX (6), and XERO (2), with the remark that all sites are located at a high altitude, and an increasing the search window by no more than four units leads to a match for 12 of the 18 sites involved.
COCO	40.0% (2/5); this type is also attributed to sites located in the climate-derived regions TUND (2) and COMX (1), with the remark that for above three sites, the value of the human footprint index exceeds five.	25.0% (2/8); for the other sites, the biomization finds the following: COMX (4), TAIG (1), and TEDE (1), with the remark that all six sites are under high anthropogenic pressure conditions, and that for five of these six sites, a definition expansion by no more than three steps leads to a match.
TEDE	90.9% (10/11); in the case of the single mismatch, this pollen-inferred biome type is attributed to a site located in the climate-derived vegetation region COCO for which an increasing the search window by two units eventually results in a match.	35.7% (10/28); for the other sites, the biomization finds the following: COMX (10), TUND (7), and XERO (1), with the remark that all 18 sites are under high anthropogenic pressure conditions, and for 10 of the 18 sites involved, a definition expansion by no more than three steps leads to a match.
COMX	31.4% (11/35); this type is also assigned to sites located in the climate-derived regions TEDE (10), TAIG (6), COCO (4), and TUND (4), with the remark that the vast majority (21 out of 24) of above sites are under high human pressure conditions.	78.6% (11/14); for the other sites, pollen data are biomized as TUND (2) and COCO (1), with the remark that all three sites are under high anthropogenic pressure conditions and are located below 1000 m a.s.l.
XERO	0.0% (0/3); this pollen-inferred biome type is assigned to sites located in the climate-derived regions TAIG (2) and TEDE (1), however, an increasing the search window by even eight units does not result in a match for any of the above sites.	No sites.
TUND	38.7% (12/31); this type is also assigned to sites located in the climate-derived regions TAIG (10), TEDE (7), and COMX (2), with the remark that the vast majority (17 out of 19) of above 19 sites are under high anthropogenic pressure conditions, and an increasing the search window by no more than four units leads to a match in the case of 10 of these 19 sites.	66.7% (12/18); for the other sites, pollen data are biomized as COMX (4) and COCO (2), with the remark that all 12 sites are located at a high altitude.

5.4 Discussion

5.4.1 Validity of the simulated biomes

Despite the obvious methodological differences (see Section 5.3.1) for both the main BIs (Fig. B.3) and biomes (Fig. 5.3), the distribution maps created in this study are consistent with those

constructed using the dataset compiled by Leemans and Cramer (1991) for the normal time period 1931–1960 (see Huntley et al. 1995 for the main BIs; see Peng et al. 1995 and Prentice et al. 1998 for the biomes). Furthermore, the main vegetation formations in the GAR determined by vegetation scientists (Bohn et al. 2003) can be properly detected by applying the BIOME model in the configuration used here. This is supported by the fact that in several cases, the dominant natural plant formation (supplementary maps in Bohn et al. 2003) that is consistent with the current climatic and edaphic conditions shows a big overlap with the climate-derived biome type (Fig. 5.3) simulated in this study (and now given in parentheses): (a) the alpine vegetation, B.2 in the central chain of the Alps (the biome type TUND), (b) the fir and spruce forests, D.4 in the Eastern Alps (the types TAIG and COCO), and (c) the beech and mixed beech forests, F.5 in the areas situated to the north–northeast of the Alps, in the southern foothills of Alps, and in the Dinaric Alps (the type COMX).

Due to the high spatial resolution of the climate fields used to create the biome map, the altitudinal stratification of plants is very well observed. In valleys characterized by less harsh conditions, where the value of GDD_5 (Fig. B.3b) exceeds the threshold of 1200 °C day, the types TEDE and COMX (Fig. 5.3) usually appear, depending on whether the value of T_C (Fig. B.3a) is above −2 °C or not. In the study area, these types occur only marginally at altitudes above 1500 m a.s.l. On the slopes, the types COCO and TAIG become dominant, replacing the "warmer" forests. This is because, on the slopes of the Alps, where sufficiently humid conditions are typical with (moderately) cold winters, only PFTs for which a smaller amount of heat is sufficient can be activated. However, where the value of GDD_5 does not exceed the threshold of 350 °C day, woody PFTs cannot activate. Here, this is mostly the case in areas at altitudes above 2000 m a.s.l., making the type TUND dominant. The altitudinal zonation of climate-based biomes simulated in this study is consistent with the position of vegetation belts revealed by phytogeographical analysis (see e.g., Fauquette et al. 2018).

5.4.2 Gaps and overlaps between the climate- and pollen-inferred biomes

The biomization procedure is able to capture regional-scale patterns of vegetation distribution in the GAR (Fig. 5.5), which has a remarkable performance in terms of the degree of human pressure on the landscape (see Fig. B.2d). However, anthropogenic pressure, together with the other above-mentioned influential factors (e.g., anomalies in pollen production), makes it difficult to make quick and unsupervised biomizations of fossil pollen data. Unfortunately, the spatial distribution of the few pollen sequences suitable for this performance assessment is non-homogeneous (Fig. 5.1): the Alps and the higher regions of the target domain are over-represented. In addition, comparisons are strongly hampered by the following facts: (a) almost all sites under low anthropogenic pressure conditions are located at high altitudes (13/14) and have high canopy openness (12/14) (see Fig. B.2), and (b) for these subgroups, the climate-inferred biomes are significantly differentiated (considering these three landscape characteristics, for 11 out of the 12 common pollen sequences, the BIOME model identifies the dominant vegetation type as either the type TUND or type TAIG) (cf. Fig. B.2 and Fig. 5.3). This makes it much more difficult to evaluate the results because the influential factors that affect different types of biomes to varying degrees can either reinforce or even mask one another.

5.4.2.1 Mixed forests everywhere

Pollen assemblages from profiles located in the region covered by the climate-based vegetation type COMX are biomized in accordance with climatic conditions (for 78.6% of these profiles, the

same biome type is detected using pollen data). However, sequences that are labelled as type COMX based on the pollen data often do not fall into the climate-derived vegetation region of the same type, leading to a matching rate of only 31.4% (i.e., for 24 of those 35 sites whose pollen data are biomized as the type COMX, a discrepancy can be observed between pollen- and climate-inferred biomes). The vast majority (21 out of 24) of the sites involved are under high anthropogenic pressure conditions, so a human impact is likely behind these discrepancies.

Biome types COMX and TEDE can be described by a similar taxon list (JSI: 0.787; see Fig. B.1). However, there are some fundamental differences between them. For example, *Picea* pollen indicates the presence of the PFT bec (see Section 5.3.1), while in the biomization procedure, the PFT "cool-temperate broad-leaved evergreen tree/shrub/liane" (wte1) is activated by the presence of pollen of ivy (*Hedera*) and holly (*Ilex*). The former PFT increases the value of the affinity score for the type COMX in the biomization, while the presence of the latter contributes to the value of type TEDE. Although ivy and holly are good climate indicators (see frost-intolerant species: Iversen 1944), in the study region, the abundance and distribution of these species decreased during the Neolithic and Bronze and Iron Ages due to anthropogenic burning (Tinner et al. 1999, 2005). In contrast, in the Swiss Alps, spruce increased in abundance (and distribution) during the Neolithic due to indirect effects (e.g., the decline of competitors), while in the last centuries due to the recovery of the timber industry (Conedera et al. 2017).

The intermingling of the biome types TEDE and COMX in the European mountains has also been shown by Binney et al. (2017), but as possible explanations for this phenomenon, the authors of the above study have indicated both the relatively fine spatial scale of vegetation mosaics and the floristic similarity of the biome types involved. But we think that due to the fine spatial resolution of the biome map used as a reference, the former effect may play a smaller role in mismatches experienced in the current study. In contrast, as already indicated by Prentice et al. (1996), through the over-representation of *Picea*, the dominance of mixed forests in this region can be much better explained by human activities, namely, the establishment of conifer plantations (Weetman 2005).

In the case of pollen profiles located in the region covered by the climate-derived vegetation types COCO and TAIG, there is also a high proportion of those for which the method used here translates pollen data into the type COMX (Table 5.1). For the first biome class, all affected sections are located at high altitudes, while for the second, the anthropogenic pressure poses a challenge for the biomization. If in addition to pollen from coniferous species (e.g., *Picea abies*, *Pinus cembra*), summergreen tree species such as common oak (*Quercus robur*) and common ash (*Fraxinus excelsior*) can also be detected in a sample, the dominant biome type is easily identified as COMX. This finding is true for most of the above-mentioned pollen profiles, with the remark that for most of these samples, there is also a high proportion of grasses (Gramineae) and/or sedges (Cyperaceae) referring to grazed meadows (Court-Picon et al. 2006). The appearance of common ash and European beech (*Fagus sylvatica*) in these samples is explained by the abandonment of traditional grazing (van der Knaap et al. 2000), which is further confirmed by the detection of grasses/sedges pollen. Identification of oak pollen in these samples can probably be attributed to the fact that in the last centuries, in alpine areas, the use of acorns to feed pigs has favoured this tree species over others (Burga 1988).

5.4.2.2 Tundra or not tundra? That is the question!

In this study, the climate-derived vegetation type TUND can only be assigned to the pollen profiles related to high altitude sites (cf. Fig. 5.5 and Fig. B.2a). The number of such sequences is 18. For

12 out of these 18 pollen profiles, the pollen-inferred biome type is the type TUND, making a significant contribution to the value of observed agreements. The biomization procedure assigns the remaining six sequences to one of the cool-temperate forest biome types. In accordance with the nature of the above subgroups, this discrepancy in the classification can be clearly explained by the upslope transport of pollen, which had been previously reported as a potential source of bias in the biomization approach (see e.g., Takahara et al. 2000; Marinova et al. 2018).

In addition, in these subgroups, there is a very high number of sequences for which the biomization scheme assigns the type TUND and for which the dominant type is one of the forest biome types according to the climatic conditions (Table 5.1). In this case, the anthropogenic opening of the closed vegetation (see e.g., Valsecchi et al. 2010; van der Knaap et al. 2000) could give a clear explanation for the observed mismatches. This may also be indicated by the fact that the vast majority (17 out of 19) of affected sites are under high anthropogenic pressure conditions. In addition to taxa that have already previously been associated with the grazing pressure (grasses and sedges), in various amounts, these pollen assemblages also contain other non-arboreal pollen taxa that indicate the proximity of (alpine) pastures (e.g., *Plantago alpina*, *Plantago lanceolata*, *Urtica*: Court-Picon et al. 2006; Appendix in Gilck and Poschlod 2019) and/or cultivated areas (e.g., *Secale cereale*, *Cerealia*-type: Behre 1981). Thus, in these cases, the dominance of the type TUND in the biomization is likely explained by a high degree of human pressure.

It is also important to underline that for 10 of the above-mentioned sites located in the region labelled as the climate-derived type TAIG, an increasing the search window by no more than four units leads to a match. Considering that the related pollen sequences are located in a topographically complex region (Fig. 5.5) and that the spatial area/scale represented by a fossil pollen site is not necessarily the same as that of the related grid cell, the observed mismatches cannot be explained by only one general rule. The following factors, alone or in combination, may be behind this discrepancy: (a) the terrain ruggedness, (b) the landscape modification by human activities, and (c) the fact that the ecotonal vegetation types (e.g., forest-tundra ecotone: Holtmeier 2009) cannot be identified by classification schemes of either climate- or pollen-inferred vegetation.

5.4.2.3 Limitations and perspectives of the PFT and biome definitions used

The appearance of the pollen-inferred biome type XERO in the Alps, where the dominant biome types are the climate-inferred types TUND and TAIG, is striking (Fig. 5.5). It can be explained by the fact that the related pollen assemblages are dominated by the taxon *Pinus* and a taxon assigned to the PFT "grass" (g). Following Binney et al. (2017), the former (i.e., pine) is assigned to the PFT "eurythermic coniferous tree/shrub" (ec) (see Tables B.1–3), which is a component of all forest biome types due to its widespread distribution (Critchfield and Little 1966). The latter, however, may only occur in the case of the type XERO of all the forest biome types. For example, in cases where, besides pine, a large number of grasses dominate a core-top sample due to human activity, the biomization procedure incorrectly identifies the climate-derived vegetation type as XERO.

The PFT and biome definitions used in this classification scheme take into account neither the ecotones between major vegetation communities nor anthropogenic biomes called anthromes (see Ellis et al. 2010). For this reason, this method is not directly applicable for reconstructing anthropogenic land use changes or for precise descriptions of the dynamics of vegetation transitions. To address these issues, Woodbridge et al. (2014) developed the so-called pseudo-

biomization approach, and this procedure was applied to surface pollen samples and tested by comparison with a remotely sensed land cover map.

Woodbridge et al. (2014) have shown that this procedure works reasonably well for "pure" (non-mixed) classes, but where due to landscape heterogeneity neither pollen-inferred nor remotely sensed vegetation data can interpret vegetation mosaics with sufficient accuracy, there is a limit to validating the method optimized for pan-European conditions. Later, Fyfe et al. (2015) applied this approach to fossil pollen data in order to produce a first synthesis of Holocene land cover changes in Europe. Although the results obtained in this study and in Fyfe et al. (2015) are not directly comparable due to differences in the implementations of classification schemes (e.g., time window, involved taxa, and weighting applied to land cover classes that include high/low pollen-producing taxa), it is important to note that for 21 (4) out of the 72 common sequences, the most recent fossil pollen assemblages are assigned by the pseudo-biomization procedure to the semi-open (arable/disturbed land) class. This fact indicates that in the GAR, a highly heterogeneous and human-modified landscape, the above aspects should be taken into account when establishing vegetation clusters that are required to explore long-term land cover changes.

In addition, it is important to emphasize that the following statement is true in about 76% of the sequences used here: the climate-inferred biome type is the same as one of the three types with the highest RBSs (see Fig. 5.4). This finding is consistent with results obtained by Woodbridge et al. (2014) indicating that the ratio of near-misses in the GAR is very high (see Fig. 4c in Woodbridge et al. 2014). In our opinion, this also reinforces the conviction that in vegetation mapping it is a good practice to use partial results of a biomization approach that is optimized for larger spatial and temporal objectives, thus avoiding a significant loss of information. This is in line with the finding of Zanon et al. (2018) that a calibrated version of the MAT method using the partial results of biomization (i.e., the PFT scores) and aiming to generate a gridded forest cover reconstruction focusing on large-scale vegetation patterns is able to track major land cover fluctuations even in complex terrain such as that of the Alpine region.

5.5 Conclusions

One of the basic aims of this study was to test one of the best-known pollen-based vegetation reconstruction approaches, called the biomization scheme, in terms of performance and potential sources of bias, following the guiding principles of initial validation experiments and making active use of improvements made in the relevant research fields over the past 25 years. The evaluation was carried out as a case study for the GAR. However, given that the climate has not been the main driver of vegetation in this highly heterogeneous and human-modified landscape for thousands of years, matching/mismatching patterns between climate- and pollen-inferred biomes did not necessarily and exclusively indicate the success or failure of the biomization.

Our results suggest that the matching rate below 50% is necessarily attributed to the fact that classification schemes used here take account of neither ecotones nor anthromes. Considering near-misses, for example, it was found that in the case of low altitude pollen sites, even a small expansion of the definition significantly increases the matching percentage: if sites with DEm below 4 are identified as a match, this rate increases from 43 to 74%. This may suggest that although the climate is not currently a major determinant of biomes in the target area, at many sites in this region, ancient woodlands have only been partially altered by human activities (e.g., the establishment of forest plantations, eradication of certain species). For high altitude sites, the area

expansion helps to eliminate the discrepancy between climate- and pollen-inferred biomes. However, this observation can be even explained by the simultaneous presence of several effects: (a) the terrain ruggedness, (b) the anthropogenic landscape alteration (e.g., opening of the closed vegetation), and/or (c) the transitional nature of the vegetation (see forest-tundra ecotone).

Considering all these findings, we believe that in the GAR, the biomization scheme alone is not a sufficient tool to circumscribe vegetational regimes in both spatial and temporal terms. This reconstruction procedure does not provide sufficient information on the dynamics/features of regime transitions and the human disturbance regimes (e.g., browsing, burning, and cultivation) through the identification of dominant biome types. However, regime transitions can be successfully monitored using quantitative vegetation reconstruction approaches that rely on the partial results of the biomization procedure, i.e., the PFT and biome scores (e.g., percentage of arboreal PFTs: Davis et al. 2015; landscape openness index: Li et al. 2019). Landscape changes related to anthropogenic land use can be tracked using pseudo-biomization (e.g., Fyfe et al. 2015) and various anthropogenic pollen indicators (see Deza-Araujo et al. 2020).

Another goal of the paper was to create a very high-resolution distribution map of climate-derived vegetation for the period 1800–1980 that can be used in further biological studies. It was found that in terms of distribution patterns, our biome map with a horizontal resolution of 0.5 arc-min that was generated using only monthly temperature and precipitation data (and two digital elevation models) is consistent with a PNV map prepared by vegetation experts. Furthermore, our results indicate that the altitudinal zonation of biomes modelled here harmonizes with the position of vegetation belts revealed by phytogeographical analysis. In the investigated period, valleys characterized by less harsh conditions were circumscribed by the types TEDE and COMX, while in areas at altitudes above 2000 m a.s.l., the type TUND was dominant. Given that *RSD* data required to generate the biome map were also estimated using the above data, the validity of vegetation distribution simulated here is remarkable. Because estimating *RSD* data is time- and resource-intensive, raster data generated here by the BIOME model (i.e., distribution maps for both biomes and the five BIs used in classification) are shared upon request with other biological studies, which are assessing spatial differences in the distribution of plants/animals in the light of climatic conditions.

Acknowledgments. The work of the first author was supported by the European Union and the State of Hungary, co-financed by the European Social Fund in the framework of TÁMOP 4.2.4. A/2-11-1-2012-0001 ‘National Excellence Program’. The work of the second author is aided by the János Bolyai Research Scholarship of the Hungarian Academy of Sciences. The authors would like to thank all members of the HISTALP (HISTorical instrumental climatological surface time series of the Greater ALPine Region) project for the use of their dataset (http://www.zamg.ac.at/histalp/). The authors thank all contributors to the European Pollen Database (EPD; http://www.europeanpollendatabase.net/) for their willingness to share their data with the scientific community. Special thanks are owed to Thomas Giesecke (University of Göttingen, Germany) and his co-authors for giving access to the revised site chronologies (https://doi.pangaea.de/10.1594/PANGAEA.804597). The authors are really grateful to the creators of the elevation map (Global 30 Arc-Second Elevation Dataset, GTOPO30) and land use/cover maps (the tree cover map from the Global Forest Change Dataset and the Human Footprint Index map) used in this study for sharing their datasets with the scientific community. The GTOPO30 digital elevation model can be downloaded from https://www.wsl.ch/lud/HSDM_Book_Data/GTOPO_30.zip. The Global Forest Change Dataset is available at https://earthenginepartners.appspot.com/science-2013-global-

forest/download_v1.7.html. The version of the Human Footprint Index map that is used here can be accessed at https://sedac.ciesin.columbia.edu/data/set/wildareas-v3-1993-human-footprint/data-download. The authors are also grateful to the software developers of the SPLASH model (https://bitbucket.org/labprentice/splash), and of the R packages "fossil" (https://github.com/cran/fossil), "raster" (https://github.com/cran/raster) and "terra" (https://github.com/cran/terra) for making their source codes available to everyone. Finally, the authors also thank Ákos János Varga (Eötvös Loránd University, Hungary) for language polishing.

6 Summary

The main findings and conclusions of this dissertation are summarized and discussed as follows.

1. **Climate of the Carpathian Region in the twentieth century based on various versions of the Holdridge life zone system** (Chapter 2)

   Using monthly temperature and precipitation data provided by the CRU TS 1.2 database, I calculated climatologies (multi-year averages) for five 20-year periods of the twentieth century (P1: 1901–1920, P2: 1921–1940, P3: 1941–1960, P4: 1961–1980, P5: 1981–2000), focusing on the Carpathian Region. The Holdridge life zone (HLZ) system was applied to these data, in order to track the temporal evolution of the spatial and altitudinal distribution patterns of HLZ types.

   Based on theoretical considerations and my own previous experience (Szelepcsényi et al. 2009), I proposed a modification to the HLZ system: both the core and transitional HLZ types were determined as separate classes. The modified model was also used to the above climatologies.

   As a validation, I compared the HLZ maps generated by both the original and modified models for P1 to an expert-based vegetation map, and determined the degree of agreement between them using the Kappa statistic (κ).

   I assessed the temporal changes in the relative coverage, the mean centre and the mean distributional altitude (MDA) for each HLZ type in order to map the ecological impacts of the recent climate change in the Carpathian Region.

   a. **Using the selected variants of the HLZ system, I demonstrated the effects of recent climate change on the potential vegetation in the Carpathian Region. Consistent with the recently observed shifts of the natural ecosystems, I showed northward and/or upward shifts of the HLZ types.**
      - During the last century, the mean centres of those HLZ types which were not related to mountains shifted northward.
      - From P1 to P3, the value of MDA increased for all HLZ types, apart from one exception, whereas from P3 to P4, a decrease in this parameter can be registered for all HLZ types. The reason for this is the fact that the climate in P4 was slightly rainier and cooler than in the former period. All in all, for the five most abundant HLZ types, the value of MDA increased during the last century.

   b. **Based on theoretical considerations, I proposed a modification to the HLZ system. By applying the proposed modification, I circumscribed the potential distribution range of the forest-steppe ecotone in the Carpathian Region.**
      - Due to the introduction of transitional HLZ types, the spatial pattern of vegetation classes is significantly rearranged: (a) the first in the coverage ranking is the core HLZ type "cool temperate moist forest", with an areal proportion of 50–60% (depending on the study period), whereas (b) the second most abundant vegetation class is the transitional HLZ type "cool temperate subhumid forest-steppe", covering a significant part of the lowland areas.
      - Comparing the distribution pattern of this transitional HLZ type in P5 and the potential areas of the forest-steppe ecotone (see Varga et al. 2000), a big overlap can be found between them.

2. **Assessment of projected climate change in the Carpathian Region using the Holdridge life zone system** (Chapter 3)

I applied the HLZ system to bias-corrected temperature and precipitation fields of 11 regional climate model (RCM) simulations provided by the ENSEMBLES project in order to evaluate the magnitude and uncertainty of the possible ecological impacts of the projected climate change in the Carpathian Region. Climatologies – and thus the spatial and altitudinal distribution patterns of HLZ types – were determined for three 30-year (T1: 1961–1990, T2: 2021–2050, T3: 2061–2090) and also 28 10-year (D1: 1951–1960, D2: 1956–1965, D3: 1961–1970, etc.) time periods.

In my assessment, the distribution patterns of HLZ types were characterized by the relative extent, the mean centre and the altitudinal range (i.e., the lower and upper altitudinal limits and also the altitudinal midpoint). I used the modified Mann-Kendall trend test to these spreading parameters generated using 10-year climatologies, in order to assess the expected temporal evolution of them, i.e., the direction and uncertainty of their predicted changes.

Using values of κ, I selected simulations, which provide the maximal and minimal distributional changes. The results for these simulations and the ensemble mean were presented in detail.

a. Using the HLZ system, I demonstrated that under a moderate emission scenario, the spatial patterns of potential vegetation types may change significantly by the end of the twenty-first century in the Carpathian Region, regardless of RCM simulations used.

- The boreal HLZ types are estimated to disappear from the region, whereas the types "warm temperate thorn steppe" and "subtropical dry forest" can appear, which can be found nowadays, for example, in Spain and Turkey.
- By the end of the twenty-first century, the relative extent of humid and perhumid HLZ types is projected to decrease by 41 ± 12 and $58 \pm 13\%$, respectively. The relative coverage of warm temperate HLZ types at the end of the century can be estimated to be 10 times as much as at present, while in the case of cool temperate HLZ types, the same value can be reduced by one or two thirds, in the same time frame.

b. I showed that the recently detected increasing temperature trend is likely to continue in the future in the Carpathian Region, for which as a response, northward and/or upward shifts of biome types are projected.

- The altitudinal ranges of potential vegetation types may expand in the future. The lower and upper altitudinal limits and also the altitudinal midpoint of HLZ types are likely to move to higher altitudes.
- A northward shift is expected for most HLZ types, and the magnitudes of these shifts can even be several times greater than those observed in the last century.

c. I pointed out that there is a considerable uncertainty in the predicted evolution of precipitation patterns in the Carpathian Region, which weakens the reliability of projections of potential vegetation distribution.

- The expected change in the coverage of the type "cool temperate steppe" is extremely uncertain because there is no consensus among the projections even in terms of the sign of the change (high inter-model variability).
- A significant trend in the westward/eastward shift is simulated just for some HLZ types (high temporal variability).

3. Estimating relative sunshine duration from commonly available meteorological variables for simulating biome distribution in the Carpathian Region (Chapter 4)

Applying the regression model of Yin (1999) to monthly temperature and precipitation data from the CarpatClim dataset, I estimated the time series of monthly mean daily value of the

relative sunshine duration (*RSD*) for each year of the period 1961–2010. Then, in each grid cell, values of the root mean square error normalized by the mean value of observed data (*RRMSE*) were computed between the observed and estimated 50-year time series of *RSD*, separately for each month.

To test the applicability of the estimation scheme to paleoclimate datasets, I calculated *RSD* values for the period 1981–2010 in two ways: (a) by averaging the time series estimated using the initial scheme for each year, and (b) by applying the scheme to 30-year averages. The estimated results were compared with the averages of the measured values over the study period.

I assessed the sensitivity of the BIOME model for estimating the spatial distribution of potential vegetation to changes in various configuration settings. The simulations were performed using climate data for the period 1981–2010. Here, I only evaluated the effects of the choice of the method used to generate the quasi-daily values and of the source of the *RSD* data on the results. With respect to the former, I performed the simulations in two ways: (a) monthly means were assumed constant over each day of the month, and (b) different mean-preserving interpolation techniques were applied.

a. I showed that in the most important period for evapotranspiration processes, the monthly time series of *RSD* can be estimated with reasonable accuracy by applying the procedure proposed by Yin (1999) to single-year time series, under varied topographic conditions.

- From May to August, the *RRMSE* between the estimated and measured *RSD* values in more than 90% of the study area does not exceed the threshold of 20% below which the model performance can be considered excellent.
- In the period from April to October, in nearly 99% of the grid cells with elevation smaller than 500 m a.s.l., the value of *RRMSE* is less than 40%, which is the limit of the model performance still considered acceptable.
- In the summer months, the *RRMSE* value in almost 90% of the lower regions (elevation < 500 m a.s.l.) does not even exceed the threshold of 15%.

b. I demonstrated that in a data poor modelling environment, *RSD* data can be adequately replaced by using a novel modelling framework based on the procedure proposed by Yin (1999), in which the data processing steps are reversed and the estimation scheme is fine-tuned.

- For the *RSD* climatologies estimated for the period 1981–2010 with the new modelling framework, from April to September (with one exception), the value of *RRMSE* calculated for the whole study area does not exceed the threshold of 10%, which indicates a very good quality of the estimates.

c. I showed that the BIOME model is insensitive to the configuration settings assessed here (i.e., the choice of the method used to generate the quasi-daily values and of the source of the *RSD* data).

- The choice of source for the monthly time series of *RSD* has no effect on the biome distribution under given space and time conditions: comparing the simulation using measured *RSD* values to both simulations driven by estimated *RSD* values, no differences between the biome maps were found.
- All biome maps generated using interpolated daily values are consistent with each other. Comparing them to the reference map, only a slight mismatch can be found. For only

0.4% of grid cells, there is a disagreement between biome maps derived using different daily weather data. In all cases, this mismatch could be explained by the discrepancy in the spatial distribution of growing degree-days above a 5 °C base (GDD_5).

4. **Comparing climate- and pollen-inferred vegetation in the Greater Alpine Region** (Chapter 5)

   Using simple statistical assumptions, I re-gridded the monthly temperature and precipitation fields derived from the HISTALP database for each year of the period 1800–1980 to a 0.5 arc-min grid of the Global 30 Arc-Second Elevation Dataset (GTOPO30). Applying the regression model of Yin (1999) to these downscaled meteorological fields, I estimated the monthly time series of *RSD* for each year within the study period. Then, I computed the mean field separately for each of the three relevant meteorological variables. Finally, I used these data to drive the BIOME model in order to simulate the distribution pattern of biomes in the Greater Alpine Region (GAR).

   I applied a refined version of the biomization procedure to 770 of the most recent fossil pollen assemblages derived from the European Pollen Database. In the next step, I calculated the relative biome scores (RBSs) obtained from the biomization for the involved 86 pollen sequences, and the type of dominant vegetation was ultimately determined for each profile.

   Using a pointwise approach, I compared the vegetation simulated by the BIOME model with the vegetation reconstructed on the basis of the RBSs characterizing the pollen sequence. To assess the effects of near-misses (i.e., assignments to a biome type with similar composition) on the comparison of climate- and pollen-based biome reconstructions, I determined the values of the area expansion and definition expansion required for matching (AEm and DEm) for each pollen profile, and aggregated these values for subgroups formed from the sequences, by using various landscape characteristics.

   a. **Using only monthly temperature and precipitation data (and digital elevation models), I generated a very high-resolution distribution map of biomes for the GAR in a modelling framework where *RSD* data required to run more sophisticated biome models were estimated using the model of Yin (1999).**

      - In the GAR, the main vegetation formations determined by vegetation scientists can be properly detected by applying the BIOME model with the configuration used here. Comparing distribution patterns of the tundra biome type simulated here and that represented by the subunit alpine vegetation (B.2) on the map of Bohn et al. (2003), there is a large overlap between them. The same conclusion holds for the following pairs: (a) the subunit fir and spruce forests (D.4) in the map of Bohn et al. (2003) and the aggregate represented by the types “taiga” and “cool conifer forest” on the biome map generated here, and (b) the subunit beech and mixed beech forests (F.5) in the expert-based vegetation map and the type “cool mixed forest” simulated here.
      - In valleys characterized by less harsh conditions, where the value of GDD_5 exceeds the threshold of 1200 °C day, the types “temperate deciduous forest” and “cool mixed forest” usually appear, depending on whether the mean temperature of the coldest month is above −2 °C or not. In the GAR, these types occur only marginally at altitudes above 1500 m a.s.l. On the slopes, the types “cool conifer forest” and “taiga” become dominant, replacing the “warmer” forests. Where the value of GDD_5 does not exceed the threshold of 350 °C day, woody plant functional types cannot activate. Here, this is mostly the case in areas at altitudes above 2000 m a.s.l., making the type “tundra” dominant. The altitudinal zonation of biomes simulated using climate data is consistent with the position

of vegetation belts revealed by phytogeographical analysis (see e.g., Fauquette et al. 2018).

b. I re-assessed discrepancies between climate- and pollen-inferred biome types in the Alpine region detected by initial validation experiments of the biomization approach, making active use of improvements made in the relevant research fields over the past 25 years.

- The vegetation type estimated by the biomization scheme is only consistent with the climate-based vegetation type in 35 of the 86 pollen sequences, representing a matching rate of only 41%.
- The following statement is true in about 76% of the sequences used here: the climate-inferred biome type is the same as one of the three types with the highest RBSs.

c. By taking into account both the impeding factors and the near-misses, I further nuanced the picture that emerged from comparing climate- and pollen-inferred vegetation types in the GAR. I pointed out that the discrepancies are not necessarily due to the inappropriateness of the biomization procedure but rather due to human impacts on the landscape.

- Considering near-misses, for example, it was found that in the case of low altitude pollen sites (elevation < 1000 m a.s.l.), even a small expansion of the definition significantly increases the matching percentage: if sites with DEm below 4 are identified as a match, this rate increases from 43 to 74%. This may suggest that although climate is currently not a major determinant of biome distribution in the GAR, at many sites in this region, ancient woodlands have only been partially altered by human activities (e.g., establishment of forest plantations, eradication of certain species).
- For high altitude sites (elevation ≥ 1000 m a.s.l.), the expansion of the search window increases the matching ratio because if sites with AEm below 4 are accepted as a match, the matching percentage increases from 39 to 77%. However, this observation can even be explained by the simultaneous presence of several effects: (a) the terrain ruggedness, (b) the anthropogenic landscape alteration (e.g., opening of the closed vegetation), and/or (c) the transitional nature of the vegetation (see forest-tundra ecotone).
- Overall, the above results suggest that the fact that the classification schemes used here do not take into account either ecotones or anthromes (i.e., intensive land-use biomes) significantly impedes comparisons.

7 Összefoglalás

A dolgozat legfontosabb eredményei és következtetései az alábbiak szerint foglalhatóak össze.

1. **A Kárpát-régió éghajlata a XX. században a Holdridge-féle életzóna rendszer különböző verziói alapján** (2. fejezet)

   A CRU TS 1.2 adatbázis által biztosított havi hőmérséklet- és csapadékadatokból a XX. század öt különböző 20 éves időszakára (P1: 1901–1920, P2: 1921–1940, P3: 1941–1960, P4: 1961–1980, P5: 1981–2000) vonatkozóan számítottam ki a klimatológiákat (többéves átlagokat) a Kárpát-régióra nézve. A Holdridge-féle életzóna (HLZ) rendszert ezekre az adatokra alkalmaztam annak érdekében, hogy nyomon kövessem a HLZ-típusok térbeli és magassági eloszlásmintázatainak az időbeli alakulását.

   Elméleti megfontolásokra és korábbi tapasztalataimra alapozva (Szelepcsényi et al. 2009) javasoltam a HLZ rendszer módosítását: mind a mag-, mind az átmeneti HLZ-típusokat külön osztályokként határoztam meg. A fenti klimatológiákra a módosított modellt is alkalmaztam.

   Validációképpen az eredeti és a módosított modell által az P1-as időszakra generált HLZ-térképeket egy szakértői alapú vegetáció-térképpel vetettem össze, és a térképek közötti egyezés mértékét a Kappa-statisztika (κ) segítségével határoztam meg.

   Megvizsgáltam az egyes HLZ-típusokra vonatkozóan a relatív lefedettség, az átlagos középpont és az átlagos előfordulási magasság (MDA) időbeli változásait annak érdekében, hogy feltérképezzem a recens éghajlatváltozás ökológiai hatásait a Kárpát-régióban.

   a. **A HLZ rendszer kiválasztott változatainak alkalmazása révén bemutattam a közelmúltbeli éghajlatváltozásnak a Kárpát-régió potenciális vegetációjára gyakorolt hatását. A természetes ökoszisztémák múlt században megfigyelt eltolódásaival összhangban kimutattam a HLZ-típusok északi irányú és/vagy felfelé irányuló eltolódásait.**
      - Azoknak a HLZ-típusoknak a középpontjai, amelyek nem kapcsolódtak a hegyvidékekhez, északi irányba tolódtak el a múlt század során.
      - Az P1-as időszakról az P3-as időszakra az MDA értéke minden HLZ-típusra vonatkozóan nőtt, egy kivételtől eltekintve, míg az P3-as időszakról az P4-as időszakra, ennek a paraméternek a csökkenése regisztrálható minden HLZ-típus esetében. Ennek az az oka, hogy a klíma az P4-as időszak során kissé csapadékosabb és hűvösebb volt, mint az azt megelőzőben. Összességében az öt leggyakoribb HLZ-típus esetében az MDA értéke nőtt a múlt században.

   b. **Elméleti megfontolásokra alapozva ajánlást fogalmaztam meg a HLZ rendszer módosítására. A javasolt módosítás alkalmazásával körülhatároltam az erdőssztyepp ökoton potenciális elterjedési területét a Kárpát-régióban.**
      - Az átmeneti HLZ-típusok bevezetése következtében a vegetációs osztályok térbeli eloszlásmintázata jelentősen átrendeződik: (a) az első a lefedettségi rangsorban a „hideg-mérsékelt üde erdő” mag-HLZ-típus, amelynek a területi aránya 50–60% (a vizsgálati időszaktól függően), míg (b) a második leggyakoribb vegetációs osztály a „hideg-mérsékelt szubhumid erdőssztyepp” átmeneti HLZ-típus, lefedve az alföldi területek jelentős részét.
      - Összehasonlítva ennek az átmeneti HLZ-típusnak az P5-es időszakban megfigyelt elterjedés-mintázatát és az erdőssztyepp ökoton potenciális területeit (lásd Varga et al. 2000), nagy átfedés mutatható ki közöttük.

2. **A Kárpát-régióban várható klímaváltozás kiértékelése a Holdridge-féle életzóna rendszerrel** (3. fejezet)

   Az ENSEMBLES projekt által biztosított 11 db regionális klímamodell (RCM) szimuláció hiba-korrigált hőmérséklet- és csapadékmezőire alkalmaztam a HLZ rendszert, hogy felmérjem a Kárpát-régióban a jövőbeli éghajlatváltozás lehetséges ökológiai hatásainak az erősségét és bizonytalanságát. A klimatológiákat – és ezáltal a HLZ-típusok térbeli és magassági elterjedés-mintázatait – három 30 éves periódusra (T1: 1961–1990, T2: 2021–2050, T3: 2061–2090) és 28 db 10 éves (D1: 1951–1960, D2: 1956–1965, D3: 1961–1970, stb.) periódusra nézve határoztam meg.

   Vizsgálataim során a HLZ-típusok elterjedés-mintázatát a relatív kiterjedés, az átlagos középpont és a magassági tartomány (azaz az alsó és felső magassági határ, valamint a magassági középpont) jellemezte. Ezekre a 10 éves klimatológiák alapján generált elterjedési paraméterekre alkalmaztam a módosított Mann-Kendall trendtesztet annak érdekében, hogy kiértékeljem azok várható időbeli alakulását, azaz a prognosztizált változások irányát és bizonytalanságát.

   A κ értékek segítségével választottam ki azokat a szimulációkat, amelyek a legkisebb és legnagyobb elterjedési változást mutatták. Az eredményeket ezekre a szimulációkra és az ensemble átlagra vonatkozóan részletesen bemutattam.

   a. **A HLZ rendszert alkalmazva kimutattam, hogy mérsékelt kibocsátási forgatókönyv esetén az alkalmazott RCM szimulációtól függetlenül jelentős mértékben megváltozhatnak a XXI. század végére a potenciális vegetáció-típusok elterjedés-mintázatai a Kárpát-régióban.**
      - A boreális HLZ-típusok a becslések szerint eltűnnek a régióból, míg megjelenhetnek azok a „meleg-mérsékelt tövises puszta” és „szubtrópusi száraz erdő” típusok, amelyek manapság például Spanyolországban és Törökországban fordulnak elő.
      - A humid és a perhumid HLZ-típusok relatív kiterjedése az előrejelzések szerint 41 ± 12, illetve 58 ± 13%-kal csökkenhet a XXI. század végére. A meleg-mérsékelt HLZ-típusok relatív lefedettsége a század végén tízszer nagyobb lehet, mint jelenleg, míg a hideg-mérsékelt HLZ-típusok esetében ugyanez az érték harmadával vagy kétharmadával csökkenthet ugyanezen időszakokat tekintve.

   b. **Megmutattam, hogy a közelmúltban észlelt növekvő hőmérsékleti trend valószínűleg a jövőben is folytatódni fog a Kárpát-régióban, amelyre válaszként a potenciális vegetáció-típusok északi irányú és/vagy felfelé irányuló eltolódása várható.**
      - A potenciális vegetáció-típusok magassági tartományai a jövőben várhatóan bővülni fognak. A HLZ-típusok alsó és felső magassági határai, valamint magassági középpontjai valószínűleg magasabbra kerülhetnek.
      - A legtöbb HLZ-típusnál északi irányú eltolódás várható, és ezen eltolódások nagysága akár többszöröse is lehet a múlt században megfigyelteknek.

   c. **Rámutattam arra, hogy a Kárpát-régió csapadékmintázatának a várható alakulása jelentős bizonytalanságot mutat, ami gyengíti a potenciális vegetáció elterjedésére vonatkozó előrejelzések megbízhatóságát.**
      - A „hideg-mérsékelt füves puszta” típus lefedettségének a várható változása rendkívül bizonytalan, mert az előrejelzések között még a változás előjelének tekintetében sincs egyetértés (nagy modellközi változékonyság).

- A nyugat/kelet irányú eltolódás szignifikáns trendje csak néhány HLZ-típus esetében várható (nagy időbeli változékonyság).

3. **A relatív napfénytartam becslése könnyen hozzáférhető meteorológiai változók alapján a biom-eloszlás szimulálásához a Kárpát-régióban** (4. fejezet)

   A Yin (1999) által javasolt regressziós modellt a CarpatClim adatkészletből vett havi hőmérséklet- és csapadékadatokra alkalmazva becsültem meg a relatív napfénytartam havi átlagos napi értékére (*RSD*-re) vonatkozó idősorokat az 1961–2010-es időszak minden egyes évére vonatkozóan. Majd minden rácscellában kiszámítottam a megfigyelt adatok átlagértékével normalizált négyzetes hiba négyzetgyökét (*RRMSE*-t) az *RSD* megfigyelt és becsült 50 éves idősoraira vonatkozóan, minden egyes hónapra külön-külön.

   Annak érdekében, hogy megvizsgáljam a becslési sémának a paleoklimatikus adatkészletekre való alkalmazhatóságát, az 1981–2010-es időszak *RSD*-értékeit kétféleképpen számítottam ki: (a) az egyes évekre vonatkozóan a kezdeti sémája alapján becsült idősorok átlagolásával, illetve (b) a sémát 30 éves átlagokra alkalmazva. A becsült eredményeket a vizsgált időszak mért értékeinek átlagaival vetettem össze.

   Megvizsgáltam, hogy a potenciális vegetáció térbeli eloszlásának becslésére szolgáló BIOME modell mennyire érzékeny a különböző konfigurációs beállítások módosítására. A szimulációkat az 1981–2010-es időszak éghajlati adatait alkalmazva készítettem el. Itt most csak azt vizsgáltam, hogy milyen hatással van az eredményekre a kvázi-napi értékek előállításához alkalmazott módszernek, illetve az *RSD*-adatok forrásának a megválasztása. Az előbbi vonatkozásában a szimulációkat kétféleképpen hajtottam végre: (a) a havi átlagokat állandónak feltételeztem a hónap minden napján, és (b) különböző átlagmegőrző interpolációs technikákat alkalmaztam.

   a. **Megmutattam, hogy a párolgás szempontjából legfontosabb időszakban változatos domborzati feltételek mellett a Yin (1999) által javasolt eljárást egyéves idősorokra alkalmazva megfelelő pontossággal becsülhető az *RSD* havi idősora.**
      - Májustól augusztusig a vizsgált terület több mint 90%-án a becsült és mért *RSD*-értékek közötti *RRMSE* nem haladja meg azt a 20%-os küszöböt, amely alatt a modell teljesítménye kiválónak tekinthető.
      - Az áprilistól októberig tartó időszakban az 500 m-nél kisebb magasságú rácscellák közel 99%-ában az *RRMSE* értéke nem éri el azt a 40%-os határértéket, amely alatt a modell teljesítménye még elfogadhatónak tekinthető.
      - A nyári hónapokban az alacsonyabb régiók (500 m-nél alacsonyabb területek) közel 90%-ában az *RRMSE* értéke a 15%-os küszöböt sem haladja meg.

   b. **Bebizonyítottam, hogy az adatfeldolgozási lépések felcserélése és a becslési séma finomhangolása mellett a Yin (1999) által javasolt eljárásra alapozva megfelelően pótolhatóak az *RSD*-adatok adatszegény szimulációs környezetben.**
      - Az új modellezési keretrendszerrel az 1981–2010-es időszakra becsült *RSD*-klimatológiák esetében áprilistól szeptemberig (egy kivételtől eltekintve) a teljes vizsgálati területre számított *RRMSE* értéke nem haladja meg a 10%-os küszöbértéket, ami a becslések nagyon jó minőségére utal.

   c. **Kimutattam, hogy a BIOME modell az itt tesztelt konfigurációs beállításokra (azaz a kvázi-napi értékek előállítási módszerének és az *RSD*-adatok forrásának a megválasztására) vonatkozóan nem érzékeny.**

- Az *RSD* havi idősorának forrásválasztása adott tér- és időviszonyok között nincs hatással a biomok eloszlására: a mért *RSD*-értékeket használó szimulációt összehasonlítva a becsült *RSD*-értékek által vezérelt mindkét szimulációval, nem találtam különbséget a biom-térképek között.
- Az interpolált napi értékek felhasználásával előállított biom-térképek összhangban vannak egymással. Ezeket a referencia-térképpel összevetve, csak egy kismértékű eltérés található. A rácscellák csak 0,4%-a esetében van eltérés a különböző napi időjárási adatok felhasználásával előállított biom-térképek között. Ezt az eltérést minden esetben az 5 °C-os bázishőmérsékletű növekedési foknap (GDD_5) területi eloszlását érintő különbség magyarázza.

4. **A klíma- és pollen-adatok alapján rekonstruált vegetáció-típusok összehasonlítása a Nagy-Alpok-régióban** (5. fejezet)

   A HISTALP adatbázis által biztosított havi hőmérséklet- és csapadékmezőket az 1800–1980-as időszak minden évére vonatkozóan a Global 30 Arc-Second Elevation Dataset (GTOPO30) 0,5 szögperces rácshálójára skáláztam le egyszerű statisztikai feltételezéseket alkalmazva. Yin (1999) regressziós modelljét alkalmaztam ezekre a leskálázott meteorológiai mezőkre annak érdekében, hogy megbecsüljem az *RSD* havi idősorát a vizsgált időszak minden egyes évére vonatkozóan. Majd származtattam a három releváns meteorológiai változóra vonatkozóan az átlagos mezőket. Végül ezekkel az adatokkal meghajtva a BIOME modellt szimuláltam a biomok elterjedés-mintázatát a Nagy-Alpok-régióban (GAR-ban).

   Az Európai Pollen Adatbázisból származó 770 db legfiatalabb fosszilis pollenegyüttesre vonatkozóan alkalmaztam a biomizációs eljárás egy finomított verzióját. A következő lépésben az érintett 86 db pollenszelvényre vonatkozóan kiszámítottam a relatív biom-pontszámokat (RBS-okat) és végül szelvényenként meghatároztam a domináns biom-típust.

   A BIOME modell segítségével szimulált vegetációt a pollenszelvények RBS-ai alapján rekonstruált vegetációval vetettem össze egy pontszerű megközelítést alkalmazva. Annak érdekében, hogy felmérjem a közeli tévesztéseknek (azaz a hasonló összetételű biom-típushoz való hozzárendeléseknek) a klíma- és pollen-adatok alapján rekonstruált biom-típusok összehasonlítására gyakorolt hatását, meghatároztam szelvényenként az egyezéshez szükséges területnövelés és definíciótágítás (AEm és DEm) értékeit, majd eme értékeket a szelvényekből képzett alcsoportokra vonatkozóan aggregáltam különböző tájkarakterisztikákat alkalmazva.

   a. **Kizárólag havi hőmérséklet- és csapadékadatok (és digitális domborzatmodellek) felhasználásával előállítottam a biomok egy nagyon nagy felbontású elterjedési térképét a GAR-ra vonatkozóan egy olyan modellezési keretrendszerben, amelyben a bonyolultabb biom modellek futtatásához szükséges *RSD*-adatokat a Yin (1999) által javasolt modell segítségével becsültem meg.**
      - A GAR-ban megfelelően beazonosíthatóak a vegetációtudósok által megállapított főbb vegetációformációk, amennyiben a BIOME modellt az itt alkalmazott konfigurációban használjuk. Amennyiben összehasonlítjuk a tundra biom-típusra nézve az itt szimuláltnak, illetve a Bohn et al. (2003) térképén az alpin vegetáció (B.2) alegység által reprezentáltnak az elterjedési mintázatát, nagy átfedés mutatható ki közöttük. Ugyanez a megállapítás érvényes a következő párok esetében is: (a) Bohn et al. (2003) térképén a jegenyefenyves és lucfenyves erdők (D.4) alegység és itt a „tajga” és „hideg tűlevelű erdő” típusokból álló aggregátum, illetve (b) a szakértői alapú térképen a bükkös és elegyes bükkös erdők (F.5) alegység és itt a „hűvös elegyes erdő” típus.

- A kevésbé zord körülményekkel jellemezhető völgyekben, ahol a GDD_5 értéke meghaladja a 1200 °C nap-os küszöbértéket, általában a „mérsékelt lombhullató erdő” és „hűvös elegyes erdő” típusok jelennek meg attól függően, hogy a leghidegebb hónap középhőmérséklete −2 °C felett van, vagy sem. Ezek a típusok a GAR-ban az 1500 m tengerszint feletti magasságokban csak elenyésző mértékben fordulnak elő. A lejtőkön a „hideg tűlevelű erdő” és „tajga” típusok válnak dominánssá, felváltva a „melegebb” erdőket. Ott, ahol a GDD_5 értéke nem haladja meg a 350 °C nap-os küszöbértéket, egyik fás növényi funkcionális típus sem tud aktiválódni. Ez itt többnyire a 2000 m tengerszint feletti magasság felett jellemző, ahol így a „tundra” típus válik uralkodóvá. A biom-típusoknak a klímaadatok alapján szimulált magassági zonációja összeegyeztethető a vegetációs övek fitogeográfiai elemzések révén feltárt pozíciójával (lásd pl. Fauquette et al. 2018).

b. A klíma- és pollen-adatok alapján becsült biom-típusok között a biomizációs megközelítés kezdeti validációs kísérletei által az Alpok-régióban kimutatott eltéréseket újraértékeltem, kiaknázva a releváns kutatási területeken az elmúlt 25 évben elért előrelépéseket.

- A biomizációs séma által becsült vegetáció-típus az összehasonlítható 86 db pollenszelvényből csupán a 35 esetében mutat egyezést a klímaadatok alapján szimulált vegetáció-típussal, ami csak 41%-os egyezési arányt jelent.
- A pollenszelvények 76%-ára vonatkozóan igaz, hogy a klímaadatok alapján becsült biom-típus megegyezik a RBS-okból képzett sorrend alapján kiválasztott első három biom-típus valamelyikével.

c. A klíma- és pollen-adatok alapján rekonstruált vegetáció-típusoknak a GAR-on belüli összevetéséből kirajzolódó képet továbbárnyaltam a hátráltató tényezők és a közeli tévesztések figyelembevétele révén. Rámutattam, hogy az eltérések nem feltétlenül a biomizációs eljárás alkalmatlanságát, hanem inkább a tájra gyakorolt emberi hatásokat tükrözik.

- A közeli tévesztések figyelembevételekor az tapasztalható, hogy az alacsony magasságban (1000 m tengerszint feletti magasságnál alacsonyabban) fekvő lelőhelyek esetén csekély mértékű definíciótágítás is jelentős mértékben növeli az egyezési arányt: ha a 4-nél kisebb DEm értékkel bíró lelőhelyeket is egyezésnek fogadjuk el, akkor az egyezési arány 43%-ról 74%-ra emelkedik. Ez arra utalhat, hogy bár a GAR-ban jelenleg nem az éghajlat a fő meghatározója a biomok eloszlásának, a régió számos lelőhelyén az ősi erdőket csak részben változtatta meg az emberi tevékenység (pl. erdőültetvények létesítése, bizonyos fajok kiirtása).
- A nagy magasságban (1000 m tengerszint feletti magasságon vagy annál magasabban) fekvő lelőhelyek esetén a területnövelés emeli meg az egyezési százalékot: ha a 4-nél kisebb AEm értékkel bíró lelőhelyeket is egyezésnek fogadjuk el, akkor az egyezési arány 39%-ról 77%-ra emelkedik. Ez a megfigyelés azonban egyszerre több tényező egyidejű jelenlétével is magyarázható: (a) a terep egyenetlenségével, (b) antropogén eredetű tájmódosulással (pl. a zárt vegetáció felhasításával), vagy éppen (c) a vegetáció átmeneti jellegével (lásd erdős tundra ökoton).
- A fenti eredmények összességében arra utalnak, hogy az összehasonlításokat jelentősen hátráltatja az a tény, miszerint az itt használt osztályozási sémák sem az ökotonokat, sem az antromokat (azaz az intenzív földhasználatú biomokat) nem veszik figyelembe.

Acknowledgments

I am extremely grateful to **Prof. Dr. Pál Sümegi** for supporting this thesis and for giving me the opportunity to carry out an independent research project in an interdisciplinary framework. I greatly appreciate the freedom he has given me to develop own ideas, as well as his confidence in me. Thanks to his encouragement, I was able to get acquainted with many quantitative approaches of the phytogeography and related disciplines. I would like to thank him for enabling me to address with various phytogeographical issues from the field of both reconstruction and simulation.

Further, my thanks go to **dr. habil. Ferenc Ács**, my former mentor, who has introduced me to the world of the bioclimatic classification methods rooted in plant geography, and has aroused my interest in the ecological climatology, which provide an interdisciplinary framework for understanding the interactions between terrestrial ecosystems and other components of the climate system through space and time. I really appreciate for providing a new perspective for me that allows me to see the world differently than others.

I would like to express my gratitude to **dr. Hajnalka Breuer**, my external consultant and my eternal mentor, who has always been opened to my ideas in working together, and has always helped me to realize them. During working with her, I have realized how many influence a tutor who has a strong vocation for his/her work has on the fate of his/her students, and how much sacrifice a mentor can make for the development of interest and skills of these students. I have acquired a lot of skills by working with her, for which I will eternally be grateful to her.

I also want to thank **dr. Nándor Fodor**, my co-supervisor, for providing a relaxed and inspiring environment for me to finish my PhD thesis over the past six years. I especially appreciate the freedom he has given me to find my own path.

I want to thank **dr. Rita Pongrácz**, my co-author, who has supported with essential data and her expertise to prepare the manuscripts that form the basis for the Chapters 3 of this thesis.

I will eternally be grateful to **dr. Anna Kis** for supporting me both professionally and personally for so many years. She has been a source of inspiration for me to get better and better in both personal and professional lives. I really appreciate her efforts and sacrifices that she has made during the intensive joint work. I apologize to her for every single “litost” from which she has suffered during the time spent with me.

I am extremely grateful to the former and current heads of the Institute of Archaeology of the Eötvös Loránd Research Network (ELKH), **Dr. Elek Benkő** and **Dr. Gabriella Kulcsár**, for their support of the completion of this thesis. As my indirect bosses, for the last two years, they were extremely patient with me, for which I am truly grateful. I am forever grateful to **Dr. Gabriella Kulcsár** for providing me with the opportunity to develop the modelling framework that underpins my research in detail, in the hope of future use in the archaeology.

I would like to thank **dr. habil. Ágnes Havasi** for improving the language of this thesis. I want to emphasize that she is not to blame for any spelling or grammatical mistakes that occur in the text because I am responsible for these mistakes. I am very thankful for her words of encouragement and the help she gave me.

I would like to thank each anonymous reviewer and editor for their suggestions and constructive comments on those manuscripts, which form the basis for the Chapters 2–5 of this thesis.

I am highly indebted to the former and current heads of the Department of Meteorology at the Eötvös Loránd University, **Prof. Dr. Judit Bartholy**, **dr. habil. Róbert Mészáros**, and the head of the Department of Geology and Palaeontology at the University of Szeged, **Prof. Dr. Pál Sümegi**, for giving me access to the IT resources of their departments after finishing my official MSc/PhD programmes. I am also grateful to the director of the Agricultural Institute of the ELKH, **Dr. Ottó Veisz**, for supporting my research by providing IT resources. In this context, I would like to thank **dr. Hajnalka Breuer**, **Bálint Csökmei** and **Tamás Cserhalmi**, who have always helped me to solve technical problems in the digital world, and have always provided effective technical support.

I am highly indebted to all the staff of the Department of Prehistoric Archaeology at the Institute of Archaeology of the ELKH for their moral support, scientific and administrative assistance. Special thanks go to my colleagues, **Dr. Mária Bondár**, **Dr. Tibor Marton** and **Dr. Krisztián Oross**, who were members of the committee of the pre-defence of my thesis. I would like to thank in particular **Dr. Krisztián Oross** for taking on the role of secretary for this pre-defence, and for helping to ensure that the proceedings ran smoothly. I also want to thank the head of the Institute of Archaeology, **Dr. Gabriella Kulcsár**, for providing the necessary personnel and infrastructure resources for the pre-defence. Finally, I am extremely grateful to each pre-opponent for their constructive advice.

I want to thank **dr. Renáta Sándor** and **dr. Csaba Szőke**, who have encouraged me to finish my PhD thesis. I will be eternally grateful to them for their support.

Thanks to **Dávid** for his continuous support and for keeping me moving for the last six years. I am grateful to him for every single swimming training, concert, hike and other leisure program.

I must say a big thank **Netti** for being there for me at the lowest and highest moments in the last five years. I would like to thank her for teaching me how to spin on my face.

I would like to thank all the staff of the Crop Production Department at the Agricultural Institute of the ELKH for providing a homely and calm atmosphere for my works. Thanks to **Tamás** and **Peti** for monitoring and helping my prosperity at Martonvásár. Special thanks to the Girls, i.e., **Gabó**, **Eszter**, **Timi**, **Anikó** and **Ildi**, who have managed to distract my attention from my work in our mid-morning coffee/tea breaks. Thanks to all the staff of the Crop Production Department and the GINOP labs at the Agricultural Institute of the ELKH for really deep and funny lunchtime talks.

Special thanks to the members of the CSEMETE brigade, i.e., **Gábor**, **Niki**, **Netti**, **Árpi**, **Vivi**, **ÁdiGábi**, **Kristóf**, **Lilla** and **Balázs** for helping me to open the valve at critical moments to release the tired steam. The moments we spent together have always served as fuel for my hard-working weekdays.

Very special thanks go to **my Mother**, who has always supported me during all the years and has always given me the freedom to choose. Without her sacrifice, this dissertation could never have been written. I thank her for everything she has done for me.

References

Abatzoglou JT, Dobrowski SZ, Parks SA, Hegewisch KC (2018) TerraClimate, a high-resolution global dataset of monthly climate and climatic water balance from 1958–2015. Sci Data 5:170191. DOI: 10.1038/sdata.2017.191

Abuzaid AH, Mohamed IB, Hussin AG (2012) Boxplot for circular variables. Comput Stat 27(3):381–392. DOI: 10.1007/s00180-011-0261-5

Alexander MR, Pearl JK, Bishop DA, Cook ER, Anchukaitis KJ, Pederson N (2019) The potential to strengthen temperature reconstructions in ecoregions with limited tree line using a multispecies approach. Quat Res 92(2):583–597. DOI: 10.1017/qua.2019.33

Allen RG (1996) Assessing integrity of weather data for reference evapotranspiration estimation. J Irrig Drain Eng 122(2):97–106. DOI: 10.1061/(ASCE)0733-9437(1996)122:2(97)

Allen JRM, Hickler T, Singarayer JS, Sykes MT, Valdes PJ, Huntley B (2010a) Last glacial vegetation of northern Eurasia. Quat Sci Rev 29(19–20):2604–2618. DOI: 10.1016/j.quascirev.2010.05.031

Allen CD, Macalady AK, Chenchouni H, Bachelet D, McDowell N, Vennetier M, Kitzberger T, Rigling A, Breshears DD, Hogg EH, Gonzalez P, Fensham R, Zhang Z, Castro J, Demidova N, Limp J-H, Allard G, Running SW, Semerci A, Cobb N (2010b) A global overview of drought and heat-induced tree mortality reveals emerging climate change risks for forests. For Ecol Manage 259(4):660–684. DOI: 10.1016/j.foreco.2009.09.001

Allen JRM, Watts WA, Huntley B (2000) Weichselian palynostratigraphy, palaeovegetation and palaeoenvironment; the record from Lago Grande di Monticchio, southern Italy. Quat Int 73–74:91–110. DOI: 10.1016/S1040-6182(00)00067-7

Araújo MB, Anderson RP, Barbosa AM, Beale CM, Dormann CF, Early R, Garcia RA, Guisan A, Maiorano L, Naimi B, O'Hara RB, Zimmermann NE, Rahbek C (2019) Standards for distribution models in biodiversity assessments. Sci Adv 5(1):eaat4858. DOI: 10.1126/sciadv.aat4858

Auer I, Böhm R, Jurkovic A, Lipa W, Orlik A, Potzmann R, Schöner W, Ungersböck M, Matulla C, Briffa K, Jones P, Efthymiadis D, Brunetti M, Nanni T, Maugeri M, Mercalli L, Mestre O, Moisselin J-M, Begert M, Müller-Westermeier G, Kveton V, Bochnicek O, Stastny P, Lapin M, Szalai S, Szentimrey T, Cegnar T, Dolinar M, Gajic-Capka M, Zaninovic K, Majstorovic Z, Nieplova E (2007) HISTALP—historical instrumental climatological surface time series of the Greater Alpine Region. Int J Climatol 27(1):17–46. DOI: 10.1002/joc.1377

Bailey RG (1976) Ecoregions of the United States (1:7 500 000). USDA Forest Service, Ogden, Utah

Bartha D (2005) Tájállapotok és vegetációállapotok, mint az erdőtermészetességi vizsgálatok viszonyítási alapjai (Landscape and vegetation states as benchmarks of forest naturalness studies). Tájökológiai Lapok 3(2):253–274 (in Hungarian)

Batista e Silva F, Marín Herrera MA, Rosina K, Ribeiro Barranco R., Freire S, Schiavina M (2018) Analysing spatiotemporal patterns of tourism in Europe at high-resolution with conventional and big data sources. Tour Manage 68:101–115. DOI: 10.1016/j.tourman.2018.02.020

Beckage B, Osborne B, Gavin DG, Pucko C, Siccama T, Perkins T (2008) A rapid upward shift of a forest ecotone during 40 years of warming in the Green Mountains of Vermont. Proc Natl Acad Sci USA 105(11):4197–4202. DOI: 10.1073/pnas.0708921105

Behre K-E (1981) The interpretation of anthropogenic indicators in pollen diagrams. Pollen Spores 23:225–245

Bellocchi G, Acutis M, Fila G, Donatelli M (2002) An indicator of solar radiation model performance based on a fuzzy expert system. Agron J 94(6):1222–1233. DOI: 10.2134/agronj2002.1222

Bennett KD, Willis KJ (2001) Pollen. In: Smol JP, Birks HJB, Last WM (eds) Tracking Environmental Change Using Lake Sediments. Volume 3. Terrestrial, Algal, and Siliceous Indicators. Kluwer Academic Publishers, Dordrecht, The Netherlands, pp 5–32. DOI: 10.1007/0-306-47668-1_2

Berényi D (1943) Magyarország Thornthwaite rendszerű éghajlati térképe és az éghajlati térképek növényföldrajzi vonatkozásai. Befejező közlemény (A Thornthwaite climatic map of Hungary and

phytogeographical aspects of climatic maps. Finishing part). Időjárás 47(7–8):117–125 (in Hungarian)

Berger A, Loutre MF (1991) Insolation values for the climate of the last 10 million years. Quat Sci Rev 10(4):297–317. DOI: 10.1016/0277-3791(91)90033-Q

Beyer RM, Krapp M, Manica A (2020) High-resolution terrestrial climate, bioclimate and vegetation for the last 120,000 years. Sci Data 7:236. DOI: 10.1038/s41597-020-0552-1

Bigelow NH, Brubaker LB, Edwards ME, Harrison SP, Prentice IC, Anderson PM, Andreev AA, Bartlein PJ, Christensen TR, Cramer W, Kaplan JO, Lozhkin AV, Matveyeva NV, Murray DF, McGuire AD, Razzhivin VY, Ritchie JC, Smith B, Walker DA, Gajewski K, Wolf V, Holmqvist BH, Igarashi Y, Kremenetskii K, Paus A, Pisaric MFJ, Volkova VS (2003) Climate change and Arctic ecosystems: 1. Vegetation changes north of 55°N between the last glacial maximum, mid-Holocene, and present. J Geophys Res Atmos 108(D19):8170. DOI: 10.1029/2002JD002558

Binney H, Edwards M, Macias-Fauria M, Lozhkin A, Anderson P, Kaplan JO, Andreev A, Bezrukova E, Blyakharchuk T, Jankovska V, Khazina I, Krivonogov S, Kremenetski K, Nield J, Novenko E, Ryabogina N, Solovieva N, Willis K, Zernitskaya V (2017) Vegetation of Eurasia from the last glacial maximum to present: Key biogeographic patterns. Quat Sci Rev 157:80–97. DOI: 10.1016/j.quascirev.2016.11.022

Birks HJB, Heiri O, Seppä H, Bjune AE (2010) Strengths and Weaknesses of Quantitative Climate Reconstructions Based on Late-Quaternary Biological Proxies. Open Ecol J 3(Special Issue 1):68–110. DOI: 10.2174/1874213001003020068

Blaney HF, Criddle WD (1950) Determining Water Requirements in Irrigated Areas from Climatological Irrigation Data. SCS Technical Paper 96. USDA Soil Conservation Service, Washington, D.C.

Böhm U, Kücken M, Ahrens W, Block A, Hauffe D, Keuler K, Rockel B, Will A (2006) CLM – The Climate Version of LM: Brief Description and Long-Term Applications. COSMO Newsl 6:225–235

Bohn U, Neuhäusl R, with contributions by Gollub G, Hettwer C, Neuhäuslová Z, Raus Th, Schlüter H, Weber H (2003) Map of the Natural Vegetation of Europe. Scale 1:2 500 000. Federal Agency for Nature Conservation, Bonn, Germany

Box EO (1981a) Macroclimate and Plant Forms: An Introduction to Predictive Modeling in Phytogeography. Springer Netherlands, The Hague, The Netherlands. DOI: 10.1007/978-94-009-8680-0

Box EO (1981b) Predicting physiognomic vegetation types with climate variables. Vegetatio 45(2):127–139. DOI: 10.1007/BF00119222

Breuer H, Ács F, Skarbit N (2017) Climate change in Hungary during the twentieth century according to Feddema. Theor Appl Climatol 127(3–4):853–863. DOI: 10.1007/s00704-015-1670-0

Brewer S, Giesecke T, Davis BAS, Finsinger W, Wolters S, Binney H, de Beaulieu J-L, Fyfe R, Gil-Romera G, Kühl N, Kuneš P, Leydet M, Bradshaw RH (2017) Late-glacial and Holocene European pollen data. J Maps 13(2):921–928. DOI: 10.1080/17445647.2016.1197613

Brewer S, Guiot J, Barboni D (2013) Use of Pollen as Climate Proxies. In: Elias SA, Mock CJ (eds) Encyclopedia of Quaternary Science (Second Edition). Elsevier, Amsterdam, The Netherlands, pp 805–815. DOI: 10.1016/B978-0-444-53643-3.00180-1

Brock TD (1981) Calculating solar radiation for ecological studies. Ecol Model 14(1–2):1–19. DOI: 10.1016/0304-3800(81)90011-9

Burga CA (1988) Swiss vegetation history during the last 18 000 years. New Phytol 110(4):581–602. DOI: 10.1111/j.1469-8137.1988.tb00298.x

Burt JE, Barber GM, Rigby DL (2009) Elementary Statistics for Geographers. Third Edition. Guildord Press, New York, NY

Castellvi F (2001) A new simple method for estimating monthly and daily solar radiation. Performance and comparison with other methods at Lleida (NE Spain); a semiarid climate. Theor Appl Climatol 69(3–4):231–238. DOI: 10.1007/s007040170028

Chakraborty A, Joshi PK, Ghosh A, Areendran G (2013) Assessing biome boundary shifts under climate change scenarios in India. Ecol Indic 34:536–547. DOI: 10.1016/j.ecolind.2013.06.013

Chen X, Zhang X-S, Li B-L (2003) The possible response of life zones in China under global climate change. Glob Planet Chang 38(3–4):327–337. DOI: 10.1016/S0921-8181(03)00115-2

Cheng Y, Liu H, Wang H, Hao Q (2018) Differentiated climate-driven Holocene biome migration in western and eastern China as mediated by topography. Earth-Sci Rev 182:174–185. DOI: 10.1016/j.earscirev.2018.05.006

Christensen JH, Carter TR, Rummukainen M, Amanatidis G (2007a) Evaluating the performance and utility of regional climate models: the PRUDENCE project. Clim Chang 81(Suppl 1):1–6. DOI: 10.1007/s10584-006-9211-6

Christensen OB, Drews M, Christensen JH, Dethloff K, Ketelsen K, Hebestadt I, Rinke A (2007b) The HIRHAM Regional Climate Model Version 5 (β). Technical Report 06-17. Danish Meteorological Institute, Copenhagen, Denmark

Chuine I, Beaubien EG (2001) Phenology is a major determinant of tree species range. Ecol Lett 4(5):500–510. DOI: 10.1046/j.1461-0248.2001.00261.x

Claussen M (1996) Variability of global biome patterns as a function of initial and boundary conditions in a climate model. Clim Dyn 12(6):371–379. DOI: 10.1007/BF00211683

Cohen J (1960) A Coefficient of Agreement for Nominal Scales. Educ Psychol Meas 20(1):37–46. DOI: 10.1177/001316446002000104

COHMAP Members (1988) Climatic Changes of the Last 18,000 Years: Observations and Model Simulations. Science 241(4869):1043–1052. DOI: 10.1126/science.241.4869.1043

Conedera M, Colombaroli D, Tinner W, Krebs P, Whitlock C (2017) Insights about past forest dynamics as a tool for present and future forest management in Switzerland. For Ecol Manage 388:100–112. DOI: 10.1016/j.foreco.2016.10.027

Court-Picon M, Buttler A, de Beaulieu J-L (2006) Modern pollen/vegetation/land-use relationships in mountain environments: an example from the Champsaur valley (French Alps). Veg Hist Archaeobot 15(3):151–168. DOI: 10.1007/s00334-005-0008-8

Cramer W (2002) Biome Models. In: Mooney HA, Canadell JG (eds) Encyclopaedia of Global Environmental Change. Volume 2. The Earth System: Biological and Ecological Dimensions of Global Environmental Change. John Wiley & Sons Ltd, Chichester, UK, pp 166–171

Cramer W, Prentice IC (1988) Simulation of regional soil moisture deficits on a European scale. Nor J Geogr 42(2–3):149–151. DOI: 10.1080/00291958808552193

Critchfield WB, Little EL (1966) Geographic distribution of the pines of the world. USDA Forest Service, Washington, D.C.

Czúcz B, Gálhidy L, Mátyás Cs (2011) Present and forecasted xeric climatic limits of beech and sessile oak distribution at low altitudes in Central Europe. Ann For Sci 68(1):99–108. DOI: 10.1007/s13595-011-0011-4

Davis BAS, Chevalier M, Sommer P, Carter VA, Finsinger W, Mauri A, Phelps LN, Zanon M, Abegglen R, Åkesson CM, Alba-Sánchez F, Anderson RS, Antipina TG, Atanassova JR, Beer R, Belyanina NI, Blyakharchuk TA, Borisova OK, Bozilova E, Bukreeva G, Bunting MJ, Clò E, Colombaroli D, Combourieu-Nebout N, Desprat S, Di Rita F, Djamali M, Edwards KJ, Fall PL, Feurdean A, Fletcher W, Florenzano A, Furlanetto G, Gaceur E, Galimov AT, Gałka M, García-Moreiras I, Giesecke T, Grindean R, Guido MA, Gvozdeva IG, Herzschuh U, Hjelle KL, Ivanov S, Jahns S, Jankovska V, Jiménez-Moreno G, Karpińska-Kołaczek M, Kitaba I, Kołaczek P, Lapteva EG, Latałowa M, Lebreton V, Leroy S, Leydet M, Lopatina DA, López-Sáez JA, Lotter AF, Magri D, Marinova E, Matthias I, Mavridou A, Mercuri AM, Mesa-Fernández JM, Mikishin YA, Milecka K, Montanari C, Morales-Molino C, Mrotzek A, Muñoz Sobrino C, Naidina OD, Nakagawa T, Nielsen AB, Novenko EY, Panajiotidis S, Panova NK, Papadopoulou M, Pardoe HS, Pędziszewska A, Petrenko TI, Ramos-Román MJ, Ravazzi C, Rösch M, Ryabogina N, Sabariego Ruiz S, Salonen JS, Sapelko TV, Schofield JE, Seppä H, Shumilovskikh L, Stivrins N, Stojakowits P, Svobodova Svitavska H, Święta-Musznicka J, Tantau I, Tinner W, Tobolski K, Tonkov S, Tsakiridou M, Valsecchi V, Zanina OG, Zimny M (2020) The Eurasian Modern Pollen Database (EMPD), version 2. Earth Syst Sci Data 12(4):2423–2445. DOI: 10.5194/essd-12-2423-2020

Davis BAS, Collins PM, Kaplan JO (2015) The age and post-glacial development of the modern European vegetation: a plant functional approach based on pollen data. Veg Hist Archaeobot 24(2):303–317. DOI: 10.1007/s00334-014-0476-9

Davis TW, Prentice IC, Stocker BD, Thomas RT, Whitley RJ, Wang H, Evans BJ, Gallego-Sala AV, Sykes MT, Cramer W (2017) Simple process-led algorithms for simulating habitats (SPLASH v.1.0): robust indices of radiation, evapotranspiration and plant-available moisture. Geosci Model Dev 10(2):689–708. DOI: 10.5194/gmd-10-689-2017

de Castro M, Gallardo C, Jylha K, Tuomenvirta H (2007) The use of a climate-type classification for assessing climate change effects in Europe from an ensemble of nine regional climate models. Clim Chang 81(Suppl 1):329–341. DOI: 10.1007/s10584-006-9224-1

Déqué M (2007) Frequency of precipitation and temperature extremes over France in an anthropogenic scenario: Model results and statistical correction according to observed values. Glob Planet Chang 57(1–2):16–26. DOI: 10.1016/j.gloplacha.2006.11.030

Déqué M, Marquet P, Jones RG (1998) Simulation of climate change over Europe using a global variable resolution general circulation model. Clim Dyn 14(3):173–189. DOI: 10.1007/s003820050216

Deza-Araujo M, Morales-Molino C, Tinner W, Henne PD, Heitz C, Pezzatti GB, Hafner A, Conedera M (2020) A critical assessment of human-impact indices based on anthropogenic pollen indicators. Quat Sci Rev 236:106291. DOI: 10.1016/j.quascirev.2020.106291

Dobor L, Barcza Z, Hlásny T Havasi Á, Horváth F, Ittzés P, Bartholy J (2015) Bridging the gap between climate models and impact studies: the FORESEE Database. Geosci Data J 2(1):1–11. DOI: 10.1002/gdj3.22

Doorenbos J, Pruitt WO (1977) Guidelines for predicting crop water requirements. FAO Irrigation and Drainage Paper No. 24, Technical Report. Food and Agriculture Organization of the United Nations, Italy, Rome

Dormann CF, Schymanski SJ, Cabral J, Chuine I, Graham C, Hartig F, Kearney M, Morin X, Römermann C, Schröder B, Singer A (2012) Correlation and process in species distribution models: bridging a dichotomy. J Biogeogr 39(12):2119–2131. DOI: 10.1111/j.1365-2699.2011.02659.x

Duffie JA, Beckman WA (1991) Solar Engineering of Thermal Processes. Second Edition. Wiley-Interscience, New York, NY

Ehret U, Zehe E, Wulfmeyer V, Warrach-Sagi K, Liebert J (2012) HESS Opinions "Should we apply bias correction to global and regional climate model data?" Hydrol Earth Syst Sci 16(9):3391–3404. DOI: 10.5194/hess-16-3391-2012

Elith J, Leathwick JR (2009) Species Distribution Models: Ecological Explanation and Prediction Across Space and Time. Annu Rev Ecol Evol Syst 40:677–697. DOI: 10.1146/annurev.ecolsys.110308.120159

Ellis EC, Klein Goldewijk K, Siebert S, Lightman D, Ramankutty N (2010) Anthropogenic transformation of the biomes, 1700 to 2000. Glob Ecol Biogeogr 19(5):589–606. DOI: 10.1111/j.1466-8238.2010.00540.x

Emanuel WR, Shugart HH, Stevenson MP (1985) Climatic change and the broad-scale distribution of terrestrial ecosystem complexes. Clim Chang 7(1):29–43. DOI: 10.1007/BF00139439

Epstein ES (1991) On Obtaining Daily Climatological Values from Monthly Means. J Clim 4(3):365–368. DOI: 10.1175/1520-0442(1991)004<0365:OODCVF>2.0.CO;2

Evans MN, Tolwinski-Ward SE, Thompson DM, Anchukaitis KJ (2013) Applications of proxy system modeling in high resolution paleoclimatology. Quat Sci Rev 76:16–28. DOI: 10.1016/j.quascirev.2013.05.024

Ewel JJ (1999) Natural systems as models for the design of sustainable systems of land use. Agrofor Syst 45(1–3):1–21. DOI: 10.1023/A:1006219721151

Fábián ÁP, Matyasovszky I (2010) Analysis of climate change in Hungary according to an extended Köppen classification system, 1971–2060. Időjárás 114(4):251–261

Falk W, Mellert KH (2011) Species distribution models as a tool for forest management planning under climate change: risk evaluation of *Abies alba* in Bavaria. J Veg Sci 22(4):621–634. DOI: 10.1111/j.1654-1103.2011.01294.x

Fan ZM, Li J, Yue TX (2012) Changes of Climate-Vegetation Ecosystem in Loess Plateau of China. Procedia Environ Sci 13:715–720. DOI: 10.1016/j.proenv.2012.01.064

Fan ZM, Li J, Yue TX (2013) Land-cover changes of biome transition zones in Loess Plateau of China. Ecol Model 252:129–140. DOI: 10.1016/j.ecolmodel.2012.07.039

Fauquette S, Suc J-P, Médail F, Muller SD, Jiménez-Moreno G, Bertini A, Martinetto E, Popescu S-M, Zheng Z, de Beaulieu J-L (2018) The Alps: A Geological, Climatic and Human Perspective on Vegetation History and Modern Plant Diversity. In: Hoorn C, Perrigo A, Antonelli A (eds) Mountains, Climate, and Biodiversity. First Edition. Wiley-Blackwell, Oxford, UK, pp 413–428

Feddema JJ (2005) A Revised Thornthwaite-Type Global Climate Classification. Phys Geogr 26(6):442–466. DOI: 10.2747/0272-3646.26.6.442

Feng S, Ho C-H, Hu Q, Oglesby RJ, Jeong S-J, Kim B-M (2012) Evaluating observed and projected future climate changes for the Arctic using the Köppen-Trewartha climate classification. Clim Dyn 38(7):1359–1373. DOI: 10.1007/s00382-011-1020-6

Fenna D (2007) Cartographic Science: A Compendium of Map Projections, with Derivations. Taylor & Francis Group, Boca Raton, Florida

Fischlin A, Ayres M, Karnosky D, Kellomäki S, Louman B, Ong C, Plattner G-K, Santoso H, Thompson I, Booth TH, Marcar N, Scholes B, Swanston C, Zamolodchikov D (2009) Future environmental impacts and vulnerabilities. In: Seppälä R, Buck A, Katila P (eds) Adaptation of Forests and People to Climate Change. A Global Assessment Report. IUFRO World Series Volume 22. International Union of Forest Research Organizations, Helsinki, Finland, pp 53–100

Führer E, Horváth L, Jagodics A, Machon A, Szabados I (2011) Application of a new aridity index in Hungarian forestry practice. Időjárás 115(3):205–216

Fyfe RM, de Beaulieu J-L, Binney H, Bradshaw RHW, Brewer S, Le Flao A, Finsinger W, Gaillard M-J, Giesecke T, Gil-Romera G, Grimm EC, Huntley B, Kunes P, Kühl N, Leydet M, Lotter AF, Tarasov PE, Tonkov S (2009) The European Pollen Database: past efforts and current activities. Veg Hist Archaeobot 18(5):417–424. DOI: 10.1007/s00334-009-0215-9

Fyfe RM, Woodbridge J, Roberts N (2015) From forest to farmland: pollen-inferred land cover change across Europe using the pseudobiomization approach. Glob Chang Biol 21(3):1197–1212. DOI: 10.1111/gcb.12776

Gallardo C, Gil V, Hagel E, Tejeda C, de Castro M (2013) Assessment of climate change in Europe from an ensemble of regional climate models by the use of Köppen-Trewartha classification. Int J Climatol 33(9):2157–2166. DOI: 10.1002/joc.3580

Gesch DB, Verdin KL, Greenlee SK (1999) New land surface digital elevation model covers the Earth. EOS Earth Space Sci News 80(6):69–70. DOI: 10.1029/99EO00050

Giesecke T, Davis B, Brewer S, Finsinger W, Wolters S, Blaauw M, de Beaulieu J-L, Binney H, Fyfe RM, Gaillard M-J, Gil-Romera G, van der Knaap WO, Kuneš P, Kühl N, van Leeuwen JFN, Leydet M, Lotter AF, Ortu E, Semmler M, Bradshaw RHW (2014) Towards mapping the late Quaternary vegetation change of Europe. Veg Hist Archaeobot 23(1):75–86. DOI: 10.1007/s00334-012-0390-y

Gilck F, Poschlod P (2019) The origin of alpine farming: A review of archaeological, linguistic and archaeobotanical studies in the Alps. Holocene 29(9):1503–1511. DOI: 10.1177/0959683619854511

Giorgi F (2019) Thirty Years of Regional Climate Modeling: Where Are We and Where Are We Going next? J Geophys Res Atmos 124(11):5696–5723. DOI: 10.1029/2018JD030094

Giorgi F, Marinucci MR, Bates GT (1993) Development of a Second-Generation Regional Climate Model (RegCM2). Part I: Boundary-Layer and Radiative Transfer Processes. Mon Weather Rev 121(10):2794–2813. DOI: 10.1175/1520-0493(1993)121<2794:DOASGR>2.0.CO;2

Gordon C, Cooper C, Senior CA, Banks H, Gregory JM, Johns TC, Mitchell JFB, Wood RA (2000) The simulation of SST, sea ice extents and ocean heat transports in a version of the Hadley Centre coupled model without flux adjustments. Clim Dyn 16(2–3):147–168. DOI: 10.1007/s003820050010

Grabherr G, Gottfried M, Pauli H (1994) Climate effects on mountain plants. Nature 369(6480):448. DOI: 10.1038/369448a0

Hakim GJ, Emile-Geay J, Steig EJ, Noone D, Anderson DM, Tardif R, Steiger N, Perkins WA (2016) The last millennium climate reanalysis project: Framework and first results. J Geophys Res Atmos 121(12):6745–6764. DOI: 10.1002/2016JD024751

Hamed KH, Rao AR (1998) A modified Mann-Kendall trend test for autocorrelated data. J Hydrol 204(1–4):182–196. DOI: 10.1016/S0022-1694(97)00125-X

Hansen MC, Potapov PV, Moore R, Hancher M, Turubanova SA, Tyukavina A, Thau D, Stehman SV, Goetz SJ, Loveland TR, Kommareddy A, Egorov A, Chini L, Justice CO, Townshend JRG (2013) High-resolution global maps of 21st-century forest cover change. Science 342(6160):850–853. DOI: 10.1126/science.1244693

Hansen MC, Stehman SV, Potapov PV (2010) Quantification of global gross forest cover loss. Proc Natl Acad Sci USA 107(19):8650–8655. DOI: 10.1073/pnas.0912668107

Hargreaves GH, Samani ZA (1985) Reference Crop Evapotranspiration from Temperature. Appl Eng Agric 1(2):96–99. DOI: 10.13031/2013.26773

Harris I, Osborn TJ, Jones P, Lister D (2020) Version 4 of the CRU TS monthly high-resolution gridded multivariate climate dataset. Sci Data 7:109. DOI: 10.1038/s41597-020-0453-3

Harrison SP (2013) Data–Model Comparisons. In: Elias SA, Mock CJ (eds) Encyclopedia of Quaternary Science (Second Edition). Elsevier, Amsterdam, The Netherlands, pp 135–146. DOI: 10.1016/B978-0-444-53643-3.00007-8

Harrison SP, Bartlein PJ, Prentice IC (2016) What have we learnt from palaeoclimate simulations? J Quat Sci 31(4):363–385. DOI: 10.1002/jqs.2842

Harsch MA, Hulme PE, McGlone MS, Duncan RP (2009) Are treelines advancing? A global meta-analysis of treeline response to climate warming. Ecol Lett 12(10):1040–1049. DOI: 10.1111/j.1461-0248.2009.01355.x

Haylock MR, Hofstra N, Klein Tank AMG, Klok EJ, Jones PD, New M (2008) A European daily high-resolution gridded data set of surface temperature and precipitation for 1950–2006. J Geophys Res 113:D20119. DOI: 10.1029/2008JD010201

He F (2011) Simulating Transient Climate Evolution of the Last Deglaciation with CCSM3. Dissertation, University of Wisconsin–Madison

Henderson-Sellers A (1994) Global terrestrial vegetation 'prediction': the use and abuse of climate and application models. Prog Phys Geogr 18(2):209–246. DOI: 10.1177/030913339401800203

Hertelendi E, Sümegi P, Szöör Gy (1992) Geochronologic and Paleoclimatic Characterization of Quaternary Sediments in the Great Hungarian Plain. Radiocarbon 34(3):833–839. DOI: 10.1017/S0033822200064146

Hickler T, Vohland K, Feehan J, Miller PA, Smith B, Costa L, Giesecke T, Fronzek S, Carter TR, Cramer W, Kühn I, Sykes MT (2012) Projecting the future distribution of European potential natural vegetation zones with a generalized, tree species-based dynamic vegetation model. Glob Ecol Biogeogr 21(1):50–63. DOI: 10.1111/j.1466-8238.2010.00613.x

Hijmans RJ (2020) raster: Geographic Data Analysis and Modeling. R package version 3.3-13. https://CRAN.R-project.org/package=raster. Accessed 25 November 2020

Hijmans RJ (2021) terra: Spatial Data Analysis. R package version 1.3-22. https://CRAN.R-project.org/package=terra. Accessed 2 November 2021

Hijmans RJ, Cameron SE, Parra JL, Jones PG, Jarvis A (2005) Very high resolution interpolated climate surfaces for global land areas. Int J Climatol 25(15):1965–1978. DOI: 10.1002/joc.1276

Hijmans RJ, van Etten J (2014) raster: Geographic Data Analysis and Modeling. R package version, 2.2-31. http://cran.r-project.org/package=raster. Accessed 14 March 2014

Holdridge LR (1947) Determination of World Plant Formations From Simple Climatic Data. Science 105(2727):367–368. DOI: 10.1126/science.105.2727.367

Holdridge LR (1959) Simple Method for Determining Potential Evapotranspiration from Temperature Data. Science 130(3375):572. DOI: 10.1126/science.130.3375.572

Holdridge LR (1967) Life zone ecology. Tropical Science Center, San Jose, Costa Rica
Hollis D, McCarthy M, Kendon M, Legg T, Simpson I (2019) HadUK-Grid—A new UK dataset of gridded climate observations. Geosci Data J 6(2):151–159. DOI: 10.1002/gdj3.78
Holtmeier F-K (2009) Mountain Timberlines. Ecology, Patchiness, and Dynamics. Springer, Dordrecht, The Netherlands. DOI: 10.1007/978-1-4020-9705-8
Hou XY, Sun SZ, Zhang JW, He MG, Wang YF, Kong DZ, Wang SQ (1982) Vegetation Map of the People's Republic of China (1:4 000 000). Map Press of China, Beijing, China
Hoyt DV (1977) Percent of Possible Sunshine and the Total Cloud Cover. Mon Weather Rev 105(5):648–652. DOI: 10.1175/1520-0493(1977)105<0648:POPSAT>2.0.CO;2
Huntley B, Berry PM, Cramer W, McDonald AP (1995) Modelling present and potential future ranges of some European higher plants using climate response surfaces. J Biogeogr 22(6):967–1001. DOI: 10.2307/2845830
Huntley B, Birks HJB (1983) An atlas of past and present pollen maps for Europe: 0–13000 years ago. Cambridge University Press, Cambridge, UK
Iqbal M (1983) An Introduction to Solar Radiation. Academic Press, London, UK. DOI: 10.1016/B978-0-12-373750-2.X5001-0
Iversen J (1944) Viscum, Hedera and Ilex as climatic indicators. Geol Fören Stockholm För 66(3):463–483. DOI: 10.1080/11035894409445689
Jaccard P (1901) Étude comparative de la distribution florale dans une portion des alpes et des jura. Bull Soc Vaud sci nat 37:547–579
Jacob D, Podzun R (1997) Sensitivity studies with the regional climate model REMO. Meteorol Atmos Phys 63(1–2):119–129. DOI: 10.1007/BF01025368
Jones RG, Noguer M, Hassell DC, Hudson D, Wilson SS, Jenkins GJ, Mitchell JFB (2004) Generating high resolution climate change scenarios using PRECIS. Met Office Hadley Centre, Exeter, UK
Juggins S, Birks HJB (2012) Quantitative Environmental Reconstructions from Biological Data. In: Birks HJB, Lotter AF, Juggins S, Smol JP (eds) Tracking Environmental Change Using Lake Sediments. Volume 5. Data Handling and Numerical Techniques. Springer, Dordrecht, The Netherlands, pp 431–494. DOI: 10.1007/978-94-007-2745-8_14
Jump AS, Mátyás Cs, Peñuelas J (2009) The altitude-for-latitude disparity in the range retractions of woody species. Trends Ecol Evol 22(12):694–701. DOI: 10.1016/j.tree.2009.06.007
Kandirmaz HM, Kaba K, Avci M (2014) Estimation of Monthly Sunshine Duration in Turkey Using Artificial Neural Networks. Int J Photoenergy 2014:680596. DOI: 10.1155/2014/680596
Kandler O, Innes JL (1995) Air pollution and forest decline in Central Europe. Environ Pollut 90(2):171–180. DOI: 10.1016/0269-7491(95)00006-D
Kaplan JO (2001) Geophysical Applications of Vegetation Modeling. Dissertation, Lund University
Kappelle M, Castro M, Acevedo H, Cordero P, González L, Méndez E, Monge H (2003) A Rapid Method in Ecosystem Mapping and Monitoring as a Tool for Managing Costa Rican Ecosystem Health. In: Rapport DJ, Lasley BL, Rolston DE, Nielsen NO, Qualset CO, Damania AB (eds) Managing for Healthy Ecosystems. Lewis Publishers, Boca Raton, Florida, pp 449–458. DOI: 10.1201/9781420032130.ch47
Karger DN, Nobis MP, Normand S, Graham CH, Zimmermann NE (in review) CHELSA-TraCE21k v1.0. Downscaled transient temperature and precipitation data since the last glacial maximum. Clim Past Discuss. DOI: 10.5194/cp-2021-30
Kendall MG (1975) Rank Correlation Methods. Fourth Edition. Charles Griffin, London, UK
Khaliq MN, Ouarda TBMJ, Gachon P, Sushama L, St-Hilaire A (2009) Identification of hydrological trends in the presence of serial and cross correlations: A review of selected methods and their application to annual flow regimes of Canadian rivers. J Hydrol 368(1–4):117–130. DOI: 10.1016/j.jhydrol.2009.01.035
Khalyani AH, Gould WA, Harmsen E, Terando A, Quinones M, Collazo JA (2016) Climate Change Implications for Tropical Islands: Interpolating and Interpreting Statistically Downscaled GCM

Projections for Management and Planning. J Appl Meteorol Climatol 55(2):265–282. DOI: 10.1175/JAMC-D-15-0182.1

Kharuk V, Ranson K, Dvinskaya M (2007) Evidence of evergreen conifer invasion into larch dominated forests during recent decades in Central Siberia. Eurasian J For Res 10(2):163–171

Köppen W (1936) Das geographische System der Klimate (The geographical system of the climate). In: Köppen W, Geiger R (eds) Handbuch der Klimatologie (Handbook of climatology). Verlag von Gebrüder Borntraeger, Berlin, Germany, pp 1–44 (in German)

Körner C (2012) Alpine Treelines. Functional Ecology of the Global High Elevation Tree Limits. Springer, Basel, Switzerland

Krapp M, Beyer RM, Edmundson SL, Valdes PJ, Manica A (2021) A statistics-based reconstruction of high-resolution global terrestrial climate for the last 800,000 years. Sci Data 8:228. DOI: 10.1038/s41597-021-01009-3

Küchler AW (1964) Potential natural vegetation of the conterminous United States (1:3 168 000). American Geographical Society, New York, NY

Kullman L (2001) 20th Century Climate Warming and Tree-limit Rise in the Southern Scandes of Sweden. Ambio 30(2):72–80. DOI: 10.1579/0044-7447-30.2.72

Leemans R (1990) Global Data Sets Collected and Compiled by the Biosphere Project. IIASA Working Paper. International Institute for Applied Systems Analysis, Laxenburg, Austria

Leemans R, Cramer WP (1991) The IIASA Database for Mean Monthly Values of Temperature, Precipitation, and Cloudiness on a Global Terrestrial Grid. IIASA Research Report. International Institute for Applied Systems Analysis, Laxenburg, Austria

Leggett J, Pepper WJ, Swart RJ (1992) Emissions Scenarios for IPCC: an Update. In: Houghton JT, Callander BA, Varney SK (eds) Climate Change 1992. The Supplementary Report to the IPCC Scientific Assessment. Cambridge University Press, Cambridge, UK, pp 69–95

Lescop-Sinclair K, Payette S (1995) Recent Advance of the Arctic Treeline Along the Eastern Coast of Hudson Bay. J Ecol 83(6):929–936. DOI: 10.2307/2261175

Li G, Wen Z, Guo K, Du S (2015) Simulating the Effect of Climate Change on Vegetation Zone Distribution on the Loess Plateau, Northwest China. Forests 6(6):2092–2108. DOI: 10.3390/f6062092

Li Q, Wu H, Yu Y, Sun A, Luo Y (2019) Large-scale vegetation history in China and its response to climate change since the Last Glacial Maximum. Quat Int 500:108–119. DOI: 10.1016/j.quaint.2018.11.016

Liebig J (1840) Die organische Chemie in ihrer Anwendung auf Agricultur und Physiologie (Organic chemistry in its applications to agriculture and physiology). Verlag von Friedrich Vieweg und Sohn, Braunschweig, Germany (in German)

Limonard CBG (1978) Missing values in time series and the implications on autocorrelation analysis. Anal Chim Acta 103(2):133–140. DOI: 10.1016/S0003-2670(01)84033-2

Liu X, Zhan T, Zhou X, Wu H, Li Q, Zhao C, Qiao Y, Jiang S, Tu L, Ma Y, Zhang J, Jiang X, Lou B, Zhang X, Zhou X (2019) Late onset of the Holocene rainfall maximum in northeastern China inferred from a pollen record from the sediments of Tianchi Crater Lake. Quat Res 92(1):133–145. DOI: 10.1017/qua.2018.137

Lüdeke MKB, Badeck FW, Otto RD, Häger C, Dönges S, Kindermann J, Würth G, Lang T, Jäkel U, Klaudius A, Ramge P, Habermehl S, Kohlmaier GH (1994) The Frankfurt Biosphere Model: A global process-oriented model of seasonal and long-term CO_2 exchange between terrestrial ecosystems and the atmosphere. I. Model description and illustrative results for cold deciduous and boreal forests. Clim Res 4(2):143–166. DOI: 10.3354/cr004143

Lugo AE, Brown SL, Dodson R, Smith TS, Shugart HH (1999) The Holdridge life zones of the conterminous United States in relation to ecosystem mapping. J Biogeogr 26(5):1025–1038. DOI: 10.1046/j.1365-2699.1999.00329.x

Magyari EK, Gasparik M, Major I, Lengyel Gy, Pál I, Virág A, Korponai J, Haliuc A, Szabó Z, Pazonyi P (2022) Mammal extinction facilitated biome shift and human population change during the last glacial termination in East-Central Europe. Sci Rep 12:6796. DOI: 10.1038/s41598-022-10714-x

Magyari EK, Pál I, Vincze I, Veres D, Jakab G, Braun M, Szalai Z, Szabó Z, Korponai J (2019) Warm Younger Dryas summers and early late glacial spread of temperate deciduous trees in the Pannonian Basin during the last glacial termination (20-9 kyr cal BP). Quat Sci Rev 225:105980. DOI: 10.1016/j.quascirev.2019.105980

Mann HB (1945) Nonparametric Tests Against Trend. Econometrica 13(3):245–259. DOI: 10.2307/1907187

Marinova E, Harrison SP, Bragg F, Connor S, de Laet V, Leroy SAG, Mudie P, Atanassova J, Bozilova E, Caner H, Cordova C, Djamali M, Filipova-Marinova M, Gerasimenko N, Jahns S, Kouli K, Kotthoff U, Kvavadze E, Lazarova M, Novenko E, Ramezani E, Röpke A, Shumilovskikh L, Tanţău I, Tonkov S (2018) Pollen-derived biomes in the Eastern Mediterranean–Black Sea–Caspian-Corridor. J Biogeogr 45(2):484–499. DOI: 10.1111/jbi.13128

Martazinova V, Ivanova O, Shandra O (2011) Climate and treeline dynamics in the Ukrainian Carpathians Mts. Folia Oecol 38(1):66–72

Mather JR, Yoshioka GA (1968) The role of climate in the distribution of vegetation. Ann Assoc Am Geogr 58(1):29–41. DOI: 10.1111/j.1467-8306.1968.tb01634.x

Mátyás Cs, Berki I, Bidló A, Csóka Gy, Czimber K, Führer E, Gálos B, Gribovszki Z, Illés G, Hirka A, Somogyi Z (2018) Sustainability of Forest Cover under Climate Change on the Temperate-Continental Xeric Limits. Forests 9(8):489. DOI: 10.3390/f9080489

Mauri A, Davis BAS, Collins PM, Kaplan JO (2014) The influence of atmospheric circulation on the mid-Holocene climate of Europe: a data–model comparison. Clim Past 10(5):1925–1938. DOI: 10.5194/cp-10-1925-2014

McMahon SM, Harrison SP, Armbruster WS, Bartlein PJ, Beale CM, Edwards ME, Kattge J, Midgley G, Morin X, Prentice IC (2011) Improving assessment and modelling of climate change impacts on global terrestrial biodiversity. Trends Ecol Evol 26(5):249–259. DOI: 10.1016/j.tree.2011.02.012

Mihailović DT, Lalić B, Dreśković N, Mimić G, Djurdjević V, Jančić M (2015) Climate change effects on crop yields in Serbia and related shifts of Köppen climate zones under the SRES-A1B and SRES-A2. Int J Climatol 35(11):3320–3334. DOI: 10.1002/joc.4209

Miletić B, Orlović S, Lalić B, Đurđević V, Mandić MV, Vuković A, Gutalj M, Stjepanović S, Matović B, Stojanović DB (2021) The potential impact of climate change on the distribution of key tree species in Serbia under RCP4.5 and RCP 8.5 scenarios. Austrian J For Sci 138(4):183–208

Miller PA, Giesecke T, Hickler T, Bradshaw RHW, Smith B, Seppä H, Valdes PJ, Sykes MT (2008) Exploring climatic and biotic controls on Holocene vegetation change in Fennoscandia. J Ecol 96(2):247–259. DOI: 10.1111/j.1365-2745.2007.01342.x

Mitchell TD, Carter TR, Jones PD, Hulme M, New M (2004) A comprehensive set of high-resolution grids of monthly climate for Europe and the globe: the observed record (1901-2000) and 16 scenarios (2001-2100). Tyndall Centre Working Paper 55. Tyndall Centre for Climate Change Research, University of East Anglia, Norwich, UK

Mitchell T, GDAL Developers (2014) Geospatial Power Tools: GDAL Raster & Vector Commands. Locate Press, Chugiak, Alaska

Mitscherlich EA (1909) Das Gesetz des Minimums und das Gesetz des abnehmenden Bodenertrags (The laws of the minimum and diminishing returns). Landwirtsch Jahrb 38:537–552 (in German)

Monserud RA, Leemans R (1992) Comparing global vegetation maps with the Kappa statistics. Ecol Model 62(4):275–293. DOI: 10.1016/0304-3800(92)90003-W

Morales P, Hickler T, Rowell DP, Smith B, Sykes MT (2007) Changes in European ecosystem productivity and carbon balance driven by regional climate model output. Glob Chang Biol 13(1):108–122. DOI: 10.1111/j.1365-2486.2006.01289.x

Móricz N, Rasztovits E, Gálos B, Berki I, Eredics A, Loibl W (2013) Modelling the potential distribution of three climate zonal tree species for present and future climate in Hungary. Acta Silvatica et Lignaria Hungarica 9(1):85–96. DOI: 10.2478/aslh-2013-0007

Moss R, Babiker M, Brinkman S, Calvo E, Carter T, Edmonds J, Elgizouli I, Emori S, Erda L, Hibbard K, Jones R, Kainuma M, Kelleher J, Lamarque JF, Manning M, Matthews B, Meehl J, Meyer L, Mitchell

J, Nakicenovic N, O'Neill B, Pichs R, Riahi K, Rose S, Runci P, Stouffer R, van Vuuren D, Weyant J, Wilbanks T, van Ypersele JP, Zurek M (2008) Towards New Scenarios for Analysis of Emissions, Climate Change, Impacts, and Response Strategies. Intergovernmental Panel on Climate Change, Geneva, Switzerland

Mucina L (2019) Biome: evolution of a crucial ecological and biogeographical concept. New Phytol 222(1):97–114. DOI: 10.1111/nph.15609

Nakicenovic N, Swart R (eds) (2000) Special Report on Emissions Scenarios. A Special Report of Working Group III of the Intergovernmental Panel on Climate Change. Cambridge University Press, Cambridge, UK

New M, Hulme M, Jones P (1999) Representing Twentieth-Century Space–Time Climate Variability. Part I: Development of a 1961–90 Mean Monthly Terrestrial Climatology. J Clim 12(3):829–856. DOI: 10.1175/1520-0442(1999)012<0829:RTCSTC>2.0.CO;2

New M, Hulme M, Jones P (2000) Representing Twentieth-Century Space–Time Climate Variability. Part II: Development of 1901–96 Monthly Grids of Terrestrial Surface Climate. J Clim 13(13):2217–2238. DOI: 10.1175/1520-0442(2000)013<2217:RTCSTC>2.0.CO;2

Oh H, Shin HJ (2016) Climatic classification over asia during the middle holocene climatic optimum based on PMIP models. J Earth Sci 27(1):123–129. DOI: 10.1007/s12583-016-0622-7

Orbán I, Birks HH, Vincze I, Finsinger W, Pál I, Marinova E, Jakab G, Braun M, Hubay K, Bíró T, Magyari EK (2018) Treeline and timberline dynamics on the northern and southern slopes of the Retezat Mountains (Romania) during the late glacial and the Holocene. Quat Int 477:59–78. DOI: 10.1016/j.quaint.2017.03.012

Pal JS, Giorgi F, Bi X, Elguindi N, Solmon F, Gao X, Rauscher SA, Francisco R, Zakey A, Winter J, Ashfaq M, Syed FS, Bell JL, Differbaugh NS, Karmacharya J, Konaré A, Martinez D, da Rocha RP, Sloan LC, Steiner AL (2007) Regional Climate Modeling for the Developing World: The ICTP RegCM3 and RegCNET. Bull Am Meteorol Soc 88(9):1395–1409. DOI: 10.1175/Bams-88-9-1395

Pearson RG (2007) Species' distribution modeling for conservation educators and practitioners. Lessons Conserv 3:54–89

Peng C (2000) From static biogeographical model to dynamic global vegetation model: a global perspective on modelling vegetation dynamics. Ecol Model 135(1):33–54. DOI: 10.1016/S0304-3800(00)00348-3

Peng CH, Guiot J, Van Campo E, Cheddadi R (1995) Temporal and spatial variations of terrestrial biomes and carbon storage since 13 000 yr BP in Europe: Reconstruction from pollen data and statistical models. Water Air Soil Pollut 82(1–2):375–390. DOI: 10.1007/BF01182848

Peñuelas J, Boada M (2003) A global change-induced biome shift in the Montseny mountains (NE Spain). Glob Chang Biol 9(2):131–140. DOI: 10.1046/j.1365-2486.2003.00566.x

Peyron O, Guiot J, Cheddadi R, Tarasov P, Reille M, de Beaulieu J-L, Bottema S, Andrieu V (1998) Climatic Reconstruction in Europe for 18,000 YR B.P. from Pollen Data. Quat Res 49(2):183–196. DOI: 10.1006/qres.1997.1961

Philipona R, Dürr B (2004) Greenhouse forcing outweighs decreasing solar radiation driving rapid temperature rise over land. Geophys Res Lett 31:L22208. DOI: 10.1029/2004GL020937

Phillips SJ, Anderson RP, Schapire RE (2006) Maximum entropy modelling of species geographic distributions. Ecol Model 190(3–4):231–259. DOI: 10.1016/j.ecolmodel.2005.03.026

Pongrácz R, Bartholy J, Kis A (2014) Estimation of future precipitation conditions for Hungary with special focus on dry periods. Időjárás 118(4):305–321

Pongrácz R, Bartholy J, Miklós E (2011) Analysis of projected climate change for Hungary using ENSEMBLES simulations. Appl Ecol Environ Res 9(4):387–398

Prentice KC (1990) Bioclimatic distribution of vegetation for general circulation model studies. J Geophys Res 95(D8):11811–11830. DOI: 10.1029/jd095id08p11811

Prentice IC, Bondeau A, Cramer W, Harrison SP, Hickler T, Lucht W, Sitch S, Smith B, Sykes MT (2007) Dynamic Global Vegetation Modeling: Quantifying Terrestrial Ecosystem Responses to Large-Scale Environmental Change. In: Canadell JG, Pataki DE, Pitelka LF (eds) Terrestrial Ecosystems in a

Changing World. Springer, Berlin, Heidelberg, Germany, pp 175–192. DOI: 10.1007/978-3-540-32730-1_15

Prentice IC, Cowling SA (2013) Dynamic Global Vegetation Models. In: Levin SA (ed) Encyclopedia of Biodiversity (Second Edition). Elsevier, Amsterdam, The Netherlands, pp 607–689. DOI: 10.1016/B978-0-12-384719-5.00412-3

Prentice IC, Cramer W, Harrison SP, Leemans R, Monserud RA, Solomon AM (1992) A global biome model based on plant physiology and dominance, soil properties and climate. J Biogeogr 19(2):117–134. DOI: 10.2307/2845499

Prentice IC, Guiot J, Huntley B, Jolly D, Cheddadi R (1996) Reconstructing biomes from palaeoecological data: a general method and its application to European pollen data at 0 and 6 ka. Clim Dyn 12(3):185–194. DOI: 10.1007/BF00211617

Prentice IC, Harrison SP, Jolly D, Guiot J (1998) The climate and biomes of Europe at 6000 yr BP: comparison of model simulations and pollen-based reconstructions. Quat Sci Rev 17(6–7):659–668. DOI: 10.1016/S0277-3791(98)00016-X

Prentice IC, Sykes MT, Cramer W (1993) A simulation model for the transient effects of climate change on forest landscapes. Ecol Model 65(1–2):51–70. DOI: 10.1016/0304-3800(93)90126-D

Priestley CHB, Taylor RJ (1972) On the assessment of surface heat flux and evaporation using large-scale parameters. Mon Weather Rev 100(2):81–92. DOI: 10.1175/1520-0493(1972)100<0081:OTAOSH>2.3.CO;2

Radu R, Déqué M, Somot S (2008) Spectral nudging in a spectral regional climate model. Tellus Ser A 60(5):898–910. DOI: 10.1111/j.1600-0870.2008.00341.x

Rasztovits E, Móricz N, Berki I, Pötzelsberger E, Mátyás Cs (2012) Evaluating the performance of stochastic distribution models for European beech at low-elevation xeric limits. Időjárás 116(3):173–194

Reid PC, Hari RE, Beaugrand G, Livingstone DM, Marty C, Straile D, Barichivich J, Goberville E, Adrian R, Aono Y, Brown R, Foster J, Groisman P, Hélaouët P, Hsu H-H, Kirby R, Knight J, Kraberg A, Li J, Lo T-T, Myneni RB, North RP, Pounds JA, Sparks T, Stübi R, Tian Y, Wiltshire KH, Xiao D, Zhu Z (2016) Global impacts of the 1980s regime shift. Glob Chang Biol 22(2):682–703. DOI: 10.1111/gcb.13106

Riley SJ, DeGloria SD, Elliot R (1999) A terrain ruggedness index that quantifies topographic heterogeneity. Interm J Sci 5(1–4):23–27

Roeckner E, Bäuml G, Bonaventura L, Brokopf R, Esch M, Giorgetta M, Hagemann S, Kirchner I, Kornblueh L, Manzini E, Rhodin A, Schlese U, Schulzweida U, Tompkins A (2003) The atmospheric general circulation model ECHAM 5. Part I: Model description. MPI-Report No. 349. Max Planck Institute for Meteorology, Hamburg, Germany

Rolland C (2003) Spatial and Seasonal Variations of Air Temperature Lapse Rates in Alpine Regions. J Clim 16(7):1032–1046. DOI: 10.1175/1520-0442(2003)016<1032:SASVOA>2.0.CO;2

Rousseau D-D (1991) Climatic transfer function from quaternary molluscs in European loess deposits. Quat Res 36(2):195–209. DOI: 10.1016/0033-5894(91)90025-Z

Rubel F, Brugger K, Haslinger K, Auer I (2017) The climate of the European Alps: Shift of very high resolution Köppen-Geiger climate zones 1800–2100. Meteorol Z 26(2):115–125. DOI: 10.1127/metz/2016/0816

Samuelsson P, Jones CG, Willén U, Ullerstig A, Gollvik S, Hansson U, Jansson C, Kjellström E, Nikulin G, Wyser K (2011) The Rossby Centre Regional Climate model RCA3: model description and performance. Tellus Ser A 63(1):4–23. DOI: 10.1111/j.1600-0870.2010.00478.x

Sitch S, Smith B, Prentice IC, Arneth A, Bondeau A, Cramer W, Kaplan JO, Levis S, Lucht W, Sykes MT, Thonicke K, Venevsky S (2003) Evaluation of ecosystem dynamics, plant geography and terrestrial carbon cycling in the LPJ dynamic global vegetation model. Glob Chang Biol 9(2):161–185. DOI: 10.1046/j.1365-2486.2003.00569.x

Skalák P, Farda A, Zahradníček P, Trnka M, Hlásny T, Štěpánek P (2018) Projected shift of Köppen–Geiger zones in the central Europe: a first insight into the implications for ecosystems and the society. Int J Climatol 38(9):3595–3606. DOI: 10.1002/joc.5520

Smith B, Prentice IC, Sykes MT (2001) Representation of vegetation dynamics in the modelling of terrestrial ecosystems: comparing two contrasting approaches within European climate space. Glob Ecol Biogeogr 10(6):621–637. DOI: 10.1046/j.1466-822X.2001.t01-1-00256.x

Spinoni J, Szalai S, Szentimrey T, Lakatos M, Bihari Z, Nagy A, Németh Á, Kovács T, Mihic D, Dacic M, Petrovic P, Kržič A, Hiebl J, Auer I, Milkovic J, Štepánek P, Zahradnícek P, Kilar P, Limanowka D, Pyrc R, Cheval S, Birsan M-V, Dumitrescu A, Deak G, Matei M, Antolovic I, Nejedlík P, Štastný P, Kajaba P, Bochnícek O, Galo D, Mikulová K, Nabyvanets Y, Skrynyk O, Krakovska S, Gnatiuk N, Tolasz R, Antofie T, Vogt J (2015) Climate of the Carpathian Region in the period 1961–2010: climatologies and trends of 10 variables. Int J Climatol 35(7):1322–1341. DOI: 10.1002/joc.4059

Stanghellini C (1981) A Simple Method for Evaluating Sunshine Duration by Cloudiness. J Appl Meteorol 20(3):320–323. DOI: 10.1175/1520-0450(1981)020<0320:ASMFES>2.0.CO;2

Stojanović DB, Kržič A, Matović B, Orlović S, Duputie A, Djurdjević V, Galić Z, Stojnić S (2013) Prediction of the European beech (*Fagus sylvatica* L.) xeric limit using a regional climate model: An example from southeast Europe. Agric For Meteorol 176:94–103. DOI: 10.1016/j.agrformet.2013.03.009

Stojanović DB, Matović B, Orlović S, Kržič A, Trudić B, Galić Z, Stojnić S, Pekeč S (2014) Future of the Main Important Forest Tree Species in Serbia from the Climate Change Perspective. South-East Eur For 5(2):117–124. DOI: 10.15177/seefor.14-16

Sturm M, Racine C, Tape K (2001) Increasing shrub abundance in the Arctic. Nature 411(6837):546–547. DOI: 10.1038/35079180

Sugita S (2007a) Theory of quantitative reconstruction of vegetation I: pollen from large sites REVEALS regional vegetation composition. Holocene 17(2):229–241. DOI: 10.1177/0959683607075837

Sugita S (2007b) Theory of quantitative reconstruction of vegetation II: all you need is LOVE. Holocene 17(2):243–257. DOI: 10.1177/0959683607075838

Sun A, Luo Y, Wu H, Chen X, Li Q, Yu Y, Sun X, Guo Z (2020) An updated biomization scheme and vegetation reconstruction based on a synthesis of modern and mid-Holocene pollen data in China. Glob Planet Chang 192:103178. DOI: 10.1016/j.gloplacha.2020.103178

Sykes MT, Prentice IC (1996) Climate change, tree species distributions and forest dynamics: A case study in the mixed conifer/northern hardwoods zone of northern Europe. Clim Chang 34(2):161–177. DOI: 10.1007/BF00224628

Sykes MT, Prentice IC, Cramer W (1996) A Bioclimatic Model for the Potential Distributions of North European Tree Species Under Present and Future Climates. J Biogeogr 23(2):203–233

Szabó B, Pazonyi P, Tóth E, Magyari EK, Kiss GI, Rinyu L, Futó I, Virág A (2021) Pleistocene and Holocene palaeoenvironmental reconstruction of the Carpathian Basin based on multiproxy analysis of cervid teeth. Hist Biol 33(12):3307–3325. DOI: 10.1080/08912963.2020.1863960

Szabóné André K, Bartholy J, Pongrácz R, Bór J (2021) Local identification of persistent cold air pool conditions in the Great Hungarian Plain. Időjárás 125(2):167–192. DOI: 10.28974/idojaras.2021.2.1

Szelepcsényi Z, Breuer H, Ács F, Kozma I (2009) Biofizikai klímaklasszifikációk. 2. rész: magyarországi alkalmazások (Bioclimatic classification methods. Part 2: Hungarian applications). Légkör 54(4):18–23 (in Hungarian)

Szelepcsényi Z, Breuer H, Sümegi P (2014a) The climate of Carpathian Region in the 20th century based on the original and modified Holdridge life zone system. Cent Eur J Geosci 6(3):293–307. DOI: 10.2478/s13533-012-0189-5

Szelepcsényi Z, Breuer H, Sümegi P (2014b) Hogyan változtak a Kárpát-medence régiójának életzónái a múlt században? (How did the Carpathian Region's life zones altered in the last century?) In: Sümegi P (ed) Környezetföldtani és környezettörténeti kutatások a dunai Alföldön (Researches in environmental geology and environmental history for the Danubian Plain). GeoLitera, Szeged, Hungary, pp 163–171 (in Hungarian)

Takahara H, Sugita S, Harrison SP, Miyoshi N, Morita Y, Uchiyama T (2000) Pollen-based reconstructions of Japanese biomes at 0, 6000 and 18,000 ^{14}C yr BP. J Biogeogr 27(3):665–683. DOI: 10.1046/j.1365-2699.2000.00432.x

Tapiador FJ, Moreno R, Navarro A, Sánchez JL, García-Ortega E (2019) Climate classifications from regional and global climate models: Performances for present climate estimates and expected changes in the future at high spatial resolution. Atmos Res 228:107–121. DOI: 10.1016/j.atmosres.2019.05.022

Tarasov PE, Andreev AA, Anderson PM, Lozhkin AV, Leipe C, Haltia E, Nowaczyk NR, Wennrich V, Brigham-Grette J, Melles M (2013) A pollen-based biome reconstruction over the last 3.562 million years in the Far East Russian Arctic – new insights into climate–vegetation relationships at the regional scale. Clim Past 9(6):2759–2775. DOI: 10.5194/cp-9-2759-2013

Tarasov PE, Cheddadi R, Guiot J, Bottema S, Peyron O, Belmonte J, Ruiz-Sanchez V, Saadi F, Brewer S (1998) A method to determine warm and cool steppe biomes from pollen data; application to the Mediterranean and Kazakhstan regions. J Quat Sci 13(4):335–344. DOI: 10.1002/(SICI)1099-1417(199807/08)13:4<335::AID-JQS375>3.0.CO;2-A

Tarasov PE, Peyron O, Guiot J, Brewer S, Volkova VS, Bezusko LG, Dorofeyuk NI, Kvavadze EV, Osipova IM, Panova NK (1999) Last Glacial Maximum climate of the former Soviet Union and Mongolia reconstructed from pollen and plant macrofossil data. Clim Dyn 15(3):227–240. DOI: 10.1007/s003820050278

Tarasov P, Williams JW, Andreev A, Nakagawa T, Bezrukova E, Herzschuh U, Igarashi Y, Müller S, Werner K, Zheng Z (2007) Satellite- and pollen-based quantitative woody cover reconstructions for northern Asia: Verification and application to late-Quaternary pollen data. Earth Planet Sci Lett 264(1–2):284–298. DOI: 10.1016/j.epsl.2007.10.007

Tatli H, Dalfes HN (2016) Defining Holdridge's life zones over Turkey. Int J Climatol 36(11):3864–3872. DOI: 10.1002/joc.4600

Theuerkauf M, Couwenberg J, Kuparinen A, Liebscher V (2016) A matter of dispersal: REVEALSinR introduces state-of-the-art dispersal models to quantitative vegetation reconstruction. Veg Hist Archaeobot 25(6):541–553. DOI: 10.1007/s00334-016-0572-0

Teutschbein C, Seibert J (2012) Bias correction of regional climate model simulations for hydrological climate-change impact studies: Review and evaluation of different methods. J Hydrol 456–457:12–29. DOI: 10.1016/j.jhydrol.2012.05.052

Teutschbein C, Seibert J (2013) Is bias correction of regional climate model (RCM) simulations possible for non-stationary conditions? Hydrol Earth Syst Sci 17(12):5061–5077. DOI: 10.5194/hess-17-5061-2013

Thornthwaite CW (1948) An Approach toward a Rational Classification of Climate. Geogr Rev 38(1):55–94. DOI: 10.2307/210739

Tian F, Cao X, Dallmeyer A, Lohmann G, Zhang X, Ni J, Andreev A, Anderson PM, Lozhkin AV, Bezrukova E, Rudaya N, Xu Q, Herzschuh U (2018) Biome changes and their inferred climatic drivers in northern and eastern continental Asia at selected times since 40 cal ka BP. Veg Hist Archaeobot 27(2):365–379. DOI: 10.1007/s00334-017-0653-8

Tinner W, Conedera M, Ammann B, Lotter AF (2005) Fire ecology north and south of the Alps since the last ice age. Holocene 15(8):1214–1226. DOI: 10.1191/0959683605hl892rp

Tinner W, Hubschmid P, Wehrli M, Ammann B, Conedera M (1999) Long-term forest fire ecology and dynamics in southern Switzerland. J Ecol 87(2):273–289. DOI: 10.1046/j.1365-2745.1999.00346.x

Tóth M, Heiri O, Vincze I, Braun M, Szabó Z, Magyari EK (2022) Limnological changes and chironomid-inferred summer air temperature from the Late Pleniglacial to the Early Holocene in the East Carpathians. Quat Res 105:151–165. DOI: 10.1017/qua.2021.36

Treml V, Chuman T (2015) Ecotonal Dynamics of the Altitudinal Forest Limit are Affected by Terrain and Vegetation Structure Variables: An Example from the Sudetes Mountains in Central Europe. Arct Antarc Alp Res 47(1):133–146. DOI: 10.1657/AAAR0013-108

Trewartha GT, Horn LH (1980) An Introduction to Climate. Fifth Edition. McGraw-Hill, New York, NY

Tuhkanen S (1980) Climatic Parameters and Indices in Plant Geography. Acta Phytogeogr Suec 67:1–110

Tüxen R (1956) Die heutige potentielle natürliche Vegetation als gegenstand der Vegetationskartierung (The recent potential natural vegetation as an object of vegetation mapping). Angew Pflanzensoziol 13:5–42 (in German)

Valdes PJ, Armstrong E, Badger MPS, Bradshaw CD, Bragg F, Crucifix M, Davies-Barnard T, Day JJ, Farnsworth A, Gordon C, Hopcroft PO, Kennedy AT, Lord NS, Lunt DJ, Marzocchi A, Parry LM, Pope V, Roberts WHG, Stone EJ, Tourte GJL, Williams JHT (2017) The BRIDGE HadCM3 family of climate models: HadCM3@Bristol v1.0. Geosci Model Dev 10(10):3715–3743. DOI: 10.5194/gmd-10-3715-2017

Valsecchi V, Carraro G, Conedera M, Tinner W (2010) Late-Holocene vegetation and land-use dynamics in the Southern Alps (Switzerland) as a basis for nature protection and forest management. Holocene 20(4):483–495. DOI: 10.1177/0959683609355178

van de Geijn SC, Goudriaan J (1996) The effects of elevated CO_2 and temperature change on transpiration and crop water use. In: Bazzaz F, Sombroek W (eds) Global climate change and agricultural production. Direct and indirect effects of changing hydrological, pedological and plant physiological processes. Food and Agriculture Organization of the United Nations, John Wiley & Sons Ltd, Chichester, UK, pp 101–122

van der Knaap WO, van Leeuwen JFN, Fankhauser A, Ammann B (2000) Palynostratigraphy of the last centuries in Switzerland based on 23 lake and mire deposits: chronostratigraphic pollen markers, regional patterns, and local histories. Rev Palaeobot Palynol 108(1–2):85–142. DOI: 10.1016/S0034-6667(99)00035-4

van der Linden P, Mitchell JFB (eds) (2009) ENSEMBLES: Climate change and its impacts: Summary of research and results from the ENSEMBLES project. Met Office Hadley Centre, Exeter, UK

van Meijgaard E, van Ulft LH, van de Berg WJ, Bosveld FC, van den Hurk BJJM, Lenderink G, Siebesma AP (2008) The KNMI regional atmospheric climate model RACMO version 2.1. KNMI Technical Report 302. Royal Netherlands Meteorological Institute, De Bilt, The Netherlands

Varga Z, Borhidi A, Fekete G, Debreczy Zs, Bartha D, Bölöni J, Molnár A, Kun A, Molnár Zs, Lendvai G, Szodfridt I, Rédei T, Facsar G, Sümegi P, Kósa G, Király G (2000) Az erdőssztyepp fogalma, típusai és jellemzésük (Concept and types of forest-steppe and their characterization). In: Molnár Zs, Kun A (eds) Alföldi erdőssztyepp-maradványok Magyarországon (Forest-steppe remnants in Hungary). WWF Magyarország, Budapest, Hungary, pp 7–19 (in Hungarian)

Vavrek MJ (2011) fossil: palaeoecological and palaeogeographical analysis tools. Palaeontol Electron 14(1):1T

Velarde SJ, Malhi Y, Moran D, Wright J, Hussain S (2005) Valuing the impacts of climate change on protected areas in Africa. Ecol Econ 53(1):21–33. DOI: 10.1016/j.ecolecon.2004.07.024

Venter O, Sanderson EW, Magrach A, Allan JR, Beher J, Jones KR, Possingham HP, Laurance WF, Wood P, Fekete BM, Levy MA, Watson JEM (2016a) Global terrestrial Human Footprint maps for 1993 and 2009. Sci Data 3:160067. DOI: 10.1038/sdata.2016.67

Venter O, Sanderson EW, Magrach A, Allan JR, Beher J, Jones KR, Possingham HP, Laurance WF, Wood P, Fekete BM, Levy MA, Watson JEM (2016b) Sixteen years of change in the global terrestrial human footprint and implications for biodiversity conservation. Nat Commun 7:12558. DOI: 10.1038/ncomms12558

von Humboldt A (1806) Ideen zu einer Physiognomik der Gewächse (Ideas for a physiognomy of plants). Cotta, Stuttgart (in German)

von Humboldt A, Bonpland A (1807) Ideen zu einer Geographie der Pflanzen nebst einem Naturgemälde der Tropenländer (Ideas for a geography of plants and a nature painting of the tropics). Cotta, Tübingen (in German)

Walther G-R, Beißner S, Burga CA (2005) Trends in the upward shift of alpine plants. J Veg Sci 16(5):541–548. DOI: 10.1111/j.1654-1103.2005.tb02394.x

Walther G-R, Post E, Convey P, Menzel A, Parmesan C, Beebee TJC, Fromentin J-M, Hoegh-Guldberg O, Bairlein F (2002) Ecological responses to recent climate change. Nature 416(6879):389–395. DOI: 10.1038/416389a

Wang L, Jiang WY, Jiang DB, Zou YF, Liu YY, Zhang EL, Hao QZ, Zhang DG, Zhang DT, Peng ZY, Xu B, Yang XD, Lu HY (2018) Prolonged Heavy Snowfall During the Younger Dryas. J Geophys Res Atmos 123(24):13748–13762. DOI: 10.1029/2018JD029271

Wang L, Ranasinghe R, Maskey S, van Gelder PHAJM, Vrijling JK (2016) Comparison of empirical statistical methods for downscaling daily climate projections from CMIP5 GCMs: a case study of the Huai River Basin, China. Int J Climatol 36(1):145–164. DOI: 10.1002/joc.4334

Watterson IG, Dix MR, Gordon HB, McGregor JL (1995) The CSIRO nine-level atmospheric general circulation model and its equilibrium present and doubled CO_2 climates. Aust Meteorol Mag 44(2):111–125

Webb III T, Anderson KH, Bartlein PJ, Webb RS (1998) Late Quaternary climate change in eastern North America: a comparison of pollen-derived estimates with climate model results. Quat Sci Rev 17(6–7):587–606. DOI: 10.1016/S0277-3791(98)00013-4

Weetman GF (2005) Silviculture and management of conifer forests. In: Andersson FA (ed) Ecosystems of the World. Volume 6. Coniferous Forests. Elsevier Science, pp 465–484

Wessel P, Smith WHF, Scharroo R, Luis J, Wobbe F (2013) Generic Mapping Tools: Improved Version Released. EOS Trans Am Geophys Union 94(45):409–410. DOI: 10.1002/2013EO450001

Williams JW, Jackson ST (2003) Palynological and AVHRR observations of modern vegetational gradients in eastern North America. Holocene 13(4):485–497. DOI: 10.1191/0959683603hl613rp

Williams JW, Summers RL, Webb III T (1998) Applying plant functional types to construct biome maps from eastern North American pollen data: comparisons with model results. Quat Sci Rev 17(6–7):607–627. DOI: 10.1016/S0277-3791(98)00014-6

Wilson MFJ, O'Connell B, Brown C, Guinan JC, Grehan AJ (2007) Multiscale terrain analysis of multibeam bathymetry data for habitat mapping on the continental slope. Mar Geod 30(1–2):3–35. DOI: 10.1080/01490410701295962

Wolf A, Callaghan TV, Larson K (2008) Future changes in vegetation and ecosystem function of the Barents Region. Clim Chang 87(1–2):51–73. DOI: 10.1007/s10584-007-9342-4

Woodbridge J, Fyfe RM, Roberts N (2014) A comparison of remotely sensed and pollen-based approaches to mapping Europe's land cover. J Biogeogr 41(11):2080–2092. DOI: 10.1111/jbi.12353

Woodward FI (1987) Climate and plant distribution. Cambridge University Press, Cambridge, UK

Wu B, Lang X, Jiang D (2021) Köppen climate zones in China over the last 21,000 years. J Geophys Res Atmos 126(6):e2020JD034310. DOI: 10.1029/2020JD034310

Xu C-Y, Singh VP (2002) Cross Comparison of Empirical Equations for Calculating Potential Evapotranspiration with Data from Switzerland. Water Resour Manage 16(3): 197–219. DOI: 10.1023/A:1020282515975

Yates DN, Kittel TGF, Cannon RF (2000) Comparing the Correlative Holdridge Model to Mechanistic Biogeographical Models for Assessing Vegetation Distribution Response to Climatic Change. Clim Chang 44(1–2):59–87. DOI: 10.1023/A:1005495908758

Yesson C, Brewer PW, Sutton T, Caithness N, Pahwa JS, Burgess M, Gray WA, White RJ, Jones AC, Bisby FA, Culham A (2007) How Global Is the Global Biodiversity Information Facility? PLoS ONE 2(11):e1124. DOI: 10.1371/journal.pone.0001124

Yin X (1997a) Optical Air Mass: Daily Integration and its Applications. Meteorol Atmos Phys 63(3–4):227–233. DOI: 10.1007/BF01027387

Yin X (1997b) Calculating daytime mean relative air mass. Agric For Meteorol 87(2–3):85–90. DOI: 10.1016/S0168-1923(97)00029-4

Yin X (1998) The Albedo of Vegetated Land Surfaces: Systems Analysis and Mathematical Modeling. Theor Appl Climatol 60(1–4):121–140. DOI: 10.1007/s007040050038

Yin X (1999) Bright Sunshine Duration in Relation to Precipitation, Air Temperature and Geographic Location. Theor Appl Climatol 64(1–2):61–68. DOI: 10.1007/s007040050111

Yue TX, Fan ZM, Liu JY (2005a) Changes of major terrestrial ecosystems in China since 1960. Glob Planet Chang 48(4):287–302. DOI: 10.1016/j.gloplacha.2005.03.001

Yue TX, Fan ZM, Liu JY, Wei BX (2006) Scenarios of major terrestrial ecosystems in China. Ecol Model 199(3):363–376. DOI: 10.1016/j.ecolmodel.2006.05.026

Yue TX, Liu JY, Jørgensen SE, Gao ZQ, Zhang SH, Deng XZ (2001) Changes of Holdridge life zone diversity in all of China over half a century. Ecol Model 144(2–3):153–162. DOI: 10.1016/S0304-3800(01)00370-2

Yue TX, Liu JY, Li ZQ, Chen SQ, Ma SN, Tian YZ, Ge F (2005b): Considerable effects of diversity indices and spatial scales on conclusions relating to ecological diversity. Ecol Model 188(2–4):418–431. DOI: 10.1016/j.ecolmodel.2004.12.019

Yue S, Wang C (2004) The Mann-Kendall Test Modified by Effective Sample Size to Detect Trend in Serially Correlated Hydrological Series. Water Resour Manage 18(3):201–218. DOI: 10.1023/B:WARM.0000043140.61082.60

Zanon M, Davis BAS, Marquer L, Brewer S, Kaplan JO (2018) European Forest Cover During the Past 12,000 Years: A Palynological Reconstruction Based on Modern Analogs and Remote Sensing. Front Plant Sci 9:253. DOI: 10.3389/fpls.2018.00253

Zhang G, Kang Y, Han G, Sakurai K (2011) Effect of climate change over the past half century on the distribution, extent and NPP of ecosystems of Inner Mongolia. Glob Change Biol 17(1):377–389. DOI: 10.1111/j.1365-2486.2010.02237.x

Zheng Y, Xie Z, Jiang L, Shimizu H, Drake S (2006) Changes in Holdridge Life Zone diversity in the Xinjiang Uygur Autonomous Region (XUAR) of China over the past 40 years. J Arid Environ 66(1):113–126. DOI: 10.1016/j.jaridenv.2005.09.005

Zimmermann NE, Jandl R, Hanewinkel M, Kunstler G, Kölling C, Gasparini P, Breznikar A, Meier ES, Normand S, Ulmer U, Gschwandtner T, Veit H, Naumann M, Falk W, Mellert K, Rizzo M, Skudnik M, Psomas A (2013) Potential Future Ranges of Tree Species in the Alps. In: Cerbu GA, Hanewinkel M, Gerosa G, Jandl R (eds) Management Strategies to Adapt Alpine Space Forests to Climate Change Risks. InTech, Rijeka, Croatia, pp 37–48. DOI: 10.5772/56279

Zohner CM, Benito BM, Svenning J-C, Renner SS (2016) Day length unlikely to constrain climate-driven shifts in leaf-out times of northern woody plants. Nat Clim Chang 6(12):1120–1123. DOI: 10.1038/nclimate3138

Zólyomi B (1967) A rekonstruált természetes növénytakaró (1:1 500 000) (Reconstructed natural vegetation (1:1 500 000)). In: Radó S (ed) Magyarország Nemzeti Atlasza (National Atlas of Hungary). Kartográfiai Vállalat, Budapest, Hungary, pp 31 (in Hungarian)

Zólyomi B (1981) Magyarország természetes növénytakarója (1:1 500 000) (Potential natural vegetation of Hungary (1:1 500 000)). In: Hortobágyi T, Simon T (eds) Növényföldrajz, társulástan és ökológia (Geobotany, coenology and ecology). Tankönyvkiadó, Budapest, Hungary, Supplementary map (in Hungarian)

Appendix A Supplementary Information to Chapter 3

Appendix A.1 – Supplemental figure for the assessment of changes in the spatial distribution of Holdridge life zone (HLZ) types

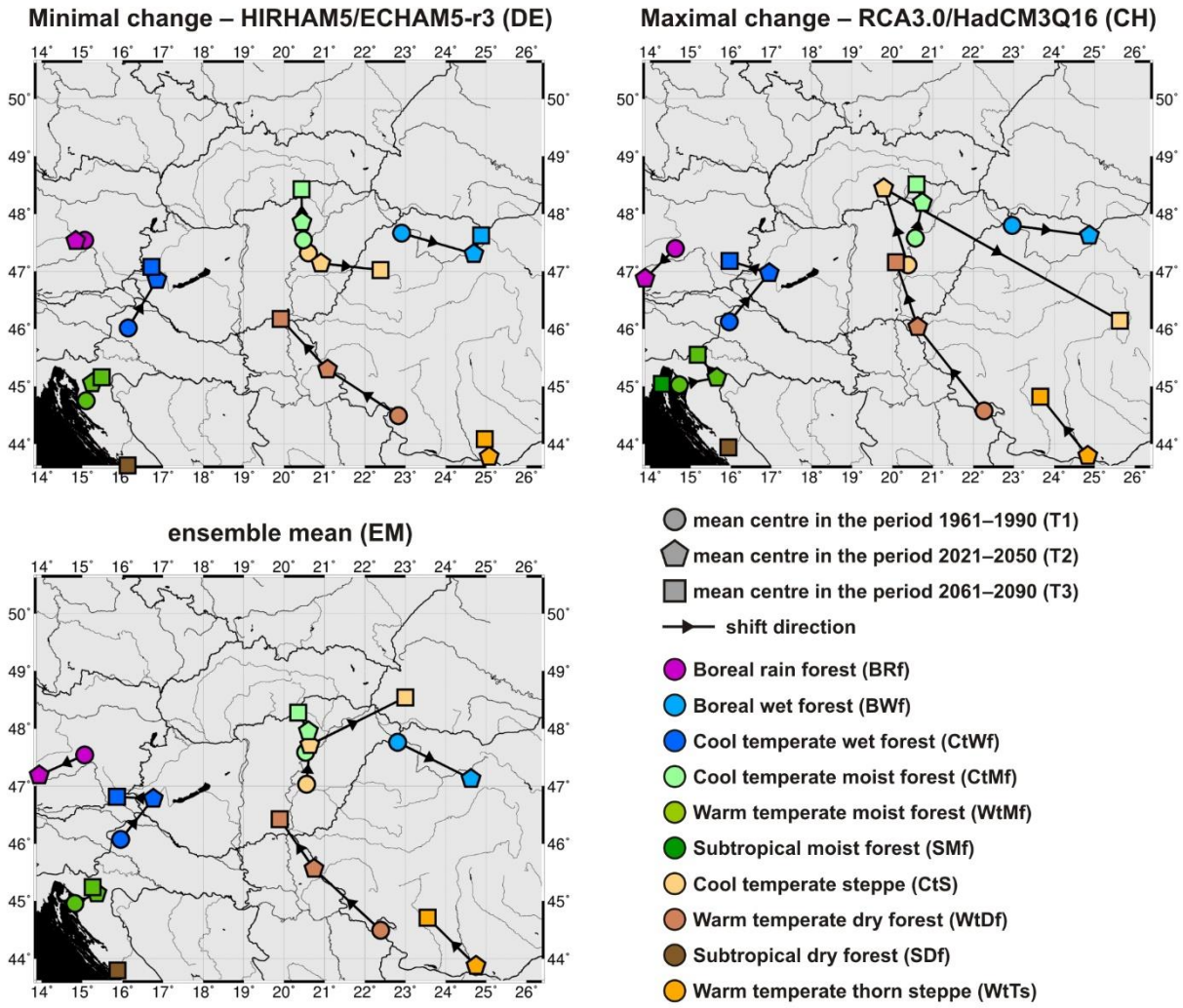

Fig. A.1 Mean centres of Holdridge life zone (HLZ) types in the Carpathian Region for the periods 1961–1990 (T1), 2021–2050 (T2) and 2061–2090 (T3) according to the ensemble mean of the selected regional climate model (RCM) simulations and those RCM simulations which provide the minimal and maximal changes in the distribution pattern of HLZ types (according to the values of Kappa statistic)

Appendix A.2 – Supplemental figure for the assessment of shifts in the altitudinal distribution of Holdridge life zone (HLZ) types

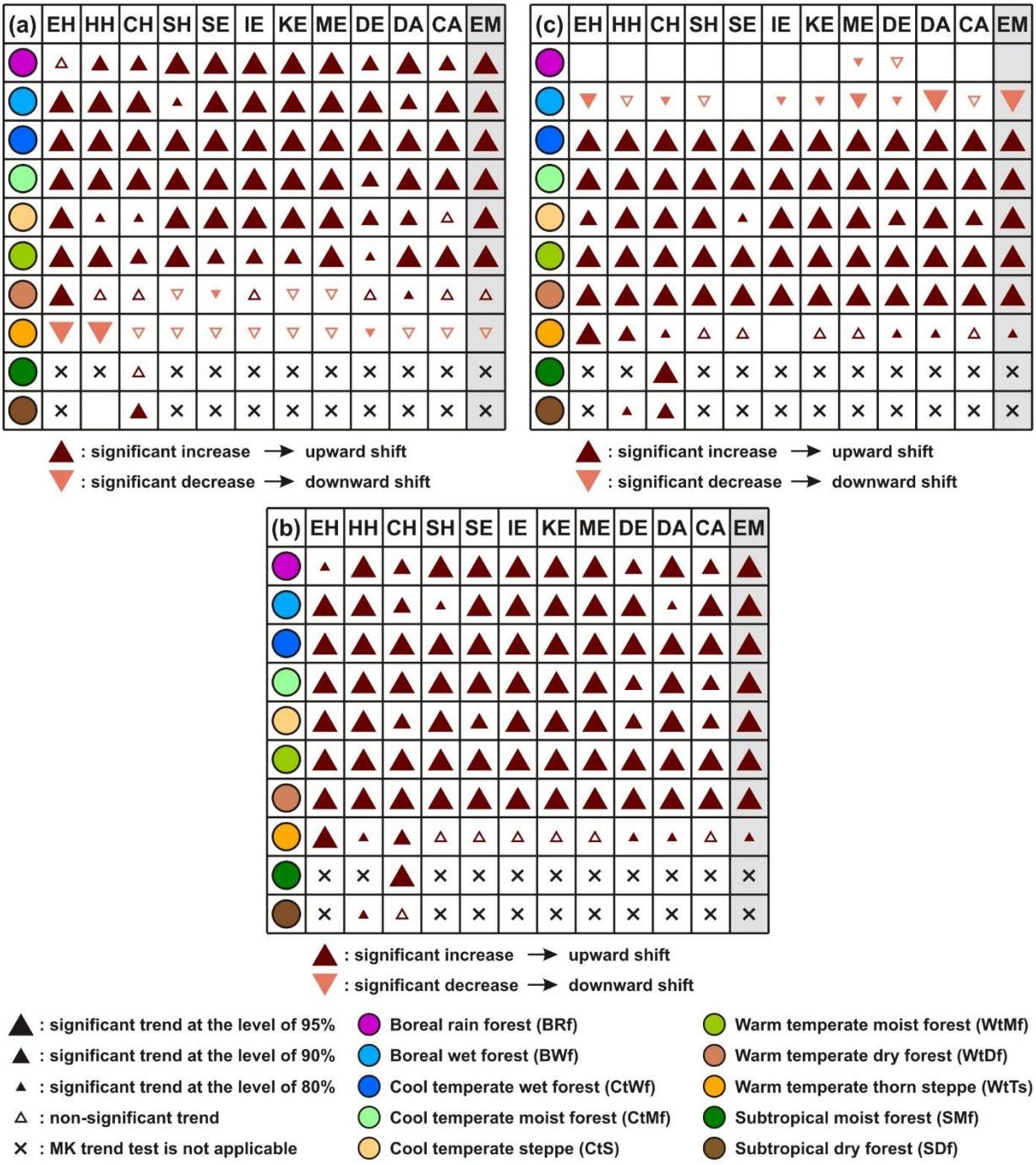

Fig. A.2 Trends in the positions of (**a**) the lower altitudinal limit, (**b**) the altitudinal midpoint and (**c**) the upper altitudinal limit of each Holdridge life zone (HLZ) type according to the selected regional climate model (RCM) simulations (whose acronyms are listed in Table 3.1) and their ensemble mean (EM). The *up-pointing* (*down-pointing*) *triangles* refer to the upward (downward) shift. A *larger filled triangle* means that the trend is significant at a higher confidence level. The *empty triangle* indicates a non-significant trend. In the case of *blank rubric* no trend could be detected. The *symbol* × refers to those cases where the Mann-Kendall (MK) trend test is not applicable

Appendix B Supplementary Information to Chapter 5

Appendix B.1 – Supplemental information for the biomization procedure

Table B.1 Assignment of pollen taxa to plant functional types (PFTs). The abbreviations of PFTs can be found in Table B.3

PFT	Pollen taxa
aa	*Aconitum*, *Androsace*, *Anemone nemorosa*-type, *Angelica palustris*, *Caltha*-type, *Dryas octopetala*, *Gentiana pneumonanthe*-type, *Geranium*, *Geum*-type, *Lloydia serotina*, *Pedicularis palustris*-type, *Primula*, *Primula hirsuta*-type, *Rubus*, *Rumex alpestris*, *Sagina*, *Saussurea*, *Saxifraga*, *Saxifraga granulata*-type, *Saxifraga oppositifolia*-type, *Saxifraga paniculata*-type, *Saxifraga stellaris*-type, Saxifragaceae, *Tofieldia*, *Trollius europaeus*, *Veratrum*.
aa/bs	*Betula*.
aa/bs/ts	*Alnus*, *Alnus viridis*, *Salix*.
aa/sf	*Allium*-type, *Anthemis*-type, *Apium*, Asteroideae, *Aster*-type, *Astragalus*-type, *Campanula medium*, Campanulaceae, *Campanula*-type, Caryophyllaceae, *Cerastium*-type, *Clematis*, Compositae, Compositae subf. Asteroideae, Compositae subf. Cichorioideae, Gentianaceae, *Helianthemum*, Liliaceae-type, *Lilium martagon*-type, *Narthecium*, *Onagraceae*, *Phyteuma*, *Phyteuma*-type, *Plantago*, *Plantago major*, *Plantago major/P. media*, *Plantago maritima*-type, *Plantago media*, *Potentilla*-type, *Primula veris*-type, Primulaceae, Ranunculaceae, *Ranunculus*, *Ranunculus acris*-type, *Ranunculus arvensis*-type, *Ranunculus sceleratus*-type, *Rosa*, Rosaceae, Rubiaceae, *Sanguisorba officinalis*, *Silene dioica*-type, *Silene vulgaris*-type, *Stellaria holostea*, *Thalictrum*, *Trifolium alpinum*-type, *Trifolium badium*-type, Umbelliferae, *Valeriana*, Valerianaceae.
bec	*Picea*.
bec/cbc	*Pinus cembra*.
bec/ctc	*Abies*.
bs	*Larix*, *Larix/Pseudotsuga*.
bs/ts	*Alnus glutinosa*-type, *Populus*, *Populus tremula*-type.
bts	*Cornus sanguinea*-type, *Lonicera*, *Lonicera nigra*, *Lonicera xylosteum*-type, *Ribes*, *Sambucus*, *Sambucus ebulus*, *Sambucus nigra/S. racemosa*, *Sambucus nigra*-type, *Sambucus racemosa*, *Sorbus aucuparia*, *Sorbus aucuparia*-type, *Sorbus*-type, *Viburnum*, *Viburnum lantana*, *Viburnum opulus*.
cgs	*Bilderdykia convolvulus*-type, *Chrysosplenium*, *Hippophae rhamnoides*, *Lysimachia*, *Lysimachia vulgaris*-type, *Parnassia palustris*, *Polygala*, *Polygonum*, *Polygonum amphibium*, *Polygonum aviculare*-type, *Polygonum bistorta*-type, *Polygonum convolvulus*-type, *Polygonum persicaria*-type, *Rhododendron*, *Rhododendron*-type, *Rumex*, *Rumex acetosa*-type, *Rumex acetosa*-type*/Oxyria*, *Rumex aquaticus/R. hydrolapathum*, *Rumex crispus*-type, *Rumex/Oxyria*.
ctc1	*Cedrus*, *Taxus baccata*.
df	*Ephedra*, *Ephedra distachya*-type.
ec	Cupressaceae, *Juniperus*-type, *Pinus*, *Pinus diploxylon*-type, *Pinus sylvestris*-type.
g	*Cerealia*-type, Gramineae, *Hordeum*-type, *Secale cereale*.
h	*Arctostaphylos*, *Calluna vulgaris*, *Empetrum nigrum*, *Erica*, Ericaceae-type, *Ledum palustre*, *Vaccinium*.
s	Cyperaceae.
sf	*Ambrosia*, *Ambrosia*-type, *Anthericum*, *Bupleurum*, Cannabaceae, *Cannabis*, *Cannabis sativa*, *Cannabis/Humulus*, *Centaurea cyanus*, *Centaurea montana*-type, *Centaurea nigra*-type, *Centaurea scabiosa*-type, *Circaea*, *Cirsium/Carduus*, *Cirsium*-type, *Convolvulus*, *Crocus*, *Dianthus superbus*-type, *Dianthus/Petrorhagia*, Dipsacaceae, *Echinops*, *Erodium*, *Eryngium*, *Fagopyrum*, *Filipendula*, *Filipendula ulmaria*, *Filipendula vulgaris*, *Gentianella campestris*-type, *Gypsophila*, *Gypsophila repens*-type, *Heracleum sphondylium*-type, *Humulus lupulus*, *Humulus/Cannabis*, *Iris pseudacorus*-type, *Jasione*-type, *Knautia*, *Linum*, *Linum catharticum*-type, *Linum usitatissimum/L. bienne*, *Lychnis*, *Lychnis flos-cuculi*, *Lythrum*, *Oxalis*, *Plantago coronopus*-type, *Plantago lanceolata*-type, *Pleurospermum austriacum*, *Polygonatum*, *Pulsatilla*, *Sanguisorba minor*-type, *Scabiosa*, *Scleranthus*, *Scleranthus annuus*, *Spergula arvensis*-type, *Succisa*, *Urtica*, *Urtica dioica*-

PFT	Pollen taxa
	type, *Urtica pilulifera*-type, Urticaceae, *Valeriana dioica*-type, *Valeriana officinalis*-type, *Valeriana tripteris*-type, *Verbena*, *Veronica*, *Veronica*-type, *Xanthium.*
sf/df	*Artemisia*, Chenopodiaceae/Amaranthaceae.
sp	*Andromeda polifolia*, *Sphagnum*.
ts	*Acer campestre*-type, *Aesculus*, *Crataegus*-type, *Euonymus*, *Fraxinus*, *Fraxinus excelsior*-type, *Prunus*-type, *Quercus*, *Quercus pubescens/Q. robur*-type, *Quercus robur*-type, *Robinia pseudacacia*, *Viscum*.
ts1	*Carpinus betulus*, *Corylus*, *Fagus*, *Frangula*, *Tilia*, *Tilia cordata*, *Tilia platyphyllos*-type, *Ulmus*, *Ulmus glabra*-type.
ts2	*Castanea*, *Cornus*, *Fraxinus ornus*, *Juglans*, *Ostrya/Carpinus orientalis*, *Platanus*, *Pterocarya*, *Rhamnus*-type, *Vitis*.
wdf	*Ephedra fragilis-type*.
wgs	*Anthyllis vulneraria*, *Armeria*-type, Boraginaceae, Crassulaceae, Cruciferae, *Cuscuta*, *Cuscuta europaea*-type, *Echium/Onosma*, *Euphorbia*, Euphorbiaceae, *Hypericum*, *Hypericum perforatum*-type, Labiatae, Leguminosae, *Lotus*-type, Malvaceae, *Melampyrum*, *Mentha*-type, *Mercurialis*, *Onobrychis*, *Onobrychis*-type, *Papaver*, *Papaver rhoeas*-type, Papaveraceae, *Peucedanum palustre*, *Peucedanum palustre*-type, *Pimpinella major*-type, *Prunella*-type, *Pulmonaria obscura*-type, *Rhinanthus*-type, Scrophulariaceae, *Scrophularia*-type, *Sedum*-type, Solanaceae, *Solanum dulcamara*, *Solanum nigrum*-type, *Stachys sylvatica*-type, *Teucrium*, *Trifolium pratense*-type, *Trifolium repens*-type, *Trifolium*-type, *Ulex*-type, *Vicia/Lathyrus*, *Viola*, *Viola palustris*-type.
wte	*Quercus ilex*-type.
wte1	*Buxus*, *Hedera*, *Ilex*.
wte2	*Cistus*, *Cistus salvifolius*, *Ligustrum vulgare*-type, *Olea europaea*, Oleaceae, *Phillyrea*, *Pistacia*.

Table B.2 Assignment of PFTs to biomes

Biome	PFTs
cold deciduous forest	h, sp, aa/bs, aa/bs/ts, bec/cbc, bs, bs/ts, ec.
taiga	h, sp, aa/bs, aa/bs/ts, bec, bec/cbc, bec/ctc, bs, bs/ts, bts, ec.
cold mixed forest	h, aa/bs, aa/bs/ts, bec/ctc, bs, bs/ts, bts, ctc1, ec, ts1.
cool coniferous forest	h, aa/bs, aa/bs/ts, bec, bec/cbc, bec/ctc, bs, bs/ts, bts, ec, ts1.
temperate deciduous forest	h, aa/bs, aa/bs/ts, bec/ctc, bs, bs/ts, bts, ctc1, ec, ts, ts1, ts2, wte1.
cool mixed forest	h, aa/bs, aa/bs/ts, bec, bec/cbc, bec/ctc, bs, bs/ts, bts, ec, ts, ts1.
warm mixed forest	h, aa/bs/ts, bs/ts, bts, ec, ts, ts1, ts2, wte, wte1.
xerophytic woodland/scrub	g, ec, wte, wte2.
cool steppe	cgs, aa/sf, g, sf, sf/df.
warm steppe	wgs, aa/sf, g, sf, sf/df.
cool desert	df, sf/df.
hot desert	wdf, df, sf/df.
tundra	aa, aa/bs, aa/bs/ts, aa/sf, g, h, s, sp.

Table B.3 Abbreviations of PFTs

Code	Name
aa	arctic–alpine forb/shrub
aa/bs	arctic–alpine/boreal summergreen tree/shrub
aa/bs/ts	arctic–alpine/boreal/ temperate summergreen tree/shrub
aa/sf	arctic–alpine/boreal/temperate forb/shrub
bec	boreal evergreen coniferous tree
bec/cbc	boreal/cool-boreal evergreen coniferous tree
bec/ctc	boreal/cool-temperate evergreen coniferous tree
bs	boreal summergreen tree
bs/ts	boreal/temperate summergreen tree/shrub
bts	boreal–temperate summergreen shrub
cgs	cool herb/shrub
ctc1	temperate coniferous tree/shrub
df	desert forb/shrub
ec	eurythermic coniferous tree/shrub

Code	Name
g	grass
h	heath
s	sedge
sf	steppe forb/shrub
sf/df	steppe/desert forb/shrub
sp	bog moss
ts	temperate summergreen tree/shrub
ts1	cool-temperate summergreen tree/shrub
ts2	warm-temperate summergreen tree/shrub
wdf	warm desert forb/shrub
wgs	warm herb/shrub
wte	warm-temperate broad-leaved evergreen tree/shrub
wte1	cool-temperate broad-leaved evergreen tree/shrub/liane
wte2	warm-temperate sclerophyll tree/shrub

Appendix B.2 – Supplemental information to compare the climate- and pollen-inferred biomes

Table B.4 Metadata of the pollen sequences related to RPSs (relevant pollen samples): (a) Entity (unique identifier for the given pollen sequence); (b) Site name; (c) Country; (d) LAT (latitude in decimal degrees); (e) LON (longitude in decimal degrees); (f) ELV (elevation in meters above sea level); (g) No RPSs (Number of relevant pollen samples) (* denotes sequences where the source of age–depth model is a calibrated chronology presented by the contributing author and not the work of Giesecke et al. 2014); (h) Publication(s) (References of the pollen sites); (i) ALT (altitude, in meters above sea level, for that 0.5 arc-min grid cell in which the site is located) from the Global 30 Arc-Second Elevation Dataset (GTOPO30: Gesch et al. 1999) (* denotes sequences where the difference between the ALT and ELV values exceeds 250 meter); (j) TRI (terrain ruggedness index, in meters, for that 0.5 arc-min grid cell in which the site is located) calculated from the GTOPO30 using the function "terrain" in the R package "raster" (Hijmans 2020); (k) TCC (tree canopy cover, in percentages, for that 0.5 arc-min grid cell of in which the site is located) extracted from the Global Forest Change Dataset (Hansen et al. 2013), for year 2000; (l) HFI (human footprint index, using a 0–50 scale, for that 0.5 arc-min grid cell of in which the site is located) developed by Venter et al. (2016), for year 1993. Here, the TCC and HFI data with different spatial resolution and grid are aggregated to the grid of the GTOPO30 using bilinear resampling technique, via the function "resample" in the R package "raster" (Hijmans 2020). The parameters a–f and the Publication(s) are derived from the European Pollen Database (Fyfe et al. 2009) but they are quality controlled and corrected if necessary

Entity	Site name	Country	LAT	LON	ELV	No RPSs	Publication(s)	ALT	TRI	TCC	HFI
79	Altenweiher	FRA	48.0133	6.9944	926	1	[1]	938	197.9	71.795	6.705
305	Cervene blato	CZE	48.8667	14.8000	470	1	[2], [67]	472	3.0	74.359	4.418
379	Le Grand Lemps	FRA	45.4244	5.4142	500	2	[3], [68]	517	49.0	60.846	23.872
513	Pelléautier	FRA	44.5211	6.0078	975	2	[4], [69]	974	43.8	2.718	15.674
553	Rotsee	CHE	47.0756	8.3256	419	1	[5], [6], [7], [70]	433	51.4	34.975	46.390
554	Rotsee	CHE	47.0756	8.3256	419	3	[5], [8], [71]	433	51.4	34.975	46.390
593	Saint Sixte	FRA	45.4250	5.6278	720	1	[3], [72]	856	92.6	83.998	11.527
637	Svatoborice-Mistrin	CZE	48.9500	17.0750	175	4	[9], [73]	154	4.4	27.156	25.655
654	Lake Balaton (Southwest)	HUN	46.8183	17.7350	104	1	[10]	84	0.0	0.000	9.221
656	Lake Balaton (Northeast)	HUN	47.0017	18.1042	104	1	[10]	84	0.0	0.000	6.503
663	Trumer Moos	AUT	47.9333	13.0667	500	1	[11], [74]	516	25.2	20.698	23.632
713	Wasenmoos beim Zellhof	AUT	47.9833	13.1000	505	1	[11], [75]	485	7.0	18.464	22.434
715	Zirbenwaldmoor	AUT	46.8583	11.0250	2150	1	[12]	2354	131.5	6.762	8.955
738	Plaine Alpe	FRA	44.9639	6.5942	1850	1	[13]	2344*	127.0	12.715	8.749
742	Schwemm	AUT	47.6583	12.3000	664	2	[14]	759	73.8	60.635	12.494
743	Schwemm	AUT	47.6583	12.3000	664	2	[14]	759	73.8	60.635	12.494

Entity	Site name	Country	LAT	LON	ELV	No RPSs	Publication(s)	ALT	TRI	TCC	HFI
903	La Beuffarde	FRA	46.8236	6.4231	1111	11	[15]	1126	24.2	84.803	6.007
921	Tourbière de Pilaz	ITA	45.8224	7.6195	1900	3	[16], [76]	2044	183.8	36.670	9.079
930	Lac de Villa	ITA	45.6855	7.6902	820	1	[16], [76]	880	189.2	68.572	27.791
978	Schwemm	AUT	47.6583	12.3000	664	1	[14]	759	73.8	60.635	12.494
982	Tourbière de Santa Anna	ITA	45.8540	7.7999	2304	1	[16], [76]	2166	291.4	0.490	4.282
1026	Feuenried	DEU	47.7437	8.9028	407	2	[17], [77]	406	8.2	22.825	27.768
1028	Steerenmoos	DEU	47.8167	8.1833	1000	5	[18]	976	40.6	13.372	25.430
1031	Nussbaumer Seen	CHE	47.6167	8.8333	434	1	[19], [20], [21], [78]	502	64.2	4.311	25.328
1055	Älbi Flue	CHE	46.5972	7.9763	1850	76	[22], [23]	1713	158.5	75.438	9.455
1057	Aletschwald	CHE	46.3886	8.0246	2017	1*	[24]	2152	212.0	74.602	8.689
1059	Aletschwald	CHE	46.3886	8.0246	2017	87	[22], [23]	2152	212.0	74.602	8.689
1061	Bachalpsee	CHE	46.6694	8.0215	2265	37	[22], [25]	2339	94.4	0.699	5.391
1062	Baldeggersee	CHE	47.2000	8.2569	463	95	[22], [26]	463	12.8	8.295	21.244
1063	La Grande Basse	FRA	48.0483	6.9517	945	4	[27]	993	53.5	87.007	9.882
1065	Alp Lüsga Belalp 2	CHE	46.3834	7.9765	2290	1	[24]	2324	265.2	0.020	7.566
1066	Lago di Bévera	ITA	45.8519	8.8942	325	9	[22], [79]	383	19.6	45.643	29.956
1072	Lac de Bretaye	CHE	46.3262	7.0725	1780	13	[22]	1763	82.2	39.582	6.143
1075	Clapeyret	FRA	44.1472	7.2389	2260	1	[4]	2319	123.1	7.959	3.150
1084	Etang de la Gruère	CHE	47.2392	7.0490	1005	8	[22], [28]	1004	8.1	59.292	22.749
1090	Lago di Ganna	ITA	45.8978	8.8258	452	21	[22], [79]	615	130.2	67.948	14.341
1091	Gerzensee	CHE	46.8296	7.5461	603	11	[22]	613	27.1	7.893	22.878
1093	Monte San Giorgio	CHE	45.9089	8.9539	990	5	[22]	687*	210.1	89.186	33.779
1095	Grächen See	CHE	46.1956	7.8450	1710	1	[29], [24]	1987*	243.8	57.743	21.494
1097	Grindjisee	CHE	46.0114	7.7911	2334	7	[22]	2438	171.5	1.755	10.864
1098	Hagelseeli	CHE	46.6729	8.0359	2339	24	[22]	2383	162.5	2.984	5.908
1105	Hinterburgseeli	CHE	46.7189	8.0689	1519	1		1895*	351.2	56.068	8.253
1106	Il Fuorn	CHE	46.6626	10.2098	1805	1*	[30]	1868	178.4	60.465	13.181
1108	Lac d'Aï	CHE	46.3639	7.0050	1891	7	[22]	1791	175.6	6.471	13.396
1121	Hopschensee	CHE	46.2524	8.0235	2017	29	[22]	1996	120.5	2.339	12.783
1122	Hopschensee	CHE	46.2524	8.0235	2017	3	[29], [24]	1996	120.5	2.339	12.783
1127	Etang de Luissel Bex	CHE	46.2362	7.0168	540	2	[24]	526	117.4	17.735	20.381

Entity	Site name	Country	LAT	LON	ELV	No RPSs	Publication(s)	ALT	TRI	TCC	HFI
1143	Riffelsee	CHE	45.9833	7.7619	2757	9	[22]	2664	90.2	0.033	8.248
1146	Alpi di Robièi Val Bavona	CHE	46.4440	8.5172	1892	1	[29], [24]	2081	243.4	5.912	2.000
1149	Praz Rodet	CHE	46.5653	6.1722	1040	30	[22], [31], [32], [33]	1056	89.6	47.622	13.027
1151	Seebergsee	CHE	46.5769	7.4439	1831	41	[22], [34]	1770	117.0	13.699	4.000
1155	Sägistalsee	CHE	46.6797	7.9764	1935	47	[22], [80]	2174	174.0	13.437	5.384
1157	Schöpfenwaldmoor	CHE	46.7435	7.8476	1450	12	[22], [35], [36]	1265	135.1	71.608	18.363
1158	Schwarzsee VS	CHE	45.9909	7.7058	2552	5	[22]	2553	176.2	0.003	8.960
1159	Schwarzsee FR	CHE	46.6667	7.2833	1046	4*	[37]	1051	103.2	23.084	4.945
1160	Schwarzsee Reschenscheideck	AUT	46.8697	10.4798	1721	3	[29], [30]	1724	102.6	82.356	13.990
1166	Trogenmoos	CHE	46.7607	7.8627	1470	15	[22]	1384	177.9	63.484	14.310
1167	Umbrail	CHE	46.5426	10.4339	2490	1	[30]	2612	159.4	0.152	7.882
1170	Wallbach Lenk	CHE	46.4274	7.4022	1885	1	[29], [24]	1887	124.0	15.168	7.770
1176	Wachseldorn Untermoos	CHE	46.8207	7.7341	980	1	[38], [29], [39], [40]	971	32.6	35.805	12.440
1178	Waxeckalm	AUT	47.0233	11.8018	1875	2	[41], [42]	2021	174.0	3.463	5.000
1179	Dortmunder Hütte	AUT	47.2109	11.0016	1915	1	[41], [42]	1987	153.2	17.453	10.892
1180	Mieminger See	AUT	47.2917	10.9764	800	3	[43]	801	56.6	28.641	23.788
1184	Seefelder See	AUT	47.3236	11.1917	1200	1	[43]	1226	103.0	23.035	37.381
1193	Sommersüss	ITA	46.7608	11.6783	870	1	[44]	902	108.2	39.662	17.150
1195	Dura-Moor	ITA	46.6400	11.4589	2080	1	[44]	1941	92.5	20.551	10.577
1199	Grünau Moor	AUT	46.9966	11.1900	2190	1*	[45]	2288	249.8	15.192	5.725
1201	Moor Alpenrose	AUT	47.0240	11.8037	1880	1	[45]	2021	174.0	3.463	5.000
1202	Rotmoos Obergurgl	AUT	46.8417	11.0250	2260	1	[46], [47]	2472	110.4	0.318	6.557
1213	Gerlos	AUT	47.2431	12.1389	1590	1	[46]	1494	90.2	70.201	12.283
1216	Le Loclat	CHE	47.0192	6.9917	432	6	[48], [49]	445	34.1	36.105	42.113
1227	Lac du Mont d'Orge Sion	CHE	46.2340	7.3382	640	9	[50]	682	116.8	15.251	40.151
1230	Marais de Charauze	FRA	45.3683	5.5669	375	1		347	30.8	2.501	34.280
1259	Fuschlsee	AUT	47.8042	13.2747	663	4	[51]	655	64.1	26.842	15.196
1262	Lac de Praver	FRA	45.0736	5.8564	1170	2	[52]	868*	295.8	82.432	28.259
1265	Tourbière de Mont Sec	FRA	45.0689	5.8067	1130	3	[52]	1104	181.0	90.422	23.982
1283	Lago Grande di Avigliana	ITA	45.0650	7.3867	353	33	[53]	384	37.1	10.925	33.184
1299	Gradenmoos	AUT	46.9655	12.8086	1920	1	[54]	2450*	393.8	26.725	5.329

Entity	Site name	Country	LAT	LON	ELV	No RPSs	Publication(s)	ALT	TRI	TCC	HFI
1398	Alsópáhok	HUN	46.7744	17.1703	126	2	[55], [56]	120	14.4	2.972	26.680
1459	Lake of Annecy	FRA	45.8567	6.1722	447	5	[57], [58], [59]	444	2.0	0.000	27.241
1476	Fangeas	FRA	44.7161	6.4494	2000	1	[60], [61]	2203	244.5	1.377	1.502
1478	Huzenbacher See	DEU	48.5756	8.3494	747	1	[62], [63]	729	88.4	79.741	7.192
1733	Kugelstattmoos	DEU	48.9531	12.8581	870	1*	[64], [65]	885	54.6	81.773	7.411
1868	Tourbière de Censeau	FRA	46.8139	6.0553	840	1*	[15]	840	6.6	12.724	18.574
1897	Tourbière du Mou de Pleure	FRA	46.9139	5.4506	214	2*	[15]	210	2.9	25.663	18.414
2220	Litzelsee	DEU	47.7689	8.9306	413	21*	[66]	417	13.6	48.219	27.922

References of pollen sequences

[1] De Valk EJ (1981) Late Holocene and present vegetation of the Kastelberg (Vosges, France). PhD Thesis, University of Utrecht, Utrecht, The Netherlands

[2] Jankovská V (1980) Paläogeobotanische Rekonstruktion der Vegetationsentwicklung im Becken Třebońská pánev während des Spätglazials und Holozäns. Vegetace ČSSR A 11, Academia, Praha

[3] Clerc J (1988) Recherches pollenanalytiques sur la paléo-écologie Tardiglaciaire et Holocene du Bas-Dauphiné. PhD Thesis, Université d'Aix-Marseille, Marseille, France

[4] de Beaulieu J-L (1977) Contribution pollenanalytique à l'histoire tardiglaciaire et Holocène de la végétation des Alpes méridionales françaices. PhD Thesis, Université d'Aix-Marseille, Marseille, France

[5] Lotter AF (1988) Paläoökologische und paläolimnologische Studie des Rotsees bei Luzern. Pollen-, grossrest-, diatomeen- und sedimentanalytische Untersuchungen. Diss Bot 124:1–187

[6] Lotter AF (1990) Die Entwicklung terrestrischer und aquatischer Ökosysteme am Rotsee (Zentralschweiz) im Verlauf der letzten 15000 Jahre. Mitt Naturforsch Ges Luzern 31:81–97. DOI: 10.5169/seals-523489

[7] Lotter AF (1988) Past water-level fluctuations at lake Rotsee (Switzerland), evidenced by diatom analysis. In: Miller U, Robertsson A-M (eds) Proceedings of the Nordic Diatomist Meeting, Stockholm, June 10–12, 1987. Department of Quaternary Research (USDQR) Report 12. University of Stockholm, Stockholm, pp 47–55

[8] Lotter AF, Eicher U, Siegenthaler U, Birks HJB (1992) Late-glacial climatic oscillations as recorded in Swiss lake sediments. J Quat Sci 7(3):187–204. DOI: 10.1002/jqs.3390070302

[9] Svobodová H (1989) Rekonstrukce přírodního prostředí a osídlení v okolí Mistřína. Palynologická studie (A reconstruction of natural environment and settlement in the environs of Mistřín. Palynological study). Památky archeologické 80(1):188–206 (in Czech)

[10] Nagy-Bodor E, Cserny T, Nagy E (1995) Unpublished report on the study performed for the European Pollen Database.

[11] Krisai R (1975) Die Ufervegetation der Trumer Seen (Salzburg). Diss Bot 29:1–197

[12] Rybníček K, Rybníčková E (1977) Mooruntersuchungen im oberen Gurgltal, Ötztaler Alpen. Folia Geobot Phytotaxon 12(3):245–291. DOI: 10.1007/BF02855878

[13] Muller SD, David F, Wicha S (2000) Impact de l'exposition des versants et de l'anthropisation sur la dynamique forestière dans les Alpes du Sud (France). Géogr Phys Quat 54(2):231–243. DOI: 10.7202/004857ar

[14] Oeggl K (1988) Beiträge zur Vegetationgeschichte Tirols VII: Das Hochmoor Schwemm bei Wachsee. Ber Naturwiss Med Ver Innsbruck 75:37–60

[15] Gauthier E (2001) Evolution de l'impact de l'homme sur la végétation du massif jurassien au cours des quatre derniers millénaires. Nouvelles données palynologiques. PhD Thesis, Université de Franche-Comté, Besançon, France

[16] Brugiapaglia E (1996) Dynamique de la végétation tardiglaciaire et holocène dans les Alpes italiennes nord-occidentales. PhD Thesis, Université d'Aix-Marseille, Marseille, France
[17] Rösch M (1997) Holocene sediment accumulation in the shallow water zone of Lower Lake Constance. Arch Hydrobiol / Suppl 107(4):541–562
[18] Rösch M (2000) Long-term human impact as registered in an upland pollen profile from the southern Black Forest, south-western Germany. Veg Hist Archaeobot 9(4):205–218. DOI: 10.1007/BF01294635
[19] Rösch M (1983) Geschichte der Nussbaumer Seen (Kanton Thurgau) und ihrer Umgebung seit dem Ausgang der letzten Eiszeit aufgrund quartärbotanischer, stratigraphischer und sedimentologischer Untersuchungen. Mitt Thurgau Naturforsch Ges 45:1–110. DOI: 10.5169/seals-593800
[20] Rösch M (1985) Nussbaumer Seen—Spät- und postglaziale Umweltsveränderungen einer Seengruppe im östlichen Schweizer Mittelland. Diss Bot 87:337–379
[21] Rösch M (1995) Geschichte des Nussbaumer Sees aus botanisch-ökologischer Sicht. Mitt Thurgau Naturforsch Ges 53:43–59. DOI: 10.5169/seals-593919
[22] van der Knaap WO, van Leeuwen JFN, Fankhauser A, Ammann B (2000) Palynostratigraphy of the last centuries in Switzerland based on 23 lake and mire deposits: chronostratigraphic pollen markers, regional patterns, and local histories. Rev Palaeobot Palynol 108(1–2):85–142. DOI: 10.1016/S0034-6667(99)00035-4
[23] Appleby PG (1998) Report on the radiometric dating of two peat cores from Älbi Flue and Aletschwald, Switzerland. Environmental Radioactivity Research Centre, Liverpool (unpublished)
[24] Welten M (1982) Vegetationsgeschichtliche Untersuchungen in den westlichen Schweizer Alpen: Bern-Wallis. Denkschr Schweiz Naturforsch Ges 95:1–104. DOI: 10.1007/978-3-0348-5359-0
[25] Lotter AF, Heiri O, Hofmann W, van der Knaap WO, van Leeuwen JFN, Walker IR, Wick L (2006) Holocene timber-line dynamics at Bachalpsee, a lake at 2265 m a.s.l. in the northern Swiss Alps. Veg Hist Archaeobot 15(4):295–307. DOI: 10.1007/s00334-006-0060-z
[26] Lotter AF, Sturm M, Teranes JL, Wehrli B (1997) Varve formation since 1885 and high-resolution varve analyses in hypertrophic Baldeggersee (Switzerland). Aquat Sci 59(4):304–325. DOI: 10.1007/BF02522361
[27] Kalis AJ, van der Knaap WO, Schweizer A, Urz R (2006) A three thousand year succession of plant communities on a valley bottom in the Vosges Mountains, NE France, reconstructed from fossil pollen, plant macrofossils, and modern phytosociological communities. Veg Hist Archaeobot 15(4):377–390. DOI: 10.1007/s00334-006-0065-7
[28] Fankhauser A (1995) Pollenanalytische Untersuchungen zur jüngsten Vegetationsgeschichte der Franches Montagnes. MSc Thesis, University of Bern, Bern, Switzerland
[29] van der Knaap WO, Ammann B (1997) Depth–age relationships of 25 well-dated Swiss Holocene pollen sequences archived in the Alpine Palynological Data-Base. Rev Paléobiol 16(2):433–480

[30] Welten M (1982) Pollenanalytische Untersuchungen zur Vegetationsgeschichte des Schweizerischen Nationalparks. Ergeb wiss Unters Schweiz Nationalpark 16(80):3–43

[31] Appleby PG, Shotyk W, Fankhauser A (1997) Lead-210 Age Dating of Three Peat Cores in the Jura Mountains, Switzerland. Water Air Soil Pollut 100(3–4):223–231. DOI: 10.1023/A:1018380922280

[32] Mitchell EAD (1995) The postglacial developmental history of the Praz Rodet bog, Vallée de Joux, Swiss Jura. MSc Thesis, University of Neuchatel, Neuchatel, Switzerland

[33] Shotyk W, Cheburkin AK, Appleby PG, Fankhauser A, Kramers JD (1997) Lead in Three Peat Bog Profiles, Jura Mountains, Switzerland: Enrichment Factors, Isotopic Composition, and Chronology of Atmospheric Deposition. Water Air Soil Pollut 100(3–4):297–310. DOI: 10.1023/A:1018384711802

[34] Hausmann S, Lotter AF, van Leeuwen JFN, Ohlendorf C, Lemcke G, Grönlund E, Sturm M (2002) Interactions of climate and land use documented in the varved sediments of Seebergsee in the Swiss Alps. Holocene 12(3):279–289. DOI: 10.1191/0959683602hl544rp

[35] Appleby PG (1998) Report on the radiometric dating of a peat core from Schöpfewaldmoor, Switzerland. Environmental Radioactivity Research Centre, Liverpool (unpublished)

[36] Appleby PG (1998) Report on radiometric dating of two peat cores from central and southern Switzerland. Environmental Radioactivity Research Centre, Liverpool (unpublished)

[37] Dapples F, Lotter AF, van Leeuwen JFN, van der Knaap WO, Dimitriadis S, Oswald D (2002) Paleolimnological evidence for increased landslide activity due to forest clearing and land-use since 3600 cal BP in the western Swiss Alps. J Paleolimnol 27(2):239–248. DOI: 10.1023/A:1014215501407

[38] Ammann B, Lotter AF (1989) Late-Glacial radiocarbon- and palynostratigraphy on the Swiss Plateau. Boreas 18(2):109–126. DOI: 10.1111/j.1502-3885.1989.tb00381.x

[39] Heeb K, Welten M (1972) Moore und Vegetationsgeschichte der Schwarzenegg und des Molassevorlandes zwischen dem Aaretal unterhalb Thun und dem obern Emmental. Mitt Naturforsch Ges Bern 29:3–54. DOI: 10.5169/seals-319573

[40] Oeschger H, Welten M, Eicher U, Möll M, Riesen T, Siegenthaler U, Wegmüller S (1980) ^{14}C and Other Parameters During the Younger Dryas Cold Phase. Radiocarbon 22(2):299–310. DOI: 10.1017/S0033822200009590

[41] Heuberger H (1977) Gletscher- und klimageschichtliche Untersuchungen im Zemmgrund. Alpenvereinsjahrbuch 102:39–50

[42] Hüttemann H, Bortenschlager S (1987) Beiträge zur Vegetationsgeschichte Tirols VI: Riesengebirge, Hohe Tatra – Zillertal, Kühtai. Ber Naturwiss Med Ver Innsbruck 74:81–112

[43] Wahlmüller N (1985) Beiträge zur Vegetationsgeschichte Tirols V: Nordtiroler Kalkalpen. Ber Naturwiss Med Ver Innsbruck 72:101–144

[44] Seiwald A (1980) Beiträge zur Vegetationsgeschichte Tirols IV: Natzer Plateau – Villanderer Alm. Ber Naturwiss Med Ver Innsbruck 67:31–72

[45] Weirich J, Bortenschlager S (1980) Beiträge zur Vegetationsgeschichte Tirols III: Stubaier Alpen – Zillertaler Alpen. Ber Naturwiss Med Ver Innsbruck 67:7–30

[46] Bortenschlager S (1984) Beiträge zur Vegetationsgeschichte Tirols I. Inneres Ötztal und unteres Inntal. Ber Naturwiss Med Ver Innsbruck 71:19–56
[47] Bortenschlager S (1970) Waldgrenz- und Klimaschwankungen im pollenanalytischen Bild des Gurgler Rotmooses. Mittl Ostalp-dinar Ges Vegetationskunde 11:19–26
[48] Hadorn P (1992) Vegetationsgeschichtliche Studie am Nordufer des Lac de Neuchâtel. Pollenanalytische Untersuchungen am Loclat, in der Bucht von Hauterive/Saint-Blaise und in den neolithischen Ufersiedlungen von Saint-Blaise/Rains des Dames. PhD Thesis, University of Bern, Bern, Switzerland
[49] Hadorn P (1994) Saint-Blaise/Bains des Dames, 1. Palynologie d'un site néolithique et histoire de la végétation des derniers 16000 ans. Archéol neuchâtel 18:1–121
[50] Welten M (1977) Résultats palynologiques sur le développement de la végétation et sa dégradation par l'homme à l'étage inférieur du Valais Central (Suisse). In: Laville H, Renault-Miskovsky J (eds) Approche écologique de l'homme fossile, Travaux du groupe 'Ouest de l'Europe' de la Commission Internationale de l'INQUA 'Palaeoecology of Early Man' (1973–1977), Supplément au Bulletin de l'Association Française pour l'Etude du Quaternaire 47. Pierre-and-Marie-Curie University, Paris, France, pp 303–307
[51] Voigt R (1996) Paläolomnolische und vegetationsgeschichtliche Untersuchungen an Sedimenten aus Fuschlsee und Chiemsee (Salzburg und Bayern). Diss Bot 270:1–303
[52] Nakagawa T (1998) Etudes palynologiques dans les Alpes Françaises centrales et méridionales: histoire de la végétation Tardiglaciaire et Holocène. PhD Thesis, Université d'Aix-Marseille, Marseille, France
[53] Finsinger W, Bigler C, Krähenbühl U, Lotter AF, Ammann B (2006) Human impacts and eutrophication patterns during the past ~200 years at Lago Grande di Avigliana (N. Italy). J Paleolimnol 36(1):55–67. DOI: 10.1007/s10933-006-0002-x
[54] Krisai R, Mayer W, Schröck C, Türk R (2006) Das Gradenmoos in der Schobergruppe (NP Hohe Tauern, Kärnten) Vegetation und Entstehung. Carinthia II 196/116(2):359–386
[55] Juhász I (2002) Reconstitution palynologique de la végétation depuis le Tardiglaciaire dans la région de Zala, sud-ouest de la Hongrie. PhD Thesis, Aix-Marseille University, Marseille, France, University of Pécs, Pécs, Hungary
[56] Zatykó Cs, Juhász I, Sümegi P (eds) (2007) Environmental archaeology in Transdanubia. Varia archaeologica Hungarica XX. Archaeological Institute of the Hungarian Academy of Sciences, Budapest, Hungary
[57] Noël H, Garbolino E, Brauer A, Lallier-Vergès E, de Beaulieu J-L, Disnar J-R (2001) Human impact and soil erosion during the last 5000 yrs as recorded in lacustrine sedimentary organic matter at Lac d'Annecy, the French Alps. J Paleolimnol 25(2):229–244. DOI: 10.1023/A:1008134517923
[58] Dearing J, Hu Y, Doody P, James P, Brauer A (2001) Preliminary reconstruction of sediment-source linkages for the past 6000 yr at the Petit Lac d'Annecy, France, based on mineral magnetic data. J Paleolimnol 25(2):245–258. DOI: 10.1023/A:1008186501993
[59] Noël H (2001) Caractérisation et calibration des flux organiques sédimentaires dérivant du bassin versant et de la production aquatique (Annecy, Le Petit Lac). Rôles respectifs

de l'Homme et du Climat sur l'évolution des flux organiques au cours des 6000 dernières années. PhD Thesis, Université d'Orléans, Orléans, France

[60] de Beaulieu J-L, Leveau P, Miramont C, Palet JM, Walsh K, Court-Picon M, Ricou F, Segard M, Sivan O, Andrieu-Ponel V, Badura M, Bertucchi G, Boutterin C, Durand A, Édouard J-L, Lavoie M, Morin A, Mocci F, Ponel P, Pothin A, Py V, Talon B, Tzortzis S, Bonet R, Columeau P, Cortot H, Garcia D (2003) Changements environnementaux postglaciaires et action de l'homme dans le bassin du Buëch et en Champsaur (Hautes-Alpes, France). Premier bilan d'une étude pluridisciplinaire. In: Muxart T, Vivien F-D, Villalba B, Burnouf J (eds) Des Milieux et des Hommes: Fragments d'Histoires Croisées. Elsevier, Paris, France, pp 93–101

[61] Walsh K, Mocci F, Dumas V, Durand A, Talon B, Tzortzis S (2003) Neuf mille ans d'occupation du sol en moyenne montagne: la vallée de Fressinières dans le Parc National des Ecrins (Fressinières, Hautes-Alpes). Archéologie du Midi Médiéval 21:185–198. DOI: 10.3406/amime.2003.1412

[62] Rösch M, Tserendorj G (2011) Der Nordschwarzwald – früher besiedelt als gedacht? Pollenprofile belegen ausgedehnte vorgeschichtliche Besiedlung und Landnutzung. Denkmalpflege in Baden-Württemberg 40(2):66–73

[63] Rösch M, Tserendorj G (2011) Florengeschichtliche Beobachtungen im Nordschwarzwald (Südwestdeutschland). Hercynia N. F. 44(1):53–71

[64] Nelle O (2002) Zur holozänen Vegetations- und Waldnutzungsgeschichte des Vorderen Bayerischen Waldes anhand von Pollen- und Holzkohlenanalysen. Hoppea Denkschr Regensb Bot Ges 63:161–361

[65] Nelle O, Dreibrodt S, Dannath Y (2010) Combining pollen and charcoal: evaluating Holocene vegetation composition and dynamics. J Archaeol Sci 37(9):2126–2135. DOI: 10.1016/j.jas.2010.02.010

[66] Rösch M, Lechterbeck J (2016) Seven Millennia of human impact as reflected in a high resolution pollen profile from the profundal sediments of Litzelsee, Lake Constance region, Germany. Veg Hist Archaeobot 25(4):339–358. DOI: 10.1007/s00334-015-0552-9

[67] Jeník J, Rektoris L, Lederer F (2002) Plant life in an endangered mire: Červené blato bog. In: Květ J, Jeník J, Soukupová L (eds) Freshwater Wetlands and their Sustainable Future: A Case Study of Trebon Basin Biosphere Reserve, Czech Republic. The Parthenon Publishing Group, New York, pp 399–408

[68] https://www.reserves-naturelles.org/etang-du-grand-lemps. Accessed 2 December 2021

[69] de Beaulieu J-L, Reille M (1983) Paléoenvironnement tardiglaciaire et holocène des lacs de Pelléautier et Siguret (Hautes-Alpes, France). I. Histoire de la végétation d'après les analyses polliniques. Ecol Mediterr 9(3):19–36

[70] Lotter AF (2010) Pollen profile RL240, Rotsee, Switzerland. European Pollen Database (EPD), PANGAEA, DOI: 10.1594/PANGAEA.739746

[71] Lotter AF (2010) Pollen profile RL250, Rotsee, Switzerland. European Pollen Database (EPD), PANGAEA, DOI: 10.1594/PANGAEA.739747

[72] Clerc J (1985) Première contribution a l'étude de la végétation Tardiglaciaire et Holocène du Piémont Dauphinois. Documents de cartographie écologique 28:65–83

[73] Svobodová H (1997) Die Entwicklung der Vegetation in Südmähren (Tschechien) während des Spätglazials und Holozäns – eine palynologische Studie. Verh Zool-Bot Ges Österr 134:317–356
[74] Krisai R (2010) Pollen profile TRUMER, Trumer Moos, Austria. European Pollen Database (EPD), PANGAEA, DOI: 10.1594/PANGAEA.739913
[75] Krisai R (2010) Pollen profile ZELLHOF, Wasenmoos beim Zellhof, Austria. European Pollen Database (EPD), PANGAEA, DOI: 10.1594/PANGAEA.739986
[76] Brugiapaglia E (1998) Paleobiogeografia della Valle d'Aosta a partire dall'ultima glaciazione. Biogeographia 19:85–104. DOI: 10.21426/B6110162
[77] Rösch M (1985) Ein Pollenprofil aus dem Feuenried bei Überlingen am Ried: Stratigraphische und landschaftsgeschichtliche Bedeutung für das Holozän im Bodenseegebiet. Materialhefte zur Vor- und Frühgeschichte in Baden-Württemberg 7:43–79
[78] Rösch M (2010) Pollen profile NUSS4, Nussbaumer Seen, Switzerland. European Pollen Database (EPD), PANGAEA, DOI: 10.1594/PANGAEA.739608
[79] Vallé F, Furlanetto G, Pini R, Brunetti M, Maggi V, Ravazzi C (2019) Reconstructing the last 3000 years climate change in N-Italy from fossil pollen archive. Geogr Fis Dinam Quat 42(2):235–244. DOI: 10.4461/GFDQ.2019.42.13
[80] Lotter AF (2010) Pollen profile SAEGIST, Sägistalsee, Switzerland. European Pollen Database (EPD), PANGAEA, DOI: 10.1594/PANGAEA.739773

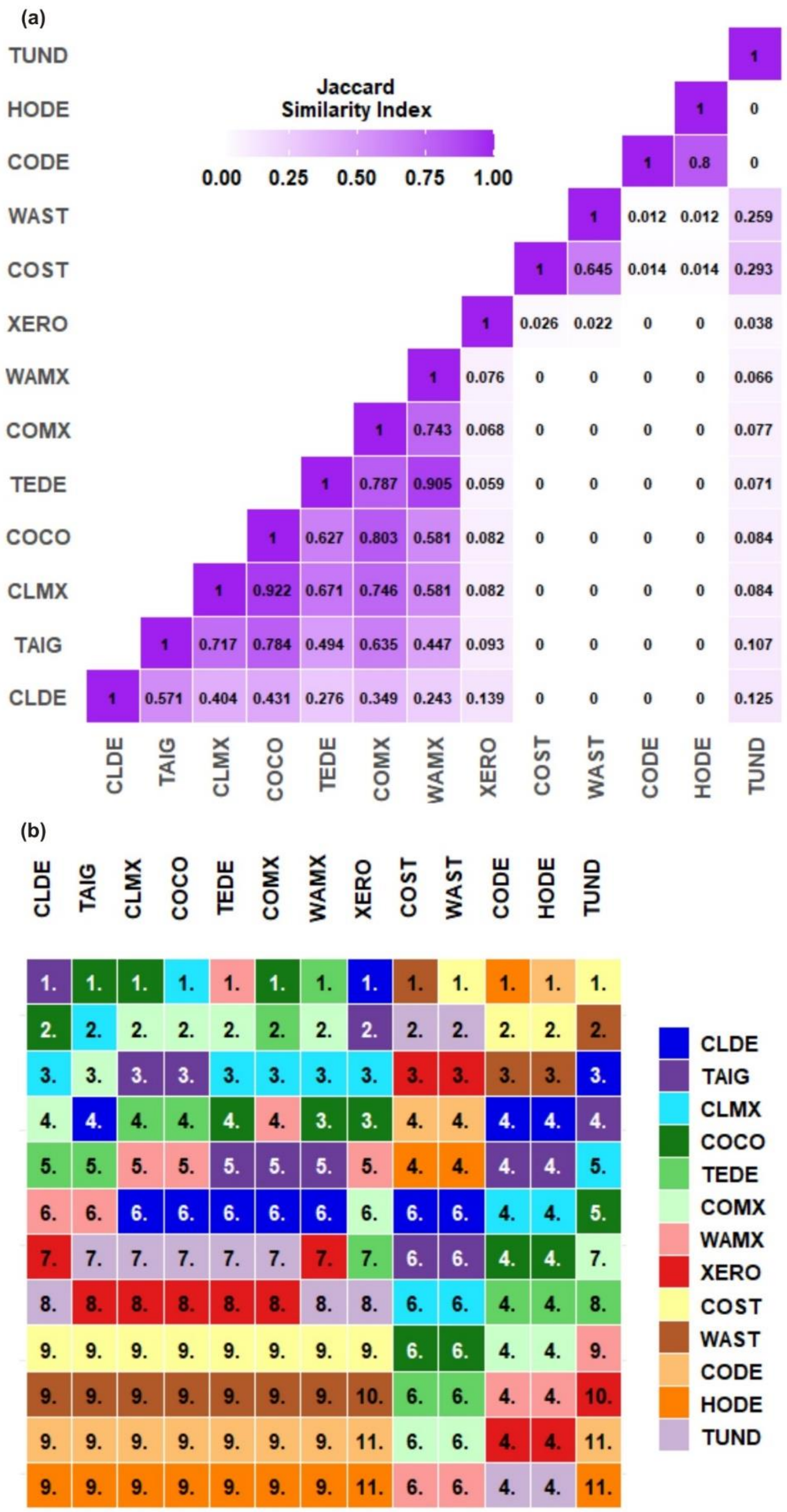

Fig. B.1 The similarity of definition of the pollen-inferred biome types used here in terms of taxonomic composition: (**a**) Values of the Jaccard similarity index (JSI: Jaccard 1901) between each pair of biomes, and (**b**) the similarity order by the above JSI values for each biome type. The value of JSI range between 0 (no similarity) and 1 (identical sets), so biome type belonging to the largest non-one JSI value is placed at the top of the ranking. These rankings are used to determine the value of the definition expansion required for matching (DEm), for each pollen sequence

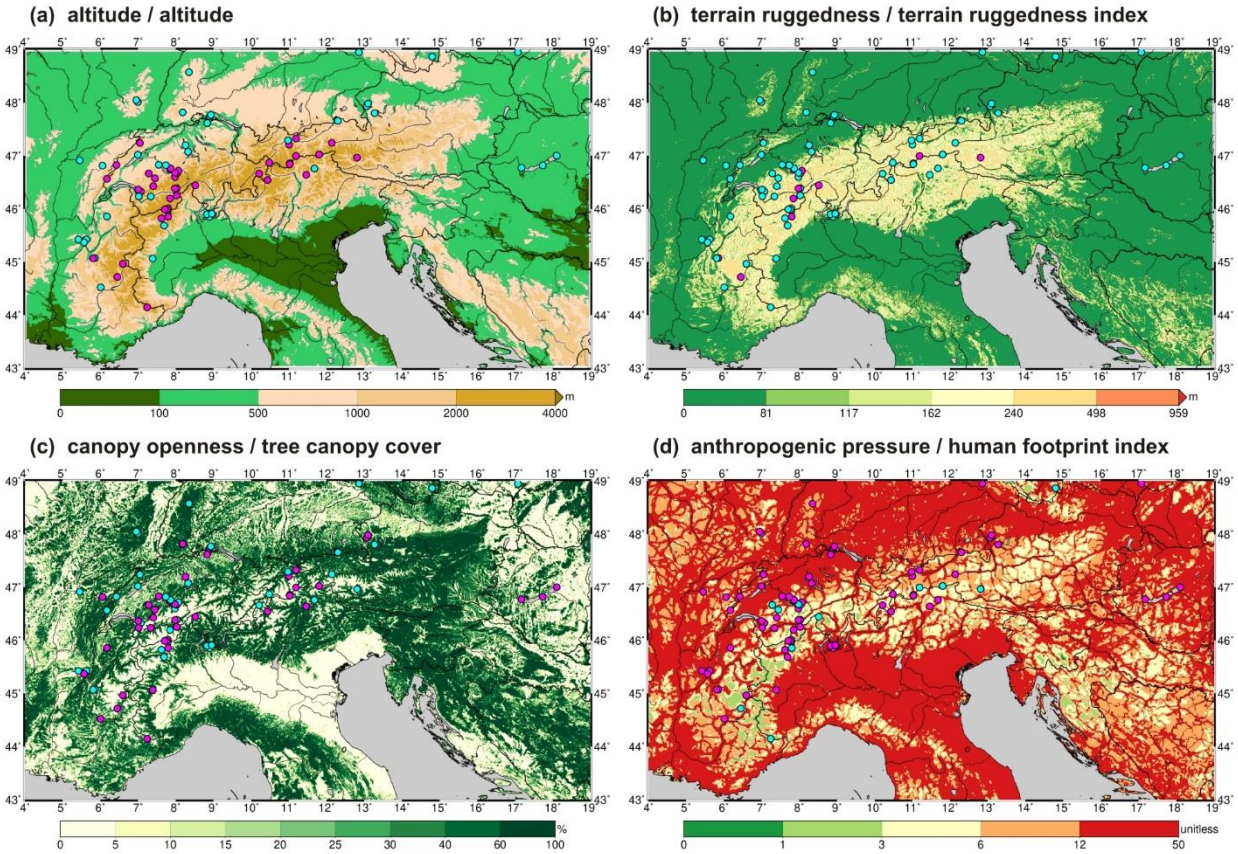

Fig. B.2 Site types superimposed on distribution maps of landscape features influencing the efficiency of the biomization process in the Greater Alpine Region. The subgroups of fossil pollen sites are generated by considering the following influential factors: (**a**) altitude (high/low altitude: 1000 m a.s.l.), (**b**) terrain ruggedness (high/low terrain ruggedness index, TRI: 240 m), (**c**) canopy openness (low/high tree canopy cover, TCC: 25%), and (**d**) anthropogenic pressure (high/low human footprint index, HFI: 6). Sites considered to be affected are marked by *magenta circles* and the remainder by *cyan circles*. Altitudinal data are derived from the Global 30 Arc-Second Elevation Dataset (GTOPO30: Gesch et al. 1999). The TRI is calculated from the GTOPO30. The TCC is extracted from the Global Forest Change Dataset (Hansen et al. 2013), for year 2000. A map of the HFI for year 1993 is developed by Venter et al. (2016). Here, the TCC and HFI data with different spatial resolution and grid are aggregated to the grid of the GTOPO30 using bilinear resampling technique

References

Fyfe RM, de Beaulieu J-L, Binney H, Bradshaw RHW, Brewer S, Le Flao A, Finsinger W, Gaillard M-J, Giesecke T, Gil-Romera G, Grimm EC, Huntley B, Kunes P, Kühl N, Leydet M, Lotter AF, Tarasov PE, Tonkov S (2009) The European Pollen Database: past efforts and current activities. Veg Hist Archaeobot 18(5):417–424. DOI: 10.1007/s00334-009-0215-9

Gesch DB, Verdin KL, Greenlee SK (1999) New land surface digital elevation model covers the Earth. EOS Earth Space Sci News 80(6):69–70. DOI: 10.1029/99EO00050

Giesecke T, Davis B, Brewer S, Finsinger W, Wolters S, Blaauw M, de Beaulieu J-L, Binney H, Fyfe RM, Gaillard M-J, Gil-Romera G, van der Knaap WO, Kuneš P, Kühl N, van Leeuwen JFN, Leydet M, Lotter AF, Ortu E, Semmler M, Bradshaw RHW (2014) Towards mapping the late Quaternary vegetation change of Europe. Veg Hist Archaeobot 23(1):75–86. DOI: 10.1007/s00334-012-0390-y

Hansen MC, Potapov PV, Moore R, Hancher M, Turubanova SA, Tyukavina A, Thau D, Stehman SV, Goetz SJ, Loveland TR, Kommareddy A, Egorov A, Chini L, Justice CO, Townshend JRG (2013) High-resolution global maps of 21st-century forest cover change. Science 342(6160):850–853. DOI: 10.1126/science.1244693

Hijmans RJ (2020) raster: Geographic Data Analysis and Modeling. R package version 3.3-13. https://CRAN.R-project.org/package=raster. Accessed 25 November 2020

Jaccard P (1901) Étude comparative de la distribution florale dans une portion des alpes et des jura. Bull Soc Vaud sci nat 37:547–579

Venter O, Sanderson EW, Magrach A, Allan JR, Beher J, Jones KR, Possingham HP, Laurance WF, Wood P, Fekete BM, Levy MA, Watson JEM (2016) Global terrestrial Human Footprint maps for 1993 and 2009. Sci Data 3:160067. DOI: 10.1038/sdata.2016.67

Appendix B.3 – Supplemental information for the simulated biome distribution

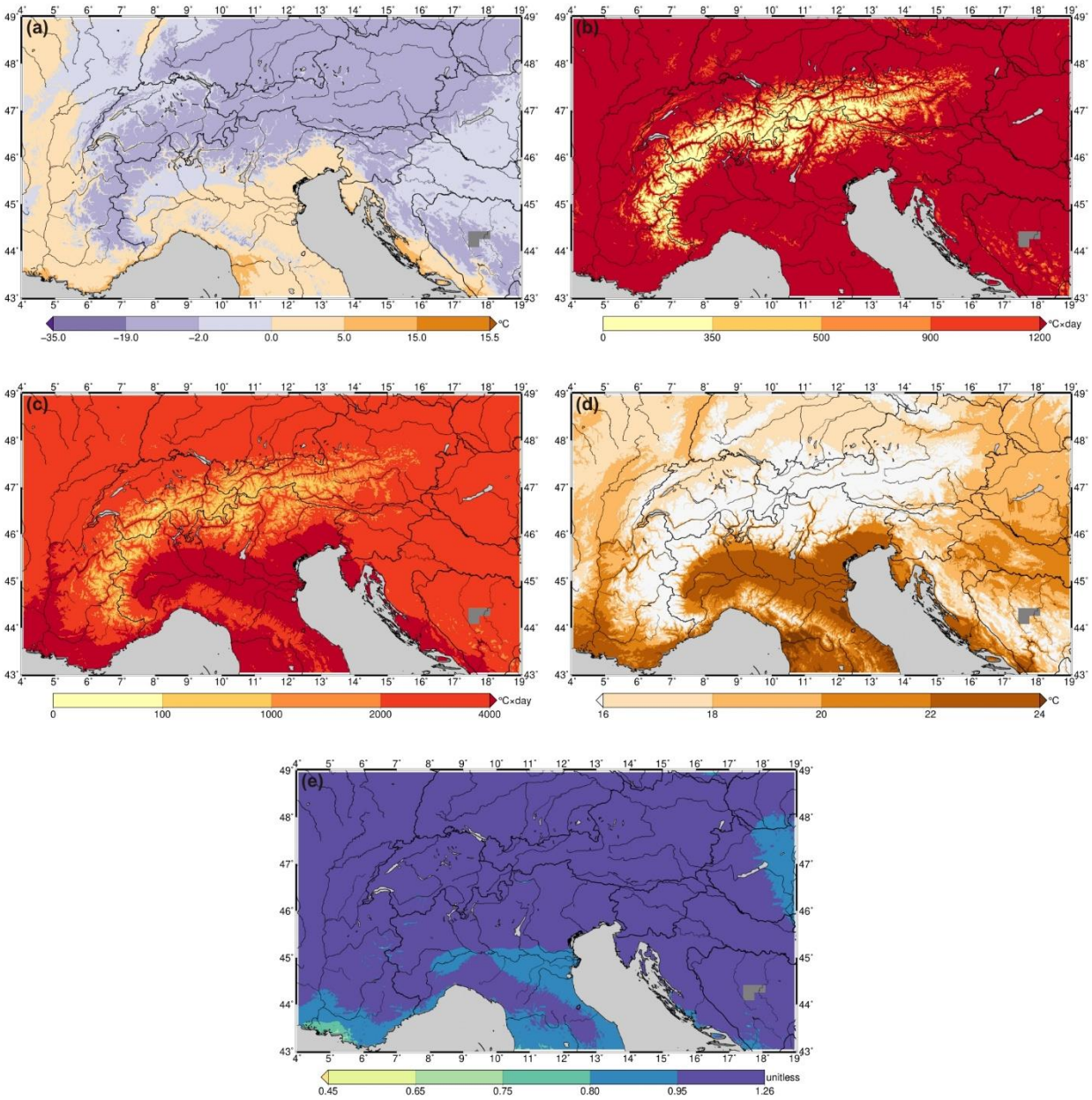

Fig. B.3 Spatial distribution patterns of the five bioclimatic indices used in the BIOME model in the Greater Alpine Region: (**a**) mean temperature of the coldest month (T_C, in °C), (**b**) growing degree-days above a 5 °C base (GDD_5, in °C day), (**c**) growing degree-days above a 0 °C base (GDD_0, in °C day), (**d**) mean temperature of the warmest month (T_W, in °C), and (**e**) Priestley–Taylor coefficient at an annual time scale (α, dimensionless)